Dissertation

Submitted to the

Combined Faculties for the Natural Sciences and for Mathematics

of the Ruperto-Carola University of Heidelberg, Germany

for the degree of

Doctor of Natural Sciences

presented by

Ikhwan Resmala Sudji

born in Sabang, Indonesia

oral examination: July 2015

Bioactivity of Steroid and Triterpenoid Saponins: Influence on Membrane Permeability and Drug Absorption

Referees: Prof. Dr. Michael Wink
Prof. Dr. Gert Fricker

Thesis declaration

I hereby declare that this thesis has been written only by the undersigned and without any assistance from third parties. Furthermore, I confirm that no sources have been used in the preparation of this thesis other than those indicated in the thesis itself.

Heidelberg, May 13, 2015

_____

Ikhwan Resmala Sudji

Look deep into nature,
and then you will understand everything better.

Albert Einstein

"Orang boleh pandai setinggi langit, tapi selama ia tidak menulis,
ia akan hilang di dalam masyarakat dan dari sejarah.
Menulis adalah bekerja untuk keabadian."

Pramoedya Ananta Toer

Acknowledgements

First and foremost, I am truly indebted and thankful to my supervisor Prof. Dr. Michael Wink for giving me the opportunity for writing this dissertation and working in his laboratory towards earning my Ph.D., and for supporting me with valuable advice from his broad knowledge and expertise. At the same time, I enjoyed the liberty of having been able to develop and pursue my own ideas.

In sincere gratefulness, I would like to thank Prof. Dr. Gert Fricker, my second supervisor, for his generous support and inspiring discussions and for giving me the opportunity to work in his lab.

My heartfelt appreciation and thanks are expressed to Prof. Dr. Ana J. García-Sáez (Membrane Biophysics Group, BioQuant) and Prof. Dr. Motomu Tanaka (Physical Chemistry of Biosystems Group, Heidelberg University) for giving me the opportunity to work on my topic within their field of membrane biophysics and for their guidance, enthusiasm, encouragement, and discussions.

Special thanks go to Dr. Ali Makky for his guidance, valuable support, and discussions regarding biomembrane models, to Dr. Nataliya Frenkel for her great support and analytical suggestions regarding the DPI and XRR measurements, to Dr. Yamunadevi Subburaj for her kind and professional help in GUV imaging by confocal microscopy, and to Eduard Hermann for developing and kindly helping with GUV software.

My sincere thanks go to the staff of the Biology Department of IPMB: to Petra Fellhauer who kindly helped in all sorts of administrative issues, to Astrid Backhaus for her kind help and technical assistance, to Heidi Staudter, Hedi Sauer-Gürth, and Dieter Holzmann for daily assistance in the lab; and to Carolin Stegmüller in the Membrane Biophysics Lab of BioQuant.

Thanks for useful advice and help are extended to Frank Sporer, Dr. Dorothea Kaufmann, Dr. Florian Herrmann, Dr. Ahmad Tahrani, Dr. Bernhard Wetterauer, Dr. Wasim Abuillan, Agatha Korytowski, Dr. Stephanie Bleicken, Max richter, Paranchai Boonsawat and Joseph Unsay.

Towards my laboratory colleagues in the three labs: Dr. Holger Schäfer, Dr. Amin Eimanifar, Eva Arnold, Agustina Nurcahyanti, Dr. Stephan Kaufmann, Mariam Vescgini, Moritz Hermann, and Dr. Monika Zelman, I would like to expressed my appreciation for your friendships and help over the years.

My warmest thanks go to my caring "Heidelberg family", Theodor C. H. Cole and Erika Siebert-Cole, for always being there for me, for keeping my spirits high, for sharing their wisdom and advice that has helped me in my endeavor towards becoming a good scientist and teacher, and for their hospitality.

My warmhearted thanks are expressed to Dr. Peter Macalister-Smith and Ritawati Abbas for their caring hospitality and friendship.

Thanks to all members of the Komunitas Indonesia Heidelberg, Dr. Endang Darmawan and family, Dr. Budi Aji, Kol. Rodon Pedrason Pedrason-Lisa Friscilla and family, M. Hasan Bashari, Kristanto Irawan Putra for kind friendship and support.

My deepest gratitude goes to my dear and loving family: especially to my parents in Sabang/Padang for their support and encouragement throughout my studies – your prayers have sustained me on this long journey. I am, and always will be, thankful and indebted for the sacrifices you made to support me.

My beloved wife, Dr. Syafrizayanti, provided emotional support throughout, and helped me to keep my faith in difficult times. I thank her for her encouragement and for the wonderful time we have been blessed with in trying to make our dreams come true.

Ikhwan Resmala Sudji

Table of Contents

Abbreviations

AFM	atomic fluorescence microscopy
BAM	Brewster angle microscopy
BSA	bovine serum albumin
CD	circular dichroism
CER	cytotoxicity enhancement ratio
Chol	cholesterol
CI	combination index
CL	cardiolipin
CM	confocal microscopy
CMC	critical micelle concentration
cryo-SEM	cryogenic scanning electron microscopy
cryo-TEM	cryogenic transmission electron microscopy
CTL	cytotoxic T lymphocytes
DLS	dynamic light scattering
DMEM	Dulbecco's Modified Eagle Medium
DMSO	dimethyl sulfoxide
DPI	dual polarization interferometry
DSC	differential scanning calorimetry
EGCG	epigallocatechin gallate
EGF	epidermal growth factor
ESI	electrospray ionization
FBS	fetal bovine serum
FCCS	fluorescence cross-correlation spectroscopy
FCS	fluorescence correlation spectroscopy
FDA	U.S. Food and Drug Association
FEMA	U.S. Flavor and Extract Manufacturers Association
FPP	farnesyl pyrophosphate
FTIR	Fourier transform infrared spectroscopy
5-FU	5-fluorouracil
GIXF	grazing-incidence X-ray fluorescence
GUVs	giant unilamellar vesicles
HPLC	high-performance liquid chromatography
IC_{50}	half-maximal inhibitory concentration
IPP	isopentenyl pyrophosphate
ISCOMs	immune-stimulating complexes
LC/MS	liquid chromatography/mass spectrometry
LUVs	large unilamellar vesicles
MAPK	mitogen-activated protein kinase
MMP-2	matrix metalloproteinase-2,
MTT	methylthiazolyltetrazolium
NMR	nuclear magnetic resonance
P	phytolaccinic acid
P-Ac	*O*-23 acetylated phytolaccinic acid
PBS	phosphate buffer saline
PC	phosphatidylcholine
Q	quillaic acid
QCM-D	quartz crystal microbalance with dissipation
Q-OH	22β-hydroxyquillaic acid
RBCs	red blood cells
RT	retention time
SAR	structure-activity relationships
SDS	sodium dodecyl sulfate
SLBs	supported lipid bilayers
SLD	scattering length density
SM	sphingomyelin
SOPC	1-stearoyl-2-oleoyl-*sn*-glycero-3-phosphocholine
SUVs	small unilamellar vesicles
TIC	total ion current
TMC	traditional Chinese medicine
VEGF	vascular endothelial growth factor
XRR	X-ray reflectivity
ΔD	dissipation shift
Δf	frequency shift

Summary

Saponins are widely distributed among flowering plants and some marine invertebrates and serve in defense for these organisms. Their amphiphilic molecules are composed of a lipophilic aglycone and one or more hydrophilic sugar moieties, giving them a high degree of structural diversity. Their biological and pharmacological activities range from antimicrobial, antifungal, anticancer, to immunomodulatory, etc. The most prominent feature of saponins is linked to their **effects on cell membranes**; they strongly affect cell membrane structure and integrity by different mechanisms depending on their chemical structure. The ability of saponins to **increase membrane permeability** can be used to facilitate the passage of drug molecules or other natural products through the cell membrane. The ability of saponins to affect cell membrane structure and integrity makes them interesting natural products in pharmacological and medical research and therapy, in particular as agents for enhancing drug efficacy. Saponins are known to interact with cholesterol in cell membranes by forming complexes. Until recently, there has been limited information on their potential as **cytotoxicity-enhancing agents** and on their **molecular mechanisms of action** on the membrane.

This study explores the mechanisms of action of saponins on membranes and their effects in enhancing the cytotoxicity of certain anticancer drugs/toxins as applied to various cancer cell lines. Two different kinds of saponins were chosen (**digitonin**, a steroid saponin, and **quillaja extract**, a triterpenoid saponin mixture). These were investigated in combination with the anticancer drugs berberine, cisplatin, doxorubicin, dexamethasone, and mitomycin C, as well as with the polar toxin ricin (extracted from castor beans), on HeLa, COS-7, MIA PaCa-2, and PANC-1 cancer cell lines. The associated molecular mechanisms of action on membranes were investigated by employing a series of bioanalytical/ biophysical techniques: 1) **MTT assay** (a formazan test) which measures cell viability; 2) **hemolysis** (microscopic screening of erythrocytes) to measure the degree of membrane destruction; 3) **dynamic light scattering (DLS)** on large unilamellar vesicles (LUVs) to observe and quantify membrane leakage; 4) **fluorescene/confocal microscopy** of giant unilamellar vesicles (GUVs) to visualize membrane permeability; 5) **quartz crystal microbalance with dissipation (QCM-D)**, **dual polarization interferometry (DPI)**, and **high-energy specular X-ray (XRR)** showing structural changes in supported lipid bilayers (SLB), and 6) **differential scanning calorimetry (DSC)** which reveals thermotropic features of membranes resulting from saponin action.

Digitonin and quillaja extract both enhance the cytotoxicity of the selected anticancer drugs in several cancer cell lines, the effect being either synergistic or additive. Quillaja saponin exerts a stronger cytotoxicity-enhancing effect than digitonin. The highly toxic monodesmosidic digitonin causes complete disruption of membranes at very low concentrations. The membrane activity of saponins strongly depends on the presence and amount of cholesterol in the membrane. **Digitonin destroys GUVs, while quillaja saponin rather leads to pore formation.** The relatively stable pores formed by the quillaja saponin-cholesterol complexes have a diameter of about 1 nm, only allowing passage of small-size molecules. **Digitonin removes cholesterol from the inner membrane layer with formation of an additional layer on the outside, which eventually leads to membrane disruption.** The quillaja saponins penetrate into the inner membrane layer forming complexes with cholesterol. The stabilized complexes form pores, which allow passage of water and other small molecules. Both sugar chains of the bidesmosidic quillaja saponins play an important role in stabilizing the pore formation in the membrane. Here, and for the first time, **we report the occurrence of monodesmosides in the employed commercial quillaja saponin extract**. The presence of both bidesmosides and monodesmosides in the quillaja saponin extract may be responsible for its bioactivity and pharmacological effects.

Zusammenfassung

Saponine sind weit verbreitete sekundäre Stoffwechselprodukte, die in Blütenpflanzen, aber auch in einigen wirbellosen Tieren vorkommen und vor allem der Verteidigung dienen. Saponine bestehen aus einem lipophilen Aglykon und einer oder mehreren hydrophilen Zuckerketten; letztere sind sehr vielgestaltig und bilden eine große Anzahl unterschiedlicher Strukturen. Das Wirkungsspektrum der Saponine erstreckt sich von antibakteriell, antimykotisch und krebshemmend bis immunstimulierend – was vor allem auf deren Interaktion mit Zellmembranen beruht. Der **Effekt auf die Zellmembran** variiert je nach Art der Molekülstruktur der Saponine. Saponine bilden in der Zellmembran komplexe Verbindungen mit Cholesterin. Die exakten Wirkmechanismen der Saponine auf die Zellmembran sind allerdings noch unzureichend erforscht.

Saponine erhöhen die **Membranpermeabilität**. Dies wird bereits genutzt, um die Wirksamkeit von intrazellulär agierenden Medikamenten zu verstärken. Die Möglichkeit der Zytotoxizitätsverstärkung von krebshemmenden Medikamenten bietet ein interessantes und weites Feld für die Zellforschung und für klinische Studien.

Die vorliegende Arbeit konzentriert sich auf die spezifischen Effekte von Saponinen auf verschiedene Membranmodelle und die Zytotoxizitätsverstärkung verschiedener Zytostatika/Toxine durch Saponine an verschiedenen Krebszelllinien. Dazu wurden zwei unterschiedliche Saponine (**Digitonin**, ein Steroidsaponin, und **Quillaja-Extrakt**, ein Triterpenoidsaponin-Gemisch) mit Berberin, Cisplatin, Doxorubicin, Dexamethason, Mitomycin C, sowie Rizin kombiniert und an vier Krebs-zelllinien untersucht (HeLa, COS-7, MIA PaCa-2, und PANC-1). Der molekulare Wirkungsmechanismus auf die Membran wurde mit verschiedenen bioanalytischen/biophysikalischen Messmethoden analysiert:

1) **MTT-Test** (ein Formazan-Test) zur Messung der Zellvitalität;
2) **Hämolyse** (Mikroskopie von Erythrozyten), ermittelt den Grad der Zerstörung von Zellmembranen;
3) **DLS (Dynamische Lichtstreuung)** an LUVs (große lamellare Vesikel), misst die Membrandurchlässigkeit;
4) **Fluorescein/Konfokalmikroskopie** an GUVs (riesige lamellare Vesikel) zur Visualisierung der Membrandurchlässigkeit;
5) **QCM-D (Quarzkristall-Mikrowaage)**, **DPI (Doppelpendelinterferometrie)**, und **XRR (Röntgenreflektometrie)**, zeigen Veränderungen der Struktur von SLBs (unterstützte Lipiddoppelschichten);
6) **DSC (Differentialkalorimetrie)**, gibt Hinweise auf thermotrope Eigen-schaften von Membranen.

Sowohl Digitonin als auch Quillajaextrakt erhöhen die Zytotoxizität der hier eingesetzten Zytostatika gegenüber mehreren Krebszelllinien, synergistisch oder additiv, je nach Zytostatikum/Toxin und Zellart. Quillajaextrakt (bestehend aus Bisdesmosiden) erhöht die Zytotoxizität der verwendeten Zytostatika in einem höheren Maße als Digitonin. Das stark giftige Digitonin (ein Monodesmosid) führt bereits bei niedriger Konzentration zur Zerstörung der Membran. Die Untersuchungen belegen, dass der Membran-Effekt hauptsächlich auf der Interaktion der Saponine mit Cholesterin beruht.

Digitonin zerstört GUV-Vesikel, während Quillajaextrakt dort lediglich zu Porenbildung führt, was die unterschiedliche Wirkung der beiden Saponine bezüglich der durch sie bedingten Erhöhung der Zytotoxizität der verwendeten Zytostatika erklärt. Die Porengröße der Quillajaextrakt-Cholesterin-Komplexe beträgt ca. 1 nm, wodurch nur entsprechend kleine Wirkstoffe in die Zelle gelangen können. **Digitonin führt zu Cholesterinverlust der inneren Membranschicht und zusätzlicher Cholesterinauflage der Außenmembran, und schließlich zur Zerstörung der Membran.**

Quillajaextrakt dringt in die innere Membranschicht ein und bildet dort mit Cholesterin stabile Komplexe und eindeutig definierbare Poren in der Membran. Wasser und andere kleine Moleküle können somit die Membran ungehindert passieren. Das Vorhandensein von zwei Zuckerketten in der Struktur der bisdesmosidischen Quillaja-Saponine spielt dabei eine wesentliche Rolle. Hier berichten wir zum ersten Mal von **Monodesmosiden in einem handelsüblichen Quillaja-Saponin**. Das Vorhandensein von sowohl Bisdesmosiden als auch Monodesmosiden in Quillaja-Extrakten scheint für die Gesamt-Bioaktivität und die pharmakologische Wirkung entscheidend zu sein.

1 Introduction

1.1 Saponins – structure and classification

Saponins are natural glycosides, which are widely distributed in the plant kingdom and some marine animals like sea cucumbers (Holothuriidae) and sea stars (Asteroidea) (Caulier et al. 2011; Andersson et al. 1989). Their amphiphilic molecular structure is due to a lipophilic aglycone and one or more hydrophilic sugar side chains. A main characteristic of saponins is their foaming, soap-like behavior in aqueous solution, leading to their name (Latin *sapo* = soap). Many plant extracts containing saponins, especially obtained from *Saponaria officinalis* (soap wort) and *Quillaja saponaria* (soapbark), traditionally have been used as soaps (Vincken et al. 2007; Augustin et al. 2011; Hostettmann and Marston 2005).

The aglycone moiety of saponins is generally referred to as the sapogenin, to which one or more sugar molecules are attached. Two classes of saponins are distinguished based on their type of aglycone; triterpene (or triterpenoid) saponins and steroid (or steroidal) saponins. Steroidal glycoalkaloids have been considered as a third type of saponins because their structural characteristics suggest a similar biosynthetic origin and their biological activities resemble those of steroidal saponins but their aglycones contain a nitrogen atom which classifies them as a separate group (Hostettmann and Marston 2005; Vincken et al. 2007). From a structural point of view, Vincken et al. suggested to omit steroidal glycoalkaloids from the class of saponins due to the occurrence of the characteristic nitrogen atom in the aglycone. Based on the carbon skeleton of the saponin aglycone, the latter authors proposed a detailed classification of saponins into 11 main classes: dammaranes, tirucallanes, lupanes, hopanes, oleananes, taraxasteranes, ursanes, cycloartanes, lanostanes, cucurbitanes, and steroids. The dammaranes, lupanes, hopanes, oleananes, ursanes, and steroids are further divided into 16 subclasses, because their carbon skeletons are subject to fragmentation, homologation, and degradation reactions. The oleanane skeleton is the most common representative in most of the orders of flowering plants (Fig. 1.1).

Both types of saponin aglycones have been synthesized from 2,3-oxidosqualene, a main metabolite in sterol biosynthesis. Saponin biosynthesis follows the isoprenoid pathway where three molecules of isopentenyl pyrophosphate (IPP), each consisting of five carbon atoms linked together in a head-to-tail manner, form a 15-carbon molecule, farnesyl pyrophosphate (FPP). Two molecules of FPP linked together resulting a 30-carbon molecule called squalene (Holstein and Hohl 2004; Vincken et al. 2007). The enzyme squalene monooxygenase converts squalene into 2,3-oxidosqualene, which becomes the precursor for the saponin aglycone.

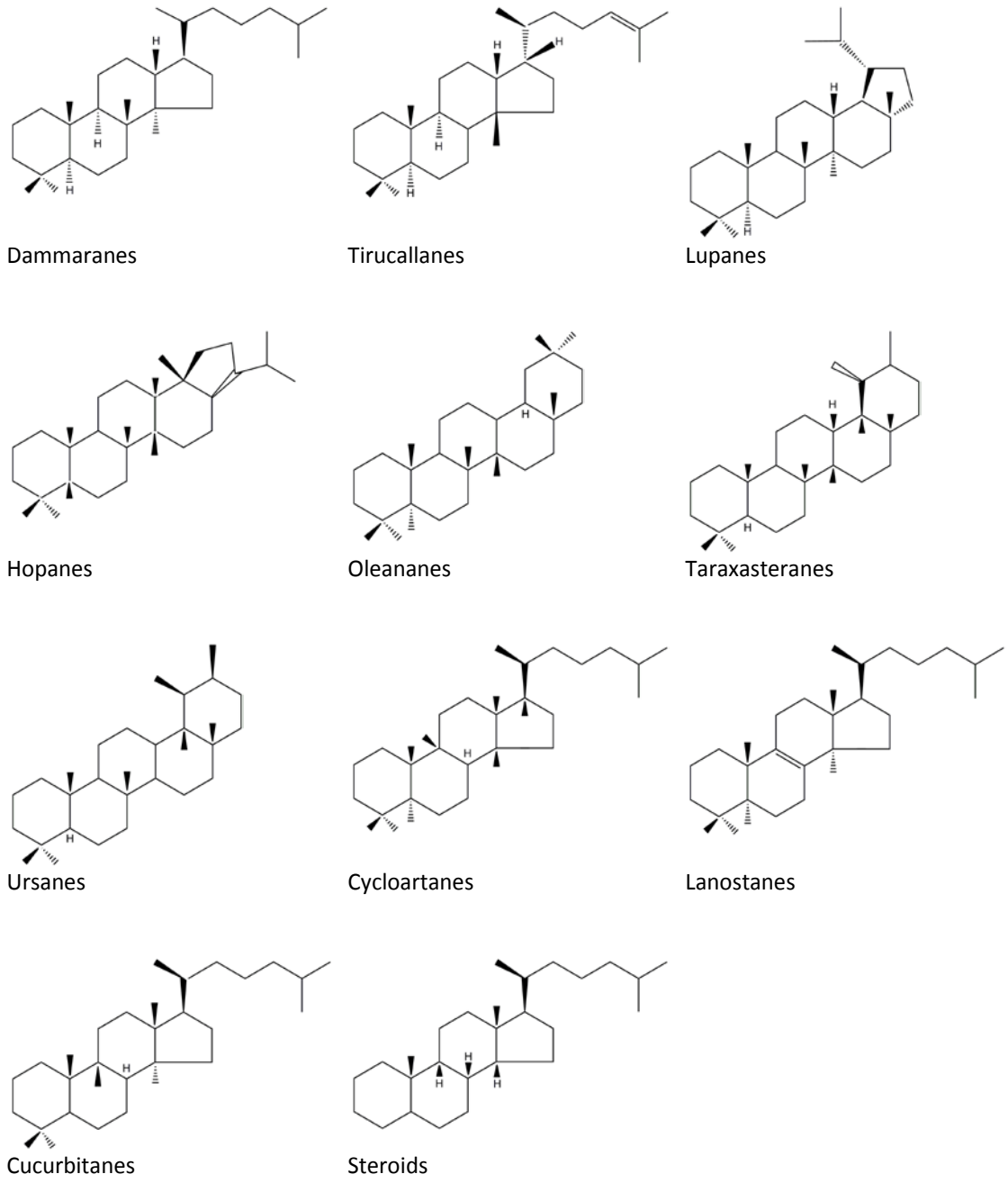

Fig. 1.1. Main classes of carbon skeletons of saponins

Cyclization of oxidosqualene leads up to all main classes of saponin aglycones. The cyclization process begins with oxidosqualene being converted into cyclic derivatives via protonation and opening of the epoxide ring leading to several types of cyclization reactions. After cyclization, subsequent rearrangements can proceed in different ways by a series of hydride shifts and/or methyl migrations, which lead to the formation of new carbocations. At the end of the process, the carbocations are neutralized by proton elimination to give double bonds or

cyclopropanyl rings or by reaction with water to give a hydroxyl group (Vincken et al. 2007; Haralampidis et al. 2002). The cyclization and rearrangement process results in triterpenoid aglycones (Abe et al. 1993; Haralampidis et al. 2002; Augustin et al. 2011) and cholesterol which can lead to steroid aglycones via oxidation at C-16, C-22, and C-26/27 and subsequent cyclization of the oxygenated cholesterol leading to the formation of the spiroketal ring (Sahu et al. 2008).

Saponins are also classified based on the number of sugars attached to the aglycone backbone. In **monodesmosidic** saponins the sugar chain is bound only to one particular position of the aglycone, mostly to the C-3 hydroxyl group. The glycosidic chain can be built of up to 11 sugar units and may also be branched. Saponins having two sugar chains attached to the aglycone are called **bidesmosidic**; here, one sugar chain is linked to the C-3 hydroxyl group and the other by an ester linkage to the C-28 carboxyl group. A third group, the tridesmosidic saponins, where three sugar chains are attached at different positions of the aglycone, is rather rare though. Aside from sugars, there may be other substances attached to the aglycone, such as small aliphatic and aromatic acids, monoterpene derivatives, or acyl groups (Vincken et al. 2007; Hostettmann and Marston 2005; Augustin et al. 2011).

1.1.1 Digitonin – a steroid saponin

Digitonin is a widely employed steroid glycoside from the plant of the foxglove, *Digitalis purpurea* (family Plantaginaceae) (Fig. 1.2). The plant is a common native to temperate Europe and naturalized in parts of North America and other regions of the temperate zone. The potency of *Digitalis purpurea* was first reported by William Withering in 1775, who referred to it as a remedy for treating dropsy. Since then chemists and pharmacologists have explored the potency of foxglove. Several active substances have been isolated, such as digitoxin, which is considered the most valuable constituent due to its cardiac activity and value as a therapeutic agent. Digitonin, in contrast, has no cardiac effect (Dixon 1912; Brown et al. 1962).

Later, digitonin was found to interact with cholesterol and affect cell membrane integrity and structure (Miller 1984; Nishikawa et al. 1984). Digitonin causes cell lysis, forming a rigid and immobilizing complex with cholesterol in model membranes. The complexes strongly perturb the lipid bilayer and induce hemolysis. However, the mechanism of digitonin-cholesterol interaction and the nature of the resulting complex are not yet clearly understood (Takagi et al. 1982).

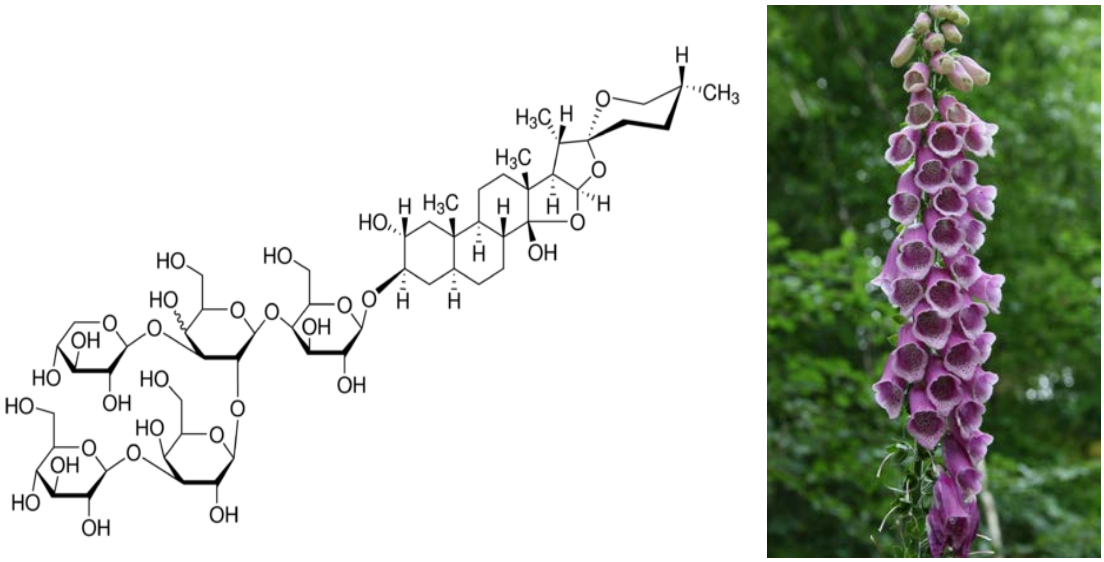

Fig 1.2. Digitonin (*left*) **from *Digitalis purpurea*** (*right*)

The chemical structure of digitonin was elucidated by mass spectrometry and ^{13}C NMR – its molecular mass is 1228. The digitonin aglycone, referred to as digitogenin, is bound to an unbranched chain consisting of five sugar units (Posthumus et al. 1978; Muhr et al. 1996). Digitonin specifically interacts with cholesterol. The structure of the digitonin-cholesterol complex has been determined by ^{13}C NMR. The steroid ring system with its 3β-hydroxyl group is essential for digitonin to form a complex with cholesterol with an equimolar stoichiometry (Takagi et al. 1982). The effect of the digitonin-cholesterol on cell membranes has been observed in different model membranes, such as liposomes and lipid monolayers. In fact, in the absence of cholesterol, digitonin neither penetrates nor affects the membranes. In membranes containing cholesterol, digitonin increases the surface pressure in penetrated lipid monolayers at the air-water interface and induces pore formation (Gögelein and Hüby 1984; Nishikawa et al. 1984). The morphology of digitonin-cholesterol complexes in the bilayer membrane is hemitubular and the structure is not correlated with the asymmetric structure of cholesterol across the membrane (Miller 1984).

Digitonin has been widely used to induce and modify membrane permeability of lipid membranes from various sources. Digitonin permeabilizes the plasma membrane allowing ions, ATP, and proteins to gain more access to intracellular spaces (Wilson and Kirshner 1983; Peppers and Holz 1986). Digitonin has also been shown to modify the permeability of mitochondrial membranes making the outer membrane lose its integrity and leading to a massive premature release of cytochrome *c* from mitochondria, which eventually induces cell

death (Duan et al. 2003; Adachi et al. 1997). Digitonin affects the cell membranes of the parasite *Trypanosoma cruzi* (Vercesi et al. 1991). Digitonin increases cell passage of a wide range of drugs, peptides and other secondary metabolites. Nontoxic concentrations of digitonin can considerably enhance drug efficacy. Thus, the potency of digitonin in modifying cell membranes is being widely used to increase the amount of drug absorption into the cytoplasm and is being used to enhance the toxicity of cisplatin (Tanaka et al. 2001; Jekunen et al. 1993) and doxorubicin (Chen et al. 2007) in cancer treatment. Digitonin has been shown to increase the uptake of peptides and (Weng et al. 2012a) increase toxicity of various plant secondary metabolites, even in multidrug-resistant cancer cells (Eid et al. 2012b; Chen et al. 2007; Eid et al. 2013; Versantvoort et al. 1992; Weng et al. 2012b; Thakur et al. 2012). However, the molecular mechanism of digitonin action in modifying membrane permeability and in supporting other drugs to enter into the cells is still not fully understood.

1.1.2 Quillaja saponin – a triterpenoid saponin

Quillaja saponin is obtained from the evergreen soap bark tree, *Quillaja saponaria* (family Rosaceae) (Fig. 1.3), which is a native to Chile, Peru, and Bolivia. The saponin content of quillaja bark is around 20% by weight as by the non-refined, commercial-grade quillaja extract (San Martín and Briones 1999). It actually is a mixture of up to 70 different saponins, the main constituent being a bidesmoside of quillaic acid (Bankefors et al. 2010). The white powder resulting from the extract of quillaja bark provokes sneezing. Its first taste is sweet, then bitter at the end. Quillaja saponin is soluble in water and produces stable foam at high concentrations. The name quillaja is derived from the Chilean *quillean* = to wash; for centuries quillaja bark has been used by natives as shampoo and soap (van Setten and van de Werken 1996). Quillaja saponin has been successfully exploited in a wide variety of commercial applications in foods, agricultural products, cosmetics, and pharmaceuticals. Based on its natural surfactant properties, quillaja saponin has been used as foaming and emulsifying agents in beverages and foods and as a wetting and cleaning agent in lipstick and shampoo. Based on its ability to form micelles, quillaja saponin has been used to produce low-cholesterol foods (San Martín and Briones 1999). Quillaja saponin extract from soapbark has been approved as an ingredient in the food and beverages industry by the United States FDA (Food and Drug Association) under Title 21 CFR 172-510, FEMA (Flavor and Extract Manufacturers Association) number 2973 and has also been approved by the European Union under code E 999 for the same purpose.

Quillaja saponin exerts various biological and pharmacological activities with a long history of use by Andean peoples as medicinal herbs for treating coughs, bronchitis and other diseases of the upper respiratory tract, antirheumatic drug and externally used to treat skin problems such as eczema (Wink et al. 2008). Recent research indicates that quillaja saponin has a great potency in activating the mammalian immune system, leading to a significant interest for applying it as a vaccine adjuvant. The chromatographic fractions and derivatives of quillaja saponin have shown strong adjuvant properties and are variously being employed as immune-stimulating complexes (ISCOMs). The derivative QS-21 is a particularly potent ISCOM with a capacity of stimulating both the Th1 immune response and producing cytotoxic T lymphocytes (CTL) against exogenous antigens, making them an ideal candidate for use in subunit vaccines and vaccines directed against intracellular pathogens, e.g., therapeutic cancer vaccines (Sun et al. 2009a; Kensil et al. 1991; Wu et al. 1992; Marciani et al. 2000; Ragupathi et al. 2011). Application of QS-21 in cancer treatment showed promising results in the clinical trial phase for different cancer types. For instance, immunizing with sTn(c)-KLH plus QS-21 and with mucin-1 keyhole limpet hemocyanin plus QS-21 in high-risk breast cancer patients boosts the vaccination effect (Gilewski et al. 2007; Gilewski et al. 2000). Application of QS-21 allows a reduction of the antigen dose applied to the patients (Evans et al. 2001). The chromatographic fraction of quillaja saponin can also act as an anticancer agent and also could increase the toxicity of other secondary metabolites in killing cancer cells (Herrmann and Wink 2011). The use of mixtures of quillaja saponin in medical applications has become common nowadays. The molecular mechanism of the interactions and activity of quillaja saponin in inducing cell membrane permeability has not been completely understood.

The notable biological and pharmacological activity of quillaja saponin results from its unique chemical structure. The basic component is quillaic acid, a triterpene of predominantly 30 carbon atoms substituted with oligosaccharides attached at C-3 and C-28. The oligosaccharide at C-3 is almost always a branched trisaccharide composed of either β-D-Glc*p*A bearing β-D-Gal*p* at its O-2 position or β-D-Xyl*p* or α-L-Rha*p* at its O-3. Many quillaic acid-based saponins have been isolated from the quillaja saponin mixture differing only in that the C-3 oligosaccharide contains either Xyl*p* or Rha*p*. The common backbone of the C-28 oligosaccharide is a disaccharide, α-L-Rha*p*-(1→2)-β-D-Fuc*p*, which is extended in most compounds by different sugar residues. The fucose O-3 and O-4 can be acylated by either an acetyl or a fatty acyl group (Fig. 1.3). Until now, more than 70 different structures of saponins from *Quillaja saponaria* have been reported and potentially many more minor components await to be discovered (Kite et al. 2004; Bankefors et al. 2011; Bankefors et al. 2010).

Commercial quillaja saponin extract (Carl Roth, Sigma, a.o.) is a heterogeneous mixture of various aglycones with different sugar moieties, the main aglycone being quillaic acid. The identity and quality control of the commercial quillaja saponin have been evaluated only by comparative HPLC fingerprints. Precise quantification of the individual contained substances of these extracts has not been performed, as individual components of the extracts are not marketed as pure substances (San Martín and Briones 2000; Thalhamer and Himmelsbach 2014).

The commercial quillaja saponin extract has mostly been considered and used as being a "**triterpenoid bidemosidic saponin"** in respect to the majority of substances contained therein (Bachran et al. 2006; Wojciechowski et al. 2014a; Gilabert-Oriol et al. 2013) and as supported by previous mass spectra from several studies (Nord and Kenne 1999; Guo et al. 1998; Kite et al. 2004; Bankefors et al. 2010; Wang et al. 2008; van Setten and van de Werken 1996)[1]. A commonly used fraction of the quillaja saponin extract employed in vaccine adjuvant field is Quil A, which contains QS-21, a triterpenoid bidesmosidic saponin ($C_{92}H_{148}O_{46}$; M_W 1988.9) (Kirk et al. 2004).

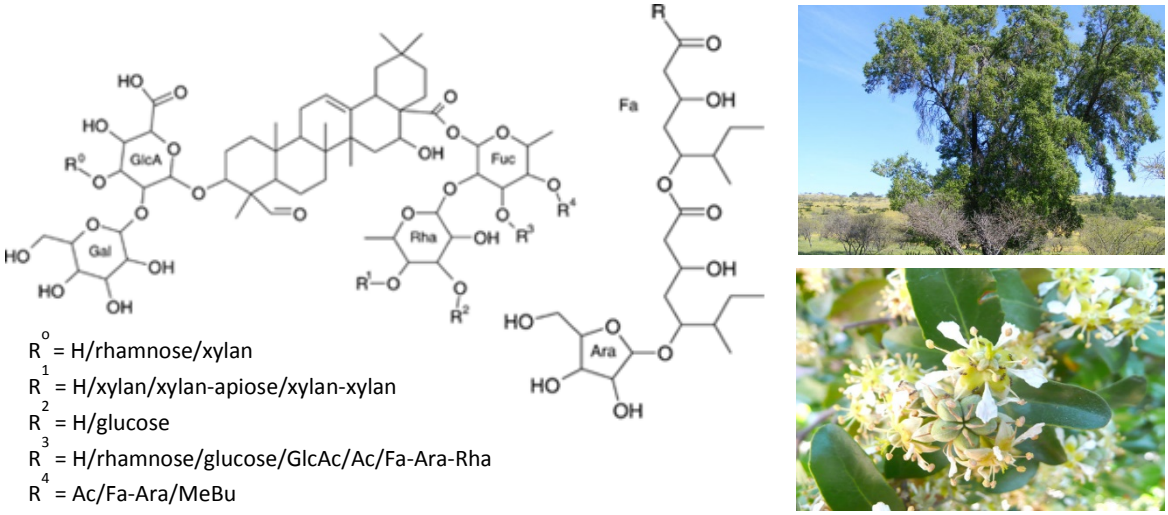

Fig 1.3. Quillaja saponin (*left*) **from *Quillaja saponaria*** (plant and flowers, *right*) (Bankefors et al. 2011; Flores-Toro and Amigo 2013)

[1] At a later stage in this Ph.D. project, we questioned whether the effects of the employed commercial "quillaja saponin" were actually attributable to the bidesmosidic saponins and reanalyzed our MS spectra to find that it in deed contained around 5% monodesmosides (see Results, p. 75). This finding is relevant for explaining the results and the according proposed mode of action as by the biophysical measurements performed by the author (see Discussion, p. 110).

The surfactant properties of quillaja saponin were investigated by Mitra and Dungan (1997). Quillaja saponin forms aggregates into micelles at concentrations above the critical micelle concentration (CMC) which is in the range of 0.5 to 0.8 g/l at 298 K. Below the CMC, quillaja saponin forms a saturated interfacial layer. The CMC value will increase along with elevated temperature and pH while increased concentrations of salt decrease the CMC. An increase of temperature decreases the intrinsic viscosity, suggesting substantial dehydration of the micelles at higher temperature (Mitra and Dungan 1997). A recent report showed that quillaja saponin occupies an area per molecule close to 1 nm^2. Based on measurements of surface tension isotherm and comparing with molecular dimensions, one can deduce that the hydrophobic triterpenoid rings of the saponin molecules lie parallel to the air-water interface, with the hydrophilic glycoside tails protruding into the aqueous phase. Upon small deformation, the saponin adsorption layers exhibit a very high surface dilatational elasticity (280 ± 30 mN/m), a much lower shear elasticity (26 ± 15 mN/m), and a negligible true dilatational surface viscosity (Stanimirova et al. 2011). Both authors mention that different quillaja saponin fractions from different commercial sources yield results that differ to a certain extent.

1.2 Saponins – biological and pharmacological activities

The main biological functions of saponins are still not fully understood. In plants, they play a role in defense (Francis et al. 2002). Many saponins from different plant extracts have been shown to be toxic to various types of organisms, from Gram-negative and Gram-positive bacteria (Oyekunle et al. 2006; Sparg et al. 2004; Avato et al. 2006) to different classes of yeasts, like *Candida albicans, Candida glabrata, Candida parapsilosis, Candida tropicalis*, and *Cryptococcus neoformans* (Yang et al. 2006; Zhang et al. 2006; Coleman et al. 2010), they are antimolluscicidal (Ekabo et al. 1996; Woldemichael and Wink 2001), act against insects (De Geyter et al. 2007; Chen 2008) and various parasites like trypanosomes and *Leishmania donovani* (Santos et al. 1997; Wink 2012), are antiviral, as shown for herpes simplex type 1 (HSV-1) and HIV (Sparg et al. 2004; Kinjo et al. 2000; Yang et al. 1999; Simões et al. 1999; Ikeda et al. 2005), and are poisonous to fish (Francis et al. 2002) and mammals (Francis et al. 2002; Sparg et al. 2004). Saponins affect various metabolic pathways in animal systems; for instance, saponins increase the dietary uptake of nonabsorbed substances by increasing the permeability of intestinal mucosal cells (Johnson et al. 1986; Sparg et al. 2004). Saponins accelerate cholesterol metabolism in the liver causing a drop of the cholesterol level in the blood serum (Stark and Madar 1993; Sparg et al. 2004). Saponins have the ability to act as

adjuvants to stimulate the immune system and enhance antibody production, one of the more interesting effects of saponins (Song and Hu 2009; Sparg et al. 2004).

Saponins are key ingredients in traditional Chinese medicines (TCM), together with polyphenols. For example, saponins from ginseng root (*Panax ginseng*) have been used in various pharmacological approaches worldwide (Park et al. 2005; Sparg et al. 2004). In mammalian cells, saponins affect various pathways at the molecular level, providing different interesting pharmacological activities: anticancer (Lacaille-Dubois and Wagner 1996; Podolak et al. 2010), anti-inflammatory (Li and Chu 1999), antiallergic (Akagi et al. 1997), immunomodulating (Song and Hu 2009), antihepatotoxic (Hikino et al. 1985), antidiabetic (Yang et al. 2010), cardiovascular (Somova et al. 2003), acting on the central nervous (Matsuda et al. 1999) and endocrine systems, and other miscellaneous effects (Lacaille-Dubois and Wagner 1996).

In analogy to the case of glucosinolates, Wink et al. have proposed that bidesmosidic saponins are stored in vacuoles that are cleaved by glycosidases upon wounding of the plant, yielding cytotoxic monodesmosides; thus, the stored bidesmosides, as biologically and pharmacologically relatively inactive substances, may function as “prodrugs” for the production of highly toxic monodesmosides for the purpose of a damage-induced mechanism of defense of the organism (Wink and Schimmer 2010; Wink and van Wyk 2008).

1.2.1 Saponins act against cancer cells

A large number of saponins with different chemical structures have been isolated from nature. Variations of the aglycone structure and different combinations with sugar molecules make saponins a group of highly variable compounds, each substance showing specific properties and biological activities. At the molecular level, saponins act by affecting membranes, various biochemical pathways, cellular organelles and cellular signals. The molecular activities of saponins have mostly been observed in cancer cell systems, where cytotoxicity has been found to be the dominant effect. Within the last decade, their cytotoxicity on different cancer cell lines has become one of the main tools in elucidating structure-activity relationships (SAR). The cytotoxicity of most saponins is generally lower than that of such reference compounds as etoposide, paclitaxel, doxorubicin, or cisplatin; this applies to both types, triterpenoid and steroid saponins (Podolak et al. 2010).

Saponins induce cell death by different means via the extrinsic pathway, which affects the stability of the plasma membrane and inhibits drug efflux, and via the intrinsic pathway, which induces different types of cell stress, affects cellular signals resulting in DNA damage,

disrupting the cell cycle, causing detachment from the cellular matrix, hypoxia, and loss of cell survival factors. The intrinsic pathway involves the release of proapoptotic proteins that activate the caspase enzyme from mitochondria but also depends on the balance between pro- and anti-apoptotic proteins from the Bcl-2 superfamily (Xu et al. 2009; Podolak et al. 2010). An overview of the molecular activities of saponins is displayed in Fig. 1.4 (Bachran et al. 2008; Podolak et al. 2010; Fuchs et al. 2009).

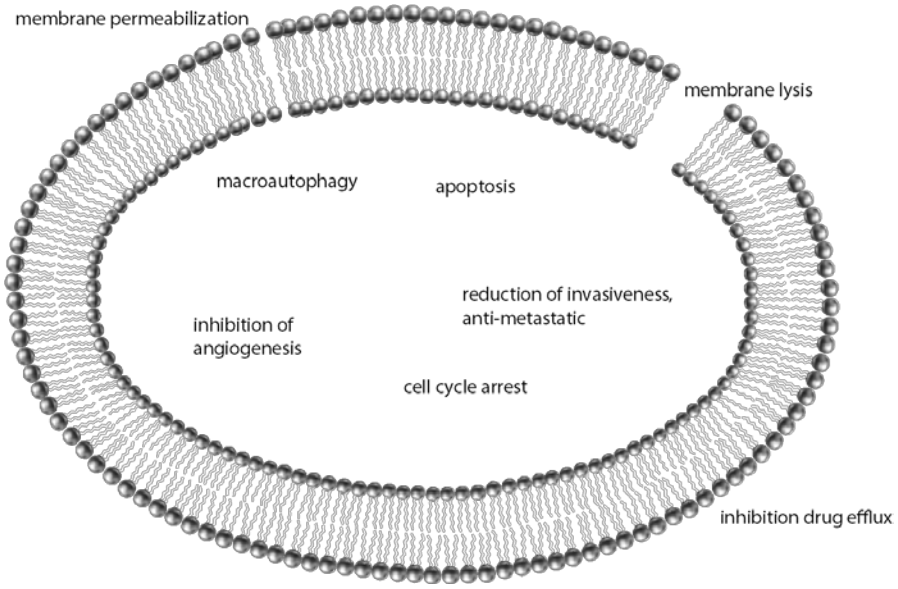

Fig. 1.4. Cellular effects of saponins. The different molecular pathways contributing to the anti-tumorigenic properties of various saponins. Note that a number of pathways are observed only for certain cell lines and certain saponins (adapted from Bachran et al. 2008; Podolak et al. 2010; Fuchs et al. 2009).

One individual saponin can target several molecular pathways while inducing cell death. For example, saikosaponins, a group of triterpenoid saponins from *Bupleurum* species, exert their effect of inducing cell death in several ways. Saikosaponin-A inhibits cell growth of HepG2 hepatoma cells by upregulating gene expression of the cyclin-dependent kinase inhibitors p-15^{INK4b} and p-16^{INK4a}, both specific inhibitors of cyclin-dependent kinase 4/6 (Wu and Hsu 2001; Wen-Sheng 2003). It inhibits the proliferation of MDA-MB-231 and MCF-7 breast cancer cell lines in a dose-dependent manner, however by affecting different apoptosis pathways. In MDA-MB-231 cells, apoptosis is independent of the P53/p21 pathway and is accompanied by an increased ratio of Bax to Bcl-2 family, higher c-myc levels, and activation of caspase-3. Apoptosis in MCF-7 is initiated by Bcl-2 and involves the p53/p21-dependent pathway and is accompanied by an increased level of c-myc (Chen et al. 2003). It also acts as an immunosuppressive it potently suppresses Con A-stimulated IL-2, IFN-γ, and TNF-α, also causing G0/G1 arrest of activated T cells through downregulating of CDK6 and cyclin D3 and upregulating p27^{kip} (Sun et al. 2009b).

Small modifications of the chemical structure of saponins affect their mechanism of action. For example, varying the sugar molecule at C-3 of the triterpene aglycone of saikosaponin leads to different molecular activities (Ashour and Wink 2011). The apoptosis mechanism induced by saikosaponin-D is different from that of saikosaponin-A, where the apoptotic effect of saikosaponin-D may be partly mediated by increases in the c-myc and p53 mRNA level accompanied by a decrease in the Bcl-2 mRNA level (Hsu et al. 2000). Saikosaponin-C shows no correlation with cell growth inhibition but induces endothelial cell migration, capillary tube formation, and angiogenesis by activating matrix metalloproteinase-2 (MMP-2), vascular endothelial growth factor (VEGF), and the p42/p44 mitogen-activated protein kinase (MAPK, ERK) (Shyu et al. 2004).

1.2.2 Saponins act on membranes

Saponins strongly affect cell membranes due to their amphiphilic properties. In particular, they cause rupturing of red blood cells. This hemolytic activity has been used to detect the presence of saponins in plant extracts and drugs. Chiefly RBCs have been used to investigate the mechanism of action of saponins on membranes (Baumann et al. 2000). The first visualization of the associated effects was reported by Dourmashkin et al. (1962) in a study on Rous sarcoma virus inactivated by “saponin” (referring to Saponin pure white/Saponinum album, Merck, a *Gypsophila* extract) (Weng et al. 2011). High concentrations of “saponin” damages the outer membrane of the virus, chicken liver cells, as well as human and guinea pig erythrocytes, creating holes (pits) with a diameter of 85 Å. The authors observed that membrane cholesterol plays a role in saponin activity. They also found that digitonin and “saponin” acted differently on membranes: “saponin” created holes (pits), while digitonin disrupted the membranes without forming holes (pits). Their experiments also confirmed that both “saponin” and digitonin specifically interact with membrane cholesterol (Dourmashkin et al. 1962).

The effect of pore formation in the membrane by saponins has become a point of interest. This effect is clearly related to the presence of cholesterol. “Saponin” forms a complex with cholesterol causing the removal of cholesterol from the membranes and thus leading to pore formation. The interaction of cholesterol with the lipophilic heads of saponin occurs at a 1 : 1 molar ratio; a ring-shaped construct is formed by twenty “saponin” molecules in a circular arrangement with a distinguishable space between each lipophilic headgroup. This was the first suggested model of interaction between “saponin” and membrane cholesterol (Bangham et al. 1963; Glauert et al. 1962) and a starting point for elucidating the basic molecular mechanism of activity of saponins in membranes. Results from several studies point to various

factors affecting the activity of saponins in perturbing membranes, such as the influence of membrane composition, especially those containing sterols (Gögelein and Hüby 1984; Armah et al. 1999; Keukens et al. 1992; Nishikawa et al. 1984; Rosenqvist et al. 1980; Stine et al. 2006; Walker et al. 2008; Böttger and Melzig 2013), different type of saponin aglycone resulting in different degrees of toxicity (Gauthier et al. 2011; Oda et al. 2000; Takechi and Wakayama 2003; Voutquenne et al. 2002; Chwalek et al. 2006; Wang et al. 2007b), the number of sugar chains attached to the aglycone (monodesmosidic or bidesmosidic) (Woldemichael and Wink 2001; Voutquenne et al. 2002), the length of the sugar chains as well as the types and linkage variants of the incorporated sugar units that affect saponin activity in the membranes (Armah et al. 1999; Chwalek et al. 2006; Nishikawa et al. 1984; Takechi and Wakayama 2003). However, due to the enormous variability of chemical structures of saponins and different experimental setups, conflicting conclusions have not allowed for a full understanding of structure-activity relationships of saponins till now.

1.2.3 Models of saponin action on membranes

Studies on the mechanisms of action of saponins on membranes have been conducted for well over 50 years and several models of action have been suggested. The effects of saponins on membranes are strongly related to the presence of cholesterol. Various methods and techniques have been used to elucidate the mechanisms of interaction of saponins with membranes. Erythrocytes have frequently been used as a natural membrane model and several other artificial membrane models like liposomes, supported lipid bilayers, and membrane monolayers have also been employed to understand the action of saponin.

The different proposed models of interaction of saponins with membranes are specific to the particular type of investigated saponin. The type of aglycone and number of sugar side chains strongly affects the mode of action. The most prominent models of saponin action on membranes are shortly summarized below.

1.2.3.1 Model of Doursmashkin-Glauert (1962)

The first model of action of saponins on membranes was suggested by Glauert et al. (1962; see also Bangham et al. 1963), based on experiments by Doursmashkin et al. (1962). Their electron microscopic observations indicated that “saponin” disrupts cell membranes of the Rous sarcoma virus, erythrocytes, and other mammalian cells forming pores with a hexagonal pattern. The hexagonal pores were reported to form by spontaneous interaction of “saponin” with cholesterol. Complexes between “saponin” and cholesterol in the membrane are

followed by association of these complexes into “two-dimensional micellar-type structures” within the membrane.

Based on close inspection of the electron micrographs of the Rous sarcoma virus and erythrocyte membranes after “saponin” treatment they suggested that the pores are constructed by twenty saponin molecules in a circular arrangement with a distinguishable space between each lipophilic headgroup forming a ring-like structure having a central hydrophilic pore, approximately 90 Å in diameter, that contain the sugar moieties of the saponin molecules. The interaction of the cholesterol molecules with the saponin aglycone (lipophilic headgroup) occurs at a 1 : 1 ratio on the outside of the circular structure (Fig. 1.5) (Glauert et al. 1962; Dourmashkin et al. 1962; Bangham et al. 1963).

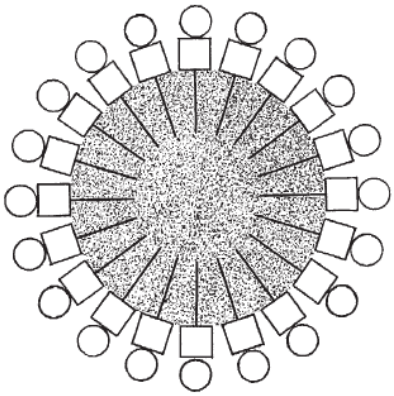

Fig. 1.5. Hypothetical micellar-type arrangement of saponin molecules with cholesterol, producing a hole (pit/pore) in the membrane; ○ cholesterol, □ "saponin" (Glauert et al. 1962).

1.2.3.2 Model of Nishikawa (1984)

Nishikawa et al. (1984) suggested a mechanism of interaction of saponins with membrane sterols that induces membrane perturbation based the observed induction of hemolysis and liposomal damage by digitonin (steroid saponin). The role of the sugar moieties in digitonin was also studied using various digitonin analogs and desglucodigitonin.

The important role of membrane cholesterol in digitonin activity was confirmed. The interaction and activity of digitonin and their analogs in the liposomal membrane completely depends on the presence of cholesterol. The ratio of digitonin bound to cholesterol in the liposomal membrane was close to 1 : 1. Digitonin-cholesterol complexes caused membrane lateral-phase separation which formed domains rich in “cholesterol-digitonin” resulting in membrane damage. The sugar chain is involved in the interaction of digitonin with cholesterol. Removal of sugar moieties from digitonin caused loss of hemolytic activity, thus no longer being able to damage liposomal membranes.

Their proposed mechanism of interaction of digitonin molecules with the membrane bilayer begins with digitonin accessing and binding with cholesterol in the membrane, then continuing with the formation of domains rich in “digitonin-cholesterol” complexes at a 1 : 1 ratio, increasing membrane permeability, and finally leading to membrane rupturing (Nishikawa et al. 1984).

1.2.3.3 Model of Keukens (1995)

From a series of observations on the activity of several glycoalkaloids in inducing membrane rupture, Keukens et al. (1995) suggested a molecular mechanism of membrane disruption by glycoalkaloids with cholesterol playing a key role as the binding target in the membrane. The interaction process of the glycoalkaloids with the membrane bilayer is shown in Fig. 1.6. The process begins with the insertion of the glycoalkaloid into the membrane surface (step 1), the aglycone part of the glycoalkaloid then reversibly binds to the membrane sterol at a ratio of 1 : 1 (step 2); when the glycoalkaloid-cholesterol complexes reach a certain density in the membrane (step 3), cooperative sugar-sugar interactions of the sugar chains of the glycoalkaloid initiate the formation of a stable irreversible matrix of glycoalkaloid-cholesterol complexes (step 4). Since the glycoalkaloid immobilizes cholesterol in the outer layer, cholesterol from the inner layer will probably flip to compensate for the “lost” cholesterol. During the formation of the matrix structure, the membrane layer will bud due to the fact that glycoalkaloid-cholesterol complexes with relatively large polar head groups do not have a cylindrical shape (step 5). The phospholipids in the inner layer of the membrane bilayer opposing the matrix get enclosed in the final structure during separation from the membrane and forming an internal purely phospholipid monolayer (step 6). The three-dimensional structure of the sugar chains leads to tubular structures which cause faster growth of the matrix in one direction.

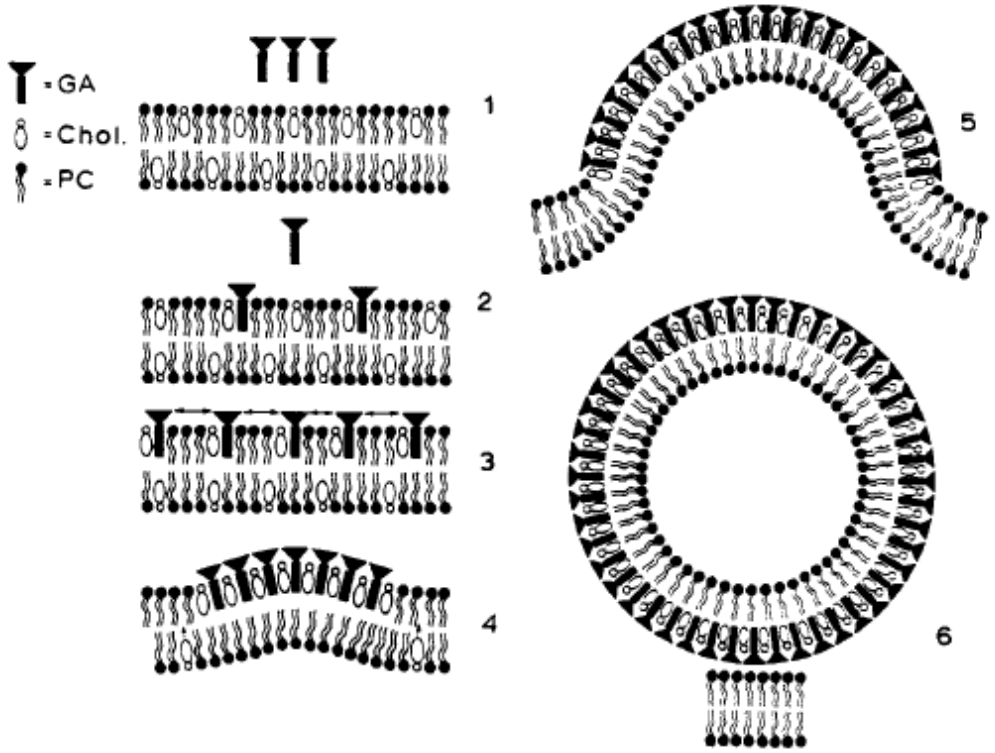

Fig. 1.6. Model of Keukens et al. (1995). Membrane disruption by glycoalkaloids (GA) – (**1**) GAs arriving at the membrane; (**2**) insertion of GAs into the membrane; (**3**) GAs bind to cholesterol; (**4**) irreversible formation of stable GA-Chol complexes by sugar-sugar interactions; (**5**) budding; (**6**) final tubular structure with GA-Chol layer on the outside and pure PC layer on the inside. GA = glycoalkaloid; Chol = cholesterol; PC = phosphatidylcholine.

1.2.3.4 Model of Armah (1999)

The triterpenoid saponin, avenacin A-1, was used to induce membrane permeability of artificial membranes, phospholipid monolayers, planar lipid bilayers, and liposomes providing new insights into the molecular mechanisms of interaction of saponins with membranes. Avenacin A-1 leads to pore formation in membranes. The mechanism of membrane pore formation by avenacin A-1 generally follows a similar route as the models of Nishikawa (Sect. 1.2.3.2) and Keukens (Sect. 1.2.3.3). The activity of avenacin A-1 in altering the lateral movement of the membrane bilayer strongly depends on the presence of cholesterol, even though it can insert into cholesterol-free membranes, while not inducing any changes in that case. The mechanism of interaction of avenacin-A1 with the membrane bilayer begins with the insertion of the aglycone portion into the membrane surface (step 1); it then binds to membrane cholesterol. The intact sugar chain of avenacin A-1 is required for reorganization of membrane cholesterol, which results in a reduction of the lateral diffusion coefficient (step 2). The final step is the formation of trans membrane pores causing an increase in membrane permeability. The mechanism by which this occurs is currently not understood. The authors

speculated that after avenacin A-1 and cholesterol form complexes, the free sugar chains of avenacin A-1 interact, causing aggregation in the avenacin A-1–cholesterol region. This may lead to rearrangement of the bilayer lipids and lead to pore formation (step 3) (Fig. 1.7). The role of the sugar chains of saponins is essential in the process of pore formation (Armah et al. 1999).

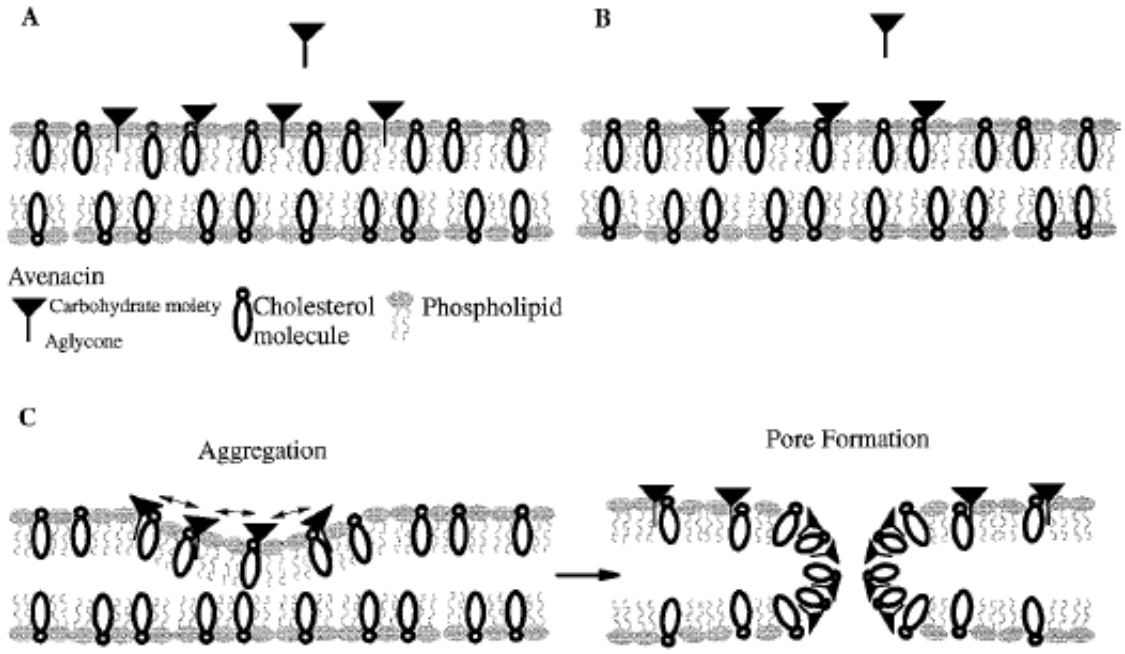

Fig. 1.7. Model of Armah et al. (1999). Pore formation by avenacin A-1. (**A**) insertion of saponin into the membrane; (**B**) saponin binds to cholesterol; (**C**) aggregation of saponin-cholesterol complexes leads to pore formation by membrane structure rearrangement.

1.2.3.5 Model of Lin and Wang (2010)

Lin and Wang (2010) presented a mechanical study on the hemolytic activity of the steroidal saponin, dioscin, using coarse-grained molecular dynamics (CGMD) simulations (Fig. 1.8). The dioscin-cholesterol complex is energetically more favorable than the cholesterol-cholesterol complex. The data supported previous experimental results on the essential role of cholesterol in membrane activity induced by saponins. The saponin appears to have two effects; firstly, the saponin penetrates and migrates to the lipid raft domain, the region enriched with cholesterol and sphingomyelin in the membrane, and then binds to cholesterol. This “abstraction” of cholesterol seizes the latter from interacting with sphingomyelin, which then causes disruption of the lipid raft microdomains. Secondly, the accumulation of saponin-cholesterol in the lipid raft microdomain will change membrane morphology because saponin molecules do not have the compact shape as other lipid-raft components. The accumulation of saponin-cholesterol at the lipid-raft domain causes severe curvature of the lipid bilayer, eventually leading to the lysis of erythrocyte membranes.

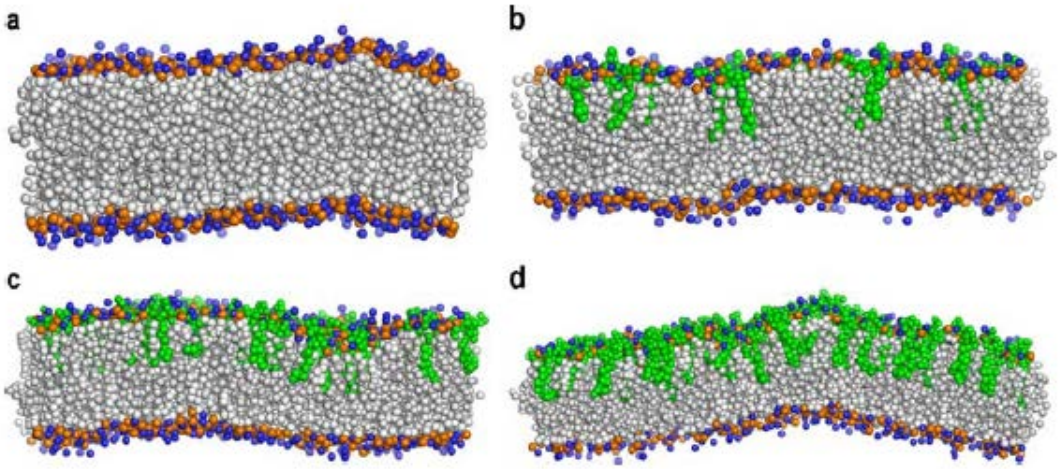

Fig. 1.8. Model of Lin and Wang (2010). Snapshots of CGMD simulations of the interaction of dioscin with the bilayer membrane. **(a)** Membrane bilayer without saponin; **(b)** penetration of saponin (*green*) into the membrane and binding to cholesterol; **(c)** membrane disruption caused by interaction of saponin with cholesterol; **(d)** accumulation of saponin-cholesterol at lipid raft domains (not shown) causes changes of membrane morphology (*blue*: cholesterol; *red*: phosphatidylcholine).

1.2.3.6 Model of Lorent (2013)

The latest interaction model of saponins with membranes has been proposed by Lorent et al. (2013, 2014) from investigations of two triterpenoid saponins, α-hederin (with two sugar moieties) and δ-hederin (with only one sugar moiety), that permeabilize the membranes of multi- and unilamellar vesicles. The molecular process leading to membrane permeability by hederins is linked to membrane curvature and is characterized by three steps; firstly, insertion of hederin into the external leaflet of the bilayer membrane which does not involve cholesterol; the interaction occurs between the negatively charged carboxyl function of the genin with the positively charged choline head group of the phospholipids. Secondly, after the initial stage, hederin binds to cholesterol. The formation of saponin-cholesterol disrupts the phospholipid/cholesterol matrix and changes the thermotropic characteristics of the membrane. The sugar moieties of hederin enhance the interaction of the saponin with cholesterol, shielding cholesterol from water, and preventing polar interactions between cholesterol and phospholipids. In a third step, α- and δ-hederin induce membrane curvature resulting in pore formation and budding. The membrane effect strongly depends on the sugar moieties of the saponin – α-hederin leads to pore formation, while δ-hederin only leads to budding (Lorent et al. 2013, 2014) (see Fig. 1.9).

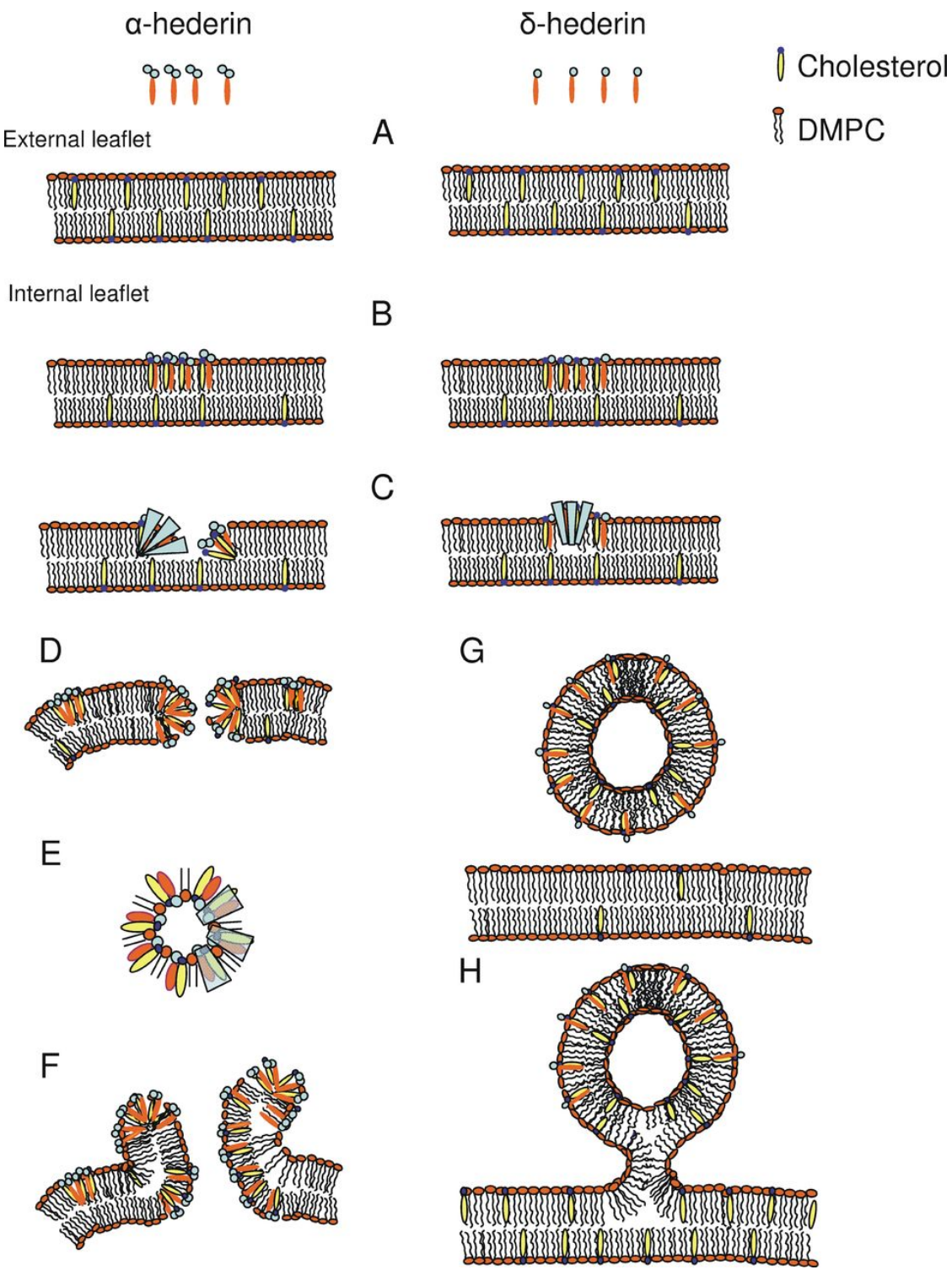

Fig. 1.9. Model of Lorent et al. (2013). Interaction of α-hederin and δ-hederin with GUVs. (**A**) Membrane bilayer; (**B**) insertion of saponin into the external leaflet of the bilayer membrane; (**C**) membrane damage; (**D**) pore formation (α-hederin); (**E**) slight negative curvature in the direction of the membrane plane; (**F**) inhomogeneous distribution of α-hederin causing rolled rims; (**G** and **H**) intermediate curvature of δ-hederin results in budding.

1.2.4 Saponins enhance the toxicity of other drugs

The natural amphiphilic properties of saponins give them the ability to reduce membrane permeability due to their interaction with other membrane amphiphilic molecules such as phospholipids and sterols. Interactions of saponins with membrane lipid components can reduce the surface tension and cause pore formation (Böttger et al. 2012). The membrane perforation effect of saponins is strongly related with their chemical structure especially the number of sugar moieties attached to the aglycone. Interaction of saponins with two sugar chains (bidesmosidic) with membrane cholesterol may cause pore formation (Gimpl et al. 1997). Therefore, the bidesmosidic saponins induce less hemolytic activity and membrane permeability than monodesmosidic saponins (Woldemichael and Wink 2001).

Formation of membrane pores by saponins is not specific or restricted to particular kinds of cells. The pore-forming effect of saponins is often used to render membranes more accessible to polar substances for enhancing drug efficacy. Many articles reported synergistic or additive effects of combined application of saponins with other antitumor drugs. This combination strategy offers improved options in cancer treatment. As an example, the cytotoxicity of the well-known cancer drug cisplatin has been synergistically increased by combining it with several saponins, such as the triterpenoid jenisseensoside saponins from campions (*Silene* spp.) (Gaidi et al. 2002) and saponins from *Panax notoginseng* (Yu et al. 2012; Zhang et al. 2013). Several triterpene saponins failed to increase the cytotoxicity of cisplatin, like the saponins from ox knee (*Achyranthes bidentata*) (Mitaine-Offer et al. 2001), the saponins from *Albizia adianthifolia* (Haddad et al. 2002), and the saponins from *Muraltia heisteria* (Elbandy et al. 2002). This shows that only certain saponins with specific structural features are able to enhance the cytotoxicity of cisplatin.

Ginsenosides are group of saponins obtained from ginseng plants (*Panax* spp.) and have been used frequently in combination with other chemotherapeutics to enhance their anticancer activity. Ginsenoside Rh2 synergistically supports the inhibitory effect of paclitaxel (Taxol™) in the prostate cancer cell model LNCaP (Xie et al. 2006). Ginsenoside Rg1, ginsenoside Rg3 and Rh1 significantly increased the toxicity of mitoxantrone and doxorubicin, which inhibit drug efflux, on drug-insensitive cell lines (Jin et al. 2006; Wang et al. 2006). Ginsenoside Rg3 increased effectiveness of cisplatin and docetaxel by inhibited NF-κB activity in prostate and colon cancer cells (Kim et al. 2009; Kim et al. 2010). A *Notoginseng* flower extract has enhanced the antiproliferation effect of 5-fluorouracil (5-FU) in colorectal cancer cells and thus reducing the applicable effective dose of 5-FU in cancer treatment (Wang et al. 2007a).

Digitonin is a steroid saponin obtained from *Digitalis purpurea* and has been used variously to improve the toxicity of many substances by increasing their passage through the cell membrane. Digitonin increases the cytotoxicity of epigallocatechin gallate (EGCG) against sporozoites but shows an additive effect on inhibiting sporozoite motility by increasing the permeability of *Plasmodium* sporozoite membranes (Hellmann et al. 2010). Digitonin synergistically increases the cytotoxicity of cisplatin by permeabilizing the plasma membrane of ovarian and lung cancer cell lines (Tanaka et al. 2001; Jekunen et al. 1993). Digitonin increases the uptake of carboplatin by liver tumor cells after intra-arterial administration with a resulting increase of cytotoxicity (Lindnér et al. 1997). In the combination with secondary metabolites, digitonin synergistically enhances the toxicity of several phytochemicals (phenolics, terpenoids, and alkaloids) towards sensitive cancer cell lines and interestingly also multidrug-resistant (MDR) cells containing high amounts of P-glycoprotein in the membrane because certain steroid saponin may also be natural substrates for P-glycoproteins (Herrmann and Wink 2011; Eid et al. 2012a; Park et al. 1996; Zhou et al. 2004). Interestingly, digitonin has led to enhanced toxicity even in combination with more than two secondary metabolites, administered simultaneously (Eid et al. 2012b).

The ability of saponins to facilitate nontargeted drug molecules to pass through the cell membrane may result in increased side effects. The combination of saponins with highly specific targeted drugs may constitute an approach to reducing these side effects. Saponinum album (or simply “saponin” Merck) (Weng et al. 2011), a triterpene saponin extract from *Gypsophila paniculata*, dramatically increases the toxicity of saporin, a ribosome inactivating protein (RIP), which specifically is linked to epidermal growth factor (EGF) via a cleavable molecular adapter forming a chimeric toxin. The application of nontoxic concentrations of Saponinum album enhanced the cytotoxicity of the chimeric toxin by 3500-fold to more than 100,000-fold, depending on the cell line. In order to ascertain whether this significant enhancing effect on drug toxicity is only restricted to Saponinum album or can also be found with other saponins, different types of saponins with different structures were tested. Analysis of the enhancing effect of different structures of saponins has shown that bidesmosidic triterpenoid saponins with an aldehyde function at the C-4 position, like Saponinum album and quillaja saponin, synergistically increased the cytotoxicity of the chimeric toxin. Quillaja saponin enhanced the cytotoxicity of the toxin in a similar way with respect to both non-targeted and targeted cells, while Saponinum album only increased the cytotoxicity towards targeted cells. The exact mechanism of toxin enhancement by saponins remains unclear to date (Fuchs et al. 2009; Bachran et al. 2006, 2008, 2009).

1.3 Drug interactions with lipid membranes

Understanding the mode of action at the molecular level of the interaction of substances or drugs with the cell membrane is of primary importance in pharmacological science. Many substances with a wide range of biological and pharmacological applications and with various chemical structures and possessing diverse properties potentially modulate different activities at the membranes, such as crossing or binding to components of the lipid membrane. Biological membranes are very complex and vary tremendously in respect to their composition. They form a carefully balanced environment and any changes that are caused by the interaction with other substances will affect the overall function and integrity of the membranes. However, it is quite difficult to investigate and elucidate the molecular mechanisms of drug interactions with biological membranes due to their high degree of complexity (Seddon et al. 2009; Bernsdorff et al. 1999; Lucio et al. 2010; Bourgaux and Couvreur 2014).

To investigate the molecular activity of substances on the membrane system, it is necessary to understand the critical aspects of membrane structure and its properties. Biological membranes are dynamic structures composed of a diverse set of lipid components such as phospholipids, glycolipids, sterols, and proteins. The fundamental structural component of all biological membranes is the lipid bilayer which is made up of two opposing layers of lipid molecules, where the hydrophilic polar head is directed outwards towards the aqueous phase and lipophilic tails pointing at the interior of the two layers. The hydrophobic interior of lipid bilayers acts as a barrier to limit the movement of polar molecules and ions in or out from the cell. The membrane's structural integrity protects the cell against various adverse external factors, in particular against toxic chemical compounds and xenobiotics. In the more general sense, the regulation and controlling of molecule movement through the cell membrane is vital in maintaining cell functions (Yeagle 2012; Seddon et al. 2009; Lucio et al. 2010). The membrane's role is not limited only to cell compartments, to protect the cell, and to transport molecules, but goes well beyond those functions as by the presence and functions of the diverse constituent membrane proteins. These are involved in various cell functions such as cell signaling (which allows cells to communicate, receive signals, and to sense their environment); to transport molecules and ions across the membranes; providing cell adhesion which allows cells to interact with each other; and the activity and properties of membrane-bound enzymes which are involved in various biochemical pathways and also implicated in a number of disease pathologies. Membrane proteins have become important targets in drug discovery (Lucio et al. 2010; Seydel and Wiese 2009).

1.4 Cholesterol and its functions in membranes

Another essential substance of eukaryotic membranes is cholesterol, a weakly amphiphilic molecule. Cholesterol plays a crucial role in membrane organization, modulating cell membrane dynamics, and affecting the functions of membrane proteins through three major molecular mechanisms: *i)* regulating the function of membrane proteins through specific interactions of sterol-proteins inside the membranes; *ii)* regulating the internal properties of the lipid bilayer of the cell membranes; and *iii)* modifying the lateral distribution of cell membrane components (Yeagle 2012). The relative amounts of cholesterol and phospholipids can change membrane fluidity and affect cell membrane curvature (Bacia et al. 2005). Cholesterol is distributed inhomogeneously in the domains of biological and artificial membranes and interacts with a subset of membrane lipids and proteins (Rukmini et al. 2001; McMullen and McElhaney 1996; Gimpl et al. 1997). Cholesterol can move between the two leaflets of a bilayer membrane, in a flip-flop manner. The cholesterol flip-flop process across lipid bilayers occurs on a very short time scale of <1 s in human erythrocytes (Steck et al. 2002; Kamp et al. 1995; Lange et al. 1981). Rapid cholesterol flip-flop has important implications on cellular and global cholesterol trafficking and also in maintaining an asymmetric distribution of cholesterol in the membrane (Hamilton 2003; Bennett et al. 2009). Cholesterol also can move and be distributed between two different and physically separate lipid vesicles through two general mechanism; *i)* between two close but separate membranes via the aqueous phase; desorption of cholesterol from the donor bilayer into the aqueous phase is activated by an increasing energy barrier in a slow process continued with collision of cholesterol with acceptor vesicles in a stochastic process (McLean and Phillips 1981); *ii)* via a water-soluble cholesterol intermediate at a distance between separate vesicle membranes even though the process is slower than the first mechanism (Yokoyama 2000; Backer and Dawidowicz 1981; Yeagle 2012).

Association of cholesterol with glycosphingolipids and protein receptors forms microdomains termed lipid rafts (Brown and London 1998). Lipid rafts are important elements in cell membrane structure, homeostasis, and most importantly in signal transduction. Lipid rafts are more ordered and tightly packed than the other lipid components and can freely float in the bilayer membrane. In general, rafts recruit proteins to new micro-environments where the phosphorylation state can be modified by local kinases and phosphatases resulting in downstream signaling (Lingwood and Simons 2010; Simons and Toomre 2000; Rajendran and Simons 2005).

Another effect of cholesterol in the membranes is in modulating membrane permeability. Cholesterol causes ordering of the lipid bilayer, repairing disorder by *trans-gauche* isomerization and thus reducing bilayer permeability. Cholesterol modulates membrane permeability by two different mechanism; *i)* by changing the electrical potential difference across the membrane-solution interface, resulting in change of the partition of charged species in the membrane; *ii)* by changing the fluidity of the interior of the bilayer membrane which affects the rate of ionic transfer and the chemical partitioning of the solute within the membrane (Szabo 1974; Papahadjopoulos et al. 1973; Parisio et al. 2013; Yeagle 2012; Ohvo-Rekilä et al. 2002).

1.5 Effects of drugs on membranes, and of membranes on drugs

Drugs can affect cell membranes in many different ways, directly or indirectly, e.g., by changing the conformation of acyl groups (*trans-gauche*), increasing the membrane surface (curvature), changing the phase separation, leading to domain formation (micro-heterogeneity), and changing the membrane thickness. They thus can lead to cell membrane disruption, increase membrane permeability, and affect membrane fluidity. All these effects are caused by the interaction between drugs and lipid membrane components like phospholipids and sterols. Numerous anesthetic drugs either in the gaseous form, like halothane and methoxyflurane, or aqueous form, like chlorpromazine and propranolol, are able to cause disordering of membranes (Goldstein 1984; Seydel and Wiese 2009). Certain anticancer drugs, like the platinum-containing agents vincristine and MRA-CN, and others such as doxorubicin, affect the electrical surface properties of membranes (Oakes et al. 1987). Other anticancer drugs affect membrane fluidity by interacting with phospholipids and cholesterol, e.g., doxorubicin has been shown to change membrane microviscosity (Marczak et al. 2006) and taxol reduces the rigidity of unsaturated lipids (Bernsdorff et al. 1999). Peptide toxins modulate membrane curvature. Cardiotoxin II from *Naja mossambicamos* strongly and specifically interacts with negatively charged phospholipids. The interaction strongly affects lipid acyl chain order and changes lipid membrane organization, modulating membrane curvature due to the different sizes of the hydrophobic and hydrophilic moieties of the peptide that leads to a rhombic shape and thus occupying large areas in the acyl chain region. Penetration of the peptide toxin mellitin into the acyl chain region also can cause surface membrane curvature (Batenburg and De Kruijff 1988).

Biological cell membranes can prevent polar drugs from passing the membrane or to become associated with them. There are several mechanisms of how membranes manage to

prevent drug action, such as limiting the rate of drug diffusion (Rhodes et al. 1985) or even completely preventing diffusion to the active site, which may cause drug resistance (Tannock et al. 2002; Gottesman 2002). Cancer cell membranes are able to develop a complex drug resistance system to prevent drugs from entering the cells, and this feature can become a serious problem in cancer treatment. Numerous multidrug-resistance mechanisms have developed in cancer cells, such as the increased drug efflux from cancer cells by ABC transporters with overexpression of P-glycoprotein transporter and reduction of drug uptake by modification or mutation of drug transporters on membrane surfaces (Gottesman 2002). Membranes may bind a drug and change the drug's conformation in such a way as to rendering it inactive (Center 1985; Luqmani 2004).

1.6 Model membranes for studying drug-membrane interactions

Identifying and elucidating the effect of drugs on cell membranes has become a major challenge in current research on biological membranes. A good understanding of drug action in membranes is indispensable for developing new drugs with high selectivity and toxic dose effectiveness and also for developing better drug-delivery systems. Such knowledge is indispensable to the pharmaceutical industry to avoid larger investments into effective drug discovery and development, which in turn increases a drug's economic value (Lucio et al. 2010). Model membranes provide free access in constructing and mimicking biological membranes and allow valuable insights into membrane structure, functions, and drug-membrane interactions. Various model membranes have been developed, from simple to sophisticated, with varying size, geometry, and composition and tailored with great precision to mimic natural membranes (Chan and Boxer 2007). At the same time, various techniques have been developed and applied to measure, characterize, and visualize membrane structures and activities for both natural and artificial membranes, such as spectroscopic and fluorescence techniques, X-ray scattering, calorimetry techniques, high-resolution nuclear magnetic resonance (NMR), microscopy, etc. (Seddon et al. 2009). Studies on drug-membrane interactions on **membrane monolayers** mostly have involved **micelles** and **phospholipid monolayers** as model membranes, while for studying **membrane bilayers** the most commonly employed model membranes are **liposomes** and **supported lipids**.

Micelles are spherical aggregates of amphiphilic molecules (surfactants) occurring as colloids in solution. They are formed when surfactants reach a certain concentration called the critical micelle concentration (CMC). Micelles have circular shapes and are composed of a single layer in which the nonpolar part of the molecules tend to form clusters, with the polar part pointing

to the outside (Tanford 1974). Micelles have been used extensively as biomimetic systems in membrane research and for elucidating structural features of drug-membrane interactions. Micelles provide several advantages in drug-membrane interaction studies, such as rapid molecular formation in aqueous solution which facilitates incorporation of drugs, allowing to characterize them by various bioanalytical techniques, like NMR, Fourier transform infrared spectroscopy (FTIR), and circular dichroism (CD). Based on the type of amphiphilic substance, it is possible to form micelles with different surface charge in order to study the electrostatic effects of drug binding to the membrane (Lucio et al. 2010). Micelles are also widely used for drug delivery across membranes (Lukyanov and Torchilin 2004; Kwon and Okano 1996).

Phospholipid monolayers (Langmuir monolayers) are model membranes that intend to mimic only one leaflet of the biological membrane. However, since the thermodynamic relationship between mono- and bilayer membranes is direct, monolayers are often used to study lipid/protein or lipid/drug interactions under specific conditions (Brockman 1999). Membrane monolayers are formed when the amphiphilic molecules arrange at the air-water interface where the hydrophilic part of the molecules (head group) point at the water phase and the hydrophobic part (tail group) towards the air. Physical characteristics of the monolayer system such as surface pressure, surface area, and number of molecules can be measured. Association or penetration of the membrane monolayer by drugs changes its thermodynamic properties. Membrane monolayers can also be used to visualize the change of lipid morphology at the air-water interface using atomic fluorescence microscopy (AFM), Brewster angle microscopy (BAM), and cryogenic scanning and transmission electron microscopy (cryo-SEM and cryo-TEM) (Wu et al. 2006; Seitz et al. 2011; Lucio et al. 2010)

Liposomes are vesicular lipid bilayers encapsulating small amounts of solutions. They share fundamental characteristics with the biological cell membrane and are relatively easy to make. Therefore they have been used extensively to characterize properties of lipid bilayers and investigate the effects of drugs on membranes. In principle, liposomes form spontaneously when dry lipid films swell in excess water or buffer (Bangham and Horne 1964; Lasic 1988) producing multilamellar vesicles. Recently, various mechanical dispersion methods have been developed to produce such vesicles. Unilamellar vesicles are made by repeated extrusion of multilamellar vesicles under moderate pressure (≤500 lb/in^2) through a polycarbonate filter, yielding unilamellar vesicles with uniform size (Hope et al. 1985). Applying a particular membrane polycarbonate pore size results in a specific size of unilamellar vesicle, e.g., a filter pore size of 100 nm will produce unilamellar vesicles ranging in diameter from 60–100 nm with trapped volumes in the region of 1–3 µl (Mayer et al. 1986). Liposomes can be classified

by their size and number of bilayers; this affects the amount of drug encapsulated inside the vesicle. Basically liposomes are classified into two groups; multilamellar vesicles and unilamellar vesicles. Unilamellar vesicles are further classified into giant unilamellar vesicles (GUVs) with diameters of 1–100 μm, large unilamellar vesicles (LUVs) with diameters from 100 nm to a few micrometers (μm), and small unilamellar vesicles (SUVs) with diameters of up to 100 nm (Akbarzadeh et al. 2013). Liposomes have variously been used in studying the effects of drugs on membranes and the effects of drug carriers through the membrane in anticancer drug research (Lasic 1998; Jesorka and Orwar 2008). Liposomes are being used as a model in studying the effect of drugs on membrane integrity and permeability. These effects can be measured by increasing the amount of fluorescence dye such as calcein, which is then released by leakage from the membrane vesicles. This leakage can be measured directly without separating the liposomes from solution (Patel et al. 2009; Katsu et al. 2007). Large and giant vesicles can be viewed by light microscopy.

Giant unilamellar vesicles (GUVs) are artificial, spherical bilayer membranes with diameters between 1–100 μm, the size range of most biological cells, and are useful models for mimicking biological processes at bilayer membranes (Morales-Penningston et al. 2010; Pott et al. 2008). GUVs are being extensively used in reconstituting membrane components for studying lipid domain formation and the physicochemical and mechanical properties of biological membranes in membrane growth, budding, fission, and fusion (Walde et al. 2010). GUVs can be produced with several techniques such as lipid hydration methods, the lipid-stabilized or surfactant-stabilized method, from lipids stabilized with or without double emulsion, by fusion of small vesicles, from an initial planar bilayer, from lipids dissolved in water-miscible solvents, or from a micellar lipid solution. Details of all techniques have been reviewed by Walde et al. (2010).

GUVs are used to reveal drug-membrane interactions and investigate drug activity. Observations on the alteration of single GUVs in the presence of particular drugs can reveal the molecular mechanisms of drug action on cell membranes, as, e.g., the antimicrobial peptide magainin 2 which interacts with membranes, inducing membrane permeability, and causing pore formation with change of vesicle shape (Tamba and Yamazaki 2005). In another example, GUVs have been employed to visualize membrane interactions with (–)-epigallocatechin gallate, the main flavonoid in green tea, causing the vesicles to burst (Tamba et al. 2007).

Supported lipid bilayers (SLB) are planar structures consisting of a lipid bilayer placed on a solid support that provides adequate stability. SLBs remain mostly intact even after applying

high flow rates, vibration, or in the case of the presence of pores in the membrane. The stability of SLBs allows an experiment to be carried out over several week or even months, an advantage not provided by other model membranes. The planar membrane structure allows a number of characterization tools to be used which are not possible in mobile or floating systems (Purrucker et al. 2001). Self-organization of SLBs starts with vesicle adsorption onto the solid support, then followed by vesicle rupture, and spreading of the lipid bilayers into planar membranes (Richter et al. 2006; Jing et al. 2014). The interactions and effects of drugs on SLBs can be characterized using several techniques, such as quartz crystal microbalance with dissipation (QCM-D), which allow investigation of the mechanisms of interaction in real time (Makky et al. 2012). Other techniques such as specular and off-specular neutron scattering (Schneck et al. 2009), X-ray reflectivity (XRR), and grazing-incidence X-ray fluorescence (GIXF) (Abuillan et al. 2013) can provide data on the physical and mechanical properties of SLBs and their interactions with drugs or other substances like peptides and proteins.

1.7 Aims of this study

Saponins, as natural surfactants, display various important biological and pharmacological activities. In plants, saponins play an essential role in defense, protecting the plants against diseases and predators. They are toxic to several classes of fungi, bacteria, insects, and parasites. The ability of saponins to affect cell membrane structure and integrity makes them interesting natural products in pharmacological and medical research and therapy, in particular as agents for enhancing drug efficacy. Their effect on membranes strongly depends on their chemical structure, which is highly variable. Until recently, there has been very little information on the activity of saponins as drug-enhancing agents and on their molecular mechanisms of action on membranes. This study tries to explore the mechanisms behind the drug-enhancing effects of saponins.

The key objectives of this study have been to explore:

- the **potency of saponins** in increasing the **efficacy of anticancer drugs** *in vitro*
- both a **steroid saponin** (digitonin) and a **triterpenoid saponin** (quillaja saponin) in respect to their **capacity of enhancing drug action**
- the **molecular mechanism** of action of **steroid and triterpenoid saponins** on biological and artifical **membranes with several biophysical methods**

2 Materials and Methods

2.1 Materials

2.1.1 Chemicals for cell cultures

DMEM (Dulbecco's Modified Eagle Medium)	Gibco® by Life Technologies
RPMI 1640 Medium	Gibco® by Life Technologies
Fetal bovine serum (FBS)	Biochrom AG, Berlin
L-Glutamine solution (200 mM, 100×)	Gibco® by Life Technologies
MEM Non-Essential Amino Acids (NAEA, 100×)	Gibco® by Life Technologies
Penicillin-streptomycin (10,000 U/ml)	Gibco® by Life Technologies
Trypan Blue solution	Sigma-Aldrich
Trypsin-EDTA (0.25%), phenol red	Gibco® by Life Technologies
Dimethyl sulfoxide (DMSO)	Sigma-Aldrich
Methylthiazoltetrazolium (MTT)	Sigma-Aldrich
NaCl	Sigma-Aldrich
KCl	Sigma-Aldrich
Na_2HPO_4	Sigma-Aldrich
KH_2PO_4	Sigma-Aldrich
NaOH	Sigma-Aldrich
Quillaja saponin	Carl Roth GmbH, Karlsruhe
Digitonin (≥ 98%)	Sigma-Aldrich
Verapamil	Sigma-Aldrich
Cisplatin	Sigma-Aldrich
Doxorubicin (adriamycin)	Sigma-Aldrich

2.1.2 Chemicals for supported lipid bilayers

Acetone	Zentralbereich Neuenheimer Feld, Heidelberg, Germany
Alexa Flour 488	LifeTechnology/Thermo Fisher, Darmstadt, Germany
Ammonium hydroxide	Sigma Aldrich, Steinheim, Germany
Bovine serum albumin (BSA)	Sigma Aldrich, Steinheim, Germany
Cardiolipin (heart, bovine) (CL)	Avanti Polar Lipids, Inc., Alabama, USA
Chloroform	Sigma Aldrich, Steinheim, Germany
Cholesterol	Avanti Polar Lipids, Inc., Alabama, USA
Desalting column PD-10	GE Healthcare, Garching, Germany
Digitonin	Sigma Aldrich, Steinheim, Germany
Dil stain (dioctadecyltetramethyl-indocarbocyanine perchlorate)	LifeTechnology/Thermo Fisher, Darmstadt, Germany
1,2-Dipalmitoyl-*sn*-glycero-3-phosphocholine (DPPC)	Avanti Polar Lipids, Inc., Alabama, USA

Ethanol	Zentralbereich Neuenheimer Feld, Heidelberg, Germany
Hellmanex	Hellma GmbH, Müllheim, Germany
Hydrogen peroxide	Grüssing GmbH, Filsum, Germany
Methanol	Zentralbereich Neuenheimer Feld, Heidelberg, Germany
Milli-Q H_2O	Thermo Electron LED GmbH, Niederelbert, Germany
L-α-Phosphatidylcholine (egg, chicken) (PC)	Avanti Polar Lipids, Inc., Alabama, USA
Phospholipids B kit	Wako Chemicals, Neuss, Germany
Sphingomyelin (egg, chicken)	Avanti Polar Lipids, Inc., Alabama, USA
1-Stearoyl-2-oleoyl-*sn*-glycero-3-phosphocholine (SOPC)	Avanti Polar Lipids, Inc., Alabama, USA
Texas Red-DHPE	Avanti Polar Lipids, Inc., Alabama, USA
Triton X-100	Sigma Aldrich, Steinheim, Germany

2.1.3 Laboratory materials

Cell culture flasks Cellstar® (25 and 75 cm^2)	Greiner bio-one GmbH, Frickenhausen
Cell culture plates Cellstar® (96- and 24-well)	Greiner bio-one GmbH, Frickenhausen
Chamber Slide™ System, NuncLab-Tek™ II	Thermo Fisher Scientific, Darmstadt, Germany
Crytubes	Greiner bio-one GmbH, Frickenhausen
Cuvettes, disposable	Carl Roth, Karlsruhe
Eppendorf safe lock reaction tubes (1.5 and 2 ml)	Eppendorf AG, Hamburg
Falcon™ conical centrifuge tubes (15 and 50 ml)	Becton Dickinson GmbH, Heidelberg
LiChrospher® 100 RP-18 (5 µm) LiChroCART® 250-4	Merck Millipore, Darmstadt
Pasteur pipettes	Carl Roth GmbH, Karlsruhe
Pipettes, serological, sterile (5, 10, and 25 ml)	Greiner bio-one GmbH, Frickenhausen
Precision spray plastic pak	Becton Dickinson GmbH, Heidelberg
Stericup® and Steritop™ 500 ml	Merck Millipore, Darmstadt
Syringe driven filter unit (0.22 and 0.45 µm)	Merck Millipore, Darmstadt
Pipette tips, natural 200 µl	Greiner bio-one GmbH
Pipette tips, natural 1000 µl	Greiner bio-one GmbH
Petri dishes, sterile, 94,0/16 mm, with vents	Greiner bio-one GmbH
Masterblock, 96 well, 1 ml, U-bottom	Greiner bio-one GmbH
Pipette tips, natural (10, 200, and 1000 µl)	Greiner bio-one GmbH

2.1.4 Instruments

Autoclave CERTOCLAV	KELOmat-Sterilizer Division, Traun, Austria
Axiovert 200 M microscope	Carl Zeiss Microscopy GmbH, Oberkochen, Germany
Beckman Coulter Gold HPLC system	Beckman Coulter GmbH, Krefeld, Germany
Cabinet TT80	FRYKA Kaltechnik, Esslingen
Centrifuge	Eppendorf AG, Hamburg, Germany
Centrifuge, Hermle ZK 364	M&S Laborgeräte GmbH, Wiesloch
Centrifuge, J12-21, Rotor JA-14	Beckmann, München
Centrifuge, Megafuge 1.0R	Hereaus Sepatech, Wiesloch
CO-150 cell culture incubator	Brunswick Scientific, Nürtingen
CO_2 incubator B5060 EK/CO_2	W.C. Heraeus GmbH, Hanau
Confocal microscope LSM 710	Carl Zeiss Microscopy GmbH, Oberkochen, Germany
Diaphragm vacuum pump	Vacuubrand GmbH & Co., Wertheim
DLS ZetasizerNano ZS	Malvern Instruments GmbH, Herrenberg
DPI sensor chips	Farfield Sensors Ltd., Crewe, UK
Dual polarization interferometer, *Ana*light® BIO200	Farfield Sensors Ltd., Crewe, UK
Heraeus oven, Model T6030	Heraeus Instrument, Hanau
YL9100 HPLC	YL Instrument Co.,Ltd., Republic of Korea
Incubator	Heraeus Holding GmbH, Hanau, Germany
Laminar air flow, Type S-2010, Model 1.2	Heto-Holten, Allerød, Denmark
Light microscope (inverted Nikon TMS)	Nikon Corporation, Tokyo, Japan
LCQ Duo ion trap mass spectrometer	Thermo Finnigan, USA
Lipid extruder	Avanti Polar Lipids, Inc., Alabama, USA
Liposome extruder, LiposoFast LF-1	Avestin, Ottawa, Canada
Liquid nitrogen tank GT35	AIR LIQUIDE GmbH, Düsseldorf
Microplate reader, Biochrom Asys UVM 340	Biochrom Ltd., Cambridge, UK
Microplate reader, Tecan Safire 2	Tecan, Crailsheim, Germany
Microplate reader, Tecan Infinite M200	Tecan, Crailsheim, Germany
Multichannel pipette 8 × 200 µl	Abimed, Langenfeld
Neubauer counting chamber	neoLab® Migge, Heidelberg
pH-meter MP 120	Biometra GmbH, Göttingen
Pipettes, PIPETMAN Classic™(2, 20, 100, 200, 1000 µl)	Gilson Inc., Middleton, USA
Pipetus® pipetting aid/controller	Hirschmann Laborgeräte, Eberstadt
Precision balance, Sartorius Basic	Sartorius AG, Göttingen
Quartz crystal microbalance with dissipation, QCM-D E4	Q-Sense/Biolin Scientific, Gothenborg, Sweden
Silicon wafer	Si-Mat Silicon Materials, Kaufering, Germany
Sonorex ultrasonic water bath, model Super RX 514	Bandelin Electronic KG, Berlin
Spectrophotometer	Eppendorf AG, Hamburg
Tip sonicator	Misonix, Inc., Farmingdale, NY, USA
Vacuum chamber	Binder GmbH, Nehren, Germany
Vortex, Heidolph Relax top	Heidolph Instruments GmbH & Co. KG, Schwabach
Water bath, Julabo P	Julabo Labortechnik GmbH, Seelbach
X-ray reflectometer	D8 Advance, Bruker, Germany

2.2 Methods

2.2.1 Cell culture

All cancer cell lines were cultured in Dulbecco's Modified Eagle Medium (DMEM + L-glutamine) supplemented with 10% heat-inactivated fetal bovine serum (FBS), 5% penicillin/streptomycin and 5% non-essential amino acids (NEAA) at 37°C in 95% humidified atmosphere and 5% CO_2. The cultures were split every two days when they reached 80% confluence using trypsin/EDTA. The cell adherence was removed by applying 3 ml of trypsin-EDTA, then incubating for 5 min at 37°C and 5% CO_2. Medium to a final volume of 10 ml was added to inactivate the trypsin-EDTA. Trypan Blue was added to differentiate between living and dead cells (10 µl TB to 100 µl of cell suspension). Numbers of living cells were counted in a Neubauer counting chamber, white cells in the four outer quadrants and in the inner square. The mean value was determined to dilute the cells with growth medium to a specific number as needed for the next experiment. All experiments were performed with cells in the logarithmic growth phase.

2.2.2 Cell proliferation assays

For cytotoxicity measurements the cells were seeded into 96-well plates at a density of 2×10^4 cells/well in 100 µl medium and then grown for 24 h before treating them with saponins and anticancer agents. Different concentrations of saponins and anticancer agents (in DMSO) were applied into the culture wells which were then incubated for 24 h. The final concentration of DMSO in the culture medium did not exceed 0.05%. Cell viability was evaluated using themethylthiazolyltetrazolium (MTT) cell viability assay. The survival of cells after treatment with saponins and anticancer agents was quantified using MTT. The test substances were replaced with fresh medium containing 0.5 mg/ml MTT, then incubated for 4 h. NAD(P)H-dependent cellular oxidoreductase enzymes from surviving cells will reduce tetrazolium dye salt into insoluble formazan which has a purple color. The MTT solution was removed from the wells and formazan crystals were dissolved in 100 µl of DMSO and then measured with a microplate reader (Biochrom UVM-340) at 570 nm. Experiments were repeated at least three times and each measurement was done as a triplicate. Controls included wells with untreated cells, wells with medium only, and wells with substance solution only. The cell viability was determined according to the formula below (Mosmann 1983). The IC_{50} values from each substance were calculated using a four-parameter logistic curve (SigmaPlot® 11.0) which representing 50% reduction of viability compared to the positive control. Results were expressed as mean and standard error (Chou 2006).

$$\%\ \text{cell viability} = \frac{\text{absorbance of sample-treated cells} - \text{absorbance of sample}}{\text{absorbance of cells} - \text{absorbance of medium}} \times 100$$

The nontoxic concentration of saponins against cancer cells was combined with the anticancer agent in order to investigate the ability of saponins to increase the toxicity of the anticancer agent in various cancer cell lines. The nontoxic concentration of saponins was taken from the IC_{20} values of saponins as determined in dose-dependent cytotoxicity experiments. Here, the IC_{20} value represents the concentration at which 80% of cells survive treatment with saponins (80% viable cells). The IC_{20} or any other IC value can be calculated from the IC_{50} equivalently to the equation below:

$$EC_F = \left(\frac{F}{100 - F}\right)^{\sqrt{H}} \times EC_{50}$$

with *F* being an index for a specified EC value, e.g., 20 for EC_{20}, and *H* the hillslope (Zhao et al. 2004).

The combination of saponins with anticancer agents in various cancer cell lines can have synergistic, additive, or antagonistic effects. The combination index (CI) between two or more drugs can be calculated by:

$$CI = \frac{C_{sap}}{IC_{50,sap}} + \frac{C_{drug}}{IC_{50,drug}}$$

Here, C_{sap} and C_{drug} are the variable concentrations of saponin and drug chosen in the combination experiments; $IC_{50,sap}$ and $IC_{50,drug}$ are the inhibitory concentrations of each of the substances; CI < 1 indicates synergistic, CI = 1 additive, and CI > 1 antagonistic effects (Chou 2006; Zhao et al. 2004).

The effect of combining saponins with anticancer drugs can also be evaluated by calculating their cytotoxicity enhancement ratio (CER), dose reduction index (DRI), or reversal ratio (RR) value. These can show how many fold the saponins can increase the toxicity of the cancer. The equation below was used to calculate CER values of saponin-anticancer agent combinations (Chou and Chou 1988).

$$CER = \frac{IC_{50,drug}}{IC_{50,sap+drug}}$$

For the combination experiment cells were treated in the same manner as for cell proliferation by the MTT cytotoxicity assay, only that the anticancer drug was mixed with saponins before being added to the cells.

2.2.3 Hemolytic activity

Defribrinated sheep blood was centrifuged at 3000 rpm for 5 min and red blood cells were then resuspended in isotonic NaCl solution to obtain a 1% erythrocyte solution. Serial dilutions of saponins were prepared in an isotonic NaCl solution. 500 µl of sample was mixed with 500 µl of erythrocytes in Eppendorf tubes and then incubated for 1 h at 37°C. After incubation the tubes were centrifuged at 1000 rpm for 5 min and then the supernatant was transferred into 96-well plate. The absorbance of hemoglobin in the supernatant was measured at 544 nm with a Biochrom UVM-340 microplate reader. As a positive control 5% Triton X-100 was employed and an isotonic NaCl solution as a negative control. Measurements were replicated three times for each saponin concentration. Hemolytic activity was calculated with the following formula (Herrmann and Wink 2011).

$$\%\ \text{hemolysis} = \frac{\text{absorbance of sample} - \text{absorbance of blank}}{\text{absorbance of positive control}} \times 100$$

2.2.4 Preparation of lipid vesicles and entrapment of calcein

Large unilamellar vesicles (LUVs) were prepared by hydration of a thin lipid film, according to the Bangham method. The desired membrane lipids, in appropriate amounts, were dissolved in chloroform, mixed properly in a round-bottom flask, and then dried under a stream of N_2 gas. The solvent was completely removed by keeping the sample in the vacuum desiccator connected to a rotary vacuum pump for more than 12 h. To prepare LUVs containing calcein, lipids were resuspended to a concentration of 4 mg/ml in 1 ml solution containing 80 mM calcein in water (pH 7.4, adjusted with NaOH) continuing with vortexing for 30 s several times at room temperature. Next, the lipid-calcein suspension was subjected to six cycles of freezing and thawing in liquid N_2. Afterwards the solution was extruded 31 times through double-stacked polycarbonate membrane (pore size, 100 nm) using a two-syringe extruder in a LiposoFast liposome extruder (Avestin) until the solution became transparent. The untrapped calcein was removed from LUVs solution through a PD-10 desalting column (GE Healthcare) equilibrated with outside buffer. The lipid concentration was estimated with the Phospholipids B kit (Wako Chemicals). Fluorescence intensities of calcein entrapment in LUVs were measured at room temperature at excitation wavelength 490 nm and emission wavelength 520 nm (García-Sáez et al. 2006).

2.2.5 Permeabilization of LUVs (calcein release assay)

Permeability activity of saponins at the LUVs was determined by measuring the intensity of calcein fluorescence released into solution from LUVs after introduction of saponins. The black 96-well plate was blocked with 10% bovine serum albumin (BSA) for 1 h at room temperature to avoid nonspecific interaction between plate material with saponins and vesicles. The BSA solution was removed from the plate, continuing with washing several times with sterile water, then dried. Following this, 100 µl of LUVs with entraped calcein was added to each well. Different concentrations of saponins were applied immediately before measurements with a Tecan Infinite M200 plate reader at fluorescence emission wavelength of 520 nm and excitation at 495 nm. The increased fluorescence intensity of calcein was monitored with time until a stationary state was reached. As a positive control 5% Triton X-100 was employed and buffer as a negative control. The percentage of calcein release from vesicles induced by saponins was calculated from:

$$\%R = 100\frac{F_f - F_i}{F_m - F_j}$$

where F_f is the calcein fluorescence intensity at a specific time after incubation with saponins, F_i the initial calcein intensity before adding saponins, and F_m the maximum intensity of calcein upon adding 5% Triton X-100 (García-Sáez et al. 2006).

2.2.6 Preparation of giant unilamellar vesicles (GUVs)

Giant unilamellar vesicles (GUVs) were prepared by the electroformation method. The desired lipid composition with and without cholesterol was mixed with Dil stain to visualize GUV membrane rims under the fluorescence microscope. The lipid mixture at 1 mg/ml in chloroform was spread onto two platinum wire electrodes at 5 µl per each wire and the solvent was evaporated for one minute. After the solvent had completely evaporated, the platinum wires were immersed in a chamber containing 300 mM sucrose solution and then the unit was connected to a power generator. The electroformation proceeded at 2.3 V and 10 Hz for 2 h, then followed by 30 min at 2 Hz at room temperature to release the GUVs from the electrode wires. The 40 µl of GUVs electroformed in 300 mM sucrose were transferred to 400 µl PBS onto an eight-chamber slide (Nunc™ Lab-Tek™ II Chamber Slide™ System) that was previously blocked with 2 mg/ml bovine serum albumin (García-Sáez et al. 2009).

2.2.7 Membrane permeability assays

For GUVs permeabilization measurements, Alexa Flour 488 was added and mixed properly with PBS containing saponin solution before GUVs were added into it. The Alexa Flour 488 fluorescence can differentiate between solution from the outside and inside of GUVs. The degree of permeabilization (filling kinetics) was determined by collecting pictures of several GUVs in different sample conditions every 20 s for 1 h. GUV images from several regions were taken after 2 h incubation with or without saponins to reach the final extent of vesicle permeabilization. Permeabilized and nonpermeabilized GUVs were counted and analyzed with homemade GUV detector software and ImageJ (http://rsbweb.nih.gov/ij/) (García-Sáez et al. 2009; Apellániz et al. 2010; Hermann et al. 2014).

2.2.8 Confocal microscopy (CM) and fluorescence correlation spectroscopy (FCS)

Membrane permeabilization by saponins was monitored with LSM710 microscope with a C-Apochromat 40×/1.2W Corr M27 water immersion objective (Zeiss, Oberkochen, Germany) in multitrack modus. The green channel consisted of excitation light from an Ar-ion 488 nm and a 505–530 nm band-pass filter. The red channel consisted of excitation light from a He-Ne 561 nm with 633 nm excitation laser and a 650 nm long-pass filter. Fluorescence cross-correlation spectroscopy (FCCS) measurements were performed at 22°C using a Confocor 3 module. Photon arrival times were recorded with a hardware correlator Flex 02-01D/C (http://correlator.com). We repeatedly scanned the detection volume with two perpendicular lines through the equator of a GUV (the distance between the two lines, *d*, was measured by photobleaching on a film of dried fluorophores). The data was analyzed using homemade software (García-Sáez et al. 2009). We binned the photon stream in 2 μs and arranged it as a matrix such that every row corresponded to one line scan. We corrected for membrane movements by calculating the maximum of a running average over several hundred line scans and shifting it to the same column. We fitted average overall rows with a Gaussian and we added only the elements of each row between –2.5 s and +2.5 s to construct the intensity trace. We computed the autocorrelation and spectral and spatial cross-correlation curves from the intensity traces and excluded irregular curves resulting from instability and distortion. The auto- and cross-correlation functions were then fitted with a nonlinear least-squares global fitting algorithm, as described by García-Sáez et al. (2009) and Bleicken et al. (2013).

2.2.9 GUV image analysis

Permeability of GUVs is defined by influx of colored solution through the GUV membranes. The percentage of GUV filling was calculated according to the equation below. The threshold for nonpermeabilized GUVs was set to <15%. Several hundred GUVs were analyzed per experiment.

$$\left[\frac{(F_t^{in} - F_0)}{(F_t^{out} - F_0)}\right] \times 100,$$

in which F_t^{in} is the average fluorescence intensities inside a GUV, F_t^{out} the average fluorescence intensities outside a GUV, and F_0 the background fluorescence at time t.

To quantify saponin binding to GUV membranes, the fluorescence intensity at the vesicle rim (F_{rim}) was calculated with ImageJ using the plug-in radial profile plot. Intensity was plotted as F_{rim}/F_{back}, where F_{back} is the background intensity outside the GUVs.

In the kinetics experiments, images were recorded every 20 s and changes in the fluorescence intensity inside GUVs were analyzed over time as

$$F_t^N = \frac{(F_t^{in} - F_0)}{(F_t^{out} - F_0)}$$

F_t^N is the normalized fluorescence intensity at time t.

To calculate the initial A_0 and relaxed A_{relax} permeabilized area of individual GUVs, as well as the relaxation time τ_{relax}, we used a multiexponential fitting described by:

$$F(t)_{in}^N = 1 - \frac{-t}{e^{\tau flux(t)}}$$

where the influx rate, τ_{flux}, decreases with time (the initial pore size relaxes to a smaller structure) according to

$$\tau_{flux}(t) = \frac{V}{A(t) \times \frac{D}{m}}$$

where V is the vesicle volume, D the dye diffusion coefficient, m the membrane thickness, and A the total permeabilized area, which varies with time according to

$$A(t) = A_{relax} + (A_0 - A_{relax}) \times \frac{-t}{e^{\tau relax}}$$

Membrane thickness was assumed to be 4.5 nm. The diffusion coefficient of cyt *c*-al488 was 196 $\mu m^2/s$ (196 ± 27 $\mu m^2/s$) as calculated by fluorescence correlation spectroscopy (FCS) (Bleicken et al. 2013).

2.2.10 Size measurement by dynamic light scattering (DLS)

In order to get an overall idea about the effects of saponins on the phospholipid bilayer membrane, the size change of small unilamellar vesicles was measured using a dynamic light scattering (DLS) technique. Different concentrations of digitonin and quillaja saponins were added to the suspension of vesicles with or without cholesterol incorporation and the size distribution was measured at room temperature before and after an incubation of 30 min. The 900 µl of vesicle solution (0.5 mg/ml) was inserted in a disposable cuvette (Roth, Karlsruhe) and measured with 11 scans of 10 s in a DLS Zetasizer Nano ZS (Malvern Instruments) at 21°C. Afterwards 100 µl of saponins was added and after incubation for 30 min at room temperature, the solution was measured once more. For the control sample instead of saponins, 100 µl of filtered Milli-Q water was added to the vesicle solution and proceeded as described above. The data was analyzed using the asymmetric Gaussian function (ExpModGauss) multipeak fitting 2 package for IGOR PRO software (Wavemetrics, OR).

2.2.11 Dual polarization interferometry (DPI)

The effects of saponins on the structure of the bilayer were further characterized in real time with another sensitive technique; Dual polarization interferometry (DPI) measurements were performed with the *Ana*light BIO200 (Farfield, UK), using a dual slab waveguide sensor chip (22 mm × 6 mm) illuminated with an alternating polarized laser beam (wavelength 632.8 nm). The chip consists of a four-layer dielectric stack of silicon oxynitride on a silicon wafer surface, which generates interference fringes at its output (integrated Young's interferometer). Upon deposition of material in the region of the evanescent field close to the surface of the top waveguide layer, spatial changes of an interference pattern occur. The optical path length of the top waveguide is affected by the change in refractive index within the evanescent field. This causes a relative phase shift corresponding to the shift of the interference fringes. The excitation of the chip with two orthogonal polarization modes provides two separate measurements of fringe shifts. The parameters refractive index n and thickness d for an adsorbed isotropic single layer are fitted to the measured phase changes with a minimization algorithm (Cross et al. 1999, 2003).

The anisotropy of the layer is considered by an additional parameter, birefringence, which describes the difference between the refractive index perpendicular and parallel to the surface (Mashaghi et al. 2008). The analysis is performed by fixing one of the parameters,

either refractive index *n,* thickness *d*, or birefringence to determine the other two. Herein a constant thickness corresponding to the thickness obtained by X-ray reflectivity is assumed.

The waveguide surfaces were cleaned according to the modified RCA cleaning procedure (Kern 1990). First, the surfaces were immersed and sonicated with acetone, ethanol, and methanol, then sonicated in a freshly prepared solution of 1 : 1 : 5 (v/v) H_2O_2 (30%)/NH_4OH (30%)/H_2O for 5 min and kept for another 45 min at 60°C to obtain hydrophilic surfaces. Finally, they were rinsed 10 times with water, thoroughly dried at 70°C and stored in a vacuum chamber prior to use. After waveguide insertion, calibrations were performed for ethanol (80%) and pure water to get a constant baseline. Liposome samples (1 mg/ml) were infused at a flow rate of 5 μl/min with a syringe pump followed by rinsing with buffer at the same flow rate at 25°C. Digitonin and quillaja saponin solution (50 μM) was infused individually at a flow rate of 4 μl/min exposing the lipid bilayer to the saponin for 1 h followed by rinsing at the same flow rate at 25°C.

2.2.12 Differential scanning calorimetry (DSC)

Differential scanning calorimetry (DSC) measurements were carried out using a VP-DSC calorimeter (MicroCal, Inc., Northampton, MA, USA). To ensure that thermal equilibrium was reached, three thermograms were recorded. The first involved heating the sample from 2°C to 15°C at a scan rate of 5°C/h, the second involved cooling from 15°C to 2°C at a scan rate of 5°C/h, and the third involved heating from 2°C to 15°C at a scan rate of 5°C/h. Only the result from the last up-scan was used. The samples used for the DSC measurements were prepared as 2 mM lipid suspensions of SOPC, SOPC/Chol (80:20), and SOPC/Chol (95:5) in PBS. For the interaction with digitonin, lipid vesicles were incubated with 50µM of digitonin for 30 min before starting the measurements.

2.2.13 QCM-D experiments

Experiments using quartz crystal microbalance with dissipation (QCM-D) monitoring were performed with a QCM-D E4 (Q-Sense). The QCM-D sensor allows the measurement of the oscillation frequency shift (Δ*f*) of a quartz crystal and simultaneous energy dissipation change (Δ*D*). Whereas changes in resonance frequency are related to the mass of the adsorbed material on or removed from the sensor, changes in energy dissipation provide information on the viscoelastic properties of the adsorbed material. AT-cut SiO_2-coated quartz crystals with a fundamental frequency of 5 MHz were provided by Q-Sense. These crystals were stored in 20 M sodium dodecyl sulfate (SDS) solution between measurements. Prior to use, they were

thoroughly rinsed with ultrapure water/ethanol/ultrapure water, dried under N_2 stream and treated with UV/ozone twice for 15 min, then separated by rinsing with ultrapure water (Makky et al. 2011).

The lipid SUV solution (0.2 mM in PBS) was flowed over the SiO_2 crystals for approx. 10 min to form a stable supported lipid bilayer. Then the crystals were rinsed with PBS buffer for 15 min to remove any unattached vesicles. Afterwards, digitonin solution (50 mM in PBS) was injected for 10 min and allowed to adsorb for another 20 min. After this time, the crystals were washed with buffer for 15 min to remove any unattached digitonin molecules on the supported planar bilayers. The peristaltic pump for liquid flow was set to 100 µl/min. All measurements on QCM-D were done with the system temperature stabilized at 25 $\pm$ 0.1°C.

2.2.14 QCM-D modelling

QCM-D detects materials adsorbed onto a quartz crystal surface. When a material is adsorbed on the crystal surface, the resonant frequency decreases with an increase in the amount of mass adsorbed on the crystal.

If the adsorbed layer is homogenous and sufficiently rigid, the frequency shift (Δf) is proportional to the adsorbed mass per unit surface (Δm) as described by the Sauerbrey (1959) equation:

$$\Delta m = -\frac{C \times \Delta f}{n}$$

where C is the mass sensitivity constant of the quartz (C = 17.7 ng/cm^2 Hz at f = 5 MHz) and n is the overtone number.

However, if the adsorbed layer is decoupled from the quartz oscillation due to the viscoelastic behavior of the adlayer and/or to the associated water molecules with the layer, then $\Delta f/n$ curves are shifted, the energy dissipation in the oscillation will increase, and the Sauerbrey equation will be invalid. In this case, the more advanced Voigt-Voinova (Voinova et al. 1999) model is often employed. In the Voigt-Voinova model, the adsorbed film is represented by a single Voigt element consisting of a parallel combination of a spring and a dashpot to represent the elastic (storage) and viscous (damping) behavior of a material, respectively. This model can be described as following:

$$G^* = G' + iG'' = \mu_f + 2\pi i f \eta_f = \mu_f (1 + 2\pi i f \tau_f)$$

where f is the oscillation frequency, μ_f the elastic shear (storage) modulus, η_f the shear viscosity (loss modulus), τ_f the characteristic relaxation time of the film ($\tau_f = \eta_f/\mu_f$),$G^*$the complex shear modulus, G' the storage modulus, and G'' the loss modulus.

The Voigt-Voinova model relates the measured frequency shift (Δf) and dissipation shift (ΔD) to the thickness and viscoelastic properties (shear modulus and shear viscosity) of the adsorbed layer using the Q-TOOLS software (Vers. 3.0.15, Q-Sense). This model assumes the quartz crystal to be purely elastic, and the surrounding solution to be purely viscous and Newtonian. In addition, it assumes that the thickness h_1 and the density ρ_1 of the film are uniform, that the viscoelastic properties of shear modulus μ_1 and viscosity η_1 are frequency independent, and that there is no slip between the adsorbed layer and the crystal during shearing. The adsorbed layer is represented with an homogeneous film on the sensor surface using four unknown parameters (ρ_1, h_1, μ_1, η_1). Above the adsorbed film is a semi-infinite bulk liquid (ρ_2, η_2).

Based on the fore mentioned, the relationship between QCM-D response and viscoelastic properties of the adsorbed layer can be explained by the following equations:

$$\Delta f \approx -\frac{1}{2\pi\rho_0 h_0}\left[\frac{\eta_2}{\delta_2} + h_1\rho_1\omega - 2h_1\left(\frac{\eta_2}{\delta_2}\right)^2 \frac{\eta_1\omega^2}{\mu_1^2 + \omega^2\eta_1^2}\right]$$

$$\Delta D \approx -\frac{1}{\pi f\rho_0 h_0}\left[\frac{\eta_2}{\delta_2} + 2h_1\left(\frac{\eta_2}{\delta_2}\right)^2 \frac{\eta_1\omega}{\mu_1^2 + \omega^2\eta_1^2}\right]$$

$$\delta = \sqrt{\frac{2\eta_2}{\rho_2\omega}}$$

where ρ_0 and h_0 are the density and thickness of the crystal, δ_2 the viscous penetration depth of the shear wave in the bulk liquid, and ω the angular frequency of the oscillation.

In the present work, three overtones (third, fifth, and seventh) were used to model the viscoelastic properties of the adsorbed layer of digitonin using the Q-TOOLS software. The fixed parameters were assumed as (*i*) the layer thickness which was determined by XRR measurement, (*ii*) fluid viscosity, 0.001 kg/m·s, and (*iii*) fluid density 1000 kg/m^3. The fitted parameters were (*i*) layer viscosity between 0.0005 and 0.01 kg/m·s, (*ii*) layer shear between 10^4 and 10^8 Pa, and (*iii*) layer density between 1000 and 1800 kg/m^3. In addition, when modelling the digitonin layer interacting with SLBs, the rigid bilayer was considered as a baseline. The thickness of the layer obtained from the Voigt model was multiplied by the density of the layer, to estimate the mass adsorbed per unit surface area.

2.2.15 High-energy specular X-ray reflectivity (XRR)

To quantify the effects of saponins on solid-support lipid bilayer a highly sensitive X-ray reflectivity technique is used. XRR measurements were performed using a D8 Advance (Bruker, Germany) equipped with a sealed X-ray tube, operating with Mo K_α radiation (E = 17.48 keV, λ = 0.0709 nm). The incident beam was collimated by various slits, reducing the beam size to 200 µm in the scattering plane. Automatic attenuator settings were used to avoid radiation damage. The scans were completed in approximately 3 h. The Si-wafer functionalized with PDA was placed on the sample holder horizontally. The momentum transfer perpendicular to the interface is given as a function of the angle of incidence α_i, $q_z = \frac{4\pi}{\lambda} \sin \alpha_i$. For each measurement point, the reflectivity was corrected for the beam footprint and for the beam intensity with the aid of an in-beam monitor. To minimize the artifacts from radiation damage, we carefully checked the reproducibility of the results by translating the sample position in the direction perpendicular to the beam. The data was fitted by using the Parratt formalism (Parratt 1954; Tolan 1999), with a genetic minimization algorithm implemented in the Motofit software package (Nelson 2006).

2.2.16 High-performance liquid chromatography (HPLC) and liquid chromatography–mass spectrometry (LC/MS)

The commercial quilllaja saponin was analyzed by YL9100 HPLC equipped with a LiChroCART RP18 column (5 µm, 250 × 4 mm, Merck). The mobile phase consisted of a gradient of water and acetonitrile, both with 0.1% formic acid. Starting from 19% acetonitrile, the gradient was run to 23% acetonitrile within 15 min, to 35% acetonitrile within the next 15 min, to 50% acetonitrile within the next 22 min, to 70% acetonitrile within the next 8 min, to 100% acetonitrile within the next 7 min, and remaining at this level for another 23 min. A flow rate of 1 ml min^{-1} was chosen (Thalhamer and Himmelsbach 2014). The chromatogram was visualized and analyzed using YL-Clarity software.

The composition of commercial quillaja saponin was determined by a LCQ Duo ion trap mass spectrometer (Thermo Finnigan, USA) fitted with an electrospray ionization (ESI) source and coupled to a Beckman Gold HPLC system (solvent module 125P, PDA detector 168) with a LiChroCART RP18 column (5 µm, 250 × 4 mm, Merck). A mobile phase gradient similar to the one used in HPLC was applied to the LC-MS system. The flow rate was 1 ml/min throughout the entire run. The absorptions were determined in background-subtracted spectra by 32 Karat™ software (Beckman Coulter, Inc.). The ESI source was operated in negative ion mode

at 4.5 kV. The heated capillary temperature was 200^{o}C. High-purity nitrogen was used as a sheath and auxiliary gas at a flow rate of 80 and 40 (arbitrary units), respectively. The mass spectrometer was set to detect ions in the range m/z 50–2000. The LCQ Duo was capable of performing single MS and MS^2 experiments in a single chromatographic run. The most abundant ions were isolated and scanned for MS/MS analysis with normalized collision energy at 35%. The mass spectra were analyzed using Xcalibur 2.0 software and the peaks were identified by comparison with published data.

3 Results

3.1 Potency of digitonin as a drug toxicity enhancer and mechanistic investigations using membrane models

3.1.1 Cytotoxicity of digitonin and selected anticancer agents

Cytotoxicity assays were performed for digitonin as well as for the selected anticancer agents berberine, cisplatin, doxorubicin, dexamethasone, and mitomycin C (Fig. 3.1). Dose response curves were established in the concentration range from 0.01 mM to 10 mM and IC_{50} and other IC values were determined. The cytotoxicity of the anticancer drugs in the four tested cancer cell lines were determined as expected (Table 3.1).

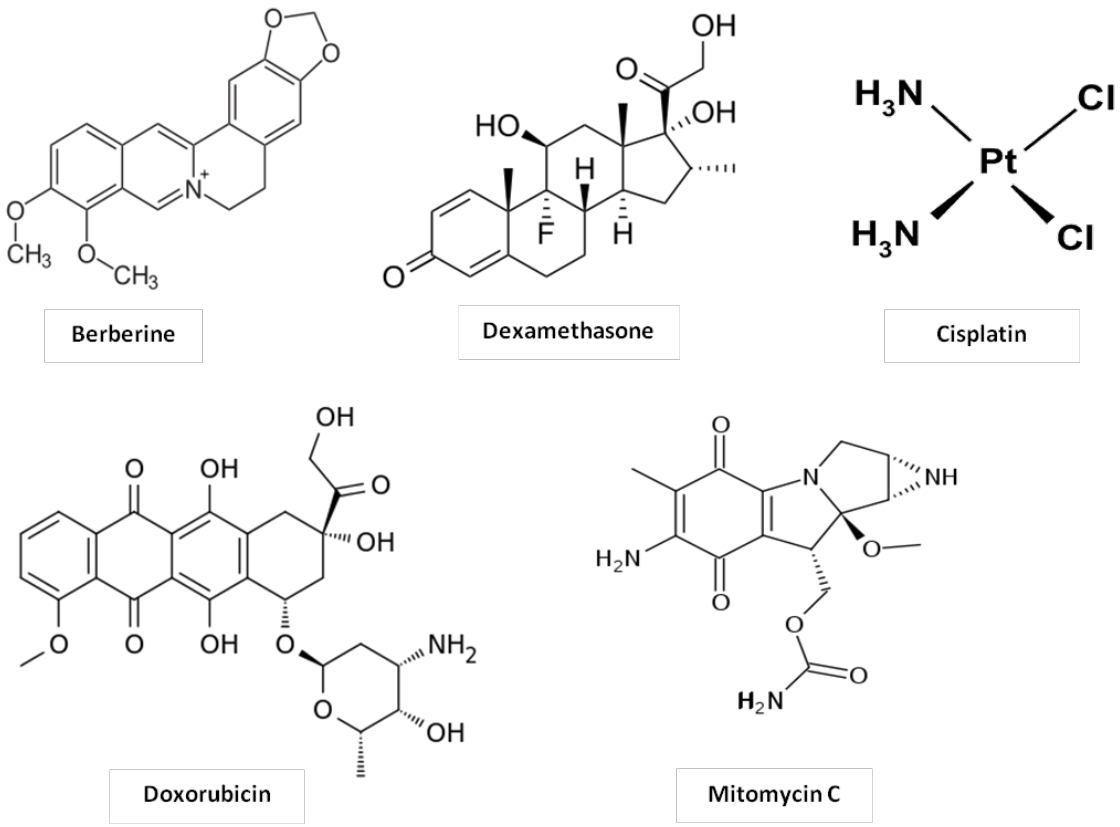

Fig. 3.1. Chemical structures of the selected anticancer agents

Table 3.1. Cytotoxicity and IC_{50} values (μM) of digitonin and of five selected anticancer agents in HeLa, COS-7, MIA PaCa-2, and PANC-1. Data indicated as mean ± standard deviation of three independent experiments, each done in triplicates.

	HeLa	COS-7	MIA PaCa-2	PANC-1
Saponin				
Digitonin (μM)	12.40 ± 3.06	11.61 ± 1.45	18.92 ± 2.39	13.41 ± 2.28
Drugs				
Berberine	334.4 ± 8.85	508 ± 0.13	103.1 ± 0.12	160.73 ± 0.01
Cisplatin	18.22 ± 5.5	30.37 ± 0.44	94 ± 0.12	99.20 ± 0.03
Doxorubicin	7.91 ± 0.16	12.76 ± 7.78	20.91 ± 5.27	57.95 ± 7.57
Dexamethasone	297 ± 0.10	340 ± 0.01	954.36 ± 0.08	1208 ± 0.25
Mitomycin C	94.40 ± 7.50	137 ± 0.02	24.2 ± 0.06	38.03 ± 0.04

3.1.2 Combining digitonin with common anticancer agents

Experiments started by applying a calculated IC_{20} concentration of digitonin and observing the actual effects on the cell cultures. The IC_{20} of digitonin is as follows for the different cell lines: 6.4 μM for HeLa, 7.7 μM for COS-7, 9.5 μM for MIA PaCa-2, and 6.5 μM for PANC-1 and these concentrations were used to test for enhanced toxicity of the five investigated anticancer agents. The cytotoxic concentrations (IC_{50}) of the individual tested anticancer agents differs for each cell line: berberine is 334.4 μM for HeLa, 508 μM for COS-7, 103.1 μM for MIA PaCa-2, and 160.73 μM for PANC-1; cisplatin is 18.22 μM for HeLa, 30.37 μM for COS-7, 94 μM for MIA PaCa-2, and 99.20 μM for PANC-1; doxorubicin is 7.91 μM for HeLa, 12.76 μM for COS-7, 20.91 μM for MIA PaCa-2, and 57.95 μM for PANC-1; dexamethasone is 297 μM for HeLa, 340 μM for COS-7, 954.36 μM for MIA PaCa-2, and 1208 μM for PANC-1; and mitomycin C is 94.40 μM for HeLa, 137 μM for COS-7, 24.2 μM for MIA PaCa-2, and 38.03 μM for PANC-1.

Anticancer agents in combination with a nontoxic concentration of digitonin generally increased the response of the cancer cell lines. The cytotoxicity enhancement ratio (CER) for each anticancer agent with digitonin was calculated by comparing IC_{50} values of the individual drugs with the IC_{50} of combined drug + digitonin for each cell line (Figs. 3.2a–d, 3.3 and Table 3.2). In general, digitonin enhanced the toxicity of all anticancer agents in all tested cancer cell lines. Among the combinations, dexamethasone + digitonin stands out: CER 3.75 in PANC-1 (IC_{50} from 1208 to 322.13 μM), 2.39 in MIA PaCa-2 (IC_{50} from 954.36 to 399.8 μM), and 1.04 in COS-7 (IC_{50} from 340 to 327.2 μM), while digitonin did not increase the cytotoxicity of dexamethasone in the HeLa cell line.

To interpret the type of interaction between anticancer agent and saponin, the isobologram method was used for determining the combination index (CI) to see whether the interaction is synergistic, additive, or antagonistic. The results indicate that the interaction of digitonin and anticancer drugs is mostly synergistic –the synergistic effect of the combination of digitonin+dexamethasone on the pancreatic cancer cell lines PANC-1 and MIA PaCa-2 being particularly strong, with CI values of 0.59 and 0.81, respectively (Fig. 3.4 and Table 3.2).

Table 3.2. Effects of digitonin (IC_{20}) + anticancer agents in HeLa, COS-7, MIA PaCa-2, and PANC-1 as reflected by the combination index (CI) and cytotoxicity enhancement ratios (CER). Data are expressed as means ±SD of cell viability for three independent experiments. The IC_{20} of digitonin was 6.4 μM in HeLa, 7.7 μM in COS-7, 9.5 μM in MIA PaCa-2, and 5.6 μM in PANC-1.

	IC_{50} (μM) of anticancer agents + IC_{20} (μM) digitonin											
	HeLa (6.4 μM)	**CI**	**CER**	**COS-7** (7.7 μM)	**CI**	**CER**	**MIA PaCa-2** (9.5 μM)	**CI**	**CER**	**PANC-1** (5.6 μM)	**CI**	**CER**
Berberine	208 ± 0.03	1.03	1.61	345 ± 0.17	1.16	1.47	58.00 ± 0.03	0.96	1.78	126.8 ± 0.33	1.11	1.27
Cisplatin	11.77 ± 8.39	1.05	1.55	15.19 ± 2.54	0.99	2.00	46.35 ± 0.01	0.89	2.03	88.36 ± 0.02	1.22	1.12
Doxorubicin	6.41 ± 0.37	1.22	1.23	6.86 ± 5.17	0.98	1.86	12.06 ± 8.21	0.97	1.73	31.26 ± 4.94	0.86	1.85
Dexamethasone	568 ± 0.14	1.35	0.52	327.2 ± 0.08	1.45	1.04	399.8 ± 0.08	0.81	2.39	322.13 ± 0.32	0.59	3.75
Mitomycin C	38.95 ± 5.76	0.82	2.42	57.52 ± 0.01	0.9	2.38	19.3 ± 0.03	1.19	1.25	22.13 ± 0.1	0.91	1.72

(a) HeLa

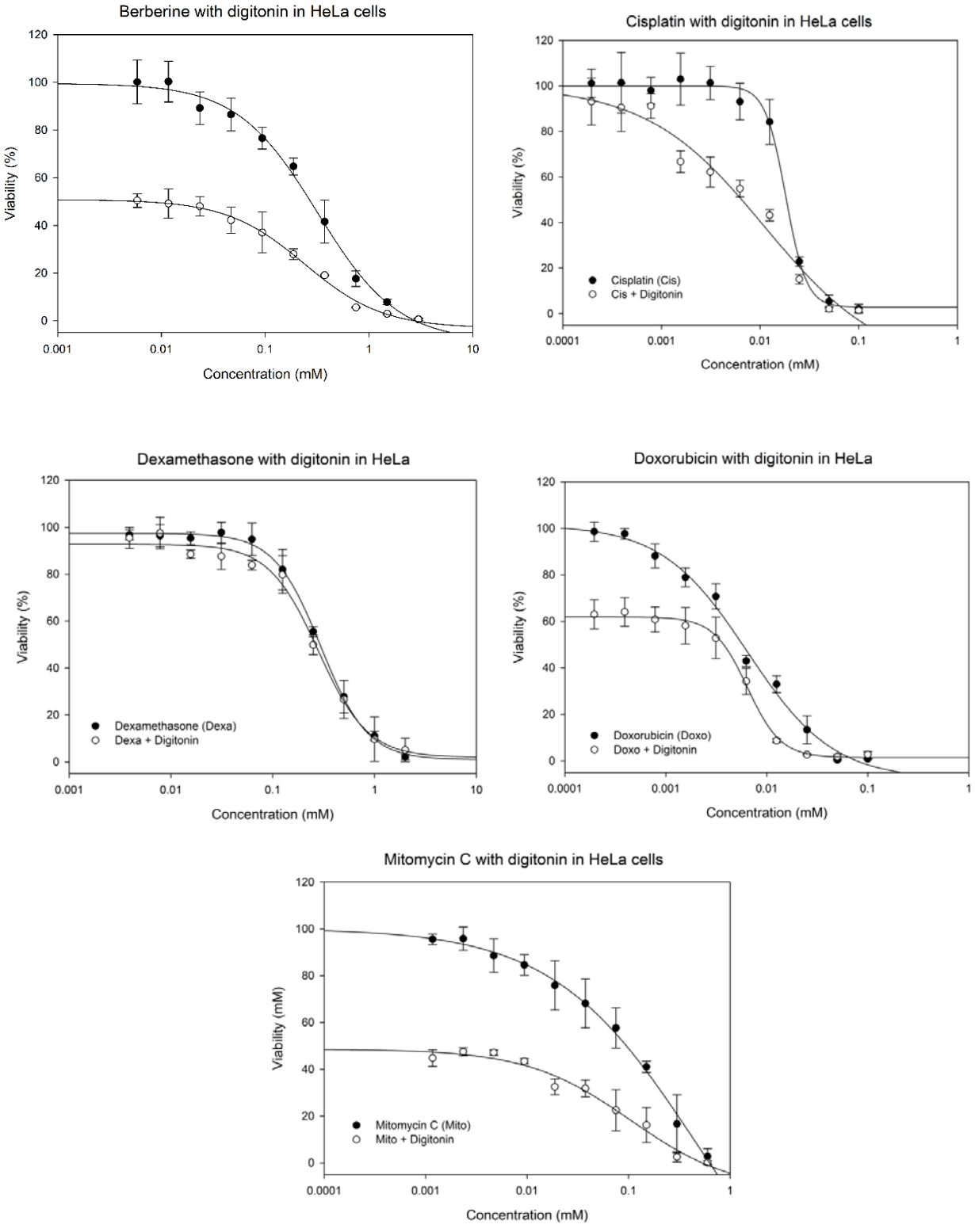

Fig. 3.2a. Dose response curves in HeLa to the anticancer agents berberine, cisplatin, dexamethasone, doxorubicin, and mitomycin C (*black data points*) and their combination with IC_{20} concentrations of digitonin (6.4 µM) (*white data points*). Data are expressed as means ±SD of cell viability from three independent experiments, each done in triplicates.

(b) COS-7

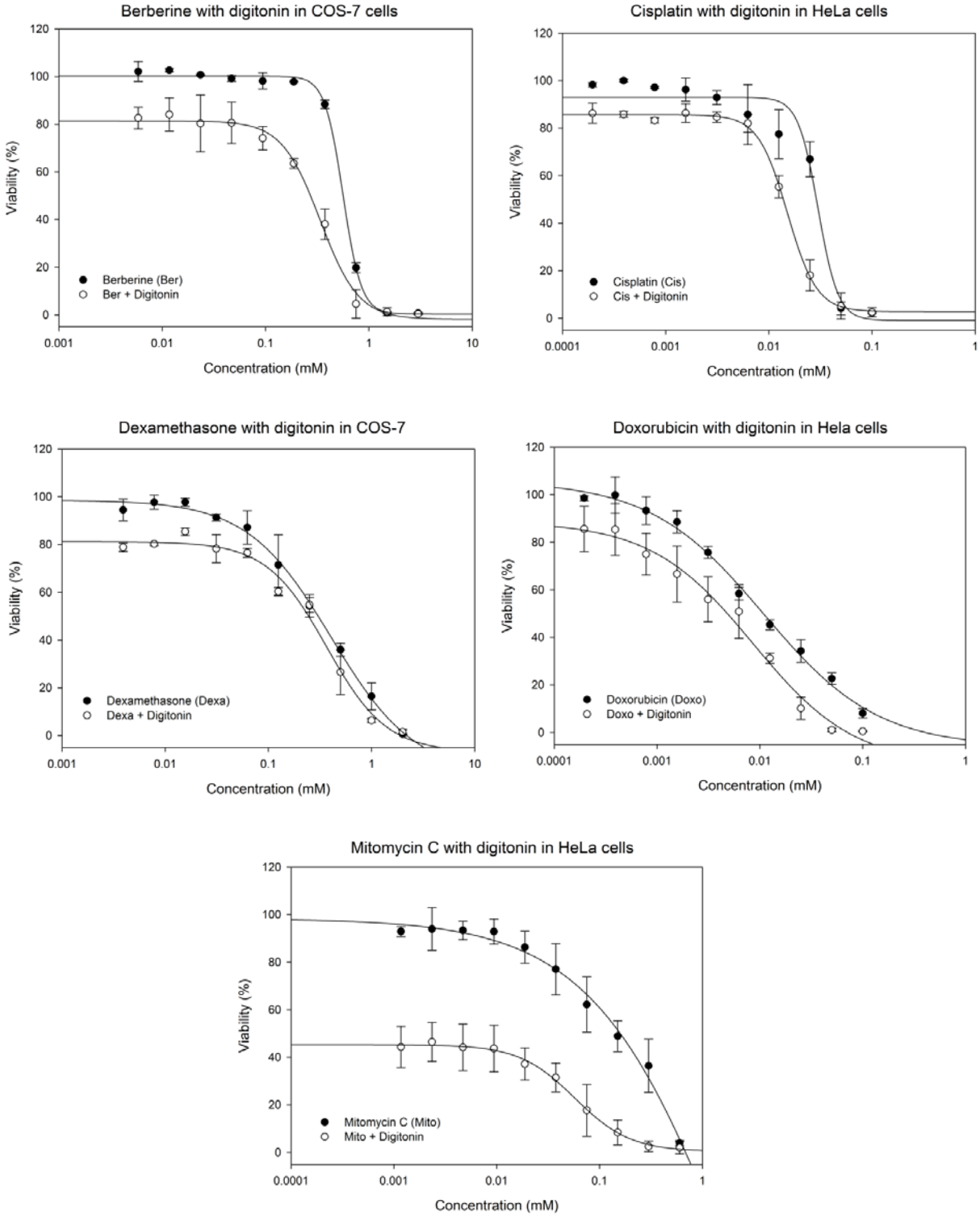

Fig. 3.2b. Dose response curves in COS-7 to the anticancer agents berberine, cisplatin, dexamethasone, doxorubicin, and mitomycin C (*black data points*) and their combination with IC_{20} concentrations of digitonin (6.4 µM) (*white data points*). Data are expressed as means ±SD of cell viability from three independent experiments, each done in triplicates.

(c) MIA PaCa-2

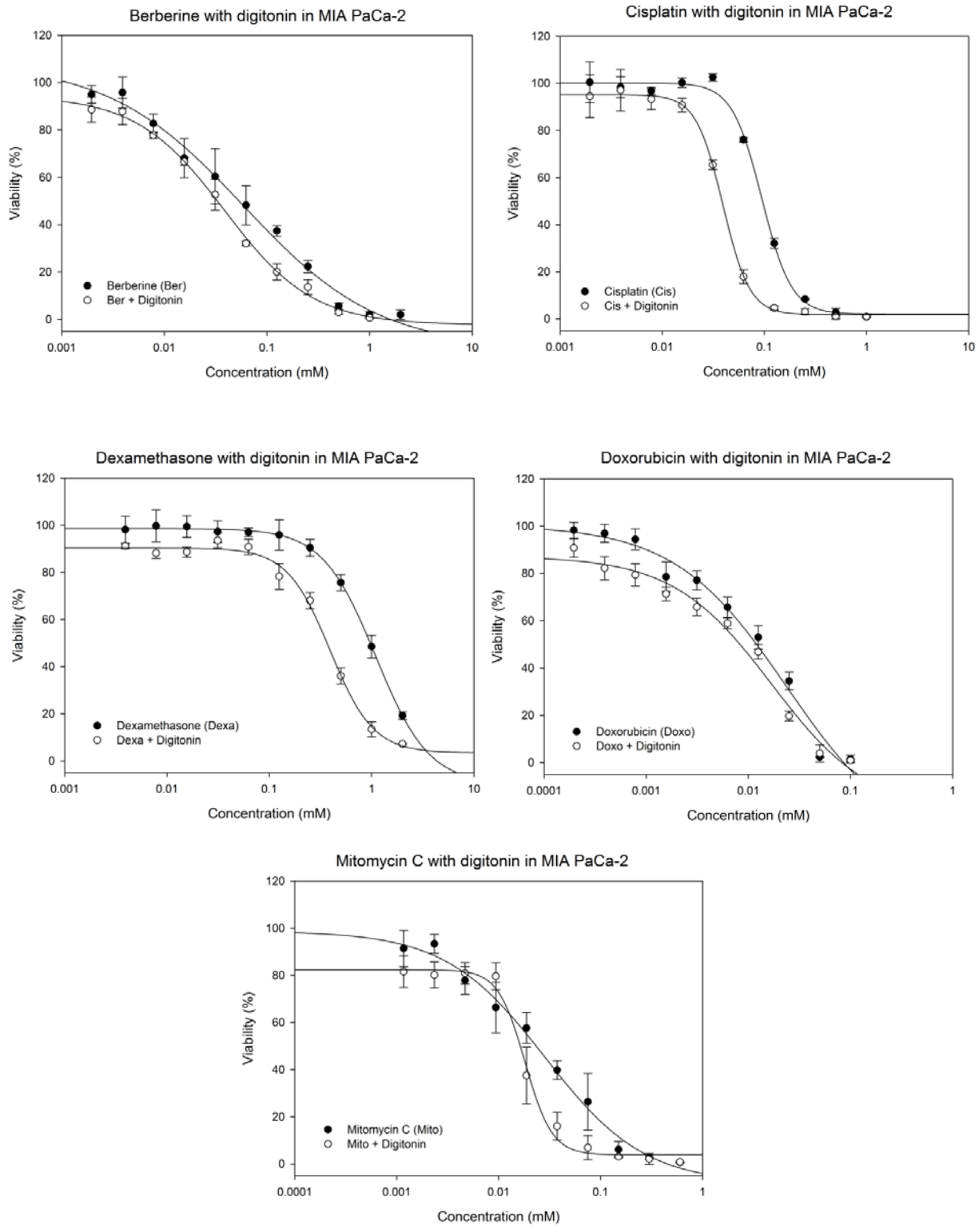

Fig. 3.2c. Dose response curves in MIA PaCa-2 to the anticancer agents berberine, cisplatin, dexamethasone, doxorubicin, and mitomycin C (*black data points*) and their combination with IC_{20} concentrations of digitonin (6.4 µM) (*white data points*). Data are expressed as means ±SD of cell viability from three independent experiments, each done in triplicates.

(d) PANC-1

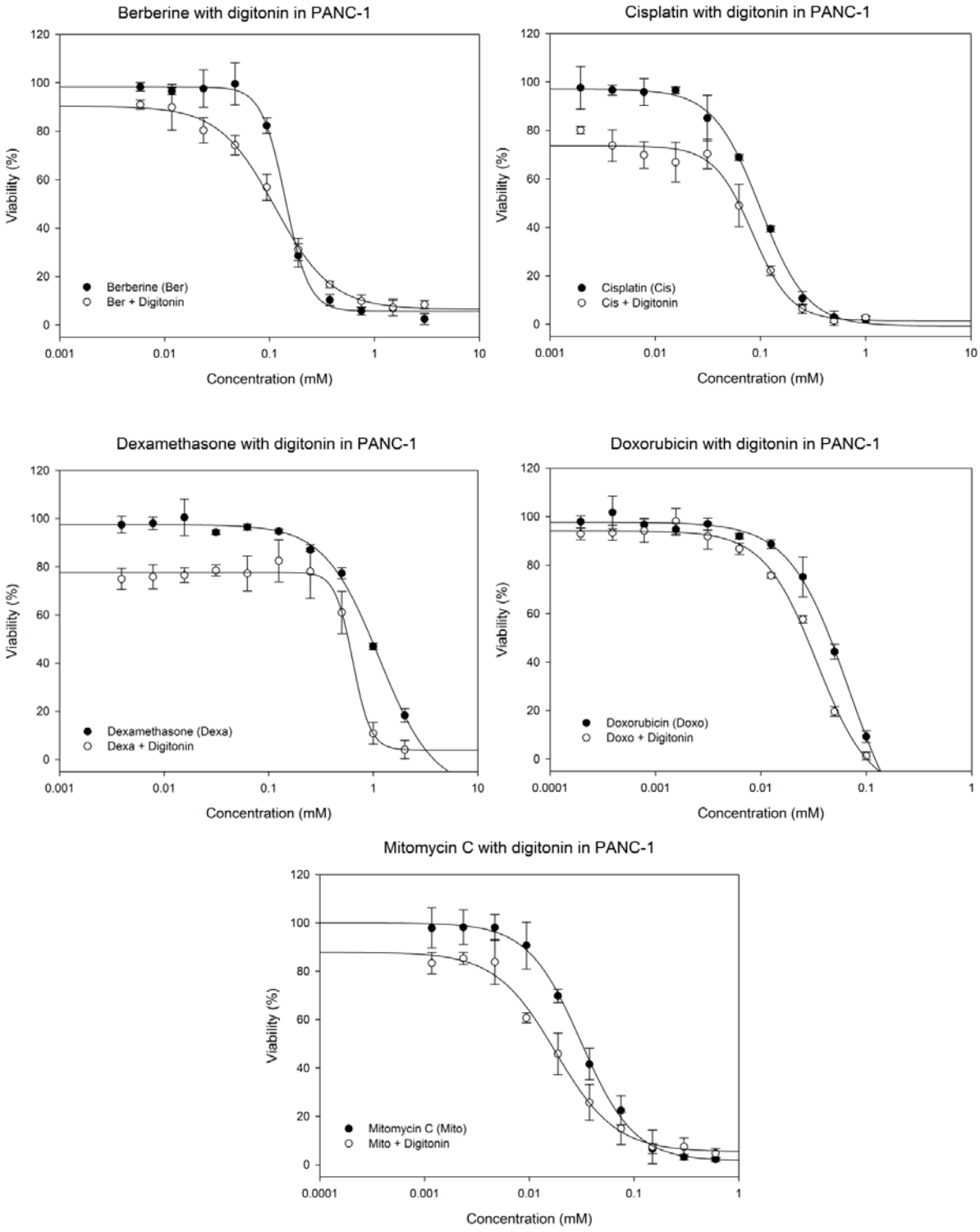

Fig. 3.2d. Dose response curves in PANC-1 of the anticancer agents berberine, cisplatin, dexamethasone, doxorubicin, and mitomycin C (*black data points*) and their combination with IC_{20} concentrations of digitonin (6.4 µM) (*white data points*). Data are expressed as means ±SD of cell viability from three independent experiments, each done in triplicates.

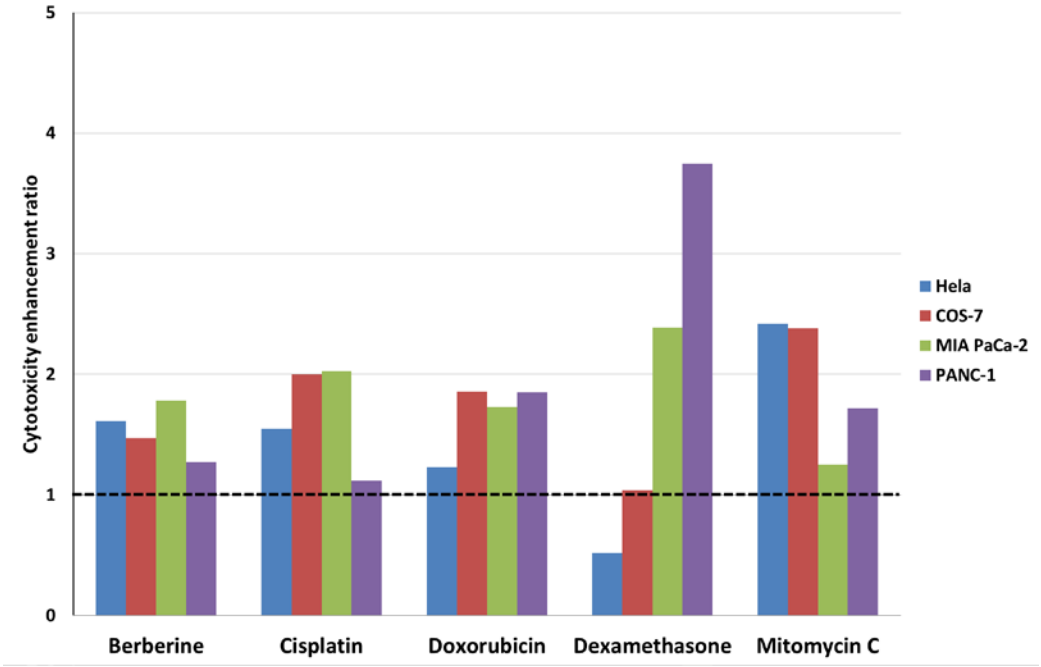

Fig. 3.3. Cytotoxicity enhancement ratios (CER) of anticancer drugs enhanced by digitonin in HeLa, COS-7, MIA PaCa-2, and PANC-1. CER values higher than 1 (*dashed line*) show the ability of digitonin to increase drug toxicity in the cancer cell lines. The cytotoxitiy enhancement profiles by digitonin differ in each case.

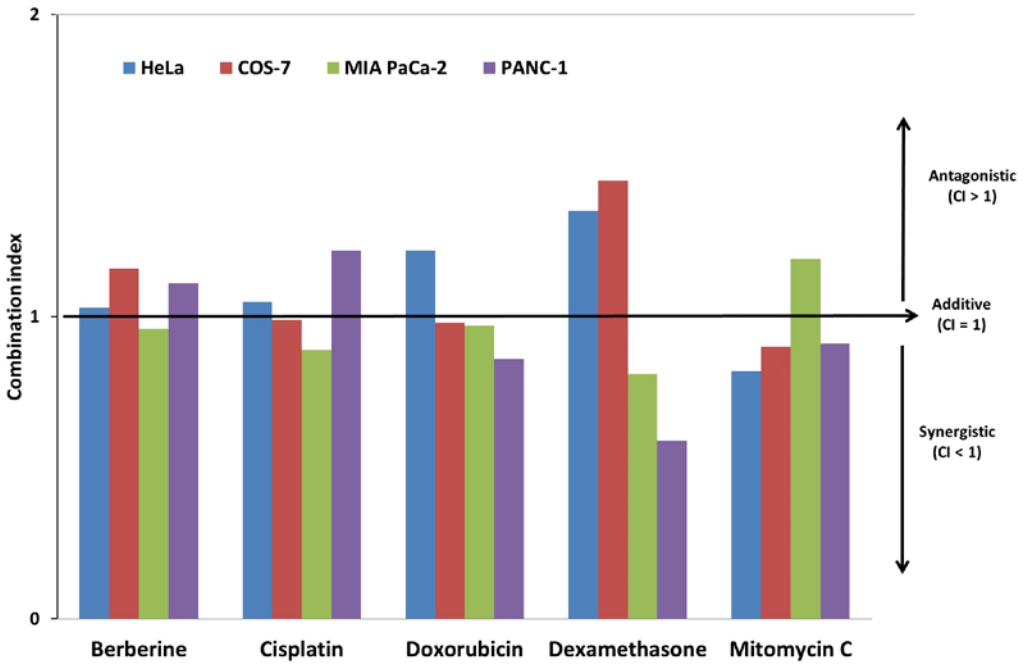

Fig. 3.4. Combination index (CI) values of digitonin (IC_{20}) with anticancer drugs in HeLa, COS-7, MIA PaCa-2, and PANC-1. CI < 1 = synergistic; CI 1 = additive; CI > 1 = antagonistic.

3.1.3 Digitonin increases the toxicity of ricin

Ricin from the seeds of *Ricinus communis* (castor bean) is a very toxic type-II ribosome-inactivating protein (RIP). Its high cytotoxicity is due to its immunotoxic, antiviral, antifungal, and insecticidal bioactivity and promises to have a potential as an anticancer agent. Mossinger et al. (1951) investigated the activity of ricin on rat sarcomas leading up to phase-I clinical studies (Fodstad 1984). Ricin is composed of an A-chain as the catalytic component and a B-chain as a sugar-specific lectin making it a nonpermeable RIP protein requiring other substances for delivery through the cell membrane. Saponins interact with cell membranes and can be used to deliver ricin into cells. Saponin from *Agrostemma githago* L. (corn cockle) increases the cytoxicity of the ribosome-inactivating lectin agrostin (Hebestreit et al. 2006; Melzig et al. 2005; Hebestreit and Melzig 2003). We explored the effect of digitonin in enhancing the toxicity of ricin.

Ricin was extracted from castor beans and identified with SDS-PAGE by submitting the aqueous fraction to gel electrophoresis, which confirmed the presence of ricin. The concentration of ricin was determined by Bradford assay. The toxic concentration of ricin in HeLa, COS-7, MIA PaCa-2, and PANC-1 was assessed by MTT assay with IC_{50} concentrations of 75.20, 99.9, 62.7, 297.15 ng/ml, respectively. The toxic and non-toxic concentration of digitonin was also determined for these cancer cell lines.

Digitonin enhances the toxicity of ricin in the cancer cell lines by more than 1.5-fold. The highest toxicity enhancements of ricin by digitonin were in the HeLa and MIA PaCa-2 cell lines with CER values of 5.41 (IC_{50} decreased from 75.2 to 13.9 ng/ml) and 5.13 (IC_{50} decreased from 62.7 to 12.2 ng/ml), respectively (Figs. 3.5 and 3.6). The combination of ricin with digitonin in HeLa, MIA PaCa-2, PANC-1 shows synergistic effects with CI values of 0.59, 0.59, and 0.90, respectively, the interaction with COS-7 is additive with a CI value of 1.04 (Fig. 3.7). Table 3.3 summarizes the cytotoxicity data of the individual substances and their combination.

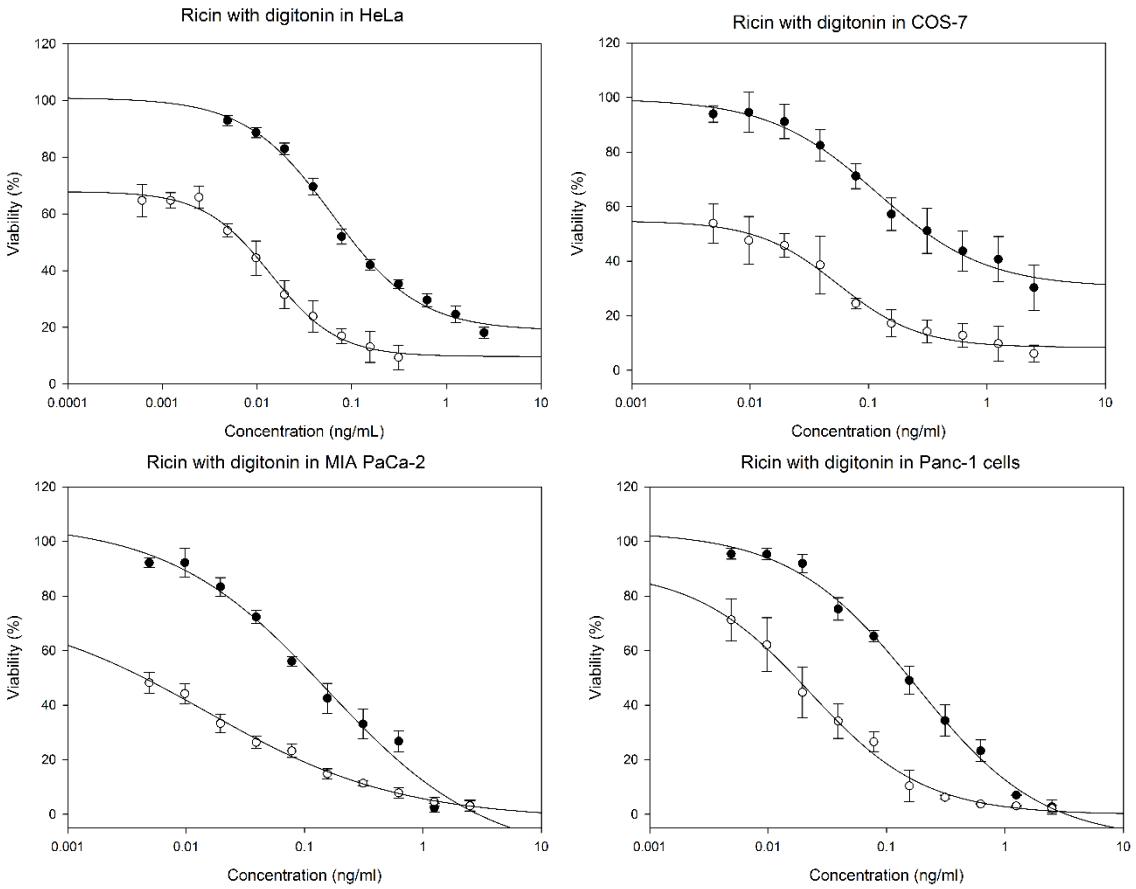

Fig. 3.5. Dose response curves of ricin in HeLa, COS-7, MIA PaCa-2, and PANC-1. Cytotoxicity of ricin (*black data points*) and its combination with IC_{20} concentrations of digitonin (6.4 µM for HeLa; 7.7 µM for COS-7; 9.5 µM for MIA PaCa-2; 5.5 µM for PANC-1) (*white data points*). Data are expressed as means ±SD of cell viability from three independent experiments, each done in triplicates.

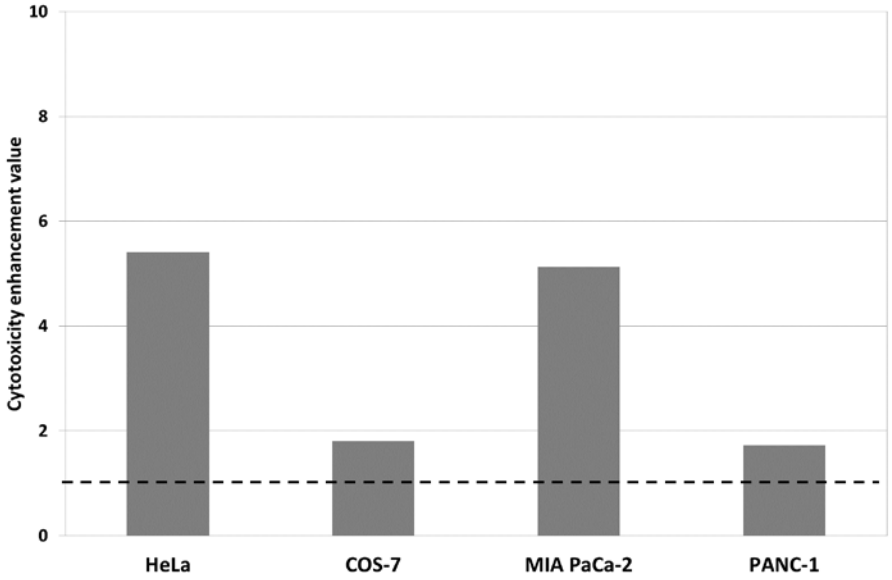

Fig. 3.6. Cytotoxicity enhancement ratio (CER) for ricin + digitonin in HeLa, COS-7, MIA PaCa-2, and PANC-1. CER values higher than 1 (*dashed line*) show the ability of digitonin to increase drug toxicity in the cancer cell lines. The cytotoxicity enhancement profiles by digitonin differ in each case.

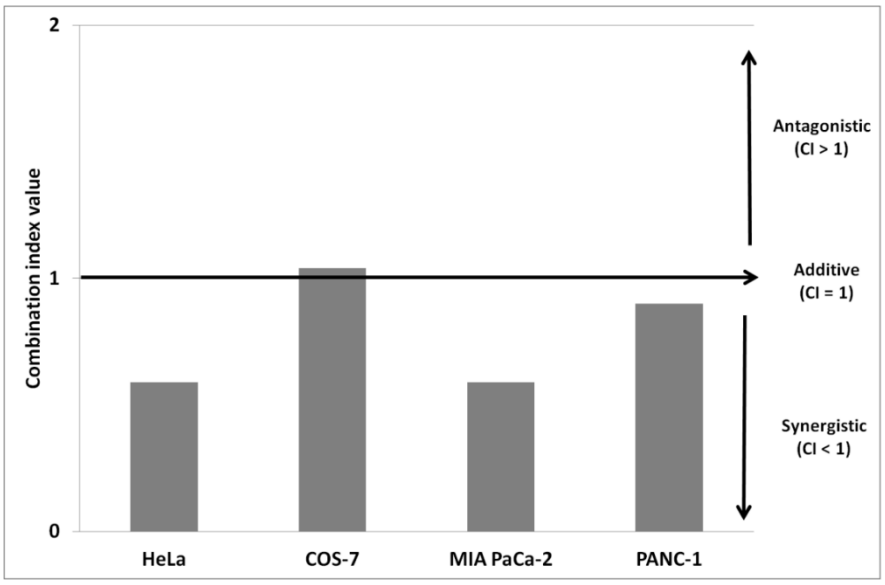

Fig. 3.7. Combination index (CI) values of digitonin (IC_{20}) + ricin in HeLa, COS-7, MIA PaCa-2, and PANC-1; CI < 1 = synergistic; CI 1 = additive; CI > 1 = antagonistic.

Table 3.3. Cytotoxicity of digitonin, of ricin, and of the combination of both in HeLa, COS-7, MIA PaCa-2, and PANC-1 cancer cell lines. The combined effect is shown by the combination index (CI) and cytotoxicity enhancement ratio (CER). Data are expressed as means ±SD of cell viability for three independent experiments.

	IC_{50} (µM) of anticancer agents + IC_{20} (µM) of digitonin											
	HeLa	**CI**	**CER**	**COS-7**	**CI**	**CER**	**MIA PaCa-2**	**CI**	**CER**	**PANC-1**	**CI**	**CER**
Saponins												
Digitonin (IC_{50}/ µM)	12.40±3.06			11.61±1.45			18.92±2.39			13.41±2.28		
Digitonin (IC_{20}/ µM)	6.4			7.7			9.5			5.6		
Ricin (ng/ml)	75.20±0.01			99.9±0.04			62.70±0.01			297.15±0.25		
Ricin + digitonin (ng/ml)	13.9 ± 0.05	0.59	5.41	55.2 ± 0.02	1.04	1.80	12.2 ± 0.1	0.59	5.13	171.1 ± 0.5	0.90	1.73

3.1.4 Digitonin ruptures RBCs

The activity of digitonin on natural cell membranes was examined with RBCs. Defebrinated sheep red blood cells were mixed with digitonin and the effect on the cell membranes was determined by photometrically measuring hemoglobin leakage out from the RBCs. Salt solution 0.9% and water were used as negative and positive controls. Digitonin affected sheep RBC membranes and rupturing them at an IC_{50} concentration of 0.0151 mM (Fig. 3.8).

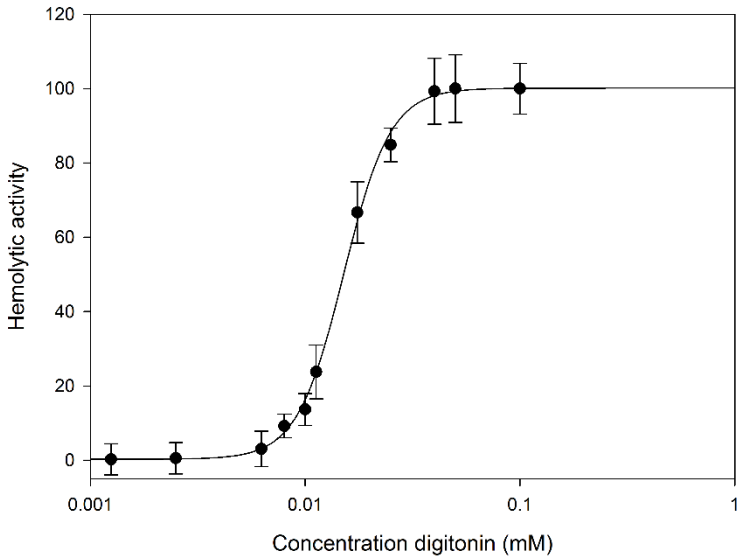

Fig. 3.8. Dose-dependent hemolytic effect of digitonin on sheep RBCs. Dose-ranging experiments were performed from 0.1 to 0.001 mM of digitonin. RBC rupturing occurred at IC_{50} 0.0151 mM. Data are expressed as means ±SD of hemolytic activity for three independent experiments.

3.1.5 Digitonin causes calcein leakage

Calcein leakage experiments were performed to investigate the specific interaction of digitonin with cell membrane components and to quantify the extent of membrane permeabilization caused by digitonin via its ability to induce leakage of lipid vesicles. Several large unilamellar vesicles (LUVs) were prepared all differing in the composition of the membrane lipids phosphatidylcholine (PC), sphingomyelin (SM), cardiolipin (CL), and cholesterol (Chol) in four different ratios: 100% PC, PC/Chol (80/20), PC/SM/Chol (40/40/20), and PC/CL (80/20). LUVs were incubated with different concentrations of digitonin and the release of calcein into the extravesicular solution was determined by fluorescence spectroscopy.

The results clearly indicate that digitonin specifically interacts with cholesterol in membranes to induce vesicle leakage and releasing entrapped calcein to the solution. The intensity of extra vesicular calcein fluorescence in the 100% PC and PC/CL (80/20) cases did not increase after incubation with digitonin for 24 h (Fig. 3.9).

Digitonin immediately interacts with cholesterol-containing membranes inducing membrane leakage within less than 2 min, then remaining stable for more than one hour, as indicated by the steady level of extravesicular calcein fluorescence (Fig. 3.10).

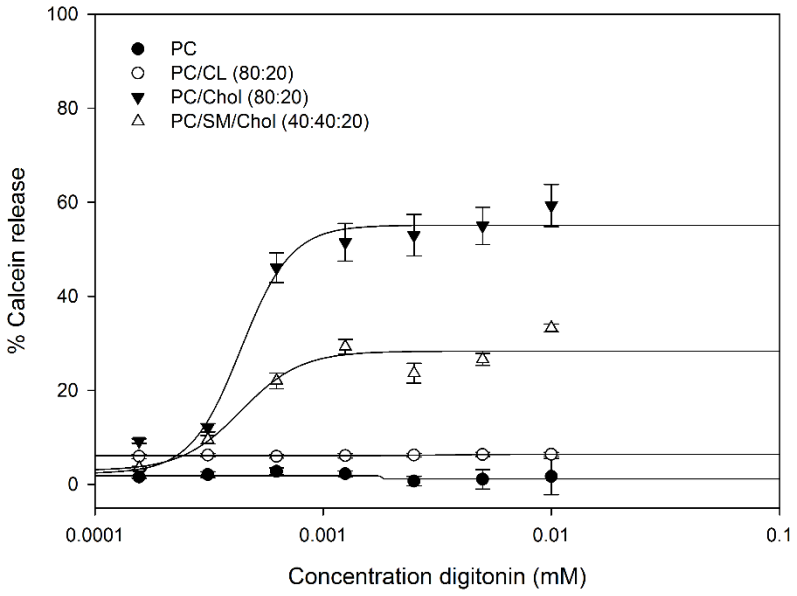

Fig. 3.9. Calcein release from different LUVs induced by digitonin. Data are expressed as means ±SD of hemolytic activity for three independent experiments. PC: phosphatidylcholine; CL: cardiolipin; Chol: cholesterol; SM: sphingomyelin.

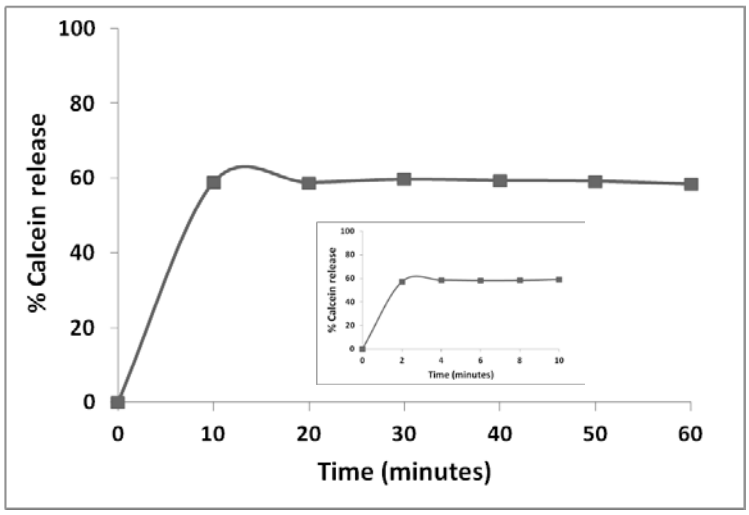

Fig. 3.10. Kinetics of calcein release of PC/Chol (80:20) LUVs induced by digitonin. Intensity of fluorescence of calcein released from LUVs by 0.01 mM digitonin was measured continuously every 120 s for 1 h. The *inset* shows the percentage of calcein release in the range time of 0–10 min.

3.1.6 Calcein release depends on membrane cholesterol concentration

Cholesterol plays an important role in the effect of digitonin on the cell membrane. We determined the extent to which cholesterol concentration has an effect on digitonin's ability to induce membrane leakage as indicated by the intensity of calcein release (Fig. 3.11).

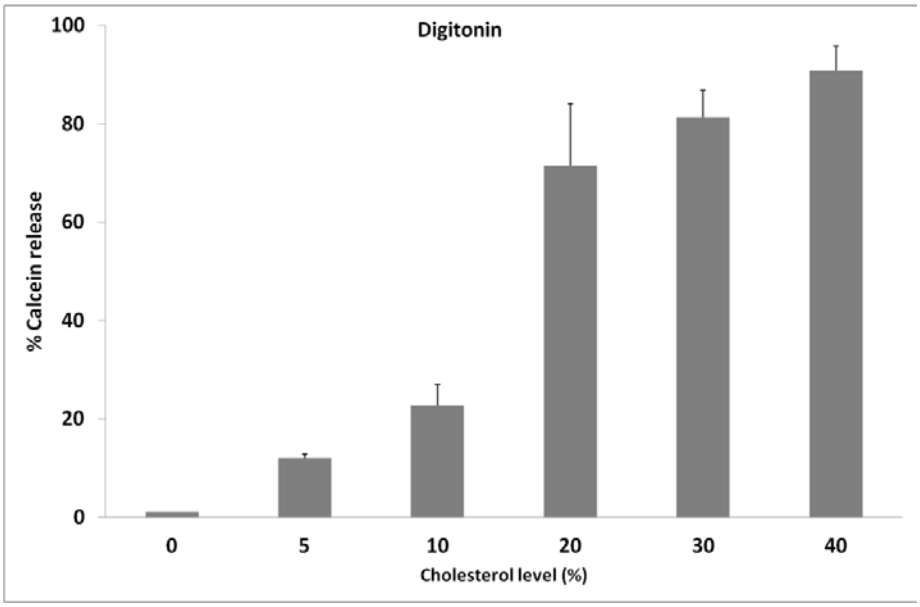

Fig. 3.11. Cholesterol concentration and effect of digitonin causing membrane leakage. PC vesicles with different concentrations of cholesterol were incubated with 0.1 mM digitonin for 1 h. Data are expressed as means ±SD of percentage of calcein release for three independent experiments.

3.1.7 Digitonin affects vesicle size only in the presence of cholesterol

To reveal possible interactions and effects of digitonin on vesicle membranes in terms of shape changes of vesicles with and without cholesterol we applied dynamic light scattering (DLS). 1-Stearoyl-2-oleoyl-*sn*-glycero-3-phosphocholine (SOPC) vesicles without and with 20% cholesterol were prepared and incubated with different concentrations of digitonin for 30 min, then measured by DLS. Shape and size of vesicles without cholesterol are similar between digitonin-treated and untreated cases, indicating that digitonin can not bind to the vesicle membranes (Fig. 3.12a). In the presence of cholesterol, shape and size of vesicles changed with increasing concentration of digitonin, and vesicle size dramatically changed when applying digitonin 100 µM (Figs. 3.12b–d).

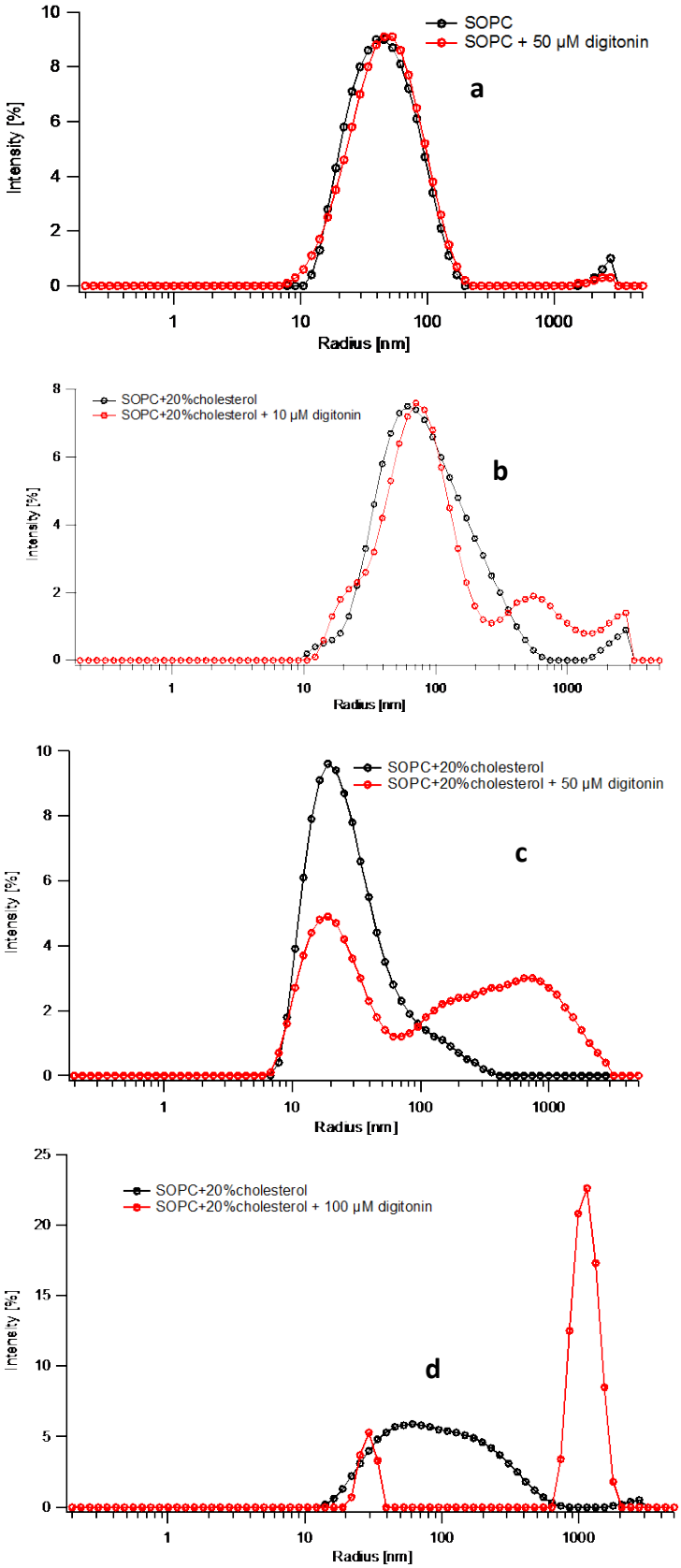

Fig. 3.12. DLS profile of vesicle sizes with and without cholesterol after incubating with different concentrations of digitonin. *Black dotted line* represents control without digitonin and *red dotted line* without digitonin. SOPC vesicles **(a)** no cholesterol + 50 µM digitonin; **(b)** 20% cholesterol + 10 µM digitonin; **(c)** 20% cholesterol + 50 µM digitonin; **(d)** 20% cholesterol + 100 µM digitonin.

3.1.8 Digitonin affects GUV membrane permeability and integrity in the presence of cholesterol

Fluorescence microscopy was employed to further investigate the interaction and permeabilization effect of digitonin on giant unilamellar vesicles (GUV) with a diameter of up to 100 µm. Dil stain was used to mark GUV membranes and Alexa Flour 488 fluorescence for coloring the extravesicular solution of GUVs. Membrane permeabilization was visualized by monitoring the presence of dye inside of GUVs (*black circle*). The kinetics and degree of membrane permeabilization can be quantified for individual vesicles.

PC-GUVs were prepared either with or without cholesterol. The membrane permeabilization effect of digitonin was monitored for 60 min. Figures 3.12 show the effects of digitonin on GUV membranes, without (Figs. 3.13a,b) and with cholesterol (Figs. 3.13c,d); (a) without cholesterol, shortly after adding the drug and (b) same, after 1 h of incubation; here, digitonin apparently cannot permeabilize the GUV membranes as these are still intact and there is no sign of influx through the membrane into the GUVs (*black interior*). (c) However, in the presence of cholesterol, digitonin affects membranes immediately; (d) after 10 min all GUVs were filled with green solution and most membranes were disrupted.

Membrane permeabilization and kinetics can be calculated by comparing the fluorescence intensity inside the individual GUVs with the background in the chosen incubation time. The degree of GUV filling represents the specific interaction between digitonin and the lipid membrane and also can be used to reveal the mechanism of membrane permeabilization. Different concentrations of digitonin were applied to determine their ability to induce membrane permeabilization with and without incorporated cholesterol. The results show that digitonin can induce membrane rupture only in the presence of cholesterol in an all-or-none mechanism and that the concentration greatly affects digitonin's ability to cause membrane disruption (Fig. 3.14).

Without Cholesterol

(a) PC–GUV + 20 µM digitonin, 0 min

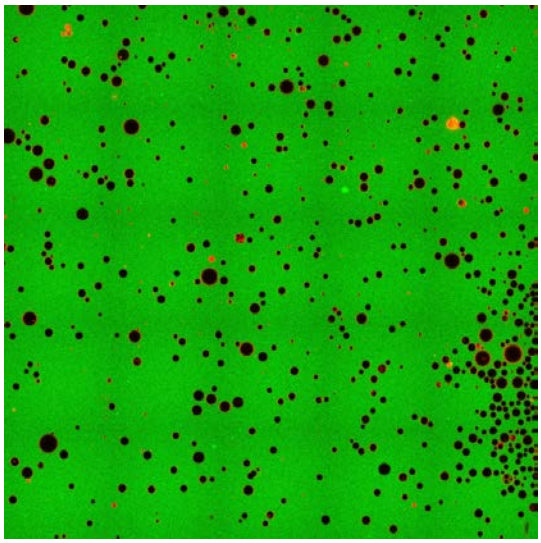

(b) PC–GUV + 20 µM digitonin, 60 min

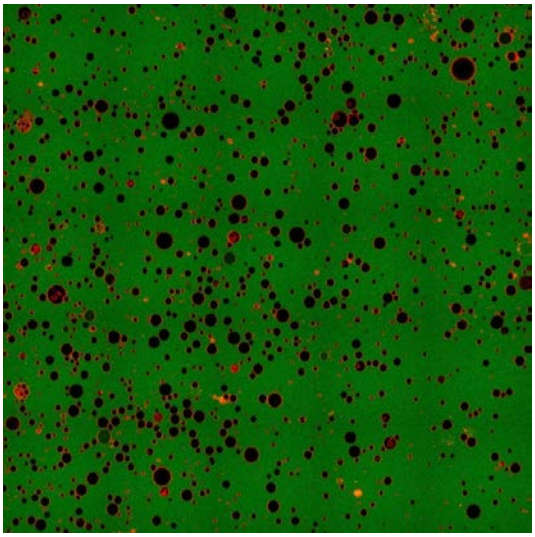

With Cholesterol

(c) PC/Chol (80:20)–GUV + 20 µM digitonin, 0 min

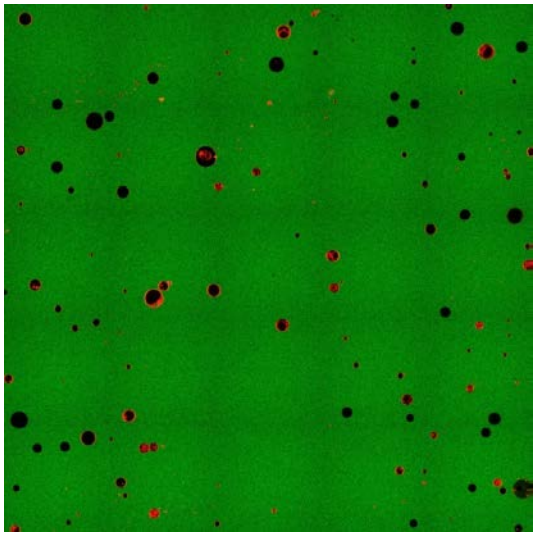

(d) PC/Chol (80:20)–GUV + 20 µM digitonin, 10 min

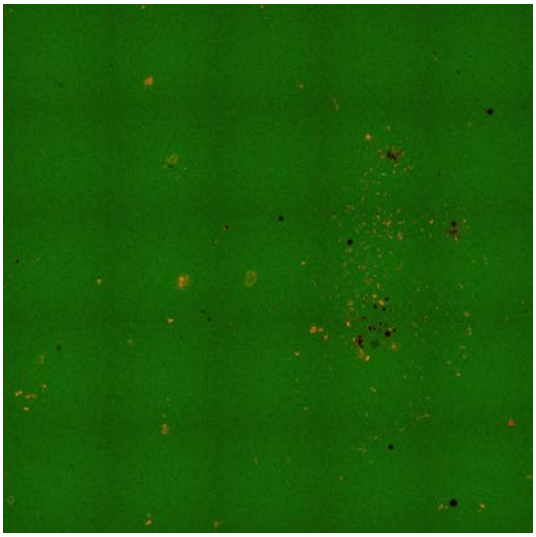

Fig. 3.13. GUV membrane permeabilization by digitonin. **(a)** PC-GUVs shortly after applying 20 µM digitonin, **(b)** PC-GUVs after incubating with 20 µM digitonin for 60 min, **(c)** PC/Chol (80:20) GUVs shortly after applying 20 µM digitonin, **(d)** PC/Chol (80:20) GUVs after incubating with 20 µM digitonin for 10 min. Solution bathing GUVs (*green*), interior of GUVs (*black*), GUV membranes (*red*).

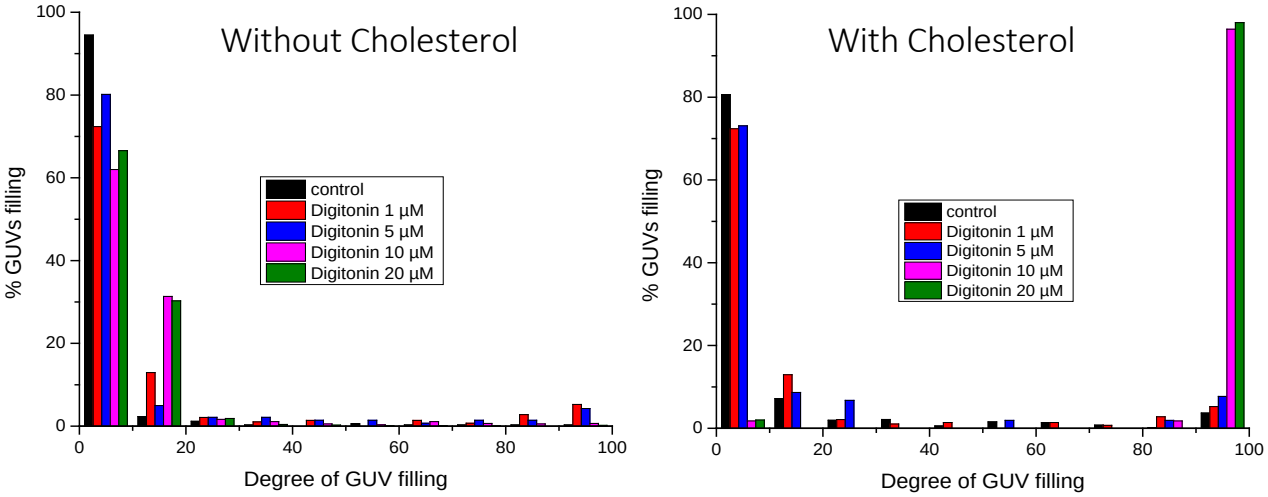

Fig. 3.14. **GUV filling upon incubating GUVs with different concentrations of digitonin. (a)** PC-GUV with digitonin incubation 60 min, **(b)** PC/Chol (80:20)-GUV with digitonin incubation 10 min.

3.1.9 Visualizing the disrupting effect of digitonin on individual PC/Chol (80:20) GUVs

The permeabilization kinetics was quantified by monitoring the permeability of individual GUVs in real time. The images were captured every 20 s for 1 h. The filling rate of PC/Chol-GUVs incubated with digitonin was very fast and most of them were filled after 10 min of incubation. The interaction of digitonin and cholesterol not only caused permeabilization but also led to vesicle rupturing (Fig. 3.15).

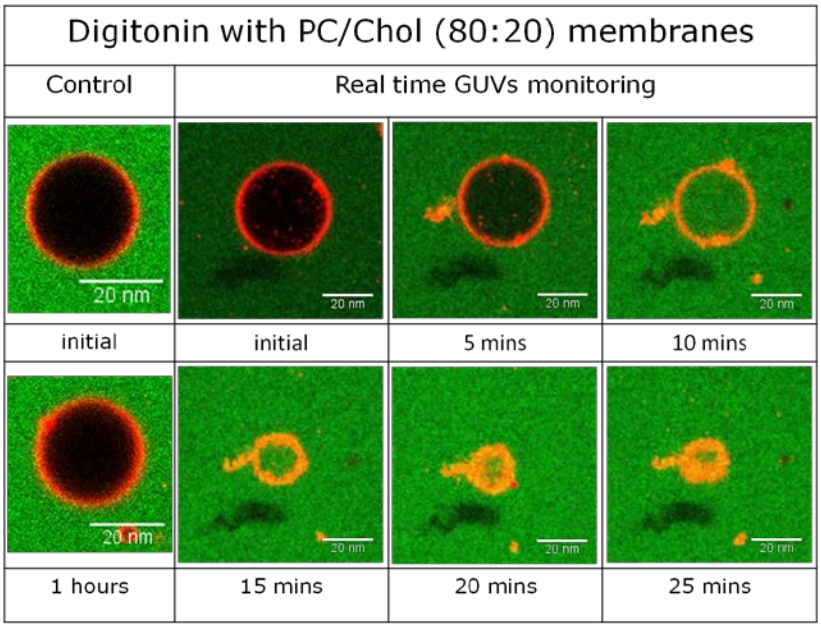

Fig. 3.15. Time dependence of individual PC/Chol (80:20)-GUV response to 20 µM digitonin. *Left images* show GUV without digitonin as a control during the incubation time. The *other images* show time lapse interaction of 20 µM digitonin with PC/Chol (80:20)-GUV. Scale bars 20 nm.

3.1.10 Quantifying structural changes of supported lipid bilayer by digitonin

In order to quantify the interaction of digitonin with cell membranes with and without cholesterol we applied four different techniques: 1) quartz crystal microbalance with dissipation (QCM-D), 2) high-energy specular X-ray reflectivity (XRR), 3) dual polarization interferometry (DPI), and 4) differential scanning calorimeter (DSC).

3.1.10.1 QCM-D

QCM-D provides information about the interaction of digitonin with membranes based on changes in frequency and dissipation. Changes in frequencies give information about mass and thickness of the lipid membrane due to substance adsorption, changes in dissipation indicate structural changes (rigidity) during the interaction.

Supported lipid bilayer (SLB) membranes were constructed by rupturing SOPC and SOPC/Chol (80:20) liposomes on the surface of SiO_2 quartz crystals. The absorption of lipid vesicles on the surface was detected by decrease of frequency to $\Delta f_{SOPC} = -50$ Hz for and $\Delta f_{SOPC/Chol} = -68$ Hz for pure SOPC and SOPC/Chol SLB membrane respectively, coupled with increasing dissipation values to $\Delta D_{SOPC} = 3.7 \times 10^{-6}$ and $\Delta D_{SOPC/Chol} = 4.1 \times 10^{-6}$. When the absorption of lipid vesicles reaches a critical density, they fuse to form planar membranes with release of water from inner space of the vesicles, resulting in increased frequency and decreased dissipation values. A frequency increase to $\Delta f = -26$ Hz and dissipation decrease to $\Delta D = 0.01 \times 10^{-6}$ for both systems, with these values remaining constant for 20 min, indicates the formation of a stable lipid bilayer membrane on the surface of the SiO_2 quartz crystal chip (Keller and Kasemo 1998) (Figs. 3.16a,b).

Digitonin (50 µM) was injected onto both SLB systems. There was no significant change of frequency and dissipation in pure SOPC membrane (Fig. 3.16c) suggesting the SLB membrane remains intact and unaffected in the presence of digitonin. However, applying digitonin onto the SOPC/Chol (80:20) membrane led to a significant decrease in frequency from $\Delta f = -26$ Hz to $\Delta f = \sim -15.5$ Hz and an increase in dissipation from $\Delta D = 0.01 \times 10^{-6}$ to $\Delta D = \sim 5 \times 10^{-6}$ and this value did not return to the initial state after rinsing with PBS buffer (Fig. 3.16d). These data indicate that digitonin permanently binds to cholesterol membranes and that this interaction is irreversible.

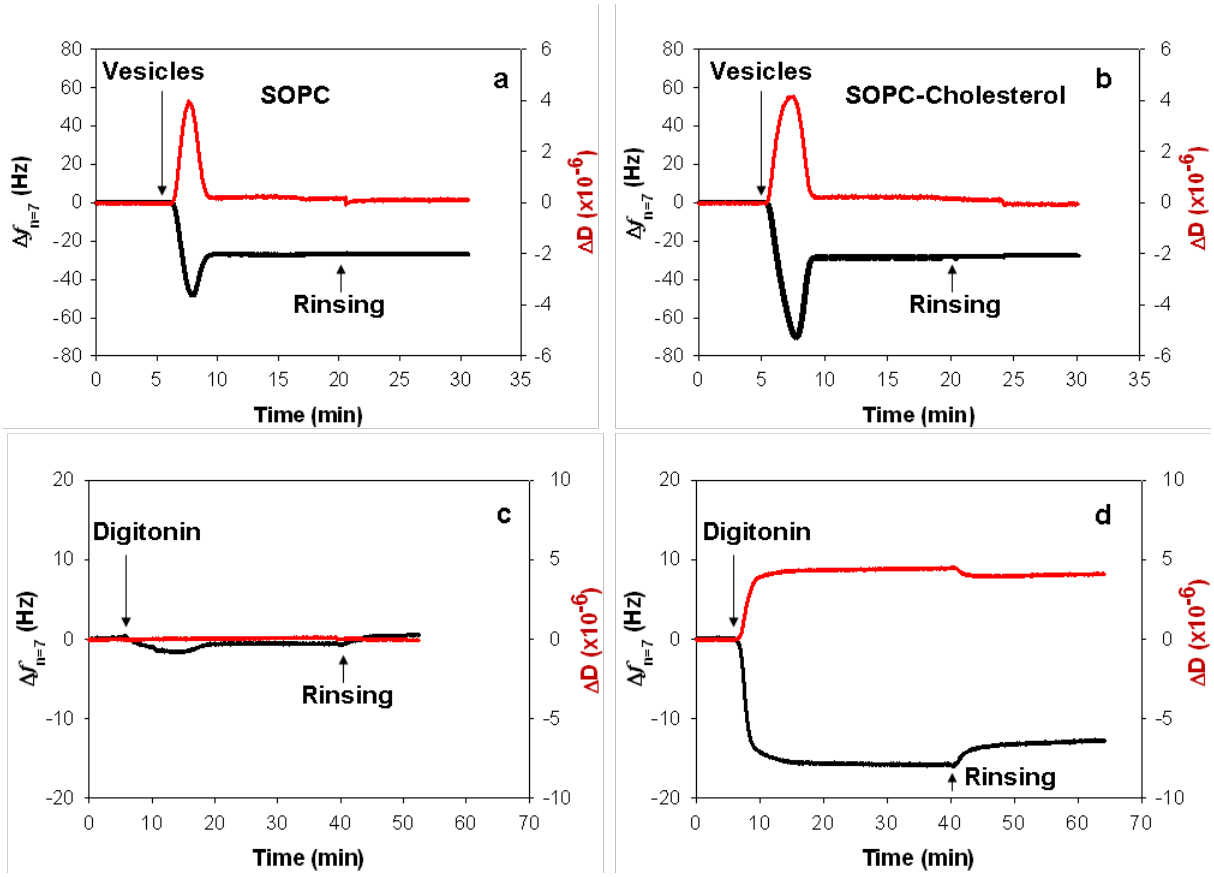

Fig. 3.16. QCM-D response to changes of frequency (Δ*f*) (*black line*) **and dissipation (ΔD)** (*red line*) of SOPC liposomes with time at 35 MHz following the injection of 50 µM digitonin **(a)** SLB formation from SOPC liposomes, **(b)** SLB formation from SOPC/Chol (80:20) liposomes, **(c)** application of digitonin onto SOPC bilayer showsno significant change, **(d)** application of digitonin onto SOPC/Chol bilayer leads to dramatical change in both Δ*f* and Δ*D*. *Arrows* indicate introduction of vesicles and digitonin and rinsings with buffer.

To deeper understand the mode of interaction of digitonin with the cholesterol membrane, the three normalized change overtones (*n* = 3, 5, 7) in frequency (Δ*f)* and dissipation (Δ*D*) were plotted and the results show no overlap, indicating that the absorbed digitonin forms a viscous layer with cholesterol on the membrane significantly altering the its mechanical characteristics. We used the Voigt-Voinova model to describe membrane mechanics with fitted experimental results and the best fit (*black lines*) yielding the change in adsorbed mass, the shear modulus (μ_1), and shear viscosity (η_1) (Fig. 3.17). The measurements and fitting results from three overtones supported the validity of this model of interaction of digitonin with cholesterol membrane with Δm_{QCMD} ~735 ng/cm^2 and density ~1638 kg/m^3 for the digitonin layer. The layer thickness used for the fitting was obtained by X-ray reflectivity measurements and set to be 45 Å for pure SOPC membrane and 47 Å for SOPC/Chol (80:20) membrane (the parameters from the best-fit models are summarize in Table 3.4).

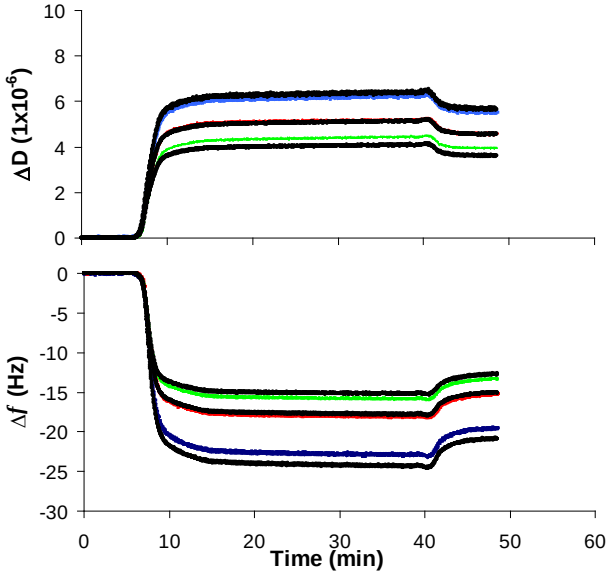

Fig. 3.17. Normalized change in frequency (Δf_n) and dissipation (ΔD) as a function of time, recorded for the three overtones (*blue*: n = 3, *red*: n = 5, and *green*: n = 7; f_0 = 5 MHz). The *black lines* correspond to the best fits based on the Voigt model for the three overtones; $h_0 = 3.34 \times 10^{-4}$ m; ρ_0 = 2650 kg/m^3; ρ_2 = 1000 kg/m^3 and $\eta_2 = 1 \times 10^{-3}$ kg/m.s. T = 25.0 ± 0.1°C.

The shear viscosity of the digitonin layer, being 1.2 mPa·s, is equal to that of water and 10 times lower than that of the supported membranes (>20 mPa·s) (Takagi et al. 1982). This value might be correlated to the hydrating water coupled to the five sugar moieties of digitonin, which was also reported for highly hydrated proteins (Larsson et al. 2003) and DNA (Malmström et al. 2007).

Table 3.4. Model parameters from QCM-D for the supported planar bilayer and the digitonin layer. The layer thickness (d) used for the fit was obtained by X-ray reflectivity measurements and was set at 45 Å and 47 Å for digitonin and SOPC/Chol layers, respectively.

Layer	Δm [ng/cm^2]	d [Å]	ρ [g/cm^3]	η [mPa·s]	μ [kPa]
Digitonin	735 ± 45	45	1.64 ± 0.10	1.1 ± 0.1	70 ± 6
SOPC/Chol	490 (465 ± 20)*	47	1.05	> 10	> 1000

* The mass value within parenthesis refers to the Sauerbrey equation using n =7, i.e., 35 MHz.

3.1.10.2 High-energy specular X-ray reflectivity (XRR)

The model of interaction between digitonin and cholesterol membrane obtained from the previous experiment requires further confirmation by structural data. Therefore, we used high-energy XRR (17.48 keV) at the solid/liquid interface to resolve the fine structure of the supported membranes. This technique provides information on thickness (d), electron density, and root-mean-square roughness (σ) in each region of the membrane, which can be used to deduce characteristic changes in the structure, enabling description of the exact mechanism of the effect of digitonin on the membrane.

Digitonin (50 µM) was applied to solid-supported lipid bilayer with and without cholesterol in the SOPC membrane for 1 h. The curves were fitted with the 5-slab model, having outer headgroups, alkyl chains, inner headgroups, water reservoir, and SiO_2 layer. The best-fit results (*red line*) together with the experimental results (*black line*) were plotted in same curve (Fig. 3.18). In the membrane system without cholesterol, digitonin treatment consistently provided no noticeable change of shape according to the experiment data and fit results (Table 3.5).

However, in presence of cholesterol, digitonin clearly induced membrane alteration, as indicated by a decrease of the SLD value of the outer headgroup layer from 11.9×10^{-6} Å^{-2} to 9.1×10^{-6} Å^{-2} and also the SLD value of the alkyl chains layer from 7.3×10^{-6} Å^{-2} to 6.8×10^{-6} Å^{-2}, suggesting that digitonin does not only adsorb on the membrane surface, but also removes some molecules from the membrane. This condition appears to be caused by complex formation of digitonin-cholesterol (Nishikawa et al. 1984). The thickness of the digitonin layer (d ~45 Å) roughly corresponds to the double of the molecular length of the digitonin molecule (l ~20 Å), and its high SLD value (7.4×10^{-6} Å^{-2}) suggests that this layer consists of dense aggregates of sterol and aglycone. The other fact was that the formation of a digitonin layer possessing a roughness of σ ~6 Å causes no significant change in the roughness of the other interfaces. Our fine-structural analysis has demonstrated for the first time that digitonin does not destroy the structural integrity of membranes, which is in a clear contrast to the previous studies suggesting the destruction of membranes by the formation of defects or surface micelles (Nishikawa et al. 1984; Gögelein and Hüby 1984). New features observed at q_z <0.1 Å^{-1} can better be interpreted as the formation of an "additional layer (slab)", rather than assuming the structural change of the existing membrane (Table 3.6).

Table 3.5. XRR best-fit parameters ($\chi^2 \leq 0.05$) for a pure SOPC membrane (see Fig. 3.18a) in the absence and presence of 50 µM digitonin.

	Without digitonin			**With digitonin**		
SOPC	***d* [Å]**	**SLD [10^{-6} Å^{-2}]**	**σ [Å]**	***d* [Å]**	**SLD [10^{-6} Å^{-2}]**	**σ [Å]**
Outer headgroup	10.6	11.8	4.5	10.9	11.9	4.9
Alkyl chain	24.6	7.4	3.8	23.8	7.3	3.9
Inner headgroup	9.1	11.6	3.3	9.3	11.9	3.9
Water	3.1	9.4	3.5	3.3	9.4	3.4
SiO_2	10.1	18.6	3.1	10.1	18.6	3.4

d = thickness, σ = roughness, SLD = scattering length density

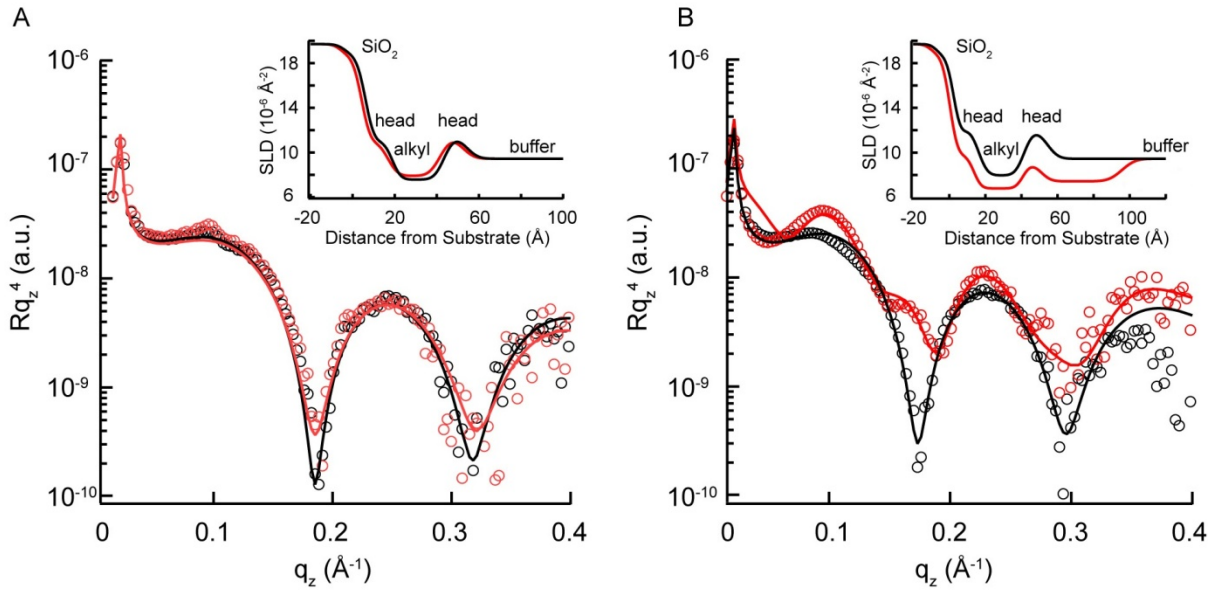

Fig. 3.18. High-energy specular X-ray reflectivity (XRR) spectra showing the fine structure of supported membranes. **(a)** Pure SOPC membrane in the absence (*black*) and presence (*red*) of 50 µM digitonin. **(b)** SOPC membrane incorporating 20 mol% cholesterol in the absence (*black*) and presence (*red*) of 50 µM digitonin. The experimental errors are within the symbol size. The *solid lines* represent the best model fits to the data.

Table 3.6. XRR best-fit parameters ($\chi^2 \leq 0.02$) for SOPC/Chol membrane incorporating 20 mol% cholesterol (see Fig. 3.17b) in the absence and presence of 50 µM digitonin.

	Without digitonin			**With digitonin**		
SOPC/Chol	***d* [Å]**	**SLD [10^{-6} Å^{-2}]**	**σ [Å]**	***d* [Å]**	**SLD [10^{-6} Å^{-2}]**	**σ [Å]**
Digitonin	–	–	–	44.8	7.4	5.9
Outer headgroup	12.9	11.9	4.1	10.1	9.1	4.2
Alkyl chain	25.6	8.0	3.9	27.3	6.8	3.4
Inner headgroup	10.1	11.8	3.9	10.1	9.7	3.2
Water	3.1	9.4	3.3	3.3	9.4	3.4
SiO_2	10.1	18.6	3.4	10.1	18.6	3.4

d = thickness, σ= roughness, SLD = scattering length density

3.1.10.3 Dual polarization interferometry (DPI)

The conformational changes occurring during interaction of digitonin with the cholesterol membrane were analyzed in real time using dual polarization interferometry (DPI). DPI monitors changes in thickness, refractive index, mass, and birefringence of thin films during adsorption of digitonin onto the lipid membrane. Diverse information on membrane conformations has been provided by previous measurements, such as change in mass by QCM-D and membrane thickness by XRR, but DPI can provide the birefringence value $\Delta n = n_0 - ne$, which differs from the ordinary and extraordinary refractive indices. For understanding supported membranes, birefringence (Δn) data can offer a perspective on the ordering of alkyl chains (Mashaghi et al. 2008; Lee et al. 2010).

Real-time monitoring phase changes in TM and TE wave guide $\Delta\Phi_{TM}$ (*black*) and $\Delta\Phi_{TE}$ (*green*) during formation of a pure SOPC and SOPC/Chol (80:20) membrane are shown in Fig. 3.18. An increase in phase ($\Delta\Phi^{SOPC}_{TM}$ ~14 rads, $\Delta\Phi^{SOPC}_{TE}$ ~11 rads and $\Delta\Phi^{SOPC\text{-}Chol}_{TM}$ ~13 rads, $\Delta\Phi^{SOPC\text{-}Chol}_{TE}$ ~9 rads) suggests the formation of a supported lipid bilayer (Mashaghi et al. 2008; Lee et al. 2010). Membranes with cholesterol present slightly different parameters from pure SOPC membranes, which can be related to the fact that alkyl chains assume a liquid ordered phase in the presence of cholesterol (Figs. 3.19a,b).

The 50 µM digitonin solution was applied to the pure SOPC membrane causing a slight change in phase, but the signal returned to the initial level after rinsing with PBS buffer ($\Delta\Phi^{SOPC}$ ~0.1 rads). This suggests that the pure SOPC membrane remained intact in the presence of 50 µM digitonin (Fig. 3.19c) and this seems consistent with previous measurements (calcein leakage, permeability GUV, QCM-D, XRR). Otherwise in the SOPC/Chol (80:20) membrane, the presence of 50 µM digitonin caused an obvious change in membrane phase. The final phase shifting after rinsing with PBS buffer ($\Delta\Phi^{SOPC\text{-}Chol}_{TM}$ ~2.7 rads, $\Delta\Phi^{SOPC\text{-}Chol}_{TE}$ ~2.5 rads) was higher than the initial value (Fig. 3.19d).

The best parameters from DPI measurement for the SOPC/Chol (80:20) membrane with and without applied digitonin are presented in Table 3.7. To obtain the structural parameters of the layer prior to the injection of digitonin, the thickness of the lipid membrane was fixed at d = 47 ± 2 Å, taking the value obtained by XRR. We found that the injection of digitonin led to a significant increase in the mass (Δm_{DPI} = 70 ± 7 ng/cm^2) as well as the average density ($\Delta\rho$ = 0.15 ± 0.01 g/cm^3). Taking Δm obtained by QCM-D (Δm_{QCMD} = 685 ± 47 ng/cm^2), the fraction of the hydrating water H (in wt%) can be calculated as:

$$H = \frac{m_{\text{water}}}{m_{\text{acoustic}}} = \frac{m_{\text{QCM-D}} - m_{\text{DPI}}}{m_{\text{QCM-D}}} \times 100 \approx 90 \text{ wt \%}$$

This result seems to be consistent with the shear viscosity and shear modulus values, which are close to those of water (Table 3.4).

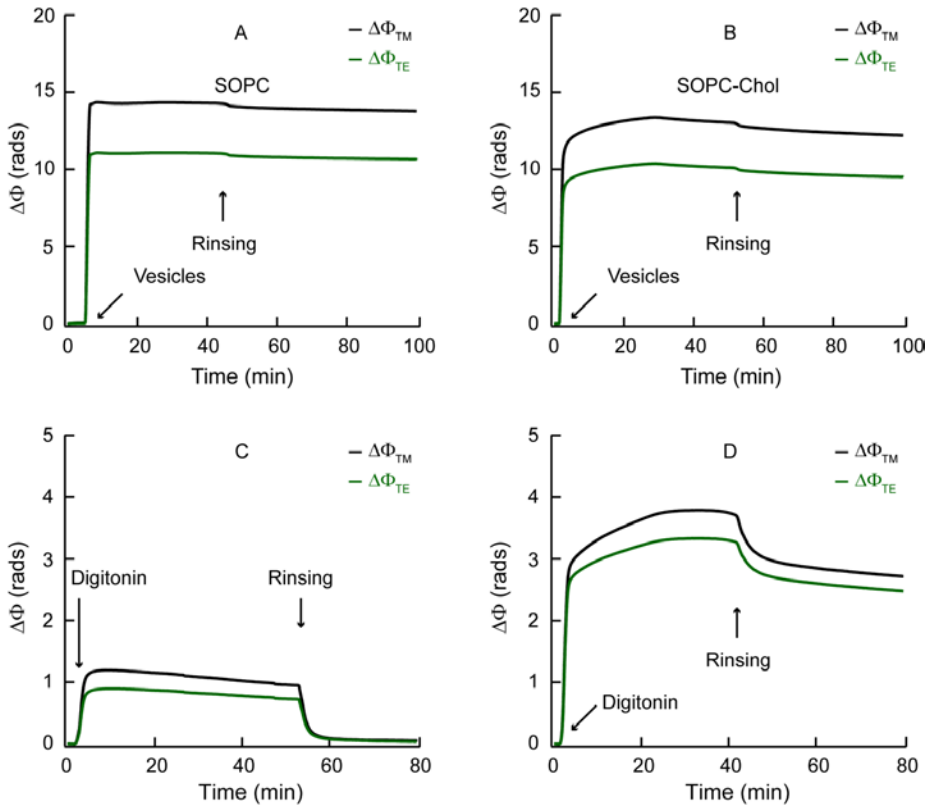

Fig. 3.19. Real-time phase changes of SLBs in TM and TE waveguide mode $\Delta\Phi_{TM}$ (*black*) and $\Delta\Phi_{TE}$ (*green*) of **(a)** a pure SOPC membrane and **(b)** a SOPC/Chol membrane prior to the incubation with digitonin, confirming the formation of supported membranes. **(c)** The injection of 50 µM digitonin resulted in a minor phase shift in the case of pure SOPC membrane, **(d)** while the membrane with cholesterol exhibited a pronounced phase shift even after rigorous rinsing.

Table 3.7. DPI best-fit parameters for SOPC/Chol (80:20) membranes in the absence and presence of 50 µM digitonin. A constant thickness obtained from XRR was taken for the calculation.

Layer	RI	*d* (Å)	Birefringence	Δm_{DPI} (ng/cm^2)	$\Delta\rho$ (g/cm^3)
Digitonin	1.36	45	0	70 ± 7	0.15 ± 0.01
SOPC/Chol	1.45	47	0.01	377 ± 5	0.80 ± 0.01

3.1.10.4 Differential scanning calorimeter (DSC)

XRR measurements have shown that digitonin does not only absorb onto the membrane surface but also removes cholesterol from the membrane core, as shown by a decreased SLD value of alkyl chains during contact with digitonin. However, it is technically almost impossible to quantitatively assess the significance of digitonin-cholesterol interactions. For this purpose, we used differential scanning calorimeter (DSC) to investigate thermotropic phase diagrams of the membrane in the

presence of cholesterol and digitonin. Figure 3.20 presents DSC scans of SOPC membranes incorporating (a) 0 mol%, (b) 5 mol%, and (c) 20 mol% of cholesterol in the absence (*black line*) and presence (*red line*) of digitonin 50 μM.

Figure 3.20a confirms the fact that digitonin specifically only interacts with cholesterol in the membrane. The DSC scan of pure SOPC membrane (*black line*) shows a very sharp endothermic peak at T_m = 6.0°C and ΔH = 3.9 kcal/mol, corresponding to the main thermotropic transition from the gel phase to the liquid crystalline phase. In the presence of digitonin (*red line*) the transition temperature remains almost identical but the onset of the phase transition appears at a slightly lower temperature. Nevertheless, the broadening of the transition peak and the decrease in the transition enthalpy remained below 6%, suggesting that the pure SOPC membranes remain almost intact in the presence of 50 μM digitonin.

However, in the case of liposomes containing cholesterol, the thermal behavior of the mixtures was significantly affected by the addition of digitonin. The membrane containing 5 mol% cholesterol showed a peak at 4.8°C accompanied by a subpeak (shoulder) at around 6.0°C and the transition enthalpy decreased to $\Delta H = \int C_p dT$ = 3.9 kcal/mol which relates to partial mixing of SOPC and substitutional impurity (cholesterol). The major peak at 4.8°C coincides with the transition of SOPC/Chol and the peak at 6.0°C with the transition of SOPC. The presence of 5 μM digitonin resulted in significant change in the weight balance between these two peaks, whereas the first peak (4.8°C) decreases and the second peak (6.0°C) becomes sharper. This means an increase in the ratio of pure SOPC fraction, while a decrease in the ratio of the SOPC/Chol complex fraction. The enhancement level ratio of pure SOPC fraction was caused by partial removal of cholesterol by digitonin from the SOPC/Chol membrane (Fig. 3.20b).

The incorporation of cholesterol into SOPC bilayer at 20% (mol%) suppressed the phase transition of SOPC (Fig. 3.20c) which caused the endothermic peak to become diminished due to the formation of another monophase, called the liquid-ordered phase, where alkyl chains are ordered but do not take all-*trans* conformation because cholesterol acts as a substitutional impurity (Cevc 1993). Interestingly, in the presence of 50 μM digitonin, the endothermic peak appears at 5.4°C, called “recovery” peak. The emergence of a “recovery” peak can be explained as displacement of cholesterol molecules by digitonin from the SOPC membrane with leads to an increasing level of the pure SOPC fraction as detected by a peak at around 6°C.

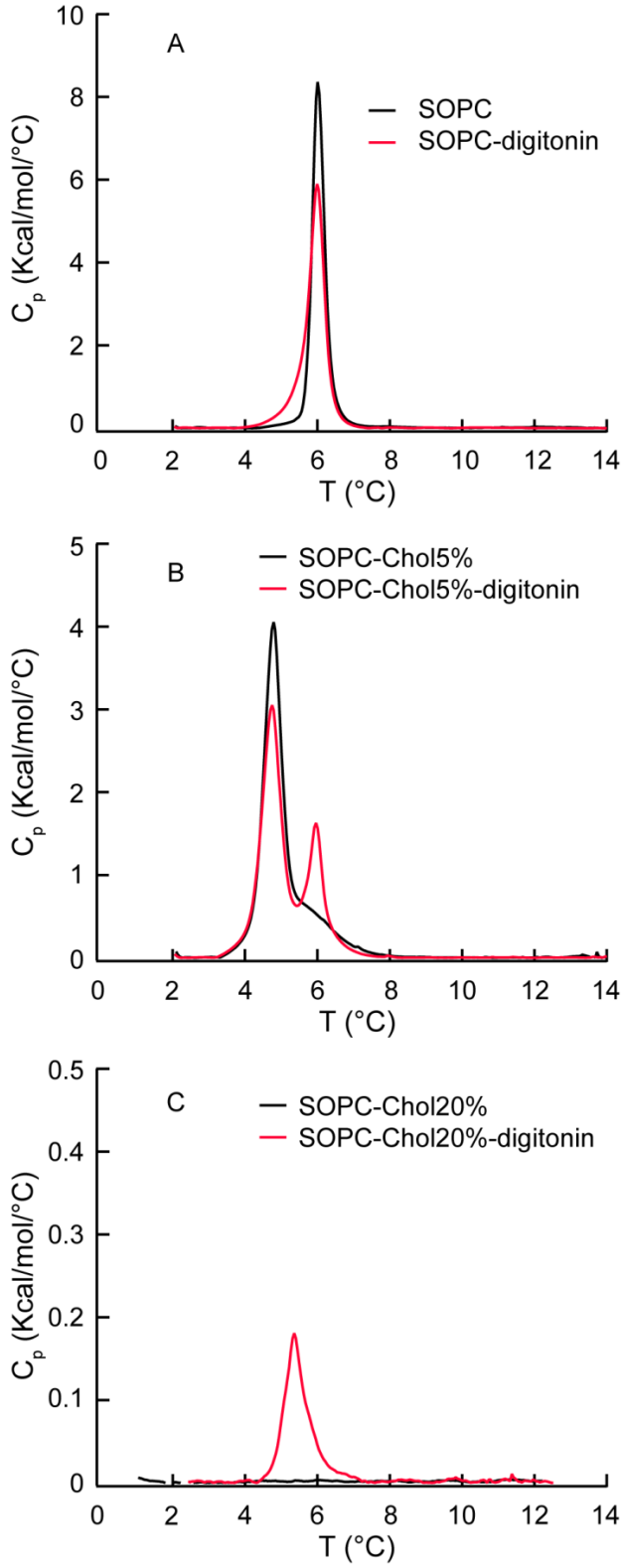

Fig. 3.20. DSC scans of SOPC liposomes with **(a)** 0 mol%, **(b)** 5 mol%, **(c)** and 20 mol% cholesterol in the absence (*black line*) and presence (*red line*) of 50 µM digitonin.

3.2 Quillaja saponin as a drug toxicity enhancer – mechanistic investigations with membrane models

3.2.1 Bidesmosides and monodesmosides in commercial quillaja saponin extract

Commercial quillaja saponin (DAB, Carl Roth, Karlsruhe) was submitted to HPLC and LC/MS to identify and quantify the saponins contained in the extract. The peak pattern of the HPLC was revealed to be similar to data reported in the literature (Kensil et al. 1991; San Martín and Briones 2000; Thalhamer and Himmelsbach 2014). The typical chromatographic peak pattern of the quillaja saponin extract starts at approximately RT 20 min, with numerous peaks up to 40 min. An intense peak that is not related to quillaja saponin was recorded at RT 5–20 min. The chromatogram intensity within the quillaja saponin retention time area (20–40 min) was lower than the intensity of the non-quillaja saponin area (5–20 min), which indicates that the amount of quillaja saponin in the extract was low. The HPLC peaks were identified using MS, as comparative individual standards of quillaja saponin compounds are not available (Fig. 3.21).

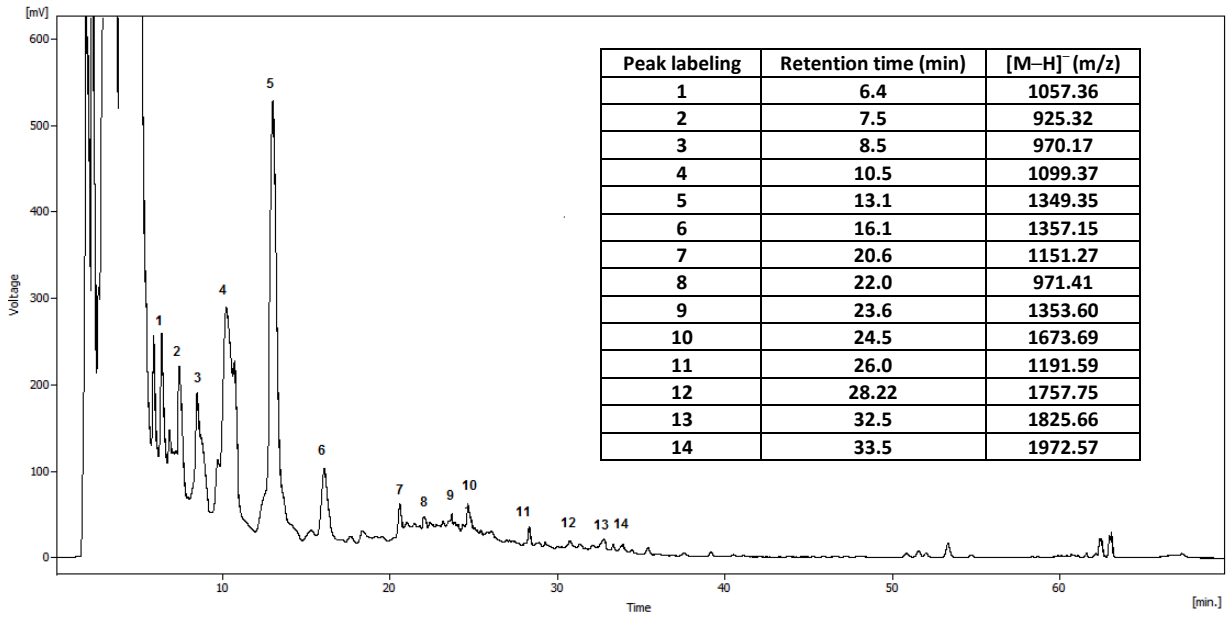

Peak labeling	Retention time (min)	$[M–H]^-$ (m/z)
1	6.4	1057.36
2	7.5	925.32
3	8.5	970.17
4	10.5	1099.37
5	13.1	1349.35
6	16.1	1357.15
7	20.6	1151.27
8	22.0	971.41
9	23.6	1353.60
10	24.5	1673.69
11	26.0	1191.59
12	28.22	1757.75
13	32.5	1825.66
14	33.5	1972.57

Fig. 3.21. Quillaja saponin – HPLC chromatogram with $[M–H]^-$ (m/z) values (*insert*).

LC/MS was applied to identify the individual saponins from the complex mixture of the above commercial quillaja saponin extract. The LC system was run similarly as applied for HPLC. Ions were detected in negative and positive modes. The negative mode showed better detection and fragmentation than the positive mode. The total ion current (TIC) run showed an opposite pattern with significantly higher intensity of the quillaja saponin than the non-quillaja saponin area (Fig. 3.22).

This result indicates that most of the quillaja saponin compounds are weak chromophores that can not be detected by ultraviolet (UV) (Kite et al. 2004).

In order to trace and identify the type of saponins inside the quillaja extract, Xcalibur 2.0 software was used to identify and calculate the molecular formula for each distinctive peak from all regions and the according MS2 spectra were analyzed if available. The MS spectra of quillaja saponin extract bear characteristic ions in the region 800–1000 m/z, here referred to as "A ions", that result from fragmentation of bidesmosides from which the oligosaccharide chain at C28 has been cleaved. The A ions represent the triterpenoid aglycone with a trisaccharide sugar attached to C3 with a varying R^0 component (Fig. 1.3). The quillaic aglycone is represented by the A ion at m/z 955 or 969, pointing to the occurrence of quillaic acid (Q) and a Xyl or Rha at R^0 position. The A ion at m/z 971 or 985 (or 62 less on occasion, 909 or 923, indicating further loss of H_2O and a carboxyl residue at C28), indicates 22β-hydroxyquillaic acid (Q-OH) as the aglycone. The A ion at m/z 853 points to phytolaccinic acid (P) and 895 represents O-23 acetylated phytolaccinic acid (P-Ac) (Wang et al. 2008; Kite et al. 2004; Bankefors et al. 2011). There were some other ion products with m/z values higher than 1100 which do not have A ions of quillaja aglycones but representing the mere quillaic acid ion at m/z 485 or 483 resulting from MS2 fragmentation of the 1560.19 precursor at RT 41.10 min. Each m/z peak from MS1 and MS2 was compared with the literature and the complete list mass data of the commercial quillaja extract is presented in the Appendix (p. 125) of this dissertation. In order to identify the presence of monodesmosidic saponins in the extract, the ions with m/z below 1000 in the MS1 and MS2 spectra were analyzed in more detail to identify the according precursors. Precursors lower than 1000 are assumed to originate from actual monodesmosides and not fragmentation products of bidesmosides.

The complete analysis of ions from the MS1 and MS2 spectra of the employed quillaja saponin extract shows that the majority of saponins contained are triterpenoid bidesmosides (>95%) and approx. 5% monodesmosides. The previously reported triterpenoid bidesmosides identified in our studies are listed in Table 3.8. The monodesmosides now being reported for the first time from commercial quillaja saponin (DAB, Carl Roth, Karlsruhe) are listed in Table 3.9. In total, 19 monodesmosides were identified, with five compounds in the quillaja saponin retention time area and the others in the non-quillaja saponin area. The MS2 fragmentation data show that the precursors originate from monodesmosides with m/z values of less than 1000.

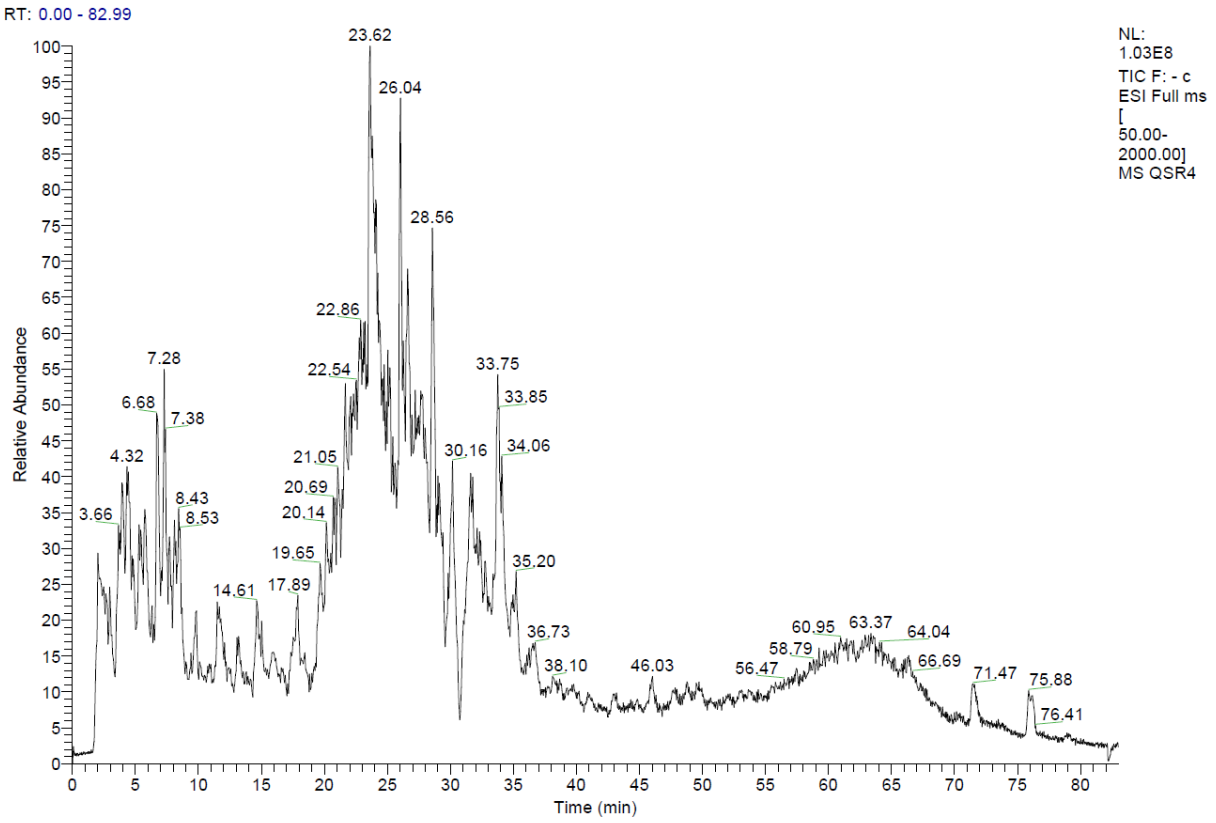

Fig. 3.22. Quillaja saponin – mass spectrometry. Total ion current (TIC) chromatogram from RT 0–80 min.

Table 3.8. Triterpenoid bidesmosidic saponins in commercial quillaja saponin extract (DAB, Carl Roth)

RT sample (min)	$[M–H]^-$ (m/z)	A ion (m/z)	Aglycone	Substituents					
				R^0	R^1	R^2	R^3	Fa	Ac
24.52	1674.71	955	Q	p	p-p	h			
25.6	1511.63	955	Q	p	p-p				
25.77	1565.71	939							
26.99	1861.8	955	Q	p	p-p	h	dh		1
27.09	1716.83	955	Q	p	p-p	h			1
27.14	1716.07	955	Q	p	p-p	h			1
27.49	1699.58	955	Q	p	p-p		dh		1
27.65	1773.6	971	Q-OH	p	p-p	h			2
28.22	1757.75	955	Q	p	p-p	h			2
28.28	1553.56	955	Q	p	p-p				1
28.96	1903.56	955	Q	p	p-p	h	dh		2
29.12	1475.75	895	P-Ac			h			3
29.3	1948.72	955	Q	p	p-p	h	dh		a
29.88	1683.63	955	Q	p	p-p			Fa/2	
30.16	1475.65	895	P-Ac			h			3
30.16	1757.71	955	Q	p	p	h	h		2
30.38	1871.71	955	Q	p	p-p			Fa-OH	
30.92	1987.84	955	Q	p	p-p			Fa-p	
31.6	1476.63	895	P-Ac			h			3
31.71	1856.75	955	Q		p-p			Fa-p	
31.91	1987.87	955	Q	p	p-p			Fa-p	
32.51	1897.74	955	Q	p	p-p			Fa	1
33.7	1559.68	895	P-Ac			h			5
34.54	1580.64	939	deOH Q	p	p-p				2
35.2	1559.73	895	P-Ac			h			5

Aglycones:

- P = phytolaccinic acid
- P-Ac = phytolaccinic acid acetylated at O-23
- Q = quillaic acid
- Q-OH = 22β-hydroxyquillaic acid
- deOH = dehydroxy quillaic acid

Substituents:

- p = pentose
- h = hexose
- dh = deoxyhexose
- Fa = fatty acyl
- Ac = acetyl

Table 3.9. **Monodesmosidic saponins in commercial quillaja saponin extract**

RT sample (min)	$[M–H]^-$ (m/z)	MS2	Precursor	Relative percentage in sample
2.95	780.82	311.13; 405.00; 466.61; 536.08; 602.02; 688.49; 720.06		1.016
16.17	745.12	373.24; 457.02; 599.13; 640.91		0.836
22.48	639.29	231.17; 325.21; 467.25; 509.23; 621.23		9.478
28.85	711.36	665.34; 711.20		5.441
29.4	793.42	306.93; 405.58; 485.42; 513.38; 567.39; 661.39; 731.47; 770.76		3.298
43.09	553.25	485.41; 523.36; 552.59		0.316
43.59	649.11	405.31; 477.08; 581.08; 605.07; 649.23; 695.92; 871.05	871.11	0.576
47.92	539.41	471.36; 492.91; 574.62; 963.43	963.43	0.343
49.5	607.19	539.40; 589.28; 715.77		0.485
62.77	757.45	349.94; 462.16; 699.19; 711.12; 739.29; 756.40; 774.52		0.758
62.84	731.43	269.21; 307.30; 390.88; 494.19; 575.53; 713.30; 730.41		0.620
62.95	593.4	187.15; 200.92; 337.02; 423.14; 524.98; 593.41		0.681
63.8	761.42	305.01; 337.48; 390.81; 466.20; 649.22; 661.02; 761.30		0.602
64.63	691.42	285.15; 413.20; 533.39; 601.16; 672.23; 691.52; 828.29	828.29	0.653
64.93	726.56	243.81; 311.21; 446.96; 465.25; 584.31; 690.51; 796.57	796.57	0.426
65.11	727.21	264.22; 463.47; 584.26; 699.65		0.498
66.36	593.38	187.08; 201.18; 337.09; 423.21; 593.37; 611.06; 812.09; 970.90	970.90	0.603
66.57	693.39	277.37; 413.18; 519.28; 665.47; 692.61; 892.81	892.81	0.538
66.63	745.57	236.17; 260.13; 335.61; 422.92; 489.31; 505.01; 727.33, 745.81		0.485

3.2.2 Quillaja saponin enhances the toxicity of five common anticancer drugs

The activity of quillaja saponin as a toxicity enhancer for berberine, cisplatin, dexamethasone, doxorubicin, and mitomycin C was explored in HeLa, COS-7, MIA PaCa-2, and PANC-1 cancer cell lines by the same procedure as for digitonin. Cell viability was measured by MTT assay.

Cytotoxicity data was obtained for quillaja saponin alone and in combination with the five selected anticancer drugs applied to four cancer cell lines (Fig. 3.23 and Table 3.10.). The IC_{50} values of quillaja saponin for all four cancer cell lines range around 100 µg/ml; the IC_{50} values of the employed anticancer agents are listed in Table 3.1. Quillaja saponin increased the cytotoxicity by each of the selected anticancer drugs on all of the cancer cell lines (Fig. 3.24). Quillaja saponin enhances the toxicity of cisplatin in HeLa, COS-7, and MIA PaCa-2 with CER values of 8.24, 4.37, 5.2, respectively, but only slightly increases toxicity of cisplatin in PANC-1 with a CER value of 1.3. The toxicity of mitomycin C also significantly increased in combination with quillaja saponin, CER values for HeLa, COS-7, MIA PaCa-2, and PANC-1 being 7.69, 7.18, 2.55, and 1.7, respectively. For doxorubicin the highest toxicity was measured in MIA PaCa-2 with CER increasing to 6.95, continued by PANC-1, COS-7, and HeLa with CERs of 3.36, 3.26, to 1.7, respectively. The cytotoxicity of berberine was only slightly increased by quillaja saponin with a CER of max. 2.92 in COS-7.

The obtained combination index (CI) values show that cisplatin with quillaja saponin has a synergistic effect on HeLa, COS-7, and MIA PaCa-2; for doxorubicin we find synergistic effects in all tested cell lines; mitomycin C has a synergistic effect on HeLa, COS-7, and MIA PaCa-2; and berberine has a synergistic effect only on COS-7; other combinations showed antagonistic effects (Fig. 3.25).

Table 3.10. Quillaja saponin alone and in combination with anticancer drugs – effects on HeLa, COS-7, MIA PaCa-2, and PANC-1.

	IC_{50} (µM) of anticancer agents + IC_{20} (µM) of quillaja saponin											
	HeLa	**CI**	**CER**	**COS-7**	**CI**	**CER**	**MIA PaCa-2**	**CI**	**CER**	**PANC-1**	**CI**	**CER**
Saponins												
Quillaja saponin (IC_{50})	103.95±9.91			105.80±26.62			109.49±9.10			98.21±11.57		
Quillaja saponin (IC_{20})	35			44			66			68		
Drug												
Berberine	260±0.03	1.10	1.29	174±0.04	0.75	2.92	73.00±0.09	1.30	1.41	61.30±0.1	1.07	2.62
Cisplatin	2.21±1.85	0.45	8.24	6.95±3.61	0.63	4.37	18.06±0.01	0.79	5.20	76.53±0.01	1.46	1.30
Doxorubicin	4.64±0.16	0.91	1.70	3.80±0.78	0.70	3.36	3.01±2.74	0.74	6.95	17.80±1.80	0.99	3.26
Dexamethasone	298.8±0.04	1.39	0.99	216.8±0.10	1.04	1.57	904.5±1.61	1.54	1.06	301.11±0.04	1.03	4.01
Mitomycin C	12.27±11.5	0.45	7.69	19.07±5.02	0.54	7.18	9.50±0.02	0.99	2.55	22.33±0.5	1.27	1.70

(a) HeLa

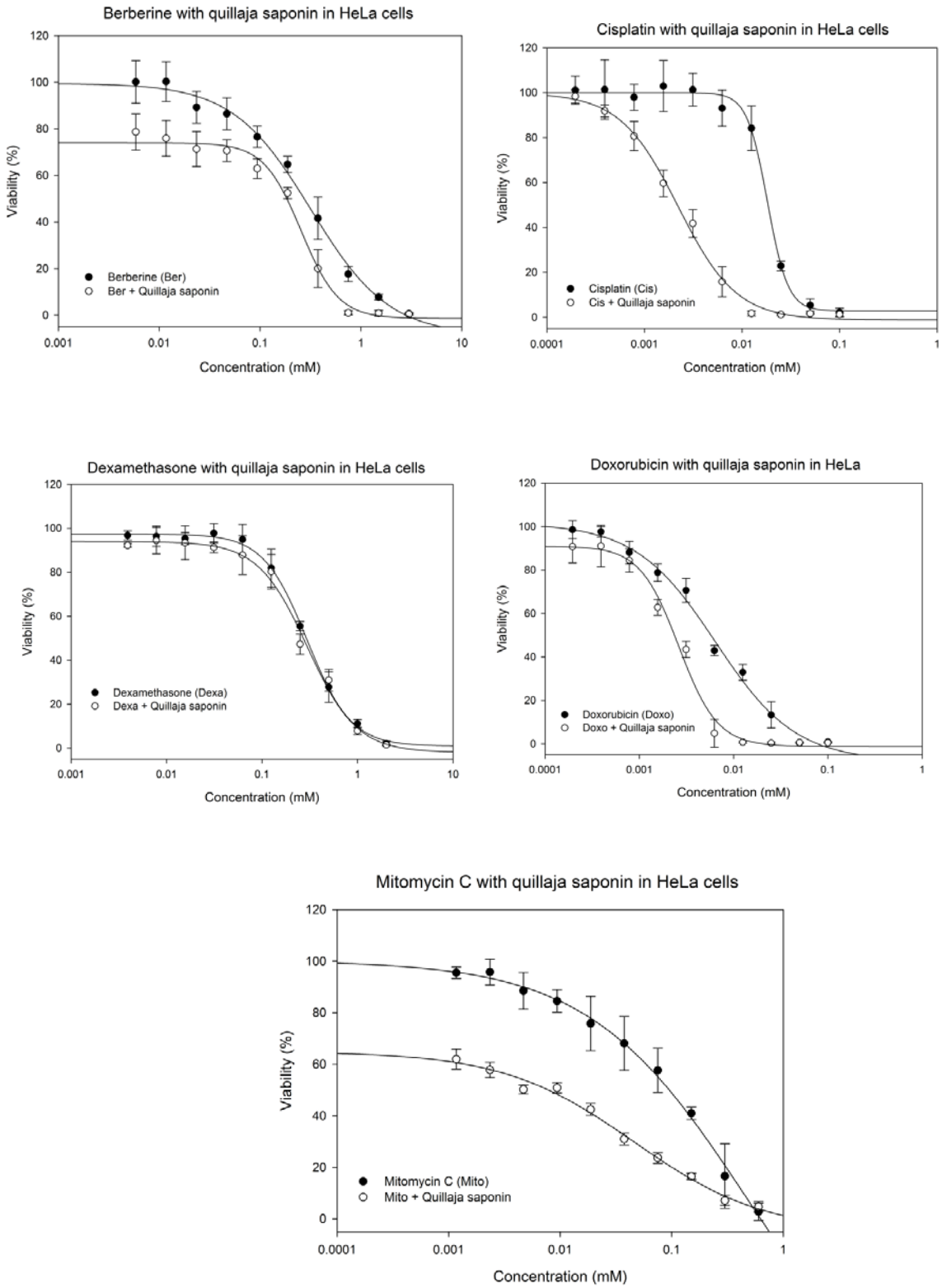

Fig. 3.23a. Dose response curves in HeLa to the anticancer agents berberine, cisplatin, dexamethasone, doxorubicin, and mitomycin C (*black data points*) and their combination with IC_{20} concentrations of quillaja saponin (35 µg/ml) (*white data points*). Data are expressed as means ±SD of cell viability from three independent experiments, each done in triplicates.

(b) COS-7

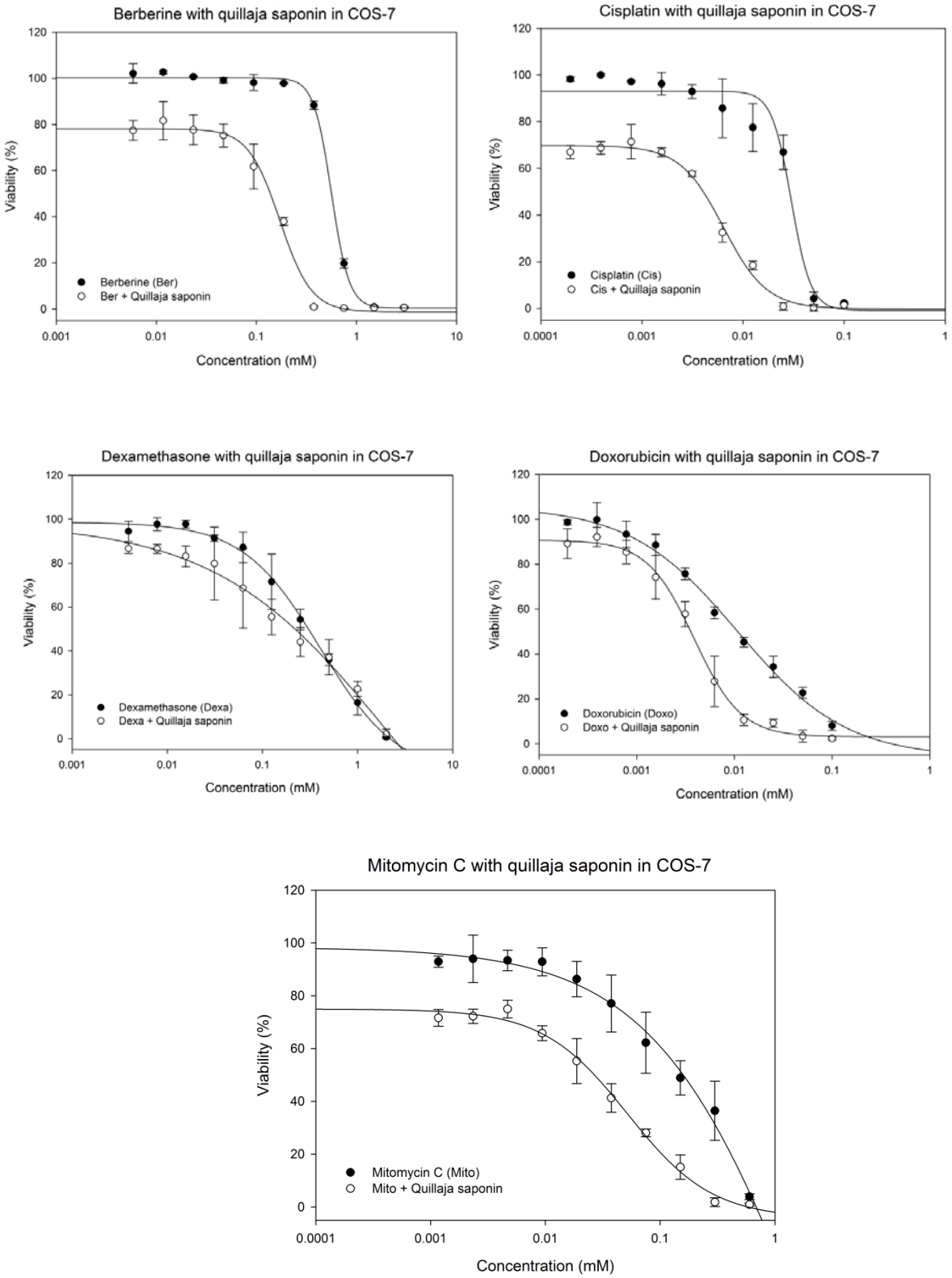

Fig. 3.23b. Dose response curves in COS-7 to the anticancer agents berberine, cisplatin, dexamethasone, doxorubicin, and mitomycin C (*black data points*) and their combination with IC_{20} concentrations of quillaja saponin (44 µg/ml) (*white data points*). Data are expressed as means ±SD of cell viability from three independent experiments, each done in triplicates.

(c) MIA PaCa-2

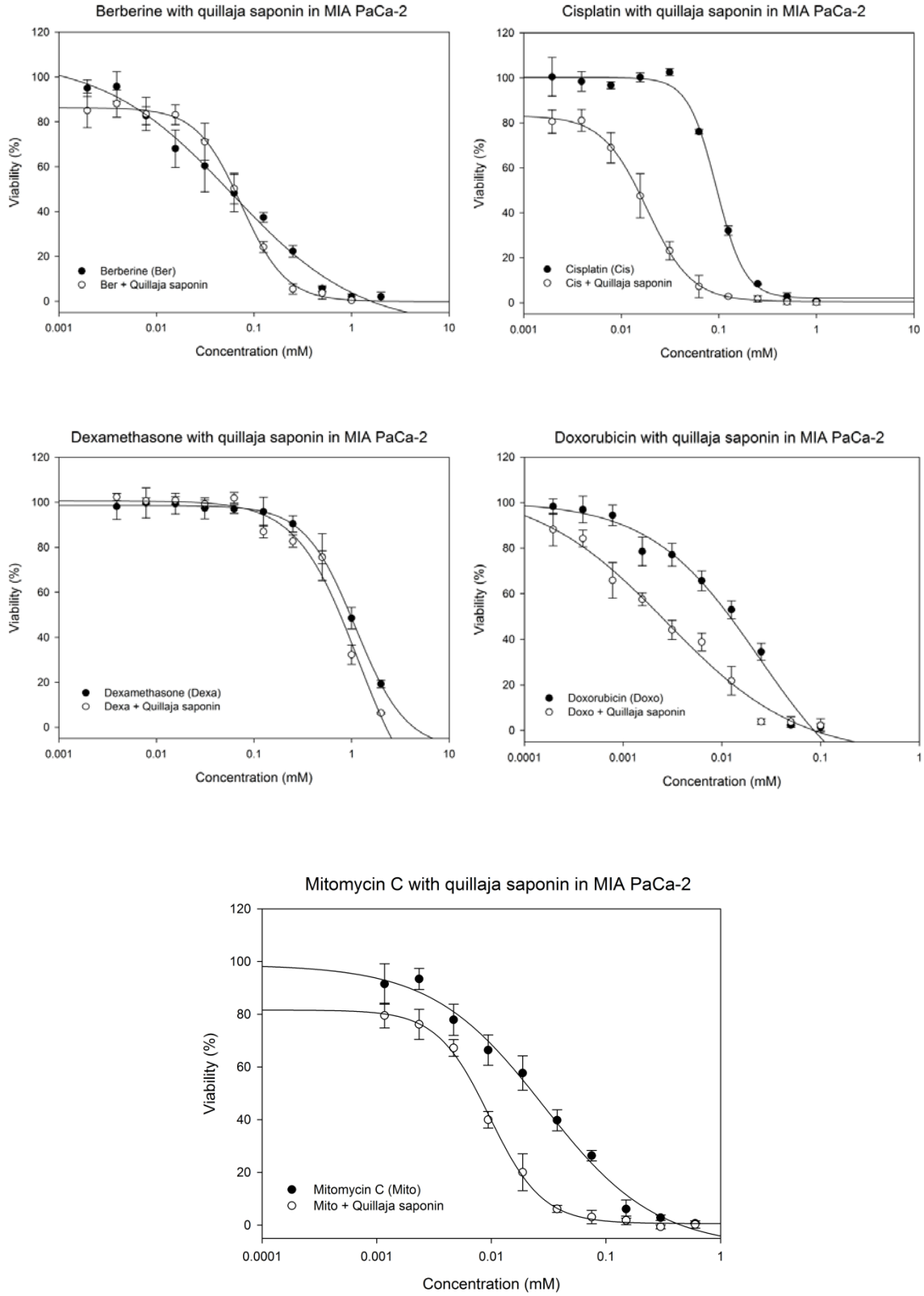

Fig. 3.23c. Dose response curves in MIA PaCa-2 to the anticancer agents berberine, cisplatin, dexamethasone, doxorubicin, and mitomycin C (*black data points*) and their combination with IC_{20} concentrations of quillaja saponin (66 µg/ml) (*white data points*). Data are expressed as means ±SD of cell viability from three independent experiments, each done in triplicates.

(d) PANC-1

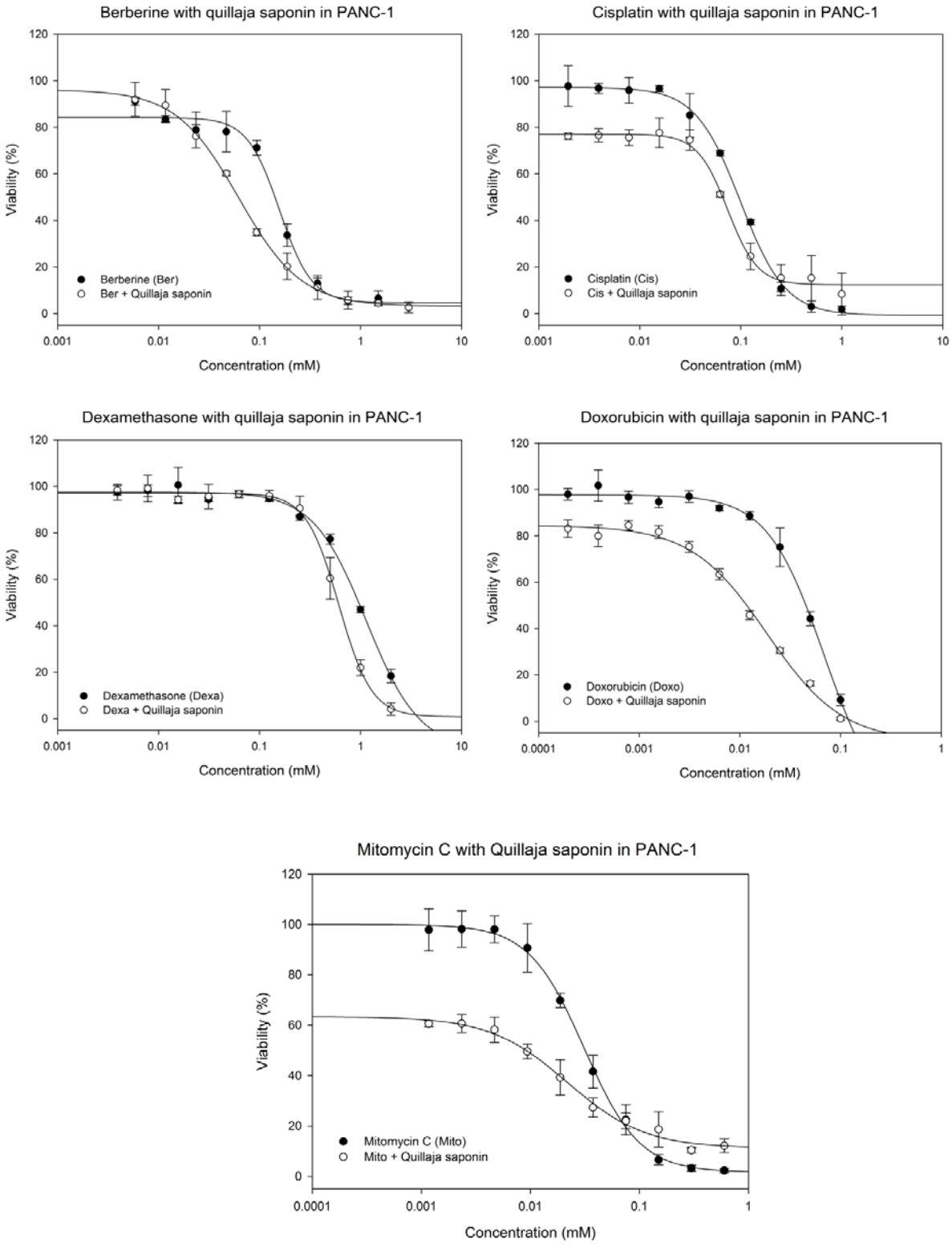

Fig. 3.23d. Dose response curves in PANC-1 to the anticancer agents berberine, cisplatin, dexamethasone, doxorubicin, and mitomycin C (*black data points*) and their combination with IC_{20} concentrations of quillaja saponin (68 µg/ml) (*white data points*). Data are expressed as means ±SD of cell viability from three independent experiments, each done in triplicates.

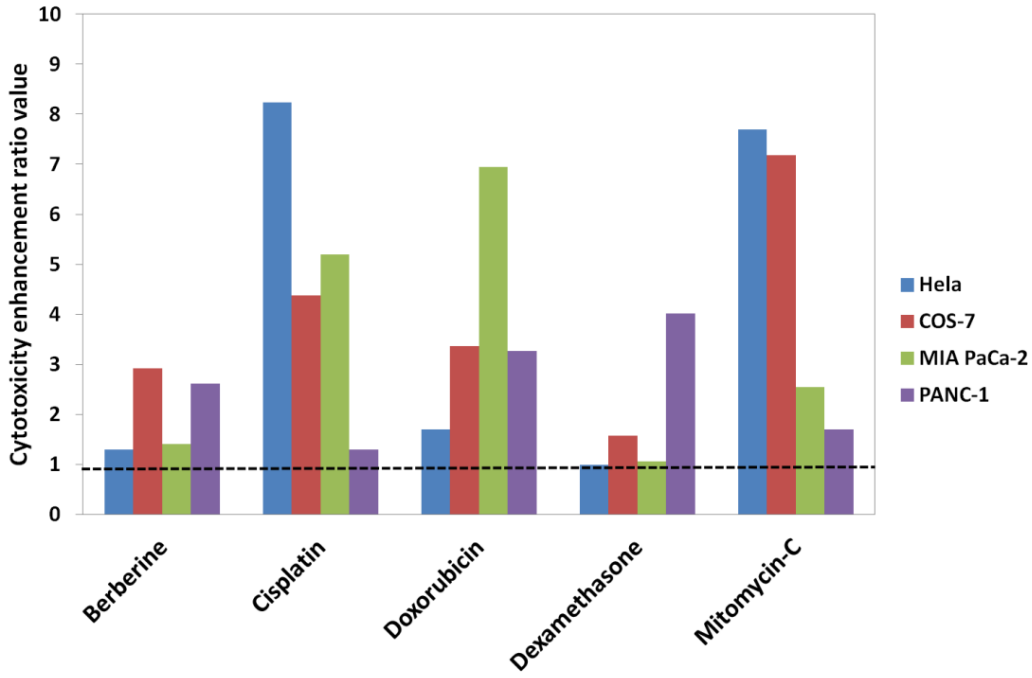

Fig. 3.24. Cytotoxicity enhancement ratios (CER) of anticancer drugs enhanced by quillaja saponin in HeLa, COS-7, MIA PaCa-2, and PANC-1. CER values higher than 1 (*dashed line*) show the ability of quillaja saponin to increase drug toxicity in the cancer cell lines. The cytotoxicity enhancement profiles by quillaja saponin differ in each case.

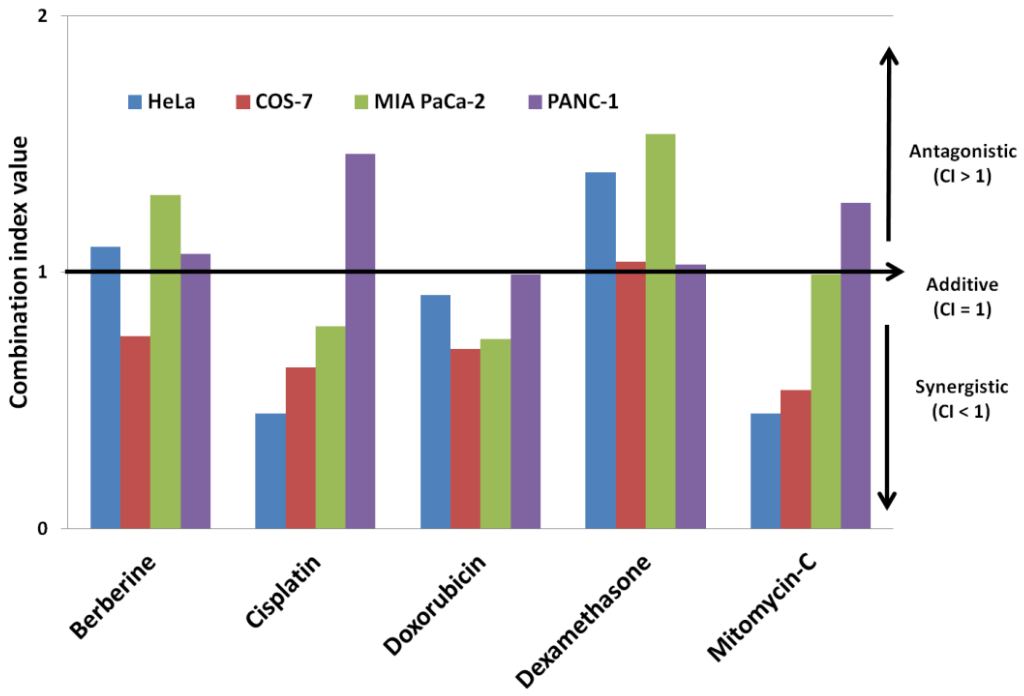

Fig. 3.25. Combination index (CI) values of quillaja saponin (IC_{20}) with anticancer drugs in HeLa, COS-7, MIA PaCa-2, and PANC-1. CI < 1 = synergistic; CI 1 = additive; CI > 1 = antagonistic.

3.2.3 Quillaja saponin significantly increases the toxicity of ricin

Quillaja saponin significantly enhances effect of ricin in all tested cancer cell lines. The lowest level of ricin toxicity enhancement was measured with a CER of 2.54 (IC_{50} from 62.70 to 24.70 ng/ml) in MIA PaCa-2 and the highest of CER 76.85 (IC_{50} from 99.9 to 1.3 ng/ml) in COS-7. The toxicity enhancement in PANC-1 and HeLa were found with a CER of 11.57 (IC_{50} from 297.15 to 22.50 ng/ml) and 13.11 (IC_{50} from 75.20 to 6.50 ng/ml), respectively (Figs. 3.26 and 3.27). As quillaja saponin increases membrane permeability, ricin will pass through the cell membrane more easily, explaining the strong cytotoxicity enhancement effect. Quillaja saponin and ricin interact synergistically as indicated by combination indexes (CI) of less than 1 (Fig. 3.28). Table 3.11 summarizes the cytotoxicity data of the individual substances and their combination.

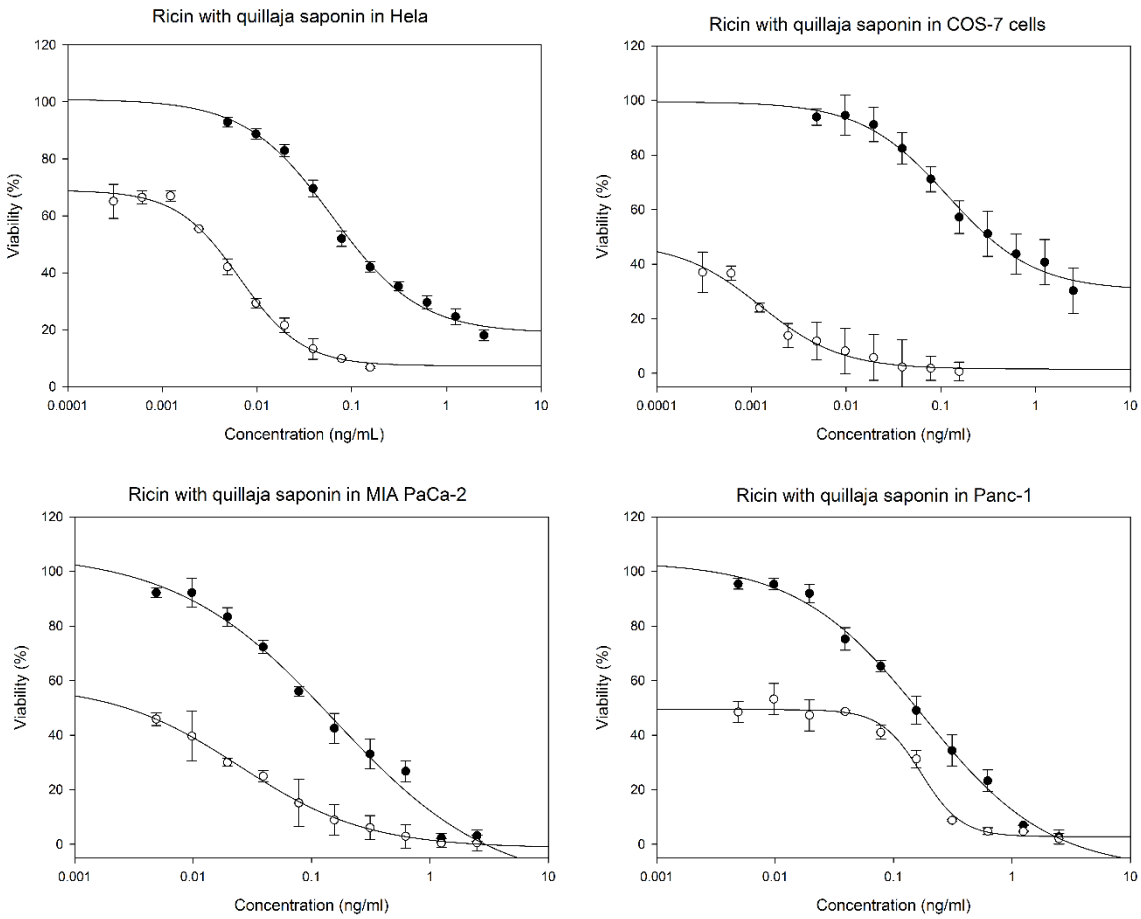

Fig. 3.26. Dose response curves of Ricin in HeLa, COS-7, MIA PaCa-2 and PANC-1. Cytotoxicity of ricin (*black data points*) and its combination with IC_{20} concentrations of quillaja saponin (35 µM for HeLa; 44 µM for COS-7; 66 µM for MIA PaCa-2; 68 µM for PANC-1) (*white data points*). Data are expressed as means ±SD of cell viability from three independent experiments, each done in triplicates.

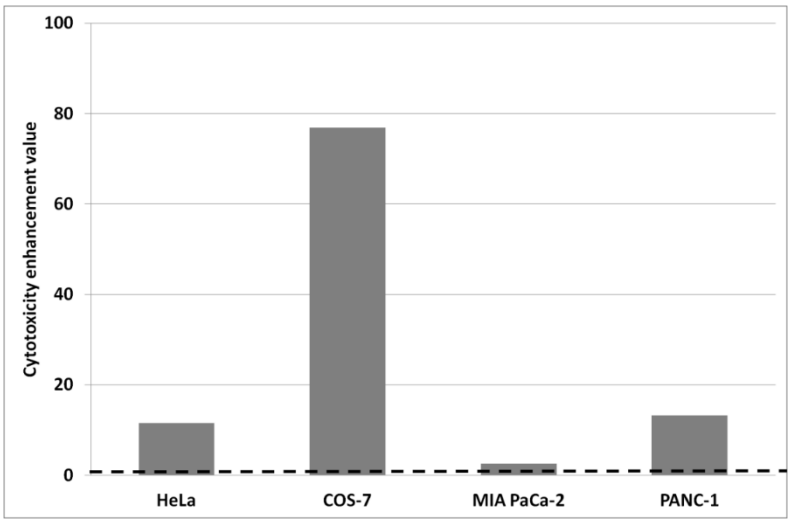

Fig. 3.27. Cytotoxicity enhancement ratio (CER) for quillaja saponin + ricin in HeLa, COS-7, MIA PaCa-2, and PANC-1. CER values higher than 1 (*dashed line*) show the ability of quillaja saponin to increase drug toxicity in the cancer cell lines. The cytotoxicity enhancement profiles by quillaja saponin differ in each case.

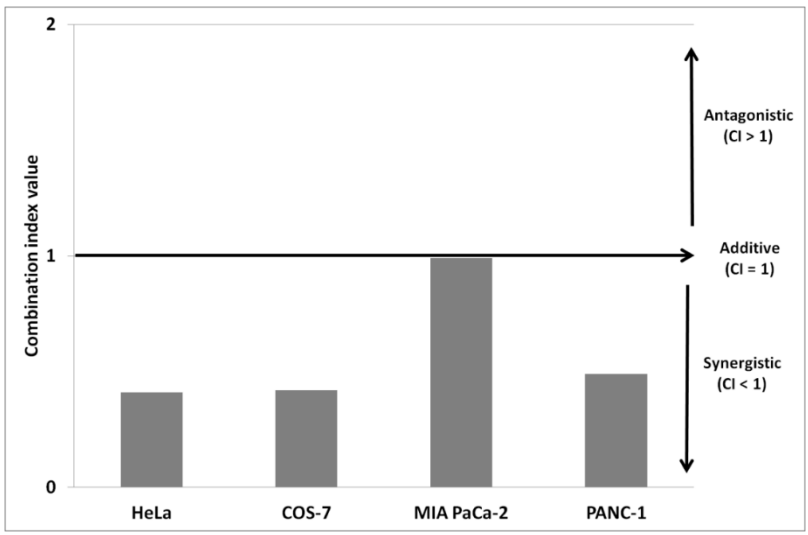

Fig. 3.28. Combination index (CI) values of quillaja saponin (IC_{20}) + ricin in HeLa, COS-7, MIA PaCa-2, and PANC-1; CI < 1 = synergistic; CI 1 = additive; CI > 1 = antagonistic.

Table 3.11. Quillaja saponin + ricin – effect on HeLa, COS-7, MIA PaCa-2, and PANC-1.

	IC_{50} of anticancer agent + IC_{20} of quillaja saponin											
	HeLa	**CI**	**CER**	**COS-7**	**CI**	**CER**	**MIA PaCa-2**	**CI**	**CER**	**PANC-1**	**CI**	**CER**
Saponins												
Quillaja saponin (IC_{50} µg/ml)	103.95±9.91			105.80±26.62			109.49±9.10			98.21±11.57		
Quillaja saponin (IC_{20} µg/ml)	35			44			66			68		
Ricin (ng/ml)	75.20±0.01			99.9±0.04			62.70±0.01			297.15±0.25		
Ricin+quillaja saponin (ng/ml)	6.50 ± 0.04	0.41	11.57	1.3 ± 0.01	0.42	76.85	24.7 ± 0.04	0.99	2.54	22.50 ± 0.3	0.49	13.21

3.2.4 Quillaja saponin ruptures RBCs

The hemolytic activity of quillaja saponin was examined with defebrinated sheep RBCs. Quillaja saponin can disrupt erythrocyte membranes causing release of hemoglobin, which can be detected photometrically. The concentration of quillaja saponin inducing 50% RBC lysis is 0.3507 mM. The hemolytic effect of quillaja saponin is not as strong as that of digitonin (Fig. 3.29).

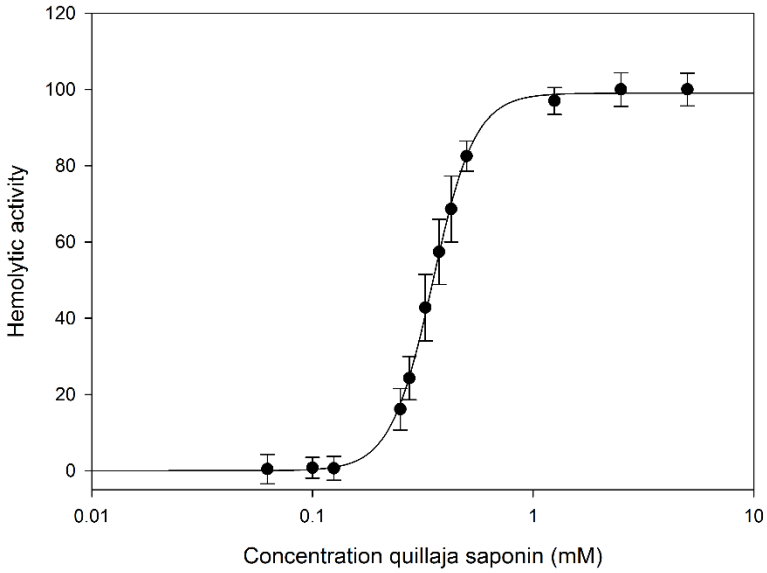

Fig. 3.29. Quillaja saponin – dose-dependent hemolytic effect on sheep RBCs. Dose-ranging experiments were performed from 0.1 to 0.001 mM of quillaja saponin. RBC rupturing occurred at IC_{50} 0.3507 mM. Data are expressed as means ±SD of hemolytic activity for three independent experiments.

3.2.5 Quillaja saponin causes calcein leakage

The activity of quillaja saponin to induce membrane leakage was measured for different lipid compositions of LUVs applying the same preparatory and experimental procedures as for digitonin (see Sect. 3.1.5). The results show that the effect of quillaja saponin on membranes also depends on the presence of cholesterol. Calcein fluorescence in LUV membranes without cholesterol remained unchanged upon addition of quillaja saponin (Fig. 3.30), while in LUVs containing cholesterol quillaja saponin addition immediately induced membrane leakage (<4 min) and calcein fluorescence remained constant for more than 1 h (Fig. 3.31).

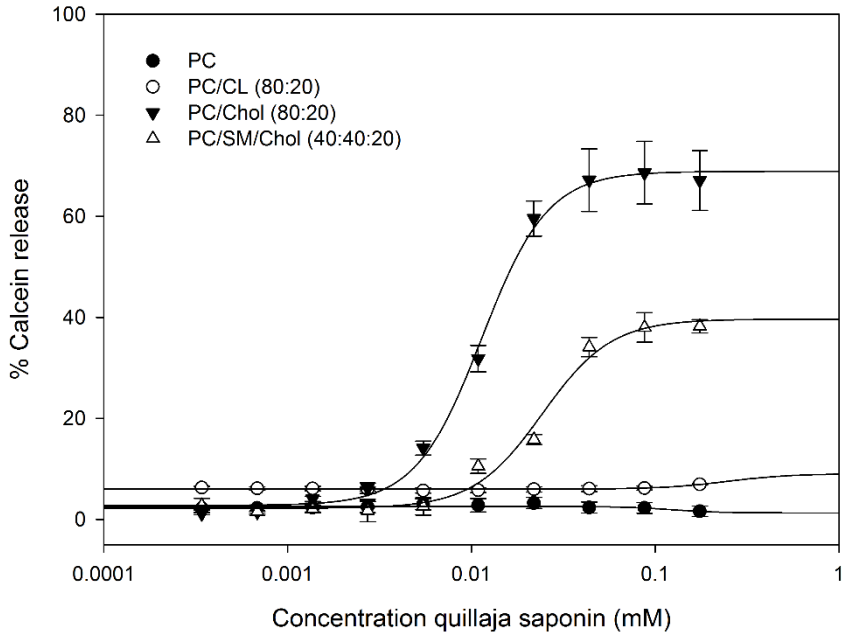

Fig. 3.30. Calcein release from different LUVs induced by quillaja saponin. Data are expressed as means ±SD of hemolytic activity for three independent experiments. PC: phosphatidylcholine; CL: cardiolipin; Chol: cholesterol; SM: sphingomyelin.

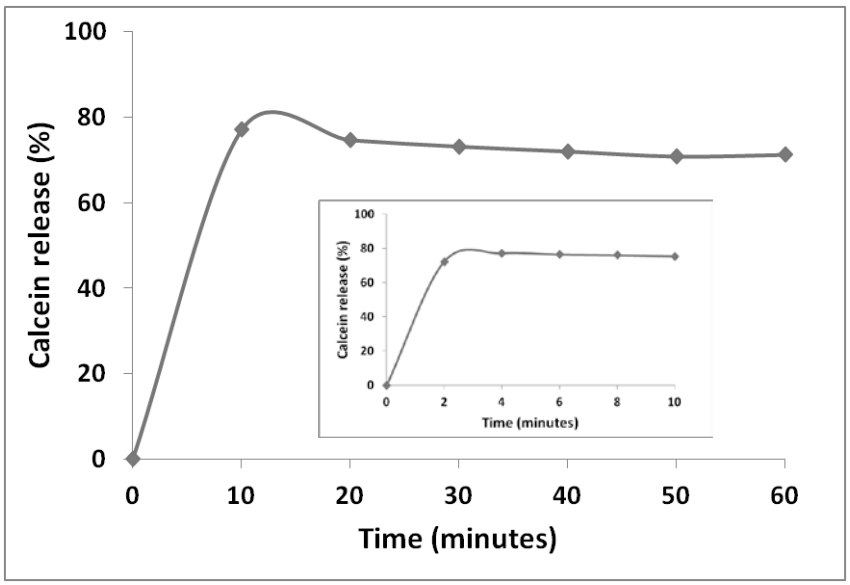

Fig. 3.31. Kinetics of calcein release of PC/Chol (80:20) LUVs induced by quillaja saponin. Intensity of fluorescence of calcein released from LUVs by 0.1 mM quillaja saponin was measured continuously every 120 s for 1 h. The *inset* shows the percentage of calcein release in the range time of 0–10 min.

3.2.6 Influence of cholesterol concentration on calcein release

The effect of cholesterol on membrane response to quillaja saponin was investigated by monitoring the percentage of calcein release at different concentrations of cholesterol in the liposomes. The results confirm that the level of cholesterol in the membrane greatly affects membrane rupture induced by quillaja saponin (Fig. 3.32). In "pure-PC" LUVs, the intensity of calcein fluorescence increased only slightly after adding quillaja saponin. Thus one can assume that quillaja saponin interacts to a minor extent with phosphatidylcholine to induce membrane leakage.

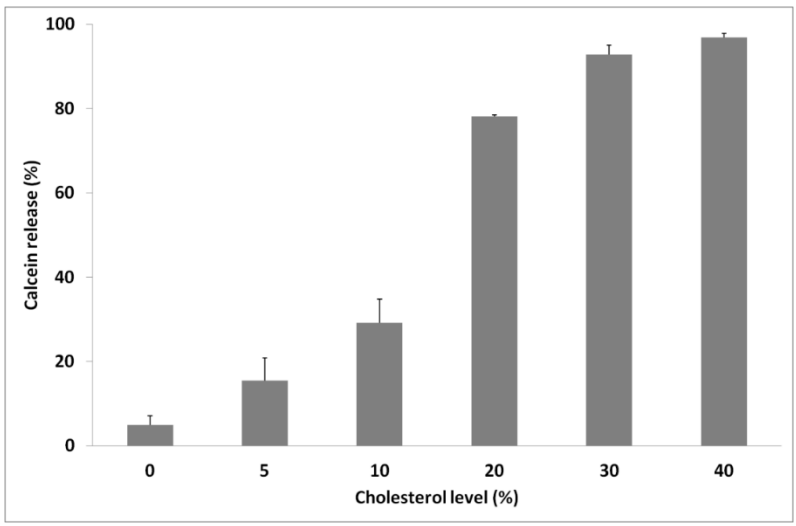

Fig. 3.32. Membrane leakage caused by quillaja saponin depending on cholesterol concentration. PC vesicles with different concentrations of cholesterol were incubated with 0.1 mM quillaja saponin for 1 h. Data are expressed as means ±SD of percentage of calcein release for three independent experiments.

3.2.7 Quillaja saponin affects vesicle size with or without cholesterol

Dynamics light scattering (DLS) measurements were carried out to elucidate the effect of quillaja saponin in increasing membrane permeability. Quillaja saponin does not cause substantial size changes to liposomes. The obtained DLS data provides additional evidence that quillaja saponin interacts only slightly with membranes that do not bear cholesterol. Quillaja saponin at 50 µM slightly affected SOPC vesicle size (Fig. 3.33a). Possibly, quillaja saponin may lead to membrane perforation allowing buffer solution to enter the vesicles and increase their size. With cholesterol present in the vesicle membranes, quillaja saponin also did not induce significant size change of the vesicles (Figs. 3.33b–d). These data corroborate the assumption that interaction of quillaja saponin with membranes in the absence or presence of cholesterol leads to membrane perforation.

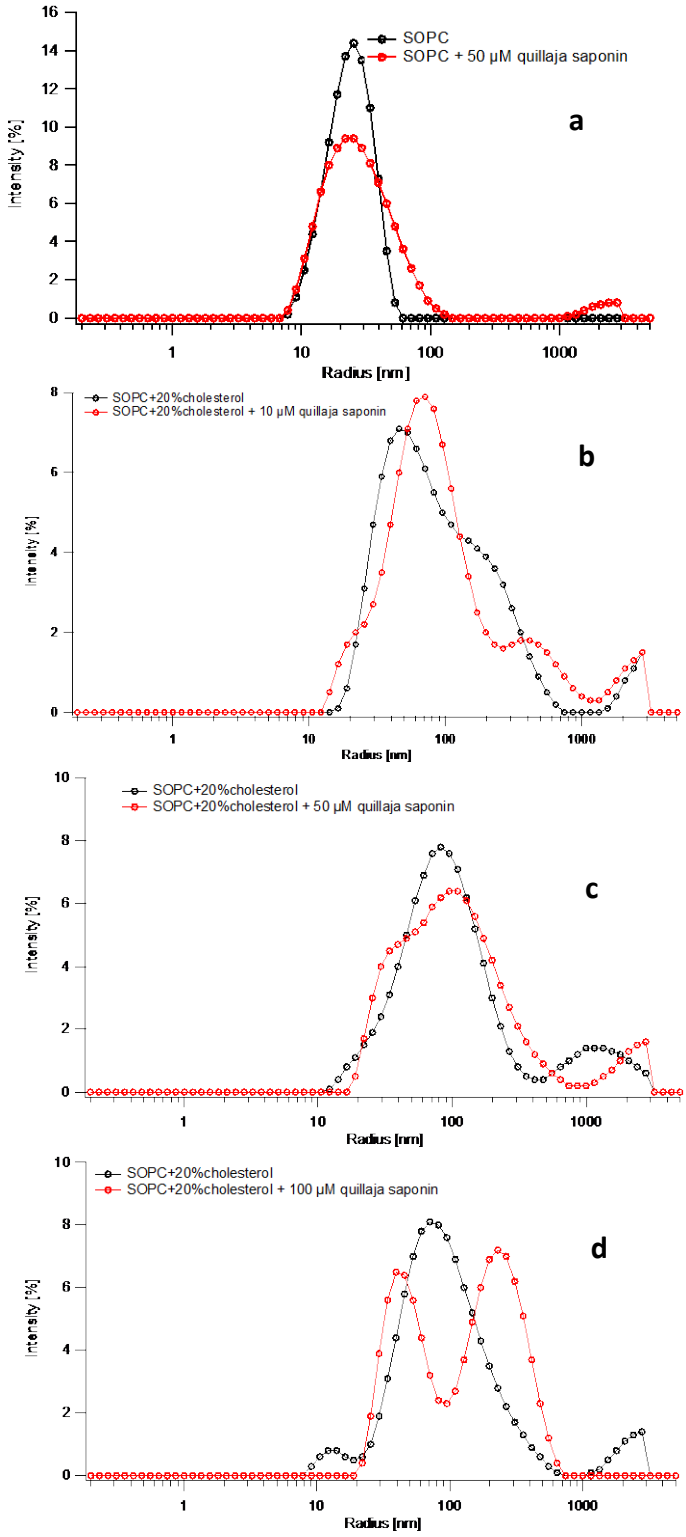

Fig. 3.33. DLS profile of vesicle sizes with and without cholesterol incubated with different concentrations of quillaja saponin. *Black data points* represent control without quillaja saponin and *red data points* without quillaja saponin. SOPC vesicles **(a)** no cholesterol + 50 µM quillaja saponin; **(b)** 20% cholesterol + 10 µM quillaja saponin; **(c)** 20% cholesterol + 50 µM quillaja saponin; **(d)** 20% cholesterol + 100 µM quillaja saponin.

3.2.8 Quillaja saponin strongly affects GUV membrane permeability and integrity in the presence of cholesterol

The interaction of quilllaja saponin with membranes and the associated induced permeabilization can be nicely studied with giant unilamellar vesicles (GUV). Thus, GUVs with and without cholesterol were prepared by electroformation. The green fluorescing dye Alexa Flour 488 was used to visualize the interaction of quillaja saponin with the GUV membrane. The dye permeates the membrane and enters the GUVs in response to quillaja saponin. The effect can be observed by monitoring the shape change of GUVs. The results were consistent with the correspondingly obtained calcein leakage and DLS data. In the non-cholesterol vesicles, quilllaja saponin induced permeability of only few GUVs after 1 h of incubation; about 10% of GUVs were filled with green solution (Fig. 3.34a,b). However, in the presence of cholesterol all GUVs were filled after 1 h of incubation (Figs. 3.34c,d). As the vesicles remained intact, this supports the assumption that quilllaja saponin leads to pore formation. The membrane permeabilization effected by quillaja saponin is presented in Fig. 3.35.

Without cholesterol

(a) PC–GUV + 50 µM quillaja saponin, 0 min

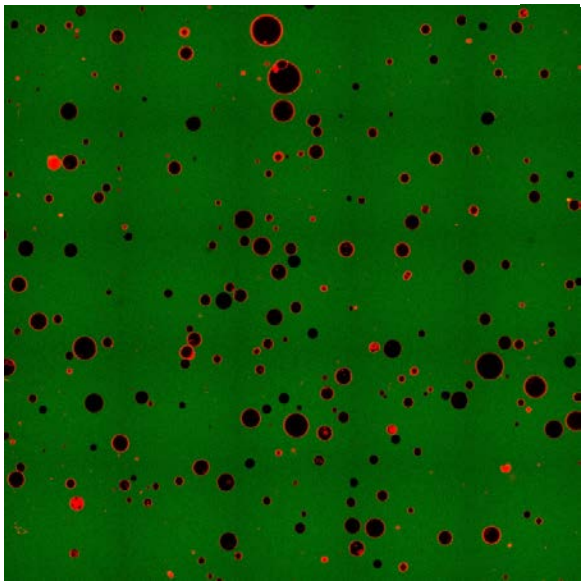

(b) PC–GUVs + 50 µM quillaja saponin 60 min

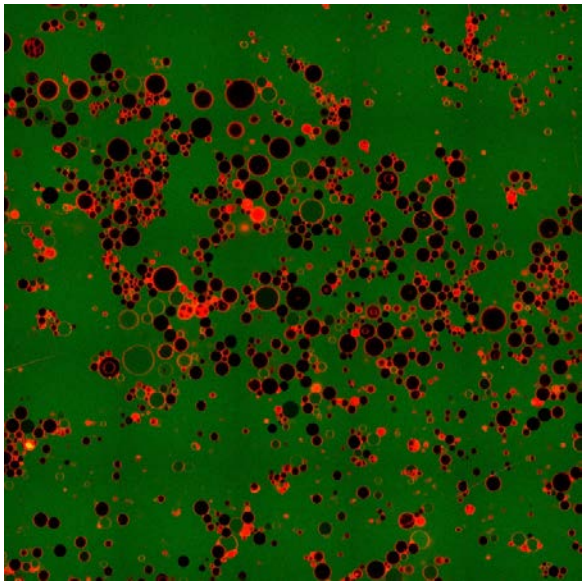

With cholesterol

(c) PC/Chol (80:20)–GUV + 50 µM quillaja saponin, 0 min

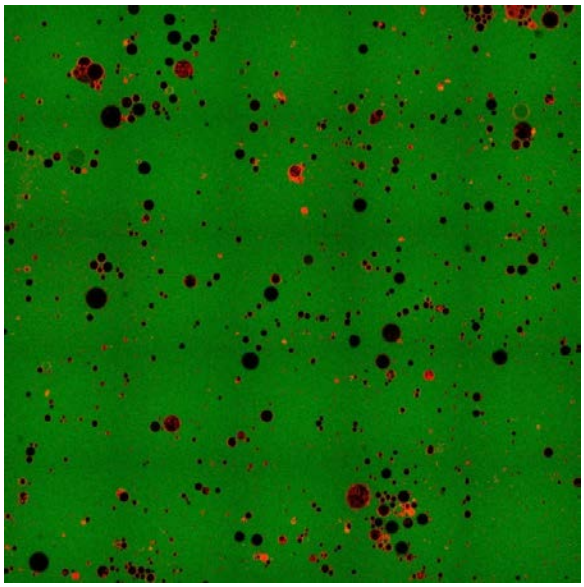

(d) PC/Chol (80:20)–GUV + 50 µM quillaja saponin, 60 min

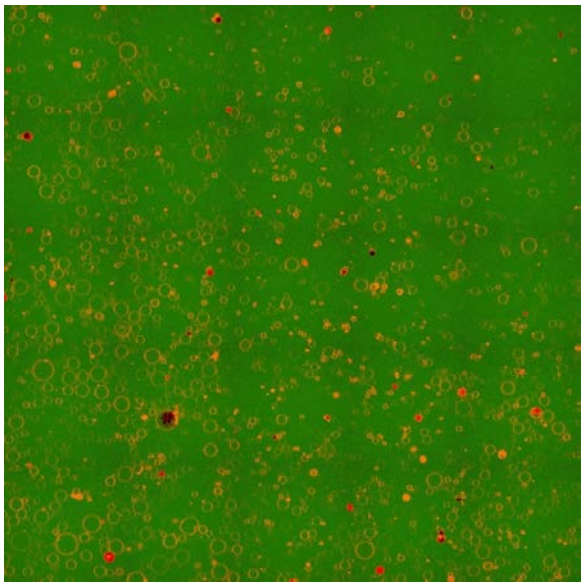

Fig. 3.34. GUV membrane permeabilization by quillaja saponin. **(a)** PC-GUVs shortly after applying 50 µM quillaja saponin, **(b)** PC-GUVs after incubating with 50 µM quillaja saponin for 60 min, **(c)** PC/Chol (80:20) GUVs shortly after applying 50 µM quillaja saponin, **(d)** PC/Chol (80:20) GUVs after incubating with 50 µM quillaja saponin for 60 min. Solution bathing GUVs (*green*), interior of GUVs (*black*), GUV membranes (*red*).

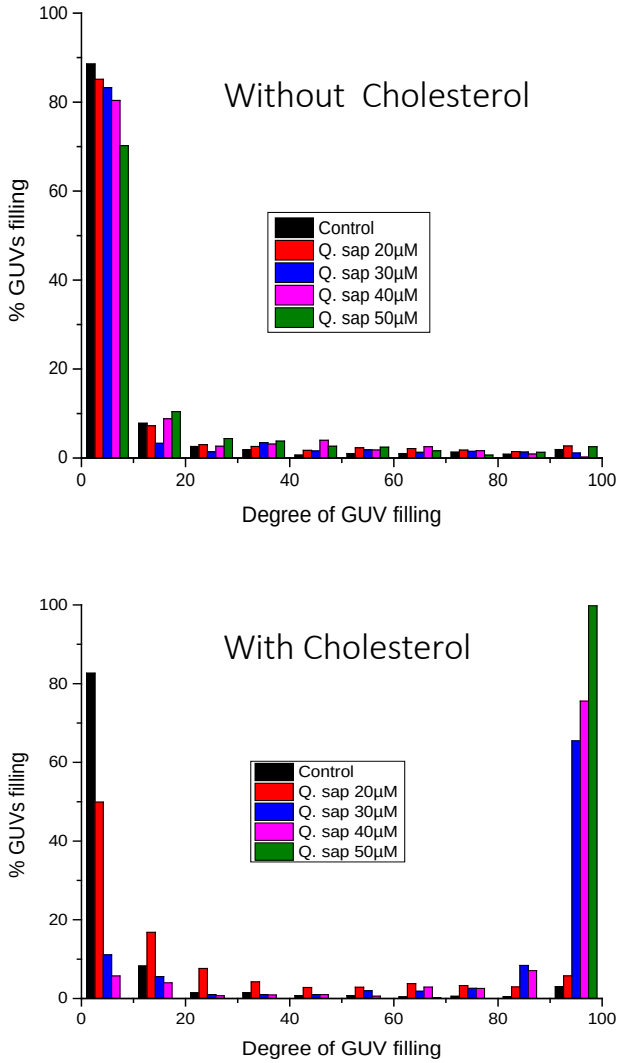

Fig. 3.35. GUV filling upon incubating GUVs with different concentrations of quillaja saponin. (a) PC-GUV with quillaja saponin, incubation 60 min, **(b)** PC/Chol (80:20)-GUV with quillaja saponin, incubation 60 min.

3.2.9 Visualizing the disrupting effect of quillaja saponin on individual PC/Chol (80:20) GUVs

Close-up views of the effect of 50 µM quillaja saponin in causing membrane permeabilization in individual GUVs with 20% membrane cholesterol content were recorded in real time. GUV filling started shortly after adding quillaja saponin to the system; the diffusion process takes about 20 min to be completed (Fig. 3.36). GUVs remained intact after complete diffusion, indicating that quillaja saponin does not induce membrane rupture. Based on these GUV observations, we conclude that quillaja saponin leads to small pores in the GUV membranes, especially when they contain cholesterol.

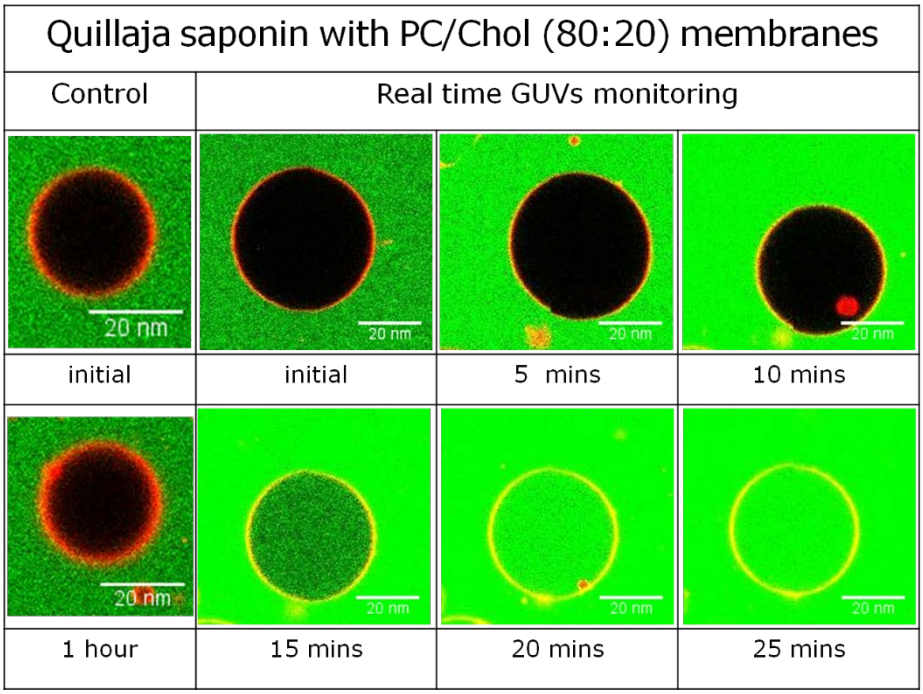

Fig. 3.36. Time dependence of individual PC/Chol (80:20)-GUV response to 50 µM quillaja saponin. *Left images* show GUV without digitonin as a control during the incubation time. The other images show time lapse interactions of 50 µM quillaja saponin with PC/Chol (80:20)-GUV. Scale bars 20 nm.

3.2.10 Quantifying structural changes of supported lipid bilayers by quillaja saponin

In order to quantify the interaction of quillaja saponin with cell membranes with and without cholesterol we applied two different techniques: quartz crystal microbalance with dissipation (QCM-D) and high-energy specular X-ray reflectivity (XRR).

3.2.10.1 QCM-D

The absorption of quillaja saponin into supported lipid bilayer membranes was quantified by measurements using quartz crystal microbalance with dissipation (QCM-D). The same system and procedure used for digitonin was also applied with quillaja saponin (see Sect. 3.1.10.1). The quality of both types of SLB membranes was evaluated by their response to frequency and their dissipation. The frequency increased to $\Delta f = -26$ Hz from $\Delta f_{SOPC} = -50$ Hz and $\Delta f_{SOPC/Chol} = -68$ Hz for pure SOPC and SOPC/Chol SLB, respectively. Also, constant dissipation values of $\Delta D = 0.01 \times 10^{-6}$ were measured for both systems, dropping from $\Delta D_{SOPC} = 3.7 \times 10^{-6}$ and $\Delta D_{SOPC/Chol} = 4.1 \times 10^{-6}$, respectively. These values indicate the formation of stable lipid bilayers on the quartz crystal chip surface (Figs. 3.37a,b).

The 50 µM quillaja saponin was introduced to the pure SOPC bilayer membrane and onlys light positive changes in frequency and negative changes in dissipation were recorded after rinsing with buffer. A higher concentration of 250 µM quillaja saponin was applied to amplify the effect. During the injection process, the frequency increased to Δf = ~ +2 Hz and dissipation decreased to ΔD = ~0.5 × 10^{-6}, but after buffer rinsing the frequency dropped to Δf = ~ +1 Hz and the dissipation value increased to close to the initial value of ΔD = ~0.3 × 10^{-6}. These results indicate an interaction of quillaja saponin with the SOPC membrane and there was a small mass change in the bilayer. The positive value of Δf indicates that small amounts of mass were being removed by buffer rinsing. The decreased dissipation value, finally being close to the initial value, indicates that no change in membrane conformation had taken place (membrane remained rigid) (Fig. 3.37c). Because of the weak dissipation response of the adsorbed layer, the Kelvin-Voigt viscoelastic model was applied to describe the interaction instead of the Sauerbrey equation model. Unfortunately, the obtained fitting result with the Kelvin-Voigt viscoelastic model provided unrealistic data, probably because of the low absolute dissipation value caused by the presence of water in the bilayer membrane. The same problem was also reported by other researchers (Wojciechowski et al. 2014b).

At the SLB membrane with cholesterol, neither frequency nor dissipation was changed by adding 50 µM quillaja saponin; while 250 µM quillaja saponin, caused the frequency to increase to Δf = ~ +2 Hz remaining constant after buffer rinsing and the dissipation decreased to ΔD = ~0.5 × 10^{-6}; at 1 mM quillaja saponin the frequency increased to Δf = ~ +6.52 Hz and remained constant after rinsing, the dissipation dropped to ΔD = ~ −1 × 10^{-6} and then increased to near initial value ΔD = ~ −0.3 × 10^{-6}. These results indicate that the interaction of quillaja saponin with cholesterol leads to mass changes in the membrane. The higher values of positive frequency suggest that the bilayer membrane losses significant mass at 1 mM quillaja saponin and final rinsing. The higher dissipation values at 250 µM quillaja saponin suggest that the quillaja saponin-cholesterol complex makes the membrane less rigid. However, the dissipation returning to close to the initial value after final rinsing in the case of 1 mM quillaja saponin suggests that the membrane becomes more rigid (Fig. 3.37d). The data on Δf and ΔD suggest that the quillaja saponin-cholesterol complex leads to pore formation by pulling up the cholesterol from the membrane causing the membrane to lose mass and allowing more water to enter the intermembrane space which in turn would make the membrane less rigid.

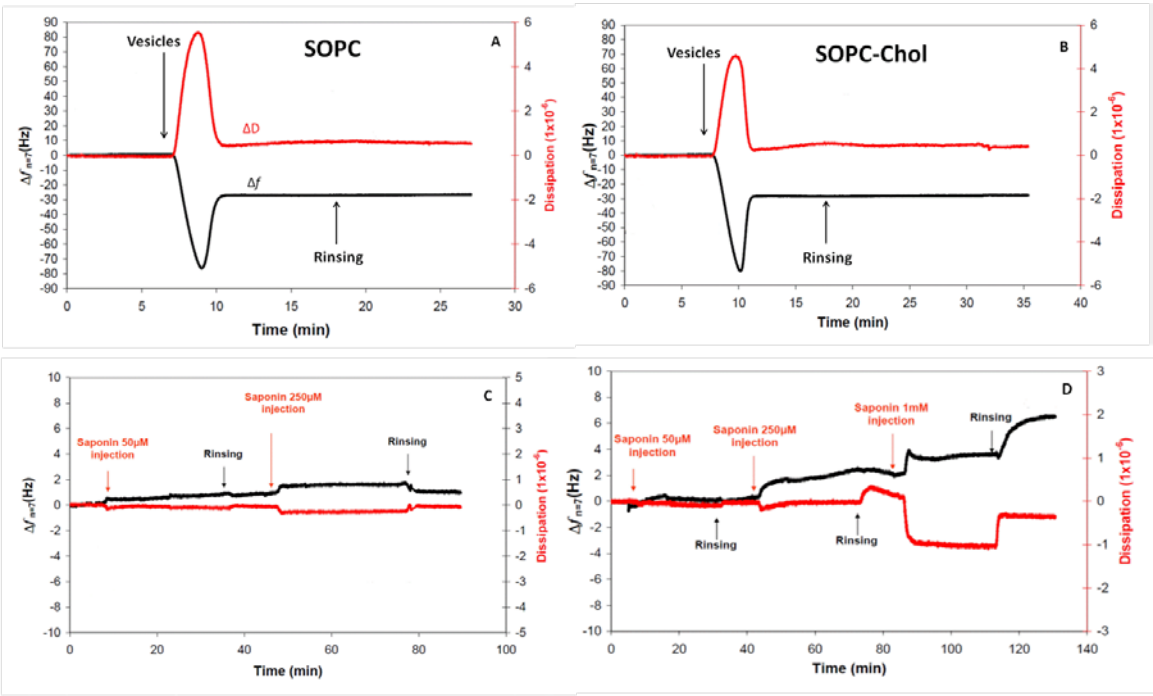

Fig. 3.37. QCM-D response to changes of frequency (Δ*f*) (*black line*) and dissipation (ΔD) (*red line*) of SOPC liposomes with time at 35 MHz following the injection of 50 μM, 250 μM, and 1 mM quillaja saponin **(a)** SLB formation from SOPC liposomes, **(b)** SLB formation from SOPC/Chol (80:20) liposomes, **(c)** application 50 mM and 250 μM quillaja saponin onto SOPC bilayer and show slightly significant change, **(d)** application of 50 μM, 250 μM, and 1 mM quillaja saponin onto SOPC/Chol bilayer and injection of 50 μM show no significant change in both Δ*f* and Δ*D*. Injection of 250 mM and 1 mM of quillaja saponins leads to significant change in both Δ*f* and Δ*D*. *Arrows* indicate introduction of vesicles and quillaja saponin and rinsings with buffer.

3.2.10.2 High-energy specular X-ray reflectivity (XRR)

In order to observe changes in the structure of supported bilayer membranes in the presence of quillaja saponin we employed high-energy specular X-ray reflectivity (XRR). Four layers of supported lipid membrane bilayers on SiO_2 surface were prepared using the same procedure as previously applied for digitonin (see Sect. 3.1.10.2). Changes occurring in the membranes in terms of thickness (*d*), electron density, and root mean square (rms) roughness (*σ*) were used to characterize the mechanism membrane binding of quillaja saponin.

XRR best-fit curves were obtained for 50 μM quillaja saponin in the solid-supported lipid bilayer membrane consisting of pure SOPC (Fig. 3.38a). The curves were fitted with the 5-slab model, having outer headgroups, alkyl chains, inner headgroups, water reservoir, and SiO_2 layer. The scattering length density (SLD) profiles from the best-fit results were also determined. Quillaja saponin applied to pure SOPC membranes induces changes in the outer headgroups of the membrane whose density increased from 9.7 Å to 10.8 Å, roughness from 4.0 Å to 5.3 Å, and a slightly increased SLD value from 11.4×10^{-6} Å^{-2} to 11.7×10^{-6} Å^{-2}.

The SLD values from the alkyl chains decreased from 8.8 × 10^{-6} $Å^{-2}$ to 11.7 × 10^{-6} $Å^{-2}$. These data suggest that quillaja saponin adsorbs to the head groups of the lipid membrane as shown by the increased density and roughness. This interaction also induced changes in the inner headgroup layer in which the density decreased from 8.8 Å to 8.5 Å, SLD decreased from 11.9 × 10^{-6} $Å^{-2}$ to 11.3 × 10^{-6} $Å^{-2}$, and roughness from 3.9 Å to 3.7 Å. This indicates that the space between the headgroups increased, making the membrane more permeable (data summarized in Table 3.12).

The presence of 50 µM quillaja saponin in the SOPC/Chol membrane caused slight changes in membrane conformation (Fig. 3.38b). In the outer headgroup of the bilayer membrane the density increased from 10.0 Å to 10.8 Å, the SLD increased only slightly from 11.4 × 10^{-6} $Å^{-2}$ to 11.5 × 10^{-6} $Å^{-2}$. Interestingly, the surface roughness decreased from 6.3 Å to 5.8 Å which indicates that the number of molecules in the lipid headgroup layer increased, but the membrane surface becomes more smooth. We thus assume that quillaja saponin penetrates down to the alkyl chains. Changes occurring in the alkyl chains appear to prove this assumption as density increased from 23.8 Å to 25.4 Å, SLD increased from 7.4 × 10^{-6} $Å^{-2}$ to 7.7 × 10^{-6} $Å^{-2}$, and roughness from 4.2 Å to 4.4 Å. These data indicate that quillaja saponin locates in the alkyl chain layer bound to cholesterol there, increasing the space between complex quillaja saponin-cholesterol and SOPC. Changes also occur in the inner headgroups where the density decreased from 8.7 Å to 8.4 Å, SLD slightly increased from 11.9 × 10^{-6} $Å^{-2}$ to 11.0 × 10^{-6} $Å^{-2}$, and no change occurred in roughness, indicating that the quillaja saponin-cholesterol complex is big enough to force additional distance between headgroups of inner layer. The distance formed between headgroups in the outer and inner layer increases membrane permeability forming small pores of sizes ranging around 1 $Å^{-2}$. These small pores are permanent but the membrane remains intact, as shown by our GUV experiments (the according data for the SOPC/Chol SLB membrane are summarized in Table 3.13).

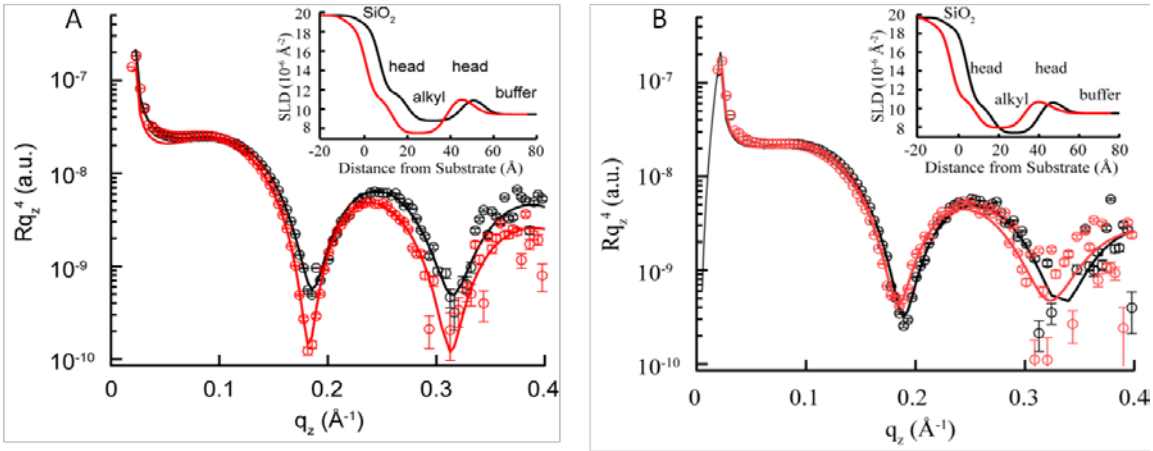

Fig. 3.38. High-energy specular X-ray reflectivity (XRR) spectra showing the fine structure of supported membranes. **(a)** Pure SOPC membrane in the absence (*black*) and presence (*red*) of 50 µM quillaja saponin. **(b)** SOPC membrane incorporating 20 mol% cholesterol in the absence (*black*) and presence (*red*) of 50 µM quillaja saponin. The experimental errors are within the symbol size. The *solid lines* represent the best-fit model to the data.

Table 3.12. XRR best-fit parameters ($\chi^2 \leq 0.05$) for a pure SOPC membrane (see Fig. 3.38a) in the absence and presence of 50 µM quillaja saponin.

	Without quillaja saponin $\chi^2 < 0.01$			**With quillaja saponin $\chi^2 < 0.04$**		
SOPC	***d* [Å]**	**SLD [10^{-6} Å^{-2}]**	**σ [Å]**	***d* [Å]**	**SLD [10^{-6} Å^{-2}]**	**σ [Å]**
Outer headgroup	**9.7**	11.4	**4.0**	10.8	**11.7**	**5.3**
Alkyl chain	**25.6**	8.8	**4.4**	26.0	**7.5**	**4.4**
Inner headgroup	8.8	11.9	3.9	8.5	11.3	3.7
Water	3.1	9.4	3.1	3.1	9.4	3.3
SiO_2	10.1	18.6	3.5	10.2	18.6	3.5

d = thickness, σ = roughness, SLD = scattering length density

Table 3.13. XRR best-fit parameters ($\chi^2 \leq 0.02$) for SOPC membrane incorporating 20 mol% cholesterol (see Fig. 3.38b) in the absence and presence of 50 µM quillaja saponin.

	Without quillaja $\chi^2 < 0.04$			**With quillaja $\chi^2 < 0.05$**		
SOPC/Chol	***d* [Å]**	**SLD [10^{-6} Å^{-2}]**	**σ [Å]**	***d* [Å]**	**SLD [10^{-6} Å^{-2}]**	**σ [Å]**
Outer headgroup	**10.0**	11.4	**6.3**	**10.8**	11.5	**5.8**
Alkyl chain	**23.8**	7.4	**4.2**	**25.4**	7.7	**4.4**
Inner headgroup	8.7	11.9	3.9	8.4	11.0	3.9
Water	3.3	9.4	3.3	3.4	9.4	3.3
SiO_2	10.3	18.6	3.5	10.2	18.6	3.5

d = thickness, σ = roughness, SLD = scattering length density

4 Discussion

4.1. Cytotoxicity of saponins

Saponins exert a broad spectrum of biological and pharmacological activities in various organisms – from membrane activity, targeting metabolic pathway, affects cellular signals resulting in DNA damage (Lacaille-Dubois and Wagner 1996; Fuchs et al. 2009). Their anticancer properties have been intensively studied in various cancer cell lines and different mechanisms of action have been revealed. Saponins act at the extracellular and intracellular level on tumor cells. At the extracellular level, saponins affect membrane permeability and structure and also inhibit membrane proteins leading to drug efflux inhibition. Inside the cells they can induce apoptosis and cell cycle arrest (Podolak et al. 2010). As saponins increase membrane permeability, this effect may be used to enhance drug toxicity in a synergistic way (Bachran et al. 2009; Eid et al. 2012a; Herrmann and Wink 2011; Bachran et al. 2006). The degree of cytotoxicity and membrane permeability enhancing activity of saponins is determined by both the aglycone type (whether steroid or triterpenoid) and by the number of sugar moieties (Chwalek et al. 2006; Wang et al. 2007b).

In this study, we have tested the cytotoxicity and membrane permeability enhancing effect of both steroid and triterpenoid saponins as represented by digitonin and quillaja saponin, respectively, in five selected cancer cell lines. As a single drug, digitonin is more than 5 times as toxic as quillaja saponin. Low concentrations of digitonin affect cells both on the extra- and intracellular levels. The steroid aglycone exerts its strong anticancer effect via modulation of multiple cell signaling factors leading to inhibition of cell proliferation, blocking cell-cycle signaling in the G_0/G_1 phase, inducing apoptosis, modulating cyclooxygenase and lipoxygenase, and inhibiting fatty acid synthase (FAS), all observed in the case of diosgenin (Trouillas et al. 2005; Raju and Mehta 2008). Digitonin, as a monodesmosidic saponin, has strong detergent properties due to its ability to insert itself into the membrane and form a complex with cholesterol, which can disturb membrane permeability (Wink 2008). Quillaja saponin is a mixture of bidesmosidic saponins with small amounts of monodesmosides. The bidesmosides bear two sugar chains attached to C-3 and C-28 of the triterpenoid aglycone, making it less toxic than the monodesmosidic saponin. The high polarity of the sugar moiety of quillaja saponin allegedly prevents this bidesmosidic saponin from reaching the cytoplasm (Podolak et al. 2010).

4.2. Saponins enhance the toxicity of selected antitumor agents and ricin

The capacity of saponins to affect membranes and increase their permeability has been used to improve the cytotoxicity of antitumor drugs (Bachran et al. 2006; Gaidi et al. 2002) and natural products in a synergistic way (Eid et al. 2012a; Herrmann and Wink 2011). In nature, the synergistic effect between saponins and polar molecules show in *Agrostemma githago* seed which contain lectin and *Agrostemma* saponins. Lectins are very toxic polar compounds with a quite low cytotoxicity if applied as a single drug. However, when lectins are combined with *Agrostemma* saponins the cytotoxic effect is dramatically increased (Hebestreit and Melzig 2003). This phenomenon offered an interesting new focus in cancer treatment for combining saponins with other antitumor drugs. This enhancing effect of saponins is strongly related to the type of aglycone and number of sugar moieties in their structures.

To explore the role of the molecular structure in regard to the cytotoxicity-enhancing effect, we tested the monodesmosidic steroid saponin, digitonin, and the bidesmosidic triterpenoid saponin, quillaja saponin, with selected antitumor drugs on selected cancer cell lines. The application of a nontoxic concentration of the saponins (IC_{20} concentration) increased the toxicity of selected drugs more than two-fold. On average, the cytotoxicity enhancement ratio (CRE) of digitonin was around 1.5 with a maximum of 3.75 for dexamethasone in PANC-1. In combination with ricin, the highest CER was around 5.4 in MIA PaCa-2 and HeLa cell lines and only 1.5 for COS-7 and PANC-1. In combination with several classes of secondary metabolites, the average CRE by digitonin was also in the range of 1.3 to 2.3 in drug-resistant human cancer cell lines and drug-sensitive cell lines (Eid et al. 2012a). The combination of digitonin with two secondary metabolites generally led to CER values in the range of 1 to 5, only particular combinations displayed higher values (Eid et al. 2012b). Digitonin increased the toxicity of cisplatin by 4.4-fold to 6.5-fold depending on the concentration of digitonin (Jekunen et al. 1993). The combination index values from our results and related literature indicate that digitonin mostly influences the cytotoxicity of other anticancer agents in a synergistic way but that some combinations have additive and antagonistic effects depending on the substance and the type of cells (Eid et al. 2012a,b; Hellmann et al. 2010; Herrmann and Wink 2011). This suggests that the toxicity enhancing capability of digitonin is determined by the applied concentration of digitonin in combination, the drugs' properties, and cell type. The monodesmosidic steroid saponin digitonin is very toxic to the cell membrane and appears to rupture the membrane completely.

Otherwise, bidesmosidic triterpenoid saponin quillaja saponin presented better enhancement effect than digitonin. The average cytotoxicity enhancement ratio show by quillaja saponin higher than 6-folds but they are much selected with the substances. Quillaja saponin increased the toxicity of cisplatin, doxorubicin, and mitomycin-C by more than 5-fold from individual treatment, but only slightly increased the toxicity of berberine and dexamethasone. Quillaja saponin significantly increased the toxicity of ricin by more than 75-fold in COS-7 and more than 10-fold in HeLa and PANC-1. Combinations of quillaja saponin with anticancer drugs and ricin yielded CER values above 2 and thus synergistic effects. These effects of quillaja saponin are similar to those reported for 'Saponinum album' from *Gypsophila paniculata* L. (baby's breath), Caryophyllaceae, a mixture of chiefly bidesmosidic triterpenoid saponins, which has been shown to enhance the toxicity of the saporin chimeric toxins Sap-3 and SA2E in breast cancer cell lines by more than 1000-fold. The aglycones of both quillaja saponin and 'Saponinum album' are triterpenes with an aldehyde function at the C-4 position, which seems to be critical for the synergistic action. Bidesmosidic saponins have shown to be more active as enhancer agents than monodesmosidic saponins (Bachran et al. 2006; Fuchs et al. 2009). The drug enhancement activity of quillaja saponin depends on the drug's characteristics and cell type.

4.3 Saponins cause membrane leakage in the presence of cholesterol

To reveal the mechanism of saponin action on membrane activity we tested the hemolytic activity and role of cholesterol for digitonin and quillaja saponin.

Red blood cells (RBC) are a suitable natural model in evaluating the effect of saponins on biological membranes. Saponins disrupt RBCs and this hemolytic activity depends on the chemical structure of the applied saponin (aglycones and sugar moieties). Many studies have shown that steroid saponins have stronger hemolytic effects than triterpenoid saponins (Nakamura et al. 1979). Both aglycone types are strongly hemolytic if they have only one sugar chain attached at C-3 (monodesmosidic) rather than two sugar chains (bidesmosidic) (Woldemichael and Wink 2001). Our results support this finding: the monodesmosidic digitonin shows 30-times higher hemolytic activity than the bidesmosidic quillaja saponin.

Cholesterol plays a special role in the action of saponins on cell membranes. Saponins target cholesterol and upon binding leads to membrane leakage with change in membrane permeability or pore formation allowing free diffusion to and from the cytoplasm (Böttger and Melzig 2013; Hu et al. 1996; Yu et al. 1984; Gögelein and Hüby 1984; Li et al. 2005; Seeman et al. 1973; Shany et al. 1974; Armah et al. 1999). We used unilamellar vesicles as a membrane

model to further elucidate the mechanism of this effect. We confirm that cholesterol is the target for saponins in the membrane. Saponins did not appear to interact with other lipid membrane components such as to phosphatidylcholines, sphingomyelin, or cardiolipin. Both saponin aglycones induced a permeability change of LUV membranes containing cholesterol. The sugar chain seems play a crucial role in hemolytic activity, the monodesmoside being more active in the membrane than the bidesmoside. The rate of membrane permeability induced by the saponins was relatively fast depending on saponin and cholesterol concentrations in the membrane. One of the main functions of cholesterol in lipid bilayers and biological membranes is in maintaining the membrane lipids in the *liquid-ordered state* causing the membrane to be laterally more condensed with increased packing density of the phospholipids. This increases the mechanical strength and decreases the permeability of the membranes (Ohvo-Rekilä et al. 2002; Yeagle 2012). Saponin can very easily change the structure of membranes that contain a high amount of cholesterol, as, e.g., RBCs with 45 mol% cholesterol. Hemolysis and calcein release data suggest the ratio of the interaction complex of saponin:cholesterol as being 1:1 (Mitra and Dungan 2001; Akiyama et al. 1980; Yu and Choi 1986). This may explain the different observed effects of saponins on the different kinds of cancer cell lines.

Saponins not only affect membrane permeability but also change the membrane size. Digitonin clearly does not penetrate or change the size of pure phosphatidylcholine vesicles. In contrast, in the presence of cholesterol, the digitonin-cholesterol complex increased membrane permeability allowing buffer to enter the vesicles, dramatically changing vesicle size. Quillaja saponin, in contrast, only induces a slight permeability change on pure phosphatidylcholine vesicles, as the triterpenoid aglycone of quillaja saponin is glycosylated at both C-3 and C-28 (Hu et al. 1996). The quillaja saponin-cholesterol complex causes the membrane to become more permeable while vesicle size is retained, i.e., small pores are formed that allow diffusion, while the membrane remains intact.

4.4 Digitonin and quillaja saponin permeabilize the membrane by different modes

Giant unilamellar vesicles (GUV) are suitable for microscopic real-time monitoring of saponin-cholesterol interactions (Walde et al. 2010; Tamba et al. 2007; Tamba and Yamazaki 2005; Pott et al. 2008). We observed the response of single GUVs when exposed to various concentrations of saponins. The results support the data obtained from hemolytic and calcein leakage experiments. Cholesterol is clearly shown as the target for saponin and the effect of

inducing membrane permeability in GUVs depends on the concentration of saponin. The results revealed different modes of action between digitonin and quillaja saponin regarding increased membrane permeability.

Digitonin acted by an all-or-none mechanism: in the absence of cholesterol no observable morphological changes of vesicles where exposed even at a high concentration of ≥ 20 µM digitonin and even after more than 60 min. In contrast, inclusion of cholesterol in membranes leads to complex formation with digitonin leading to permanent pores and subsequent complete filling of vesicles. Strong permeability was displayed at concentrations above 10 µM digitonin, where all vesicles had filled with green solution. The pore size as induced by the digitonin-cholesterol complex appears to be bigger than 2 nm based on the free diffusion of Alexa 488 dye having a diameter of 1.4 nm (Bleicken et al. 2013; Weber et al. 2004; Geddes). This explains the selectivity of substance passage through the cholesterol membrane by the action of digitonin.

Digitonin leads to increased vesicle size, and at higher concentrations to membrane rupture. GUV rupturing was monitored in real time. Interestingly, vesicles start to rupture after filling is complete, the vesicles then deflate as the solution seeps out from the vesicles. The pores formed by the digitonin-cholesterol complex seem to be retained for a longer period of time but with diameters of much more than 2 nm, leading to structural membrane instability. The membranes start to reorganize to become stable again forming small compact vesicles at the end. Increased levels of cholesterol in the membranes of above 20% will cause the vesicles to suddenly burst (Menger and Keiper 1998). This result may explain the limitations of using digitonin as a toxicity enhancer: membranes are totally destroyed at higher concentrations of digitonin and cholesterol.

This is the first time that permeability effects caused by quillaja saponin have been visualized in GUVs. Quillaja saponin only slightly induces membrane permeability (less than 10%) in pure phosphatidylcholine vesicles (Hu et al. 1996), while strong activity is found in the presence of cholesterol. Membrane permeability starts to be effected at a concentration of 20 µM quillaja saponin, at 50 µM quillaja saponin all vesicles had filled with green solution (external vesicles solution). The quillaja saponin-cholesterol complex also formed stable and long-lived pores like digitonin. Interestingly, GUVs remain intact and are still visible after complete filling with green solution, which is not the case for digitonin. It seems that the quillaja saponin-cholesterol complex forms smaller pores (≤ 2 nm) than digitonin. Therefore it become advantages for quillaja saponin because they could allow the substances passing through membrane as much as possible without being limited to their own concentration and

cholesterol which led total rupture of vesicles like digitonin. This may also explain the effect of quillaja saponin to increase the toxicity of the selected anticancer drugs and ricin over digitonin. The smaller pore size induced by quillaja saponin leads to selective permeability making it a good candidate for drug toxicity enhancement.

In order to further understand the mechanical interaction between both types of saponins with cholesterol in the membrane, we observed further physical changes occurring in **supported lipid bilayers (SLB)** in the presence or absence of cholesterol caused by saponins. Increase in mass of SLBs after adding saponins are followed by changes in film mechanics. These were determined by quartz crystal microbalance with dissipation (QCM-D) while further characteristics of the membrane components were obtained by high-energy specular X-ray reflectivity (XRR). Conformational changes of the membrane were monitored by dual polarization interferometry (DPI). Changes of membrane thermodynamics were observed by differential scanning calorimetry (DSC).

In the absence of cholesterol, the bilayer membrane remained almost intact with each of the saponins. The activity of digitonin in the membrane is highly dependent on the presence of cholesterol. No structural changes were found in the bilayer membrane during and after incubation with digitonin. However, quillaja saponin showed transient interactions with the membranes. A very small fraction of membrane components was removed during the rinsing process, which most likely means that quillaja saponin interacts with SOPC and extracting it from the SLB membrane, thus causing the membrane to lose some mass while the membrane conformation remains intact (Fig. 3.37c). The fine structural analysis by XRR indicated that quillaja saponin remains on the membrane surface as indicated by increased density, SLD, and roughness of the outer headgroups of the SLB. The alkyl chain and inner headgroup part appears to be pulled out to the surfaces, condensing the middle and inner part of the bilayer (Fig. 3.38a). The interaction between quillaja saponin and SOPC was not strong enough to remove all lipids from the bilayer membrane but strong enough to interfere with membrane stability to the point of slightly increasing its permeability (Hu et al. 1996).

In the presence of cholesterol, both saponins interfere with membrane stability with different modes of action.

Digitonin strongly interacts with cholesterol causing the membrane to become more viscous and elastic, as indicated by increased membrane mass (Δf) and less rigidity (ΔD) (Fig. 3.16d). XRR data shows that digitonin does not lead to significant membrane rupturing but causes cholesterol to rise to the membrane surface from the as indicated by decreased

SLD of the alkyl chains. The digitonin-cholesterol complex forms an additional layer on the membrane surface with a thickness of 45 Å and being rougher at the outermost interface with the bulk (Fig. 3.18b and Table 3.6). DSC was used to verify if cholesterol is removed from the inner membrane by formation of digitonin-cholesterol; in fact, this is clearly indicated by the reappearance of the main-phase transition of SOPC which can be explained by the removal of substitutional impurities (cholesterol molecules) that initially suppressed the phase transition by sustaining the system in the liquid-ordered phase. This was further verified by experiments with membranes incorporating 5 mol% cholesterol (Fig. 3.20). The strong digitonin-cholesterol complexes formed gaps between the alkyl chains and the inner head groups causing the solution to easily pass through the membrane in both directions, but making the membrane more unstable. The membrane bilayer with rearranged lipid molecules plus digitonin-cholesterol complexes forms stable structures in the form of small compact vesicles. In GUVs the complete process of digitonin-cholesterol interaction could be nicely observed, from the increased membrane permeability to the shrinking vesicle size forming stable membrane structures (Fig. 3.15). At high cholesterol-digitonin concentrations, the vesicles burst (Menger and Keiper 1998). The data clearly explains the ability of digitonin to destroy cell membranes. Rather than inducing pore formation (Dourmashkin et al. 1962) it causes hemitubular or tubular structures (Elias et al. 1978); pore formation does not seem to be attributable to the cell permeabilizing activity of digitonin. In addition, at higher digitonin concentrations tubules will bud from membranes and eventually cause membrane disruption (Miller and Torreyson 1977; Graham et al. 1967). Thus, digitonin does not qualify as a toxicity-enhancing agent.

Quillaja saponin shows a different mechanism of interaction with membrane cholesterol resulting from the combined effect of mono- and bidesmosides. The monodesmosides form complexes with cholesterol that accumulate on the outer membrane layer. This leads to gaps or pores that allow the bidesmosides to penetrate the membrane, which in turn stabilizes the pores. This scenario is supported by our QCM-D data which shows a loss of mass (positive Δf) of the bilayer membrane in the presence of high amounts of quillaja saponin with the membrane structure remaining steady over time, indicating the release of some of the monodesmoside-cholesterol complexes from the membrane, with the empty space being filled by bidesmosides. The membrane structure remaining steady over time, indicating that the absorption of quillaja saponin into the inner membrane does not cause dramatic structural changes. Data of Δf and ΔD show that quillaja saponin effects cylindrical pores in the membranes which allow more water to enter the intermembrane spaces and making the film less rigid (Wang et al. 2011). XRR shows that quillaja saponin inserts into the inner membrane

and remaining there The resulting membrane surface becomes smoother and the space between polar groups at the outer and inner part of the bilayer membrane increase to around 1 $Å^{-2}$ which is large enough for water and small molecules to freely enter the vesicles, the membrane remains intact for a longer period of time, as visualized by GUV (Fig. 3.36). The XRR data do not show the presence of large pores in the membrane, as indicated by the increased density of the inner head group layer by additional water (Wu et al. 2005). These observations can explain the permeability effect of quillaja saponin. Quillaja saponin thus has a potential to serve as a toxicity-enhancing agent, as also shown from cytotoxicity experiments using drug combinations. Bidesmosidic triterpenoid saponins were reported to form pores in the membranes in correlation with cholesterol content (Armah et al. 1999; Li et al. 2005; Lorent et al. 2013, 2014; Böttger and Melzig 2013), to reduce surface tension (Böttger et al. 2012), and effect membrane permeability more than steroid saponins (Gilabert-Oriol et al. 2013). Pore formation is strongly influenced by the presence of both sugar chains at C-3 and C-28 attached to the aglycone. Removing one sugar chain will lead to complete loss of pore-forming ability of triterpenoid saponins (Armah et al. 1999; Keukens et al. 1995). The aldehyde function at C-4 is critical for the toxicity-enhancing effect (Bachran et al. 2006).

4.5 Quillaja saponin – An issue of bidesmosides vs. monodesmosides

Commercial quillaja saponin (DAB, Carl Roth) contains several triterpenoid saponins composed of four types of aglycones: quillaic acid, 22β-hydroxyquillaic acid, phytolaccinic acid, and O-23 acetylated phytolaccinic acid. The type and number of saccharides attached to the aglycones vary.

A total of 70 saponins have been identified from quillaja saponin extract. Many of them are structurally similar, making it difficult to separate them by conventional HPLC. A further complication in trying to isolate the individual components is that quillaja saponins are weak chromophores. Pure standards of the individual components are not available. The identity and quality of commercial quillaja saponin have been evaluated only by comparative HPLC fingerprints. Tandem LC/MS has been used to reveal the components of quillaja saponin extracts (Thalhamer and Himmelsbach 2014; Kite et al. 2004; San Martín and Briones 2000).

The majority of saponins in commercial quillaja saponin extract are bidesmosides (>95%), and monodesmosides occur at a concentration of less than 5%. The latter finding is remarkable in that monodesmosides in commercial quillaja saponin have never been reported to date. Previous to our findings, quillaja saponin extract has always been considered to consist of bidesmosidic triterpenoid saponins such as QS–7 ($C_{83}H_{130}O_{46}$; m/z 1861.7), QS–17 ($C_{104}H_{168}O_{55}$; m/z 2297.03), QS–18 ($C_{98}H_{158}O_{51}$; m/z 2150.9) and QS–21 ($C_{92}H_{148}O_{46}$; m/z 1987.9), used as immunological adjuvants (Kensil et al. 1996; Kensil et al. 1997; Thalhamer and Himmelsbach 2014). Due to the limitations of detection of the LCQ Duo ion trap mass spectrometer with maximum mass detection to m/z 2000, precursors of QS–17 and QS–18 can not be detected. Precursors of QS–7 and QS–21 were detected and their relative amounts in the extract were 6.6% and 14.5%, respectively.

The detected monodesmosides are pure substances – The monodesmosides occurring in the quillaja saponin extract may very well contribute to the overall activity of the extract. While bidesmosides are hemolytically inactive, monodesmosides strongly interact with cholesterol and destroy the cell membranes (Woldemichael and Wink 2001; Wink 2008; Hu et al. 1996). The presence of both bidesmosides and monodesmosides in the quillaja saponin extract may be responsible for its bioactivity and pharmacological effects.

4.6 Saponins and bilayer membranes – proposed mechanisms of interaction

Based on our observations, we propose two different mechanisms of interaction for the steroid saponin digitonin and for the triterpenoid saponin quillaja saponin with cholesterol in bilayer membranes.

4.6.1 Digitonin requires cholesterol to effect bilayer membranes

Interaction and activity of digitonin in the membrane highly depends on the presence of cholesterol. Digitonin cannot interact and affect membranes which do not contain cholesterol. However, digitonin penetrates into membranes containing cholesterol and binds to cholesterol molecules. The cholesterol then migrates from the hydrophobic core region to the outer polar group region in the form of digitonin-cholesterol complex. This does not cause the membrane to rupture. The sterical hindrance between saccharide residues in these aggregates may induce changes in the curvature of the membrane's outer layer leading thus to an increase in membrane permeability. Increasing amounts of cholesterol in the membrane will cause the membrane to more easily rupture in the presence of digitonin (Fig. 4.1).

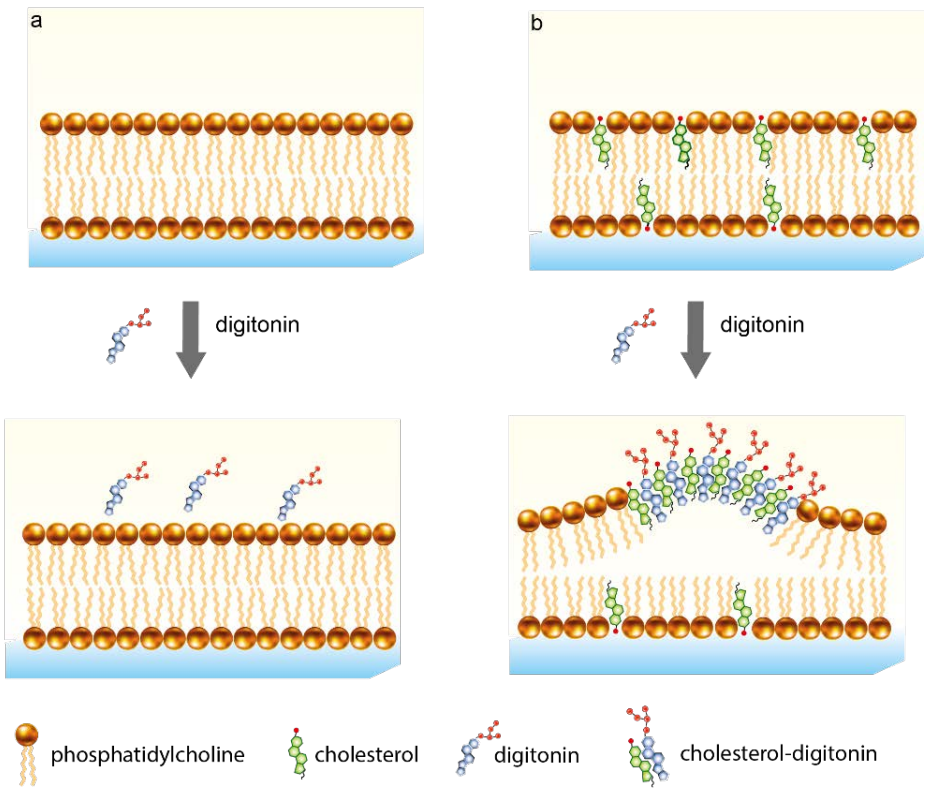

Fig. 4.1. Digitonin – model of interaction of digitonin with bilayer membrane in the absence **(a)** and presence **(b)** of cholesterol.

4.6.2 Quillaja saponin affects bilayer membranes without cholesterol, increases membrane permeability, but leaves the membrane intact

The discovery of monodesmosides in the commercial quillaja extract opens a new perspective in understanding the activities of quillaja saponin on membranes. The monodesmosides and bidesmosides appear to act together in causing membrane permeability. Monodesmosides are known to interact with cholesterol, and bidesmosides lack this ability (Woldemichael and Wink 2001). Bidesmosidic triterpenoid saponins can induce slight permeability changes of liposomal membranes without cholesterol (Fig. 4.2a). Type and number of attached sugar moieties to the triterpenoid aglycone play a great role in causing membrane permeability (Hu et al. 1996). The long polar sugar chains of quillaja saponin at C-28 interact with the hydrophilic top layer of the membrane slightly increasing the permeability, but the interaction is not as strong in the absence of cholesterol.

As proposed in Fig. 4.2b, the monodesmosides from quillaja saponin insert themselves within the lipophilic layer of the membrane and bind to cholesterol molecules there. The monodesmoside-cholesterol complexes move upward and some are released from the membrane. Thereafter, three different scenarios may apply: *i)* The bidesmosides may access the membrane and start filling the empty spaces created by the monodesmoside-cholesterol complexes; the lipophilic region would now become stabilized by the two sugar chains attached to the triterpenoid aglycone; the two sugar chains of the bidesmosides would force a distance between lipid molecules at the outer and inner polar head layer, thus leading to an increase in membrane permeability, while the membrane remains intact. *ii)* The monodesmoside-cholesterol complex could allow the bidesmosides to slip into the membrane with their sugar chains pointing upward. *iii)* The bidesmosides could alternatively form complexes with monodesmosides and cholesterol forcing a distance between the phospholipids and increase membrane permeability while the membrane remains intact.

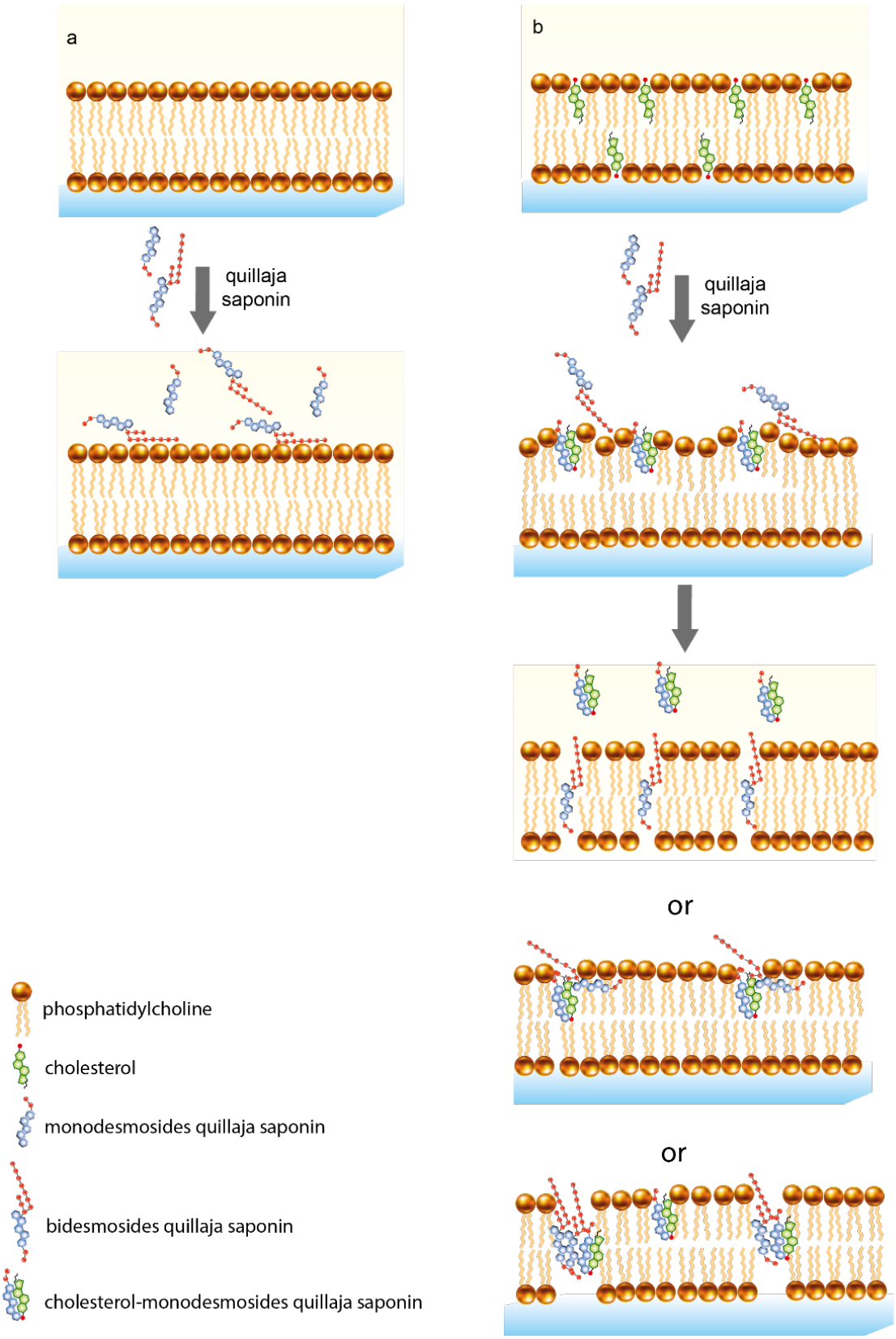

Fig. 4.2. Quillaja saponin – model of interaction of quillaja saponin with bilayer membrane in the absence **(a)** and presence **(b)** of cholesterol.

5 References

Abe I, Rohmer M, Prestwich GD (1993) Enzymatic cyclization of squalene and oxidosqualene to sterols and triterpenes. Chemical Reviews 93 (6):2189-2206

Abuillan W, Schneck E, Körner A, Brandenburg K, Gutsmann T, Gill T, Vorobiev A, Konovalov O, Tanaka M (2013) Physical interactions of fish protamine and antisepsis peptide drugs with bacterial membranes revealed by combination of specular X-ray reflectivity and grazing-incidence x-ray fluorescence. Physical Review E 88 (1):012705

Adachi S, Cross AR, Babior BM, Gottlieb RA (1997) Bcl-2 and the outer mitochondrial membrane in the inactivation of cytochrome *c* during Fas-mediated apoptosis. Journal of Biological Chemistry 272 (35):21878-21882

Akagi M, Fukuishi N, Kan T, Sagesaka YM, Akagi R (1997) Anti-allergic effect of tea-leaf saponin (TLS) from tea leaves (*Camellia sinensis* var. *sinensis*). Biological and Pharmaceutical Bulletin 20 (5):565-567

Akbarzadeh A, Rezaei-Sadabady R, Davaran S, Joo SW, Zarghami N, Hanifehpour Y, Samiei M, Kouhi M, Nejati-Koshki K (2013) Liposome: classification, preparation, and applications. Nanoscale Research Letters 8 (1):102

Akiyama T, Takagi S, Sankawa U, Inari S, Saito H (1980) Saponin-cholesterol interaction in the multibilayers of egg yolk lecithin as studied by deuterium nuclear magnetic resonance: digitonin and its analogs. Biochemistry 19 (9):1904-1911

Andersson L, Bohlin L, Iorizzi M, Riccio R, Minale L, Moreno-López W (1989) Biological activity of saponins and saponin-like compounds from starfish and brittle-stars. Toxicon 27 (2):179-188

Apellániz B, Nieva JL, Schwille P, García-Sáez AJ (2010) All-or-none versus graded: single-vesicle analysis reveals lipid composition effects on membrane permeabilization. Biophysical Journal 99 (11):3619-3628

Armah C, Mackie A, Roy C, Price K, Osbourn A, Bowyer P, Ladha S (1999) The membrane-permeabilizing effect of avenacin A-1 involves the reorganization of bilayer cholesterol. Biophysical Journal 76 (1):281-290

Ashour ML, Wink M (2011) Genus *Bupleurum*: a review of its phytochemistry, pharmacology and modes of action. Journal of Pharmacy and Pharmacology 63 (3):305-321

Augustin JM, Kuzina V, Andersen SB, Bak S (2011) Molecular activities, biosynthesis and evolution of triterpenoid saponins. Phytochemistry 72 (6):435-457

Avato P, Bucci R, Tava A, Vitali C, Rosato A, Bialy Z, Jurzysta M (2006) Antimicrobial activity of saponins from *Medicago* sp.: structure-activity relationship. Phytotherapy Research 20 (6):454-457

Bachran C, Bachran S, Sutherland M, Bachran D, Fuchs H (2008) Saponins in tumor therapy. Mini-Reviews in Medicinal Chemistry 8 (6):575-584

Bachran C, Durkop H, Sutherland M, Bachran D, Muller C, Weng A, Melzig MF, Fuchs H (2009) Inhibition of tumor growth by targeted toxins in mice is dramatically improved by saponinum album in a synergistic way. Journal of Immunotherapy 32 (7):713-725

Bachran C, Sutherland M, Heisler I, Hebestreit P, Melzig MF, Fuchs H (2006) The saponin-mediated enhanced uptake of targeted saporin-based drugs is strongly dependent on the saponin structure. Experimental Biology and Medicine 231 (4):412-420

Bacia K, Schwille P, Kurzchalia T (2005) Sterol structure determines the separation of phases and the curvature of the liquid-ordered phase in model membranes. Proceedings of the National Academy of Sciences of the United States of America 102 (9):3272-3277

Backer JM, Dawidowicz EA (1981) Mechanism of cholesterol exchange between phospholipid vesicles. Biochemistry 20 (13):3805-3810

Bangham A, Horne R (1964) Negative staining of phospholipids and their structural modification by surface-active agents as observed in the electron microscope. Journal of Molecular Biology 8 (5):660-IN610

Bangham A, Horne R, Glauert A, Dingle J, Lucy J (1963) Action of saponin on biological cell membranes. Nature (196):952-955

Bankefors J, Broberg S, Nord LI, Kenne L (2011) Electrospray ionization ion-trap multiple-stage mass spectrometry of Quillaja saponins. Journal of Mass Spectrometry 46 (7):658-665

Bankefors J, Nord LI, Kenne L (2010) Multidimensional profiling of components in complex mixtures of natural products for metabolic analysis, proof of concept: Application to *Quillaja* saponins. Journal of Chromatography B 878 (3):471-476

Batenburg A, De Kruijff B (1988) Modulation of membrane surface curvature by peptide-lipid interactions. Bioscience Reports 8 (4):299-307

Baumann E, Stoya G, Völkner A, Richter W, Lemke C, Linss W (2000) Hemolysis of human erythrocytes with saponin affects the membrane structure. Acta Histochemica 102 (1):21-35

Bennett WD, MacCallum JL, Hinner MJ, Marrink SJ, Tieleman DP (2009) Molecular view of cholesterol flip-flop and chemical potential in different membrane environments. Journal of the American Chemical Society 131 (35):12714-12720

Bernsdorff C, Reszka R, Winter R (1999) Interaction of the anticancer agent Taxol™(paclitaxel) with phospholipid bilayers. Journal of Biomedical Materials Research 46 (2):141-149

Bleicken S, Wagner C, García-Sáez AJ (2013) Mechanistic differences in the membrane activity of Bax and Bcl-xL correlate with their opposing roles in apoptosis. Biophysical Journal 104 (2):421-431

Böttger S, Hofmann K, Melzig MF (2012) Saponins can perturb biologic membranes and reduce the surface tension of aqueous solutions: A correlation? Bioorganic & Medicinal Chemistry 20 (9):2822-2828

Böttger S, Melzig MF (2013) The influence of saponins on cell membrane cholesterol. Bioorganic & Medicinal Chemistry 21 (22):7118-7124

Bourgaux C, Couvreur P (2014) Interactions of anticancer drugs with biomembranes: What can we learn from model membranes? Journal of Controlled Release 190:127-138

Brockman H (1999) Lipid monolayers: why use half a membrane to characterize protein-membrane interactions? Current Opinion in Structural Biology 9 (4):438-443

Brown B, Stafford A, Wright S (1962) Chemical structure and pharmacological activity of some derivatives of digitoxigenin and digoxigenin. British Journal of Pharmacology and Chemotherapy 18 (2):311-324

Brown D, London E (1998) Functions of lipid rafts in biological membranes. Annual Review of Cell and Developmental Biology 14 (1):111-136

Caulier G, Van Dyck S, Gerbaux P, Eeckhaut I, Flammang P (2011) Review of saponin diversity in sea cucumbers belonging to the family Holothuriidae. SPC Beche-de-mer Information Bulletin 31:48-54

Center MS (1985) Mechanisms regulating cell resistance to adriamycin evidence that drug accumulation in resistant cells is modulated by phosphorylation of a plasma membrane glycoprotein. Biochemical Pharmacology 34 (9):1471-1476

Cevc G (1993) Phospholipids Handbook. CRC Press, Boca Raton

Chan YHM, Boxer SG (2007) Model membrane systems and their applications. Current Opinion in Chemical Biology 11 (6):581-587

Chen JC, Chang NW, Chung JG, Chen KC (2003) Saikosaponin-A induces apoptotic mechanism in human breast MDA-MB-231 and MCF-7 cancer cells. American Journal of Chinese Medicine 31 (03):363-377

Chen MS (2008) Inducible direct plant defense against insect herbivores: a review. Insect Science 15 (2):101-114

Chen VY, Posada MM, Zhao L, Rosania GR (2007) Rapid doxorubicin efflux from the nucleus of drug-resistant cancer cells following extracellular drug clearance. Pharmaceutical Research 24 (11):2156-2167

Chou J, Chou T (1988) Computerized simulation of dose reduction index (DRI) in synergistic drug combinations. Pharmacologist 30:A231

Chou TC (2006) Theoretical basis, experimental design, and computerized simulation of synergism and antagonism in drug combination studies. Pharmacological Reviews 58 (3):621-681

Chwalek M, Lalun N, Bobichon H, Plé K, Voutquenne-Nazabadioko L (2006) Structure–activity relationships of some hederagenin diglycosides: haemolysis, cytotoxicity and apoptosis induction. Biochimica et Biophysica Acta (BBA)-General Subjects 1760 (9):1418-1427

Coleman JJ, Okoli I, Tegos GP, Holson EB, Wagner FF, Hamblin MR, Mylonakis E (2010) Characterization of plant-derived saponin natural products against *Candida albicans*. ACS Chemical Biology 5 (3):321-332

Cross GH, Reeves AA, Brand S, Popplewell JF, Peel LL, Swann MJ, Freeman NJ (2003) A new quantitative optical biosensor for protein characterisation. Biosensors and Bioelectronics 19 (4):383-390

Cross GH, Ren Y, Freeman NJ (1999) Young's fringes from vertically integrated slab waveguides: applications to humidity sensing. Journal of Applied Physics 86 (11):6483-6488

De Geyter E, Lambert E, Geelen D, Smagghe G (2007) Novel advances with plant saponins as natural insecticides to control pest insects. Pest Technology 1 (2):96-105

Dixon WE (1912) Critical review: the digitalis preparations employed In medicine. QJM 5 (2):297-307

Dourmashkin R, Dougherty R, HARRIS R (1962) Electron microscopic observations on Rous sarcoma virus and cell membranes. Nature 194:1116-1119

Duan S, Hájek P, Lin C, Shin SK, Attardi G, Chomyn A (2003) Mitochondrial outer membrane permeability change and hypersensitivity to digitonin early in staurosporine-induced apoptosis. Journal of Biological Chemistry 278 (2):1346-1353

Eid SY, El-Readi MZ, Eldin EEMN, Fatani SH, Wink M (2013) Influence of combinations of digitonin with selected phenolics, terpenoids, and alkaloids on the expression and activity of P-glycoprotein in leukaemia and colon cancer cells. Phytomedicine 21 (1):47-61

Eid SY, El-Readi MZ, Wink M (2012a) Digitonin synergistically enhances the cytotoxicity of plant secondary metabolites in cancer cells. Phytomedicine 19 (14):1307-1314

Eid SY, El-Readi MZ, Wink M (2012b) Synergism of three-drug combinations of sanguinarine and other plant secondary metabolites with digitonin and doxorubicin in multi-drug resistant cancer cells. Phytomedicine 19 (14):1288-1297

Ekabo OA, Farnsworth NR, Henderson TO, Mao G, Mukherjee R (1996) Antifungal and molluscicidal saponins from *Serjania salzmanniana*. Journal of Natural Products 59 (4):431-435

Elbandy M, Miyamoto T, Chauffert B, Delaude C, Lacaille-Dubois MA (2002) Novel acylated triterpene glycosides from *Muraltia heisteria*. Journal of Natural Products 65 (2):193-197

Elias PM, Goerke J, Friend DS, Brown BE (1978) Freeze-fracture identification of sterol-digitonin complexes in cell and liposome membranes. Journal of Cell Biology 78 (2):577-596

Evans TG, McElrath MJ, Matthews T, Montefiori D, Weinhold K, Wolff M, Keefer MC, Kallas EG, Corey L, Gorse GJ (2001) QS-21 promotes an adjuvant effect allowing for reduced antigen dose during HIV-1 envelope subunit immmunization in humans. Vaccine 19 (15):2080-2091

Flores-Toro L, Amigo J (2013) Flora autóctona de la cordillera el melón y del cerro tabaco, sitios prioritarios para la conservación de la biodiversidad, Región de Valparaíso, Chile. Native flora of cordillera El Melón and Tabaco mountain, prioritary sites for biodiversity conservation, Región de Valparaíso, Chile. Chloris Chilensis 16 (1)

Francis G, Kerem Z, Makkar HP, Becker K (2002) The biological action of saponins in animal systems: a review. British Journal of Nutrition 88 (6):587-605

Fuchs H, Bachran D, Panjideh H, Schellmann N, Weng A, Melzig M, Sutherland M, Bachran C (2009) Saponins as tool for improved targeted tumor therapies. Current Drug Targets 10 (2):140-151

Gaidi G, Correia M, Chauffert B, Beltramo JL, Wagner H, Lacaille-Dubois MA (2002) Saponins-mediated potentiation of cisplatin accumulation and cytotoxicity in human colon cancer cells. Planta Medica 68 (1):70-72

García-Sáez AJ, Ries J, Orzáez M, Pérez-Payà E, Schwille P (2009) Membrane promotes tBID interaction with BCLXL. Nature Structural & Molecular Biology 16 (11):1178-1185

García-Sáez AJ, Coraiola M, Serra MD, Mingarro I, Müller P, Salgado J (2006) Peptides corresponding to helices 5 and 6 of Bax can independently form large lipid pores. FEBS Journal 273 (5):971-981

Gauthier C, Legault J, Piochon-Gauthier M, Pichette A (2011) Advances in the synthesis and pharmacological activity of lupane-type triterpenoid saponins. Phytochemistry Reviews 10 (4):521-544

Geddes CD Reviews in Fluorescence 2007.

Gilabert-Oriol R, Mergel K, Thakur M, von Mallinckrodt B, Melzig MF, Fuchs H, Weng A (2013) Real-time analysis of membrane permeabilizing effects of oleanane saponins. Bioorganic Medicinal Chemistry 21 (8):2387-2395

Gilewski T, Adluri S, Ragupathi G, Zhang S, Yao T-J, Panageas K, Moynahan M, Houghton A, Norton L, Livingston PO (2000) Vaccination of high-risk breast cancer patients with mucin-1 (MUC1) keyhole limpet hemocyanin conjugate plus QS-21. Clinical Cancer Research 6 (5):1693-1701

Gilewski TA, Ragupathi G, Dickler M, Powell S, Bhuta S, Panageas K, Koganty RR, Chin-Eng J, Hudis C, Norton L (2007) Immunization of high-risk breast cancer patients with clustered sTn-KLH conjugate plus the immunologic adjuvant QS-21. Clinical Cancer Research 13 (10):2977-2985

Gimpl G, Burger K, Fahrenholz F (1997) Cholesterol as modulator of receptor function. Biochemistry 36 (36):10959-10974

Glauert AM, Dingle JT, Lucy JA (1962) Action of saponin on biological cell membranes. Nature 196 (4858):953-955

Gögelein H, Hüby A (1984) Interaction of saponin and digitonin with black lipid membranes and lipid monolayers. Biochimica et Biophysica Acta (BBA)-Biomembranes 773 (1):32-38

Goldstein DB (1984) The effects of drugs on membrane fluidity. Annual Review of Pharmacology and Toxicology 24 (1):43-64

Gottesman MM (2002) Mechanisms of cancer drug resistance. Annual Review of Medicine 53 (1):615-627

Graham R, Karnovsky M, Shafer A, Glass E, Karnovsky ML (1967) Metabolic and morphological observations on the effect of surface-active agents on leukocytes. Journal of Cell Biology 32 (3):629-647

Guo S, Kenne L, Lundgren LN, Rönnberg B, Sundquist BG (1998) Triterpenoid saponins from *Quillaja saponaria*. Phytochemistry 48 (1):175-180

Haddad M, Khan I, Lacaille-Dubois MA (2002) Two new prosapogenins from *Albizia adianthifolia*. Die Pharmazie 57 (10):705-708

Hamilton JA (2003) Fast flip-flop of cholesterol and fatty acids in membranes: implications for membrane transport proteins. Current Opinion in Lipidology 14 (3):263-271

Haralampidis K, Trojanowska M, Osbourn AE (2002) Biosynthesis of triterpenoid saponins in plants. In: Scheper T (ed.) History and Trends in Bioprocessing and Biotransformation. Advances in Biochemical Engineering/Biotechnology, Vol. 75. Springer, Heidelberg Berlin New York, pp. 31-49

Hebestreit P, Melzig MF (2003) Cytotoxic Activity of the Seeds from *Agrostemma githago* var. *githago*. Planta Medica 69 (10):921-925

Hebestreit P, Weng A, Bachran C, Fuchs H, Melzig M (2006) Enhancement of cytotoxicity of lectins by Saponinum album. Toxicon 47 (3):330-335

Hellmann JK, Munter S, Wink M, Frischknecht F (2010) Synergistic and additive effects of epigallocatechin gallate and digitonin on Plasmodium sporozoite survival and motility. PloS one 5 (1):e8682

Hermann E, Bleicken S, Subburaj Y, García-Sáez AJ (2014) Automated analysis of giant unilamellar vesicles using circular Hough transformation. Bioinformatics 30 (12):1747-1754

Herrmann F, Wink M (2011) Synergistic interactions of saponins and monoterpenes in HeLa cells, Cos7 cells and in erythrocytes. Phytomedicine 18 (13):1191-1196

Hikino H, Kiso Y, Kinouchi J, Sanada S, Shoji J (1985) Antihepatotoxic actions of ginsenosides from *Panax ginseng* roots. Planta Medica 51 (1):62-64

Holstein SA, Hohl RJ (2004) Isoprenoids: remarkable diversity of form and function. Lipids 39 (4):293-309

Hope M, Bally M, Webb G, Cullis P (1985) Production of large unilamellar vesicles by a rapid extrusion procedure. Characterization of size distribution, trapped volume and ability to maintain a membrane potential. Biochimica et Biophysica Acta (BBA)-Biomembranes 812 (1):55-65

Hostettmann K, Marston A (2005) Saponins. Cambridge University Press, Cambridge/New York

Hsu MJ, Cheng JS, Huang HC (2000) Effect of saikosaponin, a triterpene saponin, on apoptosis in lymphocytes: association with c-myc, p53, and bcl-2 mRNA. British Journal of Pharmacology 131 (7):1285-1293

Hu M, Konoki K, Tachibana K (1996) Cholesterol-independent membrane disruption caused by triterpenoid saponins. Biochimica et Biophysica Acta (BBA)-Lipids and Lipid Metabolism 1299 (2):252-258

Ikeda T, Yokomizo K, Okawa M, Tsuchihashi R, Kinjo J, Nohara T, Uyeda M (2005) Anti-herpes virus type 1 activity of oleanane-type triterpenoids. Biological and Pharmaceutical Bulletin 28 (9):1779

Jekunen AP, Shalinsky DR, Hom DK, Albright KD, Heath D, Howell SB (1993) Modulation of cisplatin cytotoxicity by permeabilization of the plasma membrane by digitonin in vitro. Biochemical Pharmacology 45 (10):2079-2085

Jesorka A, Orwar O (2008) Liposomes: technologies and analytical applications. Annual Reviews in Analytical Chemistry 1: 801-832

Jin J, Shahi S, Kang HK, van Veen HW, Fan TP (2006) Metabolites of ginsenosides as novel BCRP inhibitors. Biochemical and Biophysical Research Communications 345 (4):1308-1314

Jing Y, Trefna H, Persson M, Kasemo B, Svedhem S (2014) Formation of supported lipid bilayers on silica: relation to lipid phase transition temperature and liposome size. Soft Matter 10 (1):187-195

Johnson I, Gee JM, Price K, Curl C, Fenwick G (1986) Influence of saponins on gut permeability and active nutrient transport in vitro. Journal of Nutrition 116 (11):2270-2277

Kamp F, Zakim D, Zhang F, Noy N, Hamilton JA (1995) Fatty acid flip-flop in phospholipid bilayers is extremely fast. Biochemistry 34 (37):11928-11937

Katsu T, Imamura T, Komagoe K, Masuda K, Mizushima T (2007) Simultaneous measurements of K^+ and calcein release from liposomes and the determination of pore size formed in a membrane. Analytical Sciences 23 (5):517-522

Keller C, Kasemo B (1998) Surface specific kinetics of lipid vesicle adsorption measured with a quartz crystal microbalance. Biophysical Journal 75 (3):1397-1402

Kensil C, Wu J, Anderson C, Wheeler D, Amsden J (1997) QS-21 and QS-7: purified saponin adjuvants. Developments in Biological Standardization 92:41-47

Kensil CR, Patel U, Lennick M, Marciani D (1991) Separation and characterization of saponins with adjuvant activity from *Quillaja saponaria* Molina cortex. Journal of Immunology 146 (2):431-437

Kensil CR, Soltysik S, Wheeler DA, Wu JY (1996) Structure/function studies on QS-21, a unique immunological adjuvant from *Quillaja saponaria*. In: Waller GR, Yamasaki K (eds.) Saponins Used in Traditional and Modern Medicine. Advances in Experimental Medicine and Biology, Vol. 404. Springer, Heidelberg Berlin New York, pp. 165-172

Kern W (1990) The evolution of silicon wafer cleaning technology. Journal of the Electrochemical Society 137 (6):1887-1892

Keukens EA, de Vrije T, Fabrie CH, Demel RA, Jongen WM, de Kruijff B (1992) Dual specificity of sterol-mediated glycoalkaloid induced membrane disruption. Biochimica et Biophysica Acta (BBA)-Biomembranes 1110 (2):127-136

Keukens EA, de Vrije T, van den Boom C, de Waard P, Plasman HH, Thiel F, Chupin V, Jongen WM, de Kruijff B (1995) Molecular basis of glycoalkaloid induced membrane disruption. Biochimica et Biophysica Acta (BBA)-Biomembranes 1240 (2):216-228

Kim SM, Lee SY, Cho JS, Son SM, Choi SS, Yun YP, Yoo HS, Oh KW, Han SB, Hong JT (2010) Combination of ginsenoside Rg3 with docetaxel enhances the susceptibility of prostate cancer cells via inhibition of NF-κB. European Journal of Pharmacology 631 (1):1-9

Kim SM, Lee SY, Yuk DY, Moon DC, Choi SS, Kim Y, Han SB, Oh KW, Hong JT (2009) Inhibition of NF-κB by ginsenoside Rg3 enhances the susceptibility of colon cancer cells to docetaxel. Archives of Pharmaceutical Research 32 (5):755-765

Kinjo J, Yokomizo K, Hirakawa T, Shii Y, Nohara T, Uyeda M (2000) Anti-herpes virus activity of fabaceous triterpenoidal saponins. Biological & Pharmaceutical Bulletin 23 (7):887-889

Kirk DD, Rempel R, Pinkhasov J, Walmsley AM (2004) Application of *Quillaja saponaria* extracts as oral adjuvants for plant-made vaccines. Expert Opinion on Biological Therapy 4 (6):947-958

Kite GC, Howes MJR, Simmonds MS (2004) Metabolomic analysis of saponins in crude extracts of *Quillaja saponaria* by liquid chromatography/mass spectrometry for product authentication. Rapid Communications in Mass Spectrometry 18 (23):2859-2870

Kwon GS, Okano T (1996) Polymeric micelles as new drug carriers. Advanced Drug Delivery Reviews 21 (2):107-116

Lacaille-Dubois MA, Wagner H (1996) A review of the biological and pharmacological activities of saponins. Phytomedicine 2 (4):363-386

Lange Y, Dolde J, Steck TL (1981) The rate of transmembrane movement of cholesterol in the human erythrocyte. Journal of Biological Chemistry 256 (11):5321-5323

Larsson C, Rodahl M, Höök F (2003) Characterization of DNA immobilization and subsequent hybridization on a 2D arrangement of streptavidin on a biotin-modified lipid bilayer supported on SiO_2. Analytical Chemistry 75 (19):5080-5087

Lasic DD (1988) The mechanism of vesicle formation. Biochemical Journal 256 (1):1

Lasic DD (1998) Novel applications of liposomes. Trends in Biotechnology 16 (7):307-321

Lee TH, Hall KN, Swann MJ, Popplewell JF, Unabia S, Park Y, Hahm KS, Aguilar MI (2010) The membrane insertion of helical antimicrobial peptides from the N-terminus of *Helicobacter pylori* ribosomal protein L1. Biochimica et Biophysica Acta (BBA)-Biomembranes 1798 (3):544-557

Li SH, Chu Y (1999) Anti-inflammatory effects of total saponins of *Panax notoginseng*. Zhongguo yao li xue bao. Acta Pharmacologica Sinica 20 (6):551-554

Li XX, Davis B, Haridas V, Gutterman JU, Colombini M (2005) Proapoptotic triterpene electrophiles (avicins) form channels in membranes: cholesterol dependence. Biophysical Journal 88 (4):2577-2584

Lin F, Wang R (2010) Hemolytic mechanism of dioscin proposed by molecular dynamics simulations. Journal of Molecular Modeling 16 (1):107-118

Lindnér PG, Heath D, Howell SB, Naredi PL, Hafström LR (1997) Digitonin enhances the efficacy of carboplatin in liver tumour after intra-arterial administration. Cancer Chemotherapy and Pharmacology 40 (5):444-448

Lingwood D, Simons K (2010) Lipid rafts as a membrane-organizing principle. Science 327 (5961):46-50

Lorent J, Le Duff CS, Quetin-Leclercq J, Mingeot-Leclercq MP (2013) Induction of highly curved structures in relation to membrane permeabilization and budding by the triterpenoid saponins, α- and δ-hederin. Journal of Biological Chemistry 288: 14000-14017

Lorent J, Lins L, Domenech O, Quetin-Leclercq J, Brasseur R, Mingeot-Leclercq MP (2014) Domain formation and permeabilization induced by the saponin α-hederin and its aglycone hederagenin in a cholesterol-containing bilayer. Langmuir 30 (16):4556-4569

Lucio M, Lima J, Reis S (2010) Drug-membrane interactions: significance for medicinal chemistry. Current Medicinal Chemistry 17 (17):1795-1809

Lukyanov AN, Torchilin VP (2004) Micelles from lipid derivatives of water-soluble polymers as delivery systems for poorly soluble drugs. Advanced Drug Delivery Reviews 56 (9):1273-1289

Luqmani Y (2004) Mechanisms of drug resistance in cancer chemotherapy. Medical Principles and Practice: International Journal of Kuwait University, Health Science Centre 14:35-48

Makky A, Daghildjian K, Michel JP, Maillard P, Rosilio V (2012) Assessment of the relevance of supported planar bilayers for modeling specific interactions between glycodendrimeric porphyrins and retinoblastoma cells. Biochimica et Biophysica Acta (BBA)-Biomembranes 1818 (11):2831-2838

Makky A, Michel JP, Maillard P, Rosilio V (2011) Biomimetic liposomes and planar supported bilayers for the assessment of glycodendrimeric porphyrins interaction with an immobilized lectin. Biochimica et Biophysica Acta 1808 (3):656-666

Malmström J, Agheli H, Kingshott P, Sutherland DS (2007) Viscoelastic modeling of highly hydrated laminin layers at homogeneous and nanostructured surfaces: quantification of protein layer properties using QCM-D and SPR. Langmuir 23 (19):9760-9768

Marciani D, Press J, Reynolds R, Pathak A, Pathak V, Gundy L, Farmer J, Koratich M, May R (2000) Development of semisynthetic triterpenoid saponin derivatives with immune stimulating activity. Vaccine 18 (27):3141-3151

Marczak A, Kowalczyk A, Wrzesień-Kus´ A, Robak T, Jóźwiak Z (2006) Interaction of doxorubicin and idarubicin with red blood cells from acute myeloid leukaemia patients. Cell Biology International 30 (2):127-132

Mashaghi A, Swann M, Popplewell J, Textor M, Reimhult E (2008) Optical anisotropy of supported lipid structures probed by waveguide spectroscopy and its application to study of supported lipid bilayer formation kinetics. Analytical Chemistry 80 (10):3666-3676

Matsuda H, Li Y, Yamahara J, Yoshikawa M (1999) Inhibition of gastric emptying by triterpene saponin, momordin Ic, in mice: roles of blood glucose, capsaicin-sensitive sensory nerves, and central nervous system. Journal of Pharmacology and Experimental Therapeutics 289 (2):729-734

Mayer L, Hope M, Cullis P (1986) Vesicles of variable sizes produced by a rapid extrusion procedure. Biochimica et Biophysica Acta (BBA)-Biomembranes 858 (1):161-168

McLean L, Phillips M (1981) Mechanism of cholesterol and phosphatidylcholine exchange or transfer between unilamellar vesicles. Biochemistry 20 (10):2893-2900

McMullen TP, McElhaney RN (1996) Physical studies of cholesterol-phospholipid interactions. Current Opinion in Colloid & Interface Science 1 (1):83-90
Melzig M, Hebestreit P, Gaidi G, Lacaille-Dubois MA (2005) Structure-activity-relationship of saponins to enhance toxic effects of agrostin. Planta Medica 71 (11):1088-1090
Menger FM, Keiper JS (1998) Digitonin as a chemical trigger for the selective transformation of giant vesicles. Angewandte Chemie International Edition 37 (24):3433-3435
Miller RG (1984) Interactions between digitonin and bilayer membranes. Biochimica et Biophysica Acta (BBA)-Biomembranes 774 (1):151-157
Miller RG, Torreyson P (1977) Crystalline patterns of myelin lipids visualized by freeze fracture. Biochimica et Biophysica Acta (BBA)-Biomembranes 466 (2):325-335
Mitaine-Offer AC, Marouf A, Hanquet B, Birlirakis N, Lacaille-Dubois MA (2001) Two triterpene saponins from *Achyranthes bidentata*. Chemical and Pharmaceutical Bulletin 49 (11):1492-1494
Mitra S, Dungan SR (1997) Micellar properties of quillaja saponin. 1. Effects of temperature, salt, and pH on solution properties. Journal of Agricultural and Food Chemistry 45 (5):1587-1595
Mitra S, Dungan SR (2001) Cholesterol solubilization in aqueous micellar solutions of quillaja saponin, bile salts, or nonionic surfactants. Journal of Agricultural and Food Chemistry 49 (1):384-394
Morales-Penningston NF, Wu J, Farkas ER, Goh SL, Konyakhina TM, Zheng JY, Webb WW, Feigenson GW (2010) GUV preparation and imaging: Minimizing artifacts. Biochimica et Biophysica Acta (BBA) - Biomembranes 1798 (7):1324-1332
Mosmann T (1983) Rapid colorimetric assay for cellular growth and survival: application to proliferation and cytotoxicity assays. Journal of Immunological Methods 65 (1):55-63
Muhr P, Likussar W, Schubert-Zsilavecz M (1996) Structure investigation and proton and carbon-13 assignments of digitonin and cholesterol using multidimensional NMR techniques. Magnetic Resonance in Chemistry 34 (2):137-142
Nakamura T, Inoue K, Nojima S, Sankawa U, Shoji J, Kawasaki T, Shibata S (1979) Interaction of saponins with red blood cells as well as with the phosphatidylcholine liposomal membranes. Journal of Pharmacobiodynamics 2 (6):374-382
Nelson A (2006) Co-refinement of multiple-contrast neutron/X-ray reflectivity data using MOTOFIT. Journal of Applied Crystallography 39 (2):273-276
Nishikawa M, Nojima S, Akiyama T, Sankawa U, Inoue K (1984) Interaction of digitonin and its analogs with membrane cholesterol. Journal of Biochemistry 96 (4):1231-1239
Nord LI, Kenne L (1999) Separation and structural analysis of saponins in a bark extract from *Quillaja saponaria* Molina. Carbohydrate Research 320 (1–2):70-81
Oakes SG, Santone KS, Powis G (1987) Effect of some anticancer drugs on the surface membrane electrical properties of differentiated murine neuroblastoma cells. Journal of the National Cancer Institute 79 (1):155-161
Oda K, Matsuda H, Murakami T, Katayama S, Ohgitani T, Yoshikawa M (2000) Adjuvant and haemolytic activities of 47 saponins derived from medicinal and food plants. Biological Chemistry 381 (1):67-74
Ohvo-Rekilä H, Ramstedt B, Leppimäki P, Slotte PJ (2002) Cholesterol interactions with phospholipids in membranes. Progress in Lipid Research 41 (1):66-97
Oyekunle M, Aiyelaagbe O, Fafunso M (2006) Evaluation of the antimicrobial activity of saponins extract of *Sorghum bicolor* L. Moench. African Journal of Biotechnology 5 (23):2405-2407
Papahadjopoulos D, Cowden M, Kimelberg H (1973) Role of cholesterol in membranes effects on phospholipid-protein interactions, membrane permeability and enzymatic activity. Biochimica et Biophysica Acta (BBA)-Biomembranes 330 (1):8-26

Parisio G, Stocchero M, Ferrarini A (2013) Passive membrane permeability: beyond the standard solubility-diffusion model. Journal of Chemical Theory and Computation 9 (12):5236-5246

Park JD, Kim DS, Kwon HY, Son SK, Lee YH, Baek NI, Kim SI, Rhee DK (1996) Effects of ginseng saponin on modulation of multidrug resistance. Archives of Pharmacal Research 19 (3):213-218

Park JD, Rhee DK, Lee YH (2005) Biological activities and chemistry of saponins from *Panax ginseng* CA Meyer. Phytochemistry Reviews 4 (2-3):159-175

Parratt LG (1954) Surface studies of solids by total reflection of X-rays. Physical Review 95 (2):359

Patel H, Tscheka C, Heerklotz H (2009) Characterizing vesicle leakage by fluorescence lifetime measurements. Soft Matter 5 (15):2849-2851

Peppers SC, Holz RW (1986) Catecholamine secretion from digitonin-treated PC12 cells. Effects of Ca^{2+}, ATP, and protein kinase C activators. Journal of Biological Chemistry 261 (31):14665-14669

Podolak I, Galanty A, Sobolewska D (2010) Saponins as cytotoxic agents: a review. Phytochemistry Reviews 9 (3):425-474

Posthumus M, Kistemaker P, Meuzelaar H, Ten Noever de Brauw M (1978) Laser desorption-mass spectrometry of polar nonvolatile bio-organic molecules. Analytical Chemistry 50 (7):985-991

Pott T, Bouvrais H, Méléard P (2008) Giant unilamellar vesicle formation under physiologically relevant conditions. Chemistry and Physics of Lipids 154 (2):115-119

Purrucker O, Hillebrandt H, Adlkofer K, Tanaka M (2001) Deposition of highly resistive lipid bilayer on silicon–silicon dioxide electrode and incorporation of gramicidin studied by ac impedance spectroscopy. Electrochimica Acta 47 (5):791-798

Ragupathi G, Gardner JR, Livingston PO, Gin DY (2011) Natural and synthetic saponin adjuvant QS-21 for vaccines against cancer. Expert Review of Vaccines 10 (4):463-470

Rajendran L, Simons K (2005) Lipid rafts and membrane dynamics. Journal of Cell Science 118 (6):1099-1102

Raju J, Mehta R (2008) Cancer chemopreventive and therapeutic effects of diosgenin, a food saponin. Nutrition and Cancer 61 (1):27-35

Rhodes D, Sarmiento J, Herbette L (1985) Kinetics of binding of membrane-active drugs to receptor sites. Diffusion-limited rates for a membrane bilayer approach of 1,4-dihydropyridine calcium channel antagonists to their active site. Molecular Pharmacology 27 (6):612-623

Richter RP, Bérat R, Brisson AR (2006) Formation of solid-supported lipid bilayers: an integrated view. Langmuir 22 (8):3497-3505

Rosenqvist E, Michaelsen TE, Vistnes AI (1980) Effect of streptolysin O and digitonin on egg lecithin/cholesterol vesicles. Biochimica et Biophysica Acta (BBA)-Biomembranes 600 (1):91-102

Rukmini R, Rawat SS, Biswas SC, Chattopadhyay A (2001) Cholesterol organization in membranes at low concentrations: effects of curvature stress and membrane thickness. Biophysical Journal 81 (4):2122-2134

Sahu N, Banerjee S, Mondal N, Mandal D (2008) Steroidal saponins. In: Kräutler B, Sahu N, Banerjee S, Mondal N, Mandal D (eds.) Fortschritte der Chemie organischer Naturstoffe/Progress in the Chemistry of Organic Natural Products, Vol. 89. Springer, Heidelberg Berlin New York, pp. 45-141

San Martín R, Briones R (1999) Industrial uses and sustainable supply of *Quillaja saponaria* (Rosaceae) saponins. Economic Botany 53 (3):302-311

San Martín R, Briones R (2000) Quality control of commercial quillaja (*Quillaja saponaria* Molina) extracts by reverse phase HPLC. Journal of the Science of Food and Agriculture 80 (14):2063-2068

Santos WR, Bernardo RR, Peçanha LMT, Palatnik M, Parente J, de Sousa CBP (1997) Haemolytic activities of plant saponins and adjuvants. Effect of *Periandra mediterranea* saponin on the humoral response to the FML antigen of *Leishmania donovani*. Vaccine 15 (9):1024-1029

Sauerbrey G (1959) Use of quartz vibration for weighing thin films on a microbalance. Zeitschrift für Physik 155 (2):206-212 (in German)

Schneck E, Oliveira RG, Rehfeldt F, Demé B, Brandenburg K, Seydel U, Tanaka M (2009) Mechanical properties of interacting lipopolysaccharide membranes from bacteria mutants studied by specular and off-specular neutron scattering. Physical Review E 80 (4):041929

Seddon AM, Casey D, Law RV, Gee A, Templer RH, Ces O (2009) Drug interactions with lipid membranes. Chemical Society Reviews 38 (9):2509-2519

Seeman P, Cheng D, Iles G (1973) Structure of membrane holes in osmotic and saponin hemolysis. Journal of Cell Biology 56 (2):519-527

Seitz PC, Reif M, Yoshikawa K, Jordan R, Tanaka M (2011) Dissipative structure formation in lipid/lipopolymer monolayers. Journal of Physical Chemistry B 115 (10):2256-2263

Seydel JK, Wiese M (2009) Drug-Membrane Interactions: Analysis, Drug Distribution, Modeling, Vol. 15. John Wiley & Sons, New York

Shany S, Bernheimer AW, Grushoff PS, Kim KS (1974) Evidence for membrane cholesterol as the common binding site for cereolysin, streptolysin O and saponin. Molecular and Cellular Biochemistry 3 (3):179-186

Shyu KG, Tsai SC, Wang BW, Liu YC, Lee CC (2004) Saikosaponin C induces endothelial cells growth, migration and capillary tube formation. Life Sciences 76 (7):813-826

Simões C, Amoros M, Girre L (1999) Mechanism of antiviral activity of triterpenoid saponins. Phytotherapy Research 13 (4):323-328

Simons K, Toomre D (2000) Lipid rafts and signal transduction. Nature Reviews Molecular Cell Biology 1 (1):31-39

Somova L, Nadar A, Rammanan P, Shode F (2003) Cardiovascular, antihyperlipidemic and antioxidant effects of oleanolic and ursolic acids in experimental hypertension. Phytomedicine 10 (2):115-121

Song X, Hu S (2009) Adjuvant activities of saponins from traditional Chinese medicinal herbs. Vaccine 27 (36):4883-4890

Sparg SG, Light ME, van Staden J (2004) Biological activities and distribution of plant saponins. Journal of Ethnopharmacology 94 (2-3):219-243

Stanimirova R, Marinova K, Tcholakova S, Denkov ND, Stoyanov S, Pelan E (2011) Surface rheology of saponin adsorption layers. Langmuir 27 (20):12486-12498

Stark A, Madar Z (1993) The effect of an ethanol extract derived from fenugreek (*Trigonella foenum-graecum*) on bile acid absorption and cholesterol levels in rats. British Journal of Nutrition 69 (1):277-287

Steck TL, Ye J, Lange Y (2002) Probing red cell membrane cholesterol movement with cyclodextrin. Biophysical Journal 83 (4):2118-2125

Stine KJ, Hercules RK, Duff JD, Walker BW (2006) Interaction of the glycoalkaloid tomatine with DMPC and sterol monolayers studied by surface pressure measurements and Brewster angle microscopy. Journal of Physical Chemistry B 110 (44):22220-22229

Sun HX, Xie Y, Ye YP (2009a) Advances in saponin-based adjuvants. Vaccine 27 (12):1787-1796

Sun Y, Cai TT, Zhou XB, Xu Q (2009b) Saikosaponin a inhibits the proliferation and activation of T cells through cell cycle arrest and induction of apoptosis. International Immunopharmacology 9 (7):978-983

Szabo G (1974) Dual mechanism for the action of cholesterol on membrane permeability. Nature 252:47-49

Takagi S, Otsuka H, Akiyama T, Sankawa U (1982) Digitonin-cholesterol complex formation – effects of varying the length of the side chain. Chemical and Pharmaceutical Bulletin 30 (10):3485-3492

Takechi M, Wakayama Y (2003) Biological activities of synthetic saponins and cardiac glycosides. Phytotherapy Research 17 (1):83-85

Tamba Y, Ohba S, Kubota M, Yoshioka H, Yoshioka H, Yamazaki M (2007) Single GUV method reveals interaction of tea catechin (−)-epigallocatechin gallate with lipid membranes. Biophysical Journal 92 (9):3178-3194

Tamba Y, Yamazaki M (2005) Single giant unilamellar vesicle method reveals effect of antimicrobial peptide magainin 2 on membrane permeability. Biochemistry 44 (48):15823-15833

Tanaka T, Kaneda Y, Li TS, Matsuoka T, Zempo N, Esato K (2001) Digitonin enhances the antitumor effect of cisplatin during isolated lung perfusion. Annals of Thoracic Surgery 72 (4):1173-1178

Tanford C (1974) Theory of micelle formation in aqueous solutions. Journal of Physical Chemistry 78 (24):2469-2479

Tannock IF, Lee CM, Tunggal JK, Cowan DS, Egorin MJ (2002) Limited penetration of anticancer drugs through tumor tissue a potential cause of resistance of solid tumors to chemotherapy. Clinical Cancer Research 8 (3):878-884

Thakur M, Mergel K, Weng A, Frech S, Gilabert-Oriol R, Bachran D, Melzig MF, Fuchs H (2012) Real time monitoring of the cell viability during treatment with tumor-targeted toxins and saponins using impedance measurement. Biosensors and Bioelectronics 35 (1):503-506

Thalhamer B, Himmelsbach M (2014) Characterization of quillaja bark extracts and evaluation of their purity using liquid chromatography–high resolution mass spectrometry. Phytochemistry Letters 8:97-100

Tolan M (1999) X-Ray Scattering from Soft-Matter Thin Films. Springer, Heidelberg Berlin New York

Trouillas P, Corbière C, Liagre B, Duroux JL, Beneytout JL (2005) Structure–function relationship for saponin effects on cell cycle arrest and apoptosis in the human 1547 osteosarcoma cells: a molecular modelling approach of natural molecules structurally close to diosgenin. Bioorganic & Medicinal Chemistry 13 (4):1141-1149

van Setten DC, van de Werken G (1996) Molecular structures of saponins from *Quillaja saponaria* Molina. In: Waller GR, Yamasaki K (eds.) Saponins Used in Traditional and Modern Medicine. Advances in Experimental Medicine and Biology, Vol. 404. Springer, Heidelberg Berlin New York, pp. 185-193

Vercesi AE, Bernardes C, Hoffmann M, Gadelha F, Docampo R (1991) Digitonin permeabilization does not affect mitochondrial function and allows the determination of the mitochondrial membrane potential of *Trypanosoma cruzi* in situ. Journal of Biological Chemistry 266 (22):14431-14434

Versantvoort C, Broxterman H, Feller N, Dekker H, Kuiper C, Lankelma J (1992) Probing daunorubicin accumulation defects in non-P-glycoprotein expressing multidrug-resistant cell lines using digitonin. International Journal of Cancer 50 (6):906-911

Vincken JP, Heng L, de Groot A, Gruppen H (2007) Saponins, classification and occurrence in the plant kingdom. Phytochemistry 68 (3):275-297

Voinova MV, Rodahl M, Jonson M, Kasemo B (1999) Viscoelastic acoustic response of layered polymer films at fluid-solid interfaces: continuum mechanics approach. Physica Scripta 59 (5):391

Voutquenne L, Lavaud C, Massiot G, Men-Olivier LL (2002) Structure-activity relationships of haemolytic saponins. Pharmaceutical Biology 40 (4):253-262

Walde P, Cosentino K, Engel H, Stano P (2010) Giant vesicles: preparations and applications. ChemBioChem 11 (7):848-865

Walker BW, Manhanke N, Stine KJ (2008) Comparison of the interaction of tomatine with mixed monolayers containing phospholipid, egg sphingomyelin, and sterols. Biochimica et Biophysica Acta (BBA)-Biomembranes 1778 (10):2244-2257

Wang CZ, Luo X, Zhang B, Song WX, Ni M, Mehendale S, Xie JT, Aung HH, He TC, Yuan CS (2007a) Notoginseng enhances anti-cancer effect of 5-fluorouracil on human colorectal cancer cells. Cancer Chemotherapy and Pharmacology 60 (1):69-79

Wang KF, Nagarajan R, Mello CM, Camesano TA (2011) Characterization of supported lipid bilayer disruption by chrysophsin-3 using QCM-D. Journal of Physical Chemistry B 115 (51):15228-15235

Wang Y, Lu X, Xu G (2008) Development of a comprehensive two-dimensional hydrophilic interaction chromatography/quadrupole time-of-flight mass spectrometry system and its application in separation and identification of saponins from *Quillaja saponaria*. Journal of Chromatography A 1181 (1):51-59

Wang Y, Zhang Y, Zhu Z, Zhu S, Li Y, Li M, Yu B (2007b) Exploration of the correlation between the structure, hemolytic activity, and cytotoxicity of steroid saponins. Bioorganic & Medicinal Chemistry 15 (7):2528-2532

Wang Z, Zheng Q, Liu K, Li G, Zheng R (2006) Ginsenoside Rh2 enhances antitumour activity and decreases genotoxic effect of cyclophosphamide. Basic & Clinical Pharmacology & Toxicology 98 (4):411-415

Weber PA, Chang HC, Spaeth KE, Nitsche JM, Nicholson BJ (2004) The permeability of gap junction channels to probes of different size is dependent on connexin composition and permeant-pore affinities. Biophysical Journal 87 (2):958-973

Wen-Sheng W (2003) ERK signaling pathway is involved in p15INK4b/p16INK4a expression and HepG2 growth inhibition triggered by TPA and Saikosaponin a. Oncogene 22 (7):955-963

Weng A, Thakur M, Schindler A, Fuchs H, Melzig M (2011) Liquid-chromatographic profiling of Saponinum album (Merck). Die Pharmazie – An International Journal of Pharmaceutical Sciences 66 (10):744-746

Weng A, Thakur M, von Mallinckrodt B, Beceren-Braun F, Gilabert-Oriol R, Wiesner B, Eichhorst J, Böttger S, Melzig MF, Fuchs H (2012) Saponins modulate the intracellular trafficking of protein toxins. Journal of Controlled Release 164 (1):74-86

Wilson SP, Kirshner N (1983) Calcium-evoked secretion from digitonin-permeabilized adrenal medullary chromaffin cells. Journal of Biological Chemistry 258 (8):4994-5000

Wink M (2008) Evolutionary advantage and molecular modes of action of multi-component mixtures used in phytomedicine. Current Drug Metabolism 9 (10):996-1009

Wink M (2012) Medicinal plants: a source of anti-parasitic secondary metabolites. Molecules 17 (11):12771-12791

Wink M, Schimmer O (2010) Molecular modes of action of defensive secondary metabolites. In: Wink M (ed) Functions and Biotechnology of Plant Secondary Metabolites, 2nd edn. Annual Plant Reviews 39, pp. 21-161

Wink M, Van Wyk BE (2008) Mind-Altering and Poisonous Plants of the World. Timber Press, Portland, OR, USA

Wink M, Van Wyk BE, Wink C (2008) Handbuch der giftigen und psychoaktiven Pflanzen. Wissenschaftliche Verlagsgesellschaft, Stuttgart

Wojciechowski K, Orczyk M, Gutberlet T, Trapp M, Marcinkowski K, Kobiela T, Geue T (2014a) Unusual penetration of phospholipid mono- and bilayers by Quillaja bark saponin biosurfactant. Biochimica et Biophysica Acta (BBA)-Biomembranes 1838 (7):1931-1940

Wojciechowski K, Orczyk M, Marcinkowski K, Kobiela T, Trapp M, Gutberlet T, Geue T (2014b) Effect of hydration of sugar groups on adsorption of *Quillaja* bark saponin at air/water and Si/water interfaces. Colloids and Surfaces B: Biointerfaces 117:60-67

Woldemichael GM, Wink M (2001) Identification and biological activities of triterpenoid saponins from *Chenopodium quinoa*. Journal of Agricultural and Food Chemistry 49 (5):2327-2332

Wu G, Majewski J, Ege C, Kjaer K, Weygand MJ, Lee KYC (2005) Interaction between lipid monolayers and poloxamer 188: an X-ray reflectivity and diffraction study. Biophysical Journal 89 (5):3159-3173

Wu JC, Lin TL, Yang CP, Jeng US, Lee HY, Shih MC (2006) X-ray reflectivity and BAM studies on the LB film of mixed DPPC/DC-cholesterol monolayer. Colloids and Surfaces A: Physicochemical and Engineering Aspects 284:103-108

Wu JY, Gardner B, Murphy C, Seals J, Kensil C, Recchia J, Beltz G, Newman G, Newman M (1992) Saponin adjuvant enhancement of antigen-specific immune responses to an experimental HIV-1 vaccine. Journal of Immunology 148 (5):1519-1525

Wu WS, Hsu HY (2001) Involvement of p-15 INK4b and p-16 INK4a gene expression in saikosaponin a and TPA-induced growth inhibition of HepG2 cells. Biochemical and Biophysical Research Communications 285 (2):183-187

Xie X, Eberding A, Madera C, Fazli L, Jia W, Goldenberg L, Gleave M, Guns ES (2006) Rh2 synergistically enhances paclitaxel or mitoxantrone in prostate cancer models. Journal of Urology 175 (5):1926-1931

Xu Y, Chiu JF, He QY, Chen F (2009) Tubeimoside-1 exerts cytotoxicity in HeLa cells through mitochondrial dysfunction and endoplasmic reticulum stress pathways. Journal of Proteome Research 8 (3):1585-1593

Yang CR, Zhang Y, Jacob MR, Khan SI, Zhang YJ, Li XC (2006) Antifungal activity of C-27 steroidal saponins. Antimicrobial Agents and Chemotherapy 50 (5):1710-1714

Yang CY, Wang J, Zhao Y, Shen L, Jiang X, Xie ZG, Liang N, Zhang L, Chen ZH (2010) Anti-diabetic effects of *Panax notoginseng* saponins and its major anti-hyperglycemic components. Journal of Ethnopharmacology 130 (2):231-236

Yang XW, Zhao J, Cui YX, Liu XH, Ma CM, Hattori M, Zhang LH (1999) Anti-HIV-1 protease triterpenoid saponins from the seeds of *Aesculus chinensis*. Journal of Natural Products 62 (11):1510-1513

Yeagle PL (2012) The roles of cholesterol in the biology of cells. In: Yeagle PL (ed) The Structure of Biological Membranes, 3rd edn. CRC Press, Boca Raton, pp. 119-132

Yokoyama S (2000) Release of cellular cholesterol: molecular mechanism for cholesterol homeostasis in cells and in the body. Biochimica et Biophysica Acta (BBA)-Molecular and Cell Biology of Lipids 1529 (1):231-244

Yu BS, Choi HO (1986) The effects of digitonin and glycyrrhizin on liposomes. Archives of Pharmaceutical Research 9 (3):119-125

Yu BS, Chung HH, Kim A (1984) Effects of saponins on the osmotic behavior of multilamellar liposomes. Archives of Pharmaceutical Research 7 (1):17-22

Yu Ml, Zhang Cl, Yuan DD, Tong XH, Tao L (2012) *Panax notoginseng* saponins enhances the cytotoxicity of cisplatin via increasing gap junction intercellular communication. Biological and Pharmaceutical Bulletin 35 (8):1230-1237

Zhang C, Tong X, Qi B, Yu X, Dong S, Zhang S, Li X, Yu M (2013) Components of *Panax notoginseng* saponins enhance the cytotoxicity of cisplatin via their effects on gap junctions. Molecular Medicine Reports 8 (3):897-902

Zhang JD, Xu Z, Cao YB, Chen HS, Yan L, An MM, Gao PH, Wang Y, Jia XM, Jiang YY (2006) Antifungal activities and action mechanisms of compounds from *Tribulus terrestris* L. Journal of Ethnopharmacology 103 (1):76-84

Zhao L, Wientjes MG, Au JL (2004) Evaluation of combination chemotherapy: integration of nonlinear regression, curve shift, isobologram, and combination index analyses. Clinical Cancer Research 10 (23):7994-8004

Zhou S, Lim LY, Chowbay B (2004) Herbal modulation of P-glycoprotein. Drug Metabolism Reviews 36 (1):57-104

Appendix

Quillaja saponin (DAB, Carl Roth GmbH) – data from mass spectral analysis (M, monodesmoside)

No	RT Sample (min)	$[M–H]^-$ (m/z)	A ion (m/z)	MS2	Precursor	Note
1	1.76	1658.69		1462.03; 1469.11; 1559.10; 1802.11	1802.11	
2	2.01	1649.83		919.24; 1022.41; 1218.79; 1445.27; 1646.65; 17336.32; 1882.57	1882.57	
3	2.95	780.82		311.13; 405.00; 466.61; 536.08; 602.02; 688.49; 720.06		M
4	3.13	1641.51		541.10; 940.99; 1080.80; 1195.56; 1245.67; 1307.11; 1580.48; 1701.61	1701.61	
5	3.37	986.82		451.15; 927.20		
6	3.49	1007.33	925	340.69; 454.97; 633.30; 779.32; 861.30; 925.25; 970.59		
7	3.66	510.84		254.99; 331.33; 483.16		
8	4.32	1923.81		683.08; 750.65; 855.54; 954.08; 1055.23; 1236.83; 1454.94; 1563.38; 1664.91; 1819.50; 1854.22; 1996.35		
9	4.72	239.15		178.97; 220.99; 275.11		
10	4.83	1085.05		593.09; 611.49; 784.71; 830.62; 844.92; 1025.13; 1048.18		
11	4.89	1730.3		1028.13; 1078.72; 1176.00; 1281.07; 1342.06; 1424.75; 1479.88; 1631.69; 1683.03; 1928.47	1928.47	
12	5.01	1793.86		845.01; 1244.97; 1406.15; 1509.04; 1599.81; 1720.26; 1924.77	1924.77	
13	5.07	856.84		536.84; 557.20; 663.14; 680.86; 773.62; 809.99; 826.64; 1118.12	1118.12	
14	5.13	1676.98		1014.18; 1064.92; 1169.08; 1258.96; 1477.07; 1529.16; 1585.84; 1743.68	1743.68	
15	5.28	413.18		149.04; 195.12; 217.12; 234.59; 305.09; 394.85		
16	5.33	843.02		451.36; 625.11; 647.17; 662.97; 877.11		
17	5.51	842.89		451.36; 625.11; 647.17; 662.97; 877.11		
18	5.68	685.38		247.00; 343.18; 423.17; 467.29; 489.20; 667.18		
19	5.8	581.4		203.05; 233.05; 387.01; 419.18; 535.07; 566.12		
20	6.08	626.59		461.69; 542.89; 558.85; 575.57		
21	6.14	969.51		626.89; 742.66; 789.54; 890.50; 901.92; 923.14		
22	6.2	872.92		606.74; 655.30; 723.70; 827.05; 845.53		
23	6.26	942.96		428.99; 483.06; 618.87; 632.95; 718.89; 779.09; 900.24; 924.14; 1689.76	1689.76	
24	6.32	1071.11	925	487.08; 762.49; 779.52; 925.29; 1089.53	1089.53	
25	6.39	1220.02		525.13; 645.13; 893.28; 927.36; 1073.32; 1118.11		
26	6.45	1219.28		438.70; 524.98; 747.41; 927.18; 1073.29; 1118.35		
27	6.51	1203.39		893.35; 1057.25; 1141.10		
28	6.63	1057.36	925	307.02: 441.04; 585.38; 765.35; 911.28; 925.24, 937.18		
29	7.28	925.27		341.34; 453.26; 615.33; 761.33; 779.30; 805.14		

30	7.7	1057.37		381.13; 587.29; 731.32; 893.28; 911.28; 925.24; 937.25		
31	8.05	925.24		307.17; 455.26; 615.58; 761.44; 779.31; 805.23		
32	8.53	925.32		307.02; 487.28; 761.36; 779.28; 824.93; 970.80		
33	9.19	927.29	985	306.99; 398.81; 599.17; 633.13; 779.25; 878.39; 985.86; 1201.81	1201.81	
34	9.31	1071.42		473.31; 713.10; 779.40; 925.23; 1445.05; 1802.55	1802.55	
35	9.71	1057.38		381.34; 585.33; 765.36; 911.28; 925.21; 937.36; 1082.50	1082.5	
36	10.21	1217.19		357.20; 473.29; 617.20; 713.36; 763.23; 859.17; 925.13; 964.88; 1071.22; 1424.13	1424.13	
37	10.27	1262.56		954.21; 1115.11; 1219.24		
38	10.43	1350.45		507.14; 585.41; 747.27; 845.21; 910.99; 991.29; 1057.41; 1203.23; 1263.56; 1567.33; 1710.98		
39	10.49	1099.37		632.99; 779.17; 953.34; 1057.33; 1094.52; 1422.09; 1545.79; 1748.50	1748.5	
40	10.61	1054.68		1212.71; 1265.25; 1539.95	1539.95	
41	10.74	1009.2		1009.72; 1051.11; 1156.58; 1180.82; 1418.65; 1990.48	1990.48	
42	10.8	1136.47		1130.87; 1888.25	1888.25	
43	11.05	967.31		301.38; 529.27; 701.02; 821.18; 921.04; 1098.95	1098.95	
44	11.54	925.31		307.14; 487.11; 633.34; 779.30; 805.07; 1336.62		
45	11.84	755.05		562.88; 685.41; 708.88; 772.25; 1049.14; 1101.77; 1177.14; 1238.73	1238.73	
46	12.13	1349.36		423.32; 743.67; 895.13; 1057.36; 1203.33; 1368.54; 1671.75	1671.75	
47	12.38	925.29		306.89; 450.96; 761.27; 779.28; 860.69; 1047.50; 1394.22	1394.22	
48	13.06	1349.36		469.55; 587.01; 925.41; 1057.44; 1203.34; 1246.24, 1500.49; 1892.39	1892.39	
49	13.8	925.17		307.12; 454.85; 633.17; 779.27; 877.73; 1167.95; 1697.51; 1816.15	1816.15	
50	14.05	1217.15		470.75; 633.35; 889.19; 925.30; 1071.25; 1116.62; 1499.17	1499.17	
51	14.05	1263.44	955	453.99; 639.85; 955.15; 1217.01; 1291.02; 1612.69; 1707.94; 1840.24; 1940.43	1940.43	
52	14.61	1217.36		487.35; 578.90; 779.16; 925.26; 951.05; 1071.27; 1116.97; 1288.57	1288.57	
53	15.46	1349.33	895	441.29; 779.49; 895.47; 1057.37; 1203.34; 1245.27	1245.27	
54	15.52	1350.38		487.29; 747.01; 925.31; 1057.40; 1203.44; 1248.44; 1535.97	1535.97	
55	16.17	745.12		373.24; 457.02; 599.13; 640.91		M
56	16.2	1357.15		1163.79; 1224.33; 1272.26; 1412.18; 1584.44; 1711.82; 1767.84; 1958.59	1958.59	
57	16.2	1217.32		373.21; 778.69; 925.25; 1071.19; 1193.37; 1369.47	1369.47	
58	16.57	1071.3		779.38; 925.19; 1088.71; 1331.87; 1766.62	1766.62	
59	17.02	1295.16		920.65; 1272.33; 1447.65	1447.65	
60	17.58	1217.36		359.15; 633.12; 779.29; 925.29; 951.52; 1071.28; 1115.99; 1372.39	1372.39	
61	18.38	1279.24		908.02; 1104.25; 1132.11; 1315.46	1315.46	

62	20.14	1151.27		782.17; 1018.27; 1093.51; 1774.89	1774.89	
63	20.14	1297.25		486.13; 871.33; 928.11, 1115.77; 1150.75; 1289.14; 1488.66; 1906.45	1906.45	
64	20.63	1414.86	853	645.17; 709.21; 853.82; 1040.28; 1132.55; 1302.04; 1341.38; 1367.67; 1634.63; 1894.15	1894.15	
65	21.05	1561.14		525.67; 545.30; 650.19; 849.61; 872.09; 888.46; 1059.72; 1196.44; 1312.66; 1384.23; 1413.63; 1470.13; 1509.34; 1703.68; 1845.68; 1956.75	1956.75	
66	21.72	985.65		301.21; 449.40; 483.34; 501.40; 595.44; 641.35; 787.35; 805.41; 923.46; 967.40		A ion fragmentation
67	22.25	971.41		274.97; 355.43; 439.44; 483.67; 501.60; 595.60; 641.63; 777.57; 839.51; 909.49; 953.47		
68	22.37	1428.98		632.38; 845.36; 871.28; 921.90; 944.81; 1054.50; 1189.16; 1236.64; 1285.38; 1396.66; 1498.40; 1643.28; 1884.02; 1974.44	1974.44	
69	22.48	639.29		231.17; 325.21; 467.25; 509.23; 621.23		M
70	22.54	1515.55		503.61; 615.34; 707.44; 827.50; 974.52; 1105.58; 1237.60; 1369.67; 1426.52; 1505.64		
71	22.71	1383.51		438.90; 499.12; 645.18; 707.29; 737.16; 1075.40; 1147.49; 1237.48; 1293.44		
72	22.92	1353.62		469.20; 615.23; 665.47; 811.28; 1053.54; 1075.37; 1117.43; 1207.58; 1263.36		
73	23.56	1398.99		638.21; 659.37; 782.38; 836.45; 1237.31; 1282.33; 1326.45		
74	23.79	1353.54	985	483.22; 615.26; 707.38; 985.29; 1075.43; 1221.50; 1263.36, 1399.08	1399.08	
75	23.84	1398.86		467.26; 576.91; 625.32; 659.14; 709.41; 870.69; 942.96; 1045.27; 1158.24; 1251.44; 1325.73; 1377.74		
76	23.96	1221.47	985	439.21; 555.13; 645.22; 749.32; 925.21; 985.27; 1075.44; 1131.34; 1190.48		
77	24.01	1266.95		484.11; 822.03; 835.98; 968.90		
78	24.13	1221.47	985	422.75; 483.23; 545.42; 707.32; 730.45; 853.04; 985.10; 1075.43; 1131.34		
79	24.46	1207.55		392.39; 451.05; 469.20; 541.20; 665.35; 737.38; 793.27; 971.54; 1075.45; 1117.46		
80	24.52	1674.71	955	495.69; 579.25, 823.46; 955.53; 1205.54; 1344.80; 1541.47; 1651.49		
81	24.57	1673.69	955	485.30; 579.40; 823.48; 955.59; 1151.61; 1344.09; 1541.58; 1656.36		
82	24.68	1877				No MS2 data
83	24.74	1399		554.74; 575.31; 708.88; 842.78; 947.07; 1097.70; 1119.33; 1267.69; 1355.24; 1954.35	1954.35	
84	25.14	1191.56	955	483.34; 545.36; 615.28; 637.48; 823.66; 894.81; 955.54; 1101.38; 1173.20		
85	25.6	1511.63	955	485.42; 579.44; 823.49; 955.54; 1042.64; 1241.48; 1379.47; 1493.60	1493.6	
86	25.77	1565.71	939	512.35; 681.06; 844.22; 939.69; 1095.76; 1255.91; 1421.60; 1463.55; 1503.55; 1532.60		
87	25.93	1191.59		423.06; 483.14; 615.19; 913.44; 964.44; 1059.42; 1101; 1146.94		
88	25.93	1237		711.38; 729.11; 1208.65		

89	26.66	1105.01		580.07; 971.83; 1008.46		
90	26.72	1059.45		969.19		
91	26.99	1861.8	955	539.61; 743.26; 906.40; 955.48; 971.37; 1245.97; 1555.51; 1700.69; 1730.58; 1843.57; 1921.37	1921.37	
92	27.09	1716.83	955	485.29; 579.47; 823.58; 955.49; 1116.66; 1312.55; 1553.02; 1584.39; 1698.18; 1861.55	1861.55	
93	27.09	1863.52	955	537.18; 553.42; 743.19; 905.34; 955.54; 1233.25; 1332.69; 1611.53; 1729.53; 1843.44; 1922.10		
94	27.14	827.3		246.10; 469.30; 545.40; 733.23; 781.28; 827.16		
95	27.14	1716.07	955	485.29; 579.47; 823.58; 955.49; 1116.66; 1312.55; 1553.02; 1584.39; 1698.18; 1861.55		
96	27.2	827.26	955	247.20; 503.53; 733.24; 781.27; 826.79; 955.41	955.41	
97	27.49	1699.58	955	535.56; 579.35; 805.50; 893.53; 955.52; 1127.35; 1323.58; 1491.55; 1538.81; 1567.56; 1640.58		
98	27.65	1773.6	971	595.55; 631.39; 777.31; 909.51; 971.51; 1175.67; 1427.47; 1585.75; 1641.67; 1755.62; 1826.65	1826.65	
99	27.75	955.55		319.96; 405.57; 485.53; 579.46; 761.49; 775.49; 823.42; 893.50; 909.83		A ion fragmentation
100	28.22	1757.75	955	501.39; 579.31; 823.44; 955.51; 1186.09; 1287.56; 1535.49; 1626.70; 1697.51; 1740.54; 1898.53	1898.53	
101	28.28	1553.56	955	485.07; 689.46; 805.40; 893.44; 955.53; 1165.50; 1391.60; 1421.63; 1449.72; 1626.55; 1813.42	1813.42	
102	28.62	1331.56	895	452.38; 545.17; 650.31; 665.43; 793.36; 895.53; 939.56; 1031.46; 1271.41		
103	28.85	711.36		665.34; 711.20		M
104	28.9	1904.63	955	553.57; 699.48; 823.50; 955.52; 971.43; 1272.66; 1528.12; 1697.38; 1742.63; 1772.66; 1799.75; 1885.70; 1974.06	1974.06	
105	28.96	1903.56	955.55	554.28; 699.07; 805.43; 955.55; 971.56; 1289.59; 1433.57; 1641.60; 1741.82; 1771.80; 1918.72; 1954.32		
106	29.12	1475.75	895	516.30; 625.57; 791.64; 895.53; 937.50; 1084.55; 1295.65; 1331.60; 1373.57; 1433.63; 1518.44; 1973.42		
107	29.3	1948.72	955	581.51; 715.97; 823,49; 955.56; 973.35; 1150.58; 1330.91; 1574.50; 1699.62; 1786.60; 1816.80; 1861.74; 1929.67		
108	29.4	793.42		306.93; 405.58; 485.42; 513.38; 567.39; 661.39; 731.47; 770.76		M
109	29.7	1872.79	955	568.55; 699.34; 717.23; 793.49; 909.63; 955.50; 978.71; 1356.59; 1380.65; 1421.48; 1553.85; 1647.62; 1742.60; 1853.62; 1978.73	1978.73	
110	29.88	1683.63	955	495.58; 805.55; 939.62; 955.52; 986.32; 1308.58; 1511.67; 1553.66; 1665.63; 1696.88; 1871.56	1871.56	
111	29.94	1785.66	955	581.45; 761.32; 823.53; 955.61; 1024.70; 1263.29; 1393.33; 1621.69; 1653.69; 1699.63; 1768.61; 1860.75	1860.75	

112	30.16	1475.65	895	515.56; 671.53; 715.55; 895.58; 937.44; 1193.58; 1331.60; 1373.55; 1458.68; 1751.49	1751.49	
113	30.16	1757.71	955	501.39; 579.31; 823.44; 955.51; 1186.09; 1287.56; 1535.49; 1626.70; 1697.51; 1740.54; 1898.53	1898.53	
114	30.38	1871.71	955	565.11; 644.68; 823.56; 955.57; 995.90; 1248.60; 1289.64; 1383.84; 1511.68; 1553.65; 1665.68; 1853.68; 1905.35	1905.35	
115	30.5	1975.42	955	794.75; 837.34; 955.69; 1022.52; 1212.58; 1351.46; 1633.81; 1665.99; 1828.79; 1856.00; 1888.61; 1966. 91		
116	30.61	1885.73	823	533.72; 643.38; 823.49; 970.56; 1148.79; 1305.54; 1409.56; 1545.63; 1623.60; 1867.52; 1990.50	1990.5	
117	30.92	1987.84	955	625.43; 793.48; 955.55; 1100.65; 1407.72; 1511.66; 1553.78; 1647.78; 1819.66; 1970.65		
118	31.28	1053.48		483.21; 511.17; 699.00; 741.01; 909.32; 951.53		
119	31.6	1476.63	895	516.69; 629.65; 791.58; 895.57; 1108.52; 1252.76; 1295.49; 1373.59; 1433.58; 1518.31; 1879.62	1879.62	
120	31.71	1856.75	955	553.10; 643.49; 823.49; 955.51; 972.52; 1247.57; 1379.64; 1421.65; 1515.71; 1688.63; 1837.67; 1988.92	1988.92	
121	31.91	1987.87	955	582.65; 714.56; 836.65; 955.59; 989.56; 1227.29; 1335.39; 1511.69; 1553.59; 1647.59; 1726.60; 1820.91; 1969.61		
122	32.46	1825.69	955	567.61; 661.56; 793.51; 955.48; 1049.08; 1349.64; 1391.67; 1485.69; 1563.56; 1808.73; 1876.79; 1977.04		
123	32.51	1897.74	955	535.58; 775.44; 909.12; 955.54; 997.67; 1223.70; 1380.21; 1421.86; 1463.68; 1575.67; 1730.70; 1880.61; 1957.78		
124	32.78	1517.87	895	435.21; 667.43; 715.65; 895.47; 937.57; 1253.61; 1373.53; 1415.52; 1500.53; 1750.79; 1941.58		
125	33.43	1692.68	895	515.56; 653.44; 791.40; 895.50; 1027.57; 1089.22; 1287.57; 1420.59; 1559.62; 1589.65; 1649.65; 1723.23; 1836.60		
126	33.55	1972.57	939	583.74; 807.44; 939.53; 1007.63; 1208.45; 1405.90; 1495.73; 1537.74; 1631.69; 1709.59; 1803.65; 1954.66		
127	33.7	1559.68	895	515.48; 630.49; 791.55; 895.50; 1031.54; 1176.33; 1287.58; 1457.53; 1517.56; 1542.40; 1787.11; 1977.52		
128	34.54	1580.64	939	469.11; 547.52; 565.36; 807.46; 939.51; 1075.51; 1203.37; 1315.32; 1417.71; 1447.65; 1561.52; 1858.42		
129	34.78	1358.98		1093.00; 1134.37; 1255.29; 1317.47; 1399.19		
130	34.84	909.63		275.02; 409.54; 421.41; 535.06; 715.43; 759.45; 777.46; 862.44; 1294.34	1294.34	
131	34.9	977.32		450.20; 841.08; 909.48; 931.43; 974.61		
132	35.2	1559.73	895	483.08; 625.51; 715.60; 895.49; 937.57; 1236.46; 1415.46; 1457.62; 1517.60; 1680.82; 1996.52	1996.52	
133	36.3	1688.64	895	515.95; 626.73; 791.58; 895.49; 1108.10; 1287.60; 1317.59; 1559.49; 1602.62; 1627.65; 1669.67; 1701.13; 1861.49		
134	36.66	1680.14		483.28; 631.29; 716.98; 1099.59; 1203.46; 1339.48; 1507.18; 1619.29; 1984.64		

135	37.84	1648.57	983	555.17; 683.00; 852.53; 903.50; 983.51; 1171.55; 1307.41; 1375.62; 1516.52; 1545.57; 1606.54; 1764.18; 1943.10	1943.1	
136	38.03	1051.09		919.97; 1141.82; 1826.61	1826.61	
137	38.29	1515.57	851	586.02; 671.63; 787.81; 851.55; 893.47; 1063.63; 1234.56; 1371.59; 1413.59; 1473.63; 1682.74; 1786.26	1786.26	
138	39.28	1518.45	937	485.58; 605.19; 730.88; 937.35; 1041.48; 1177.37; 1345.46; 1498.89; 1624.92; 1904.77	1904.77	
139	39.53	1562.34		831.01; 963.03; 1069.42; 1295.36; 1440.97; 1518.61; 1543.28		
140	39.68	1385.12		1252.30; 1438.49; 1516.19	1516.17	
141	40.07	815.34		304.89; 621.43; 747.45; 769.40; 1460.62	1560.62	
142	40.19	747.47		393.29; 422.08; 497.66; 617.32; 729.51; 958.38; 958.38; 1294.17; 1475.07	1475.07	
143	40.29	883.03		646.25; 815.36; 837.33; 852.04; 1559.17	1559.19	
144	40.91	905.09		561.06; 798.32; 829.72; 1056.87; 1156.60; 1240.99	1240.99	
145	41.1	1560.19		485.58; 748.71; 833.43; 937.59; 1041.59; 1083.37; 1219.44; 1387.26; 1517.41; 1626.08	1626.08	
146	42.9	959.27		772.93; 891.29; 913.39; 940.46; 1129.73; 1598.11	1198.11	
147	43.09	553.25		485.41; 523.36; 552.59		M
148	43.59	649.11		405.31; 477.08; 581.08; 605.07; 649.23; 695.92; 871.05	871.11	M
149	44.75	952.89		804.97; 883.46; 909.40; 933.56, 1617.39; 1638.84		
150	45.53	893.61		423.43; 472.97; 587.00; 731.46; 761.47; 846.94; 1392.12; 1489.73; 1794.95	1794.95	
151	45.53	1029.28		403.60; 1125.82; 1185.38; 1269.92; 1592.99	1592.99	
152	45.59	961.45		598.61; 893.37; 915.37; 938.35; 1704.67	1704.67	
153	45.72	893.52		308.77; 423.30; 519.24; 544.42; 712.94; 743.43; 761.40; 849.31; 946.86; 1447.57	1447.57	
154	46.31	961.41		868.74; 915.43; 1039.47; 1167.53	1167.53	
155	47.53	625.11		424.10; 463.55; 556.09		
156	47.53	1661.97		870.93; 1308.69; 1380.57; 1565.93; 1529.49; 1636.21; 1819.11; 1911.78	1911.78	
157	47.77	1615.77		536.77; 967.89; 1075.51; 1221.45; 1353.49; 1483.76; 1546.62; 1970.14	1970.14	
158	47.92	539.41		471.36; 492.91; 574.62; 963.43	963.43	M
159	49.24	650.94		582.45; 622.72; 817.81; 932.77; 1073.19, 1295.65	1295.65	
160	49.5	607.19		539.40; 589.28; 715.77		M
161	50.86	1660.84		822.92; 968.25; 1336.33; 1379.42; 1613.45; 1857.68; 1925.99	1925.99	
162	52.03	1637.73		782.11; 1302.00; 1358.72; 1380.21; 1515.25; 1564.46; 1700.69; 1822.35; 1914.35	1914.35	
163	52.64	939.27		502.36; 532.98; 656.01; 802.36; 839.40; 973.98; 989.00; 1460.88; 1768.17; 1813.08	1813.08	
164	52.85	1662.89		743.42; 923.28; 1143.36; 1207.17; 1358.32; 1551.21; 1593.54; 1615.57; 1804.80; 1960.72	1960.72	

165	52.91	1663.9		764.72; 1214.88; 1398.64; 1570.30; 1594.49, 1616.27; 1807.05	1807.05	
166	53.04	1591.97		597.22; 615.31; 648.30, 945.64; 1125.02; 1207.45; 1335.49; 1445.41; 1546.57; 1618.04; 1880.60		
167	53.7	1528.95		633.25; 1265.54; 1482.26; 1510.71; 1638.42	1638.42	
168	54.42	1504.98		781.25; 1243.22; 1386.99; 1488.32; 1511.63; 1700.32	1700.32	
169	54.74	1459.61		483.07; 665.39, 751.44; 936.27, 1089.50; 1113.56; 1221.45; 1313.45; 1457.08; 1678.47; 1860.02	1860.02	
170	55.4	1486.42		482.82; 737.28; 889.13; 972.49, 1075.49; 1221.56; 1256.86; 1396.54; 1505.84; 1891.60	1891.6	
171	55.53	1531.26		818.30, 1432.81; 1484.46; 1535.67; 1677.28; 1730.81; 1940.45	1940.45	
172	55.9	1591.38		483.11; 555.12; 615.36; 805.58; 1011.70; 1113.67; 1221.44; 1353.44; 1459.55; 1501.64; 1525.86; 1708.22, 1906.69	1906.69	
173	56.88	1617.49		527.04; 555.15; 793.55; 929.69; 1113.58; 1221.56, 1335.53; 1485.63; 1510.72, 1694.46; 1990.43	1990.43	
174	59.62	828.36		253.31; 571.16; 768.43; 783.47; 951.88; 1194.47; 1478.95	1478.95	
175	59.92	593.43		187.17; 201.25; 337.06; 423.12; 549.47; 595.11; 756.99		M
176	60.1	833.61		297.06; 391.15; 526.58; 553.19; 577.09; 672.18; 833.61; 1264.97; 1646.55	1646.55	
177	60.22	1227.33		714.40; 1228.49; 1624.82; 1760.13; 1874.85	1874.85	
178	60.64	833.5		241.24; 391.24; 413.31; 553.27; 577.31; 772.54; 833.54; 886.94; 1323.40, 1613.88	1613.88	
179	60.7	1619.67		469.41; 615.12; 811.29; 931.61; 1131.55; 1221.55; 1353.51; 1487.48; 1667.13; 1777.29; 1959.34	1959.34	
180	60.89	1253.48		763.10; 1163.02; 1259.21; 1505.70; 1657.20; 1978.69	1978.69	
181	60.95	1665.06		811.30; 978.32; 1001.47; 1265.28; 1375.11; 1571.90; 1702.32; 1762.30; 1916.22	1916.22	
182	61.38	1620.55		469.04; 615.27; 737.34; 973.59; 1113.02; 1221.53; 1335.46; 1487.52; 1557.28; 1741.31; 1871.34	1871.34	
183	61.75	1227.47		943.59; 1154.90; 1177.22; 1215.11; 1354.38; 1455.88; 1577.60; 1623.45; 1658.44; 1850.26	1850.26	
184	61.99	1253.47		1197.25; 1261.60; 1328.38; 1577.88; 1636.21; 1696.72; 1848.81; 1916.32	1916.32	
185	62.36	745.38		320.74; 414.93; 509.18; 555.50; 684.28; 727.20; 744.44; 956.33; 1114.57	1114.57	
186	62.77	757.45		349.94; 462.16; 699.19; 711.12; 739.29; 756.40; 774.52		M
187	62.84	731.43		269.21; 307.30; 390.88; 494.19; 575.53; 713.30; 730.41		M
188	62.95	593.4		187.15; 200.92; 337.02; 423.14; 524.98; 593.41		M
189	63.31	1487.29	985	641.48; 749.23; 985.62; 1131.46; 1221.42; 1266.87; 1397.29; 1496.68; 1697.75; 1840.15	1840.15	
190	63.49	1532.88		642.41; 767.04; 795.27; 1017.04; 1094.34; 1462.83; 1551.27; 1672.60; 1695.56; 1789.21; 1882.07; 1968.16	1968.16	

191	63.55	1488.74		466.12; 483.26; 665.71; 749.47; 968.20, 1131.46; 1221.51; 1398.63; 1533.61; 1817.90; 1976.00	1976	
192	63.8	761.42		305.01; 337.48; 390.81; 466.20; 649.22; 661.02; 761.30		M
193	64.63	691.42		285.15; 413.20; 533.39; 601.16; 672.23; 691.52; 828.29	828.29	M
194	64.93	726.56		243.81; 311.21; 446.96; 465.25; 584.31; 690.51; 796.57	796.57	M
195	65.05	733.57		224.04; 327.34; 422.91; 477.06; 578.15; 733.02; 795.76; 973.93	973.93	
196	65.11	727.21		264.22; 463.47; 584.26; 699.65		M
197	65.47	728.42	956	223.16; 321.24; 414.55; 471.10; 552.32; 683.48; 728.29; 746.49; 956.13; 1133.08; 1232.33	1232.33	
198	66.36	593.38		187.08; 201.18; 337.09; 423.21; 593.37; 611.06; 812.09; 970.90		
199	66.57	693.39		277.37; 413.18; 519.28; 665.47; 692.61; 892.81		M
200	66.63	745.57		236.17; 260.13; 335.61; 422.92; 489.31; 505.01; 727.33, 745.81		M
201	67.47	726.22		242.81; 445.27, 616.25; 681.41; 707.39; 1157.49	1157.49	
202	68.31	669.58		242.92; 261.00; 412.78; 431.31; 499.22; 651.45		
203	69.63	687.19		447.07; 496.20; 642.69; 686.88; 837.38	837.38	
204	71.47	687.27		255.31; 452.44; 545.56; 641.71; 686.73; 1338.94	1338.94	
205	75.88	687.32		280.91; 294.77; 544.77; 641.59; 686.70; 1337.39	1337.39	